Neurocognitive Function in Patients undergoing Stereotactic Radiosurgery for Brain Metastases

---

By

Najmus Sahar Iqbal

A Thesis

Submitted to the School of Medicine

For the Degree of

Doctorate of Philosophy

Cardiff University

Doctor of Philosophy (2023)

(Medicine)

Cardiff University,

Cardiff, Wales

Title: Neurocognitive Function in Patients undergoing Stereotactic Radiosurgery for Brain Metastases

Author: Najmus Sahar Iqbal

Supervisors: Prof. John Staffurth, Dr. James Powell, Prof. Richard Wise

Number of pages: 296

Word Count: 74,681

Acknowledgements

I would like to thank Wales Cancer Research Centre and the Moondance fund at Velindre Cancer Centre for providing funding for my research time and the study. I would also like to express my gratitude to the patients who volunteered to participate in the study and undertook neurocognitive testing and MRI imaging for the study, my supervisors, Dr James Powell, Professor Richard Wise and Professor John Staffurth for providing guidance and encouragement with their expertise and throughout the research and writing period, staff at Cardiff University Brain Research Imaging Centre (CUBRIC) who taught me MRI analysis, members of staff in Velindre Cancer Centre namely, Maeve Williams, Michael Chu, Tara Daisley-Devoy, Michelle Smalley and Ceri Davies. Finally, I am indebted to me family including my husband, Aamir, and my children, Sophia and Nabeel, without their immense support this work would not have been possible.

Abbreviations for Frequently Used Terms	
ADC	Apparent Diffusion Coefficient
AFD	Apparent Fibre Density
ASL	Arterial Spin Labelling
BED	Biologically Equivalent Dose
BM	Brain Metastases
BOLD	Blood Oxygen Level Dependent
CBF	Cerebral Blood Flow
CHARMED	Composite Hindered and Restricted Model of Diffusion
Cho	Choline
COWAT	Controlled Oral Word Association Test
Cr	Creatine
CSF	Cerebrospinal Fluid
CT	Computed Tomography
DS	Digit Span
DTI	Diffusion Tensor Imaging
DWI	Diffusion Weighted Imaging
ECD	Extra-cranial Disease
EORTC	European Organisation for Research and Treatment of Cancer
FA	Fractional Anisotropy
Glx	Total Glutamate Molecules
GM	Grey Matter
GPA	Graded Prognostic Assessment
Gy	Gray
HC	Hippocampus
HVLT-R	Hopkins Verbal Learning Test-Revised
HVLT-R DR	Hopkins Verbal Learning Test-Revised Delayed Recall
HVLT-R TR	Hopkins Verbal Learning Test-Revised Total Recall
KPS	Karnofsky Performance Status
Linac	Linear Accelerator
MD	Mean Diffusivity
mI	Myo-Inositol
MRI	Magnetic Resonance Imaging
MRS	Magnetic Resonance Spectroscopy
NAA	N-Acetyl Aspartate
NCF	Neurocognitive Function
NSCLC	Non-Small Cell Lung Cancer
OS	Overall Survival
PFS	Progression Free Survival
PS	Performance Status
QoL	Quality of Life
RCT	Randomised Controlled Trial
RD	Radial Diffusivity
RPA	Recursive Partitioning Analysis
RT	Radiotherapy
SACT	Systemic Anti-Cancer Therapy
SRS	Stereotactic Radiosurgery
TE	Echo Time
TKI	Tyrosine Kinase Inhibitor
TI	Inversion Time
TMT	Trail Making Test
TR	Repetition Time

VERDICT	Vascular, Extracellular, and Restricted Diffusion for Cytometry in Tumours
WBRT	Whole Brain Radiotherapy
WHO PS	World Health Organisation Performance Status
WM	White Matter

Table of Contents

Thesis Summary

National Institute of Clinical Excellence (NICE) recommends Stereotactic radiosurgery (SRS) as the treatment of choice for patients with limited brain metastases, which is defined as volume <20 cc, with performance status 0-2, controlled or controllable extracranial disease and expected prognosis of greater than 6 months. Despite its precision, studies have reported 24-60% of patients can develop neurocognitive impairment following SRS alone. Dose to the hippocampus is thought to be related to development of neurocognitive impairment following fractionated radiotherapy for primary brain tumours and whole brain radiotherapy for brain metastases. However, this has not been studied in patients undergoing SRS.

This thesis investigates the importance of hippocampus delineation and dose delivered to this organ in patients undergoing SRS and its impact on neurocognitive decline following treatment. Multi-parametric MRI imaging identifies changes in the hippocampus structure, blood flow, metabolites, and diffusion tensor imaging of the tracts involved in the limbic system. We utilised this opportunity to perform novel microstructure MRI imaging of the metastases to understand the tumour microenvironment and oxygenation.

Below are the specific objectives related to each chapter:

Chapter 2

- Dosimetric analysis of patients who received SRS in one year
- Factors influencing hippocampal dose

Chapter 3

- Feasibility of avoiding the hippocampus during SRS treatment planning using dynamic conformal arc and volumetric arc therapy

Chapter 4

- Developing the prospective study, neurocognitive function (NCF) testing and developing MRI methods

Chapter 5

- Studying baseline clinical factors of patients and their impact on patient's survival
- NCF impairment at baseline and clinical factors influencing this

Chapter 6

- Baseline NCF Impairment and its correlation with MRI finding. Identifying confounding variables.

Chapter 7

- Changes in NCF Impairment at 1-, 3-, and 6-months following treatment
- Correlation of hippocampal dosimetry with NCF Impairment
- Multiparametric imaging of the hippocampus

Chapter 8

- Assessment of the brain metastases and impact of radiation on the surrounding brain regions

Chapter 9

- Overall conclusions, limitations of the study and future work

Chapter 1 – Introduction

1.1. Brain Metastases

There are approximately 375,000 new diagnoses of cancer in the United Kingdom every year (CRUK, 2015). Since the 1990's incidence rates of all cancers have increased by 12% and these rates are projected to rise further by 2% to 742 new cases per 100,000 population by 2035 (CRUK, 2015). With improved treatment modalities, surgical techniques, radiotherapy and systemic anti-cancer therapies, mortality rates for all cancers combined have decreased by 16% since the 1970's. Almost half of cancers are diagnosed at a late stage in England (CRUK, 2015). If cancers are diagnosed early, they can be treated radically with aim of cure. However, once cancer has metastasised from its origin, most patients have a limited life expectancy with some exceptions. Systemic anti-cancer therapies (SACT) may control metastatic cancer for many months to years. Unfortunately, this is often not the case for patients with brain metastases (BM); for these patients, survival tends to be relatively short and median overall survival is often measured in months (Tabouret *et al.*, 2012).

The exact incidence of BM is unknown. Approximately 20-40% of patients with diagnosis of cancer may develop BM during their cancer journey depending on the primary site (Barnholtz-Sloan *et al*., 2004). Lung cancer, melanoma and breast cancer are most likely to metastasise to the brain (Nieder *et al*., 2011). The concept of oligometastatic disease has been introduced recently to define metastatic disease with low tumour burden, usually represented by 1-5 metastatic sites of disease. In patients with a limited number of BM, local ablative therapies such as stereotactic radiosurgery (SRS) in combination with newer targeted agents achieve longer overall survival compared to palliation with whole brain radiotherapy (WBRT) (Andrews *et al*., 2004).

Disease specific quality of life (QoL) measures hold immense value in medicine and have been integrated into outcome reports of clinical trials. In oncology, tumour site specific validated QoL measures are used in clinical trials. In clinical trials involving patients with BMs and primary brain tumours radiotherapy induced neurocognitive impairment as well as brain

tumour specific quality of life measures should be part of follow up (Wong *et al*., 2008). This has also been endorsed by the Response Assessment of Neuro-Oncology (RANO) Group who have recommended that neurocognitive, neurological, and health-related quality of life measures should be integrated in assessments following radiation particularly in randomised controlled trials (Lin *et al*., 2013). A range of randomised controlled trials have demonstrated preserved neurocognitive function (NCF) in patients treated with SRS alone versus SRS with WBRT without impacting on overall survival (Aoyama *et al*., 2015, Brown *et al*., 2016a). Hence, SRS without WBRT is an established treatment modality for patients with limited BM (defined as volume of less than 20 cc or 1-4 metastases); recently, the overall number of BM has been removed from the NICE guidance as a criterion for treatment as there is increasing evidence of treating numerous BM with SRS (NICE, 2018). Nevertheless, despite the precision of SRS a significant proportion (ranging between 20-60%) of patients have been reported to suffer neurocognitive impairment after treatment (Brown *et al*., 2016a, Gondi *et al*., 2012).

1.1.1 Epidemiology of Brain Metastases

BM are the most common intracranial tumour and cause significant morbidity and mortality. Accurate incidence and prevalence rates of BM prove difficult to measure as there is not a nationwide systematic reporting system for metastases. Therefore, current estimation of incidence of BM is thought to be conservative. However, data collection of secondary spread of cancer is improving and it should be possible to report national data on sites of metastatic disease in the future.

Historically, autopsy studies have attempted to estimate frequency of BM and overall, the estimated frequency of BM from these studies was approximately 25% (Gavrilovic *et al.,* 2005). These varied by primary cancer histology and highest incidence was reported in non-small cell lung cancer and melanoma. Some autopsy studies have shown that 41% of cancer patients had BM (Arnold *et al*., 2001). However, these studies are outdated and largely data was collected in a single centre.

Prevalence of BM from population-based studies is challenging to calculate precisely. Mandatory reporting of primary cancer diagnosis and histological basis is recorded systematically in the national registry, however, recording sites of metastatic disease is not mandatory. The Maastricht (Netherlands) Cancer Registry captures 95% of patients with malignant disease. Using that registry, Schouten *et al*. identified 2724 patients with cancer from five common primary sites who were selected for a follow-up study, where BM were identified both by linking medical records and radiological investigations of patients. In this study, 8.5% of all patients with cancer were found to have BM, which is substantially lower than figure quoted in autopsy studies and 72% of BM occurred within a year of primary cancer diagnosis (Schouten *et al*., 2002). In another population-based study Barnholtz *et al.* collected data from 16,210 patients from the Metropolitan Detroit Cancer Surveillance System, diagnosed with BM from various primary tumours between 1973 and 2001 (Barnholtz-Sloan *et al*., 2004). The estimated overall incidence of BM reported here was 9.6%, which is similar to the Schouten study.

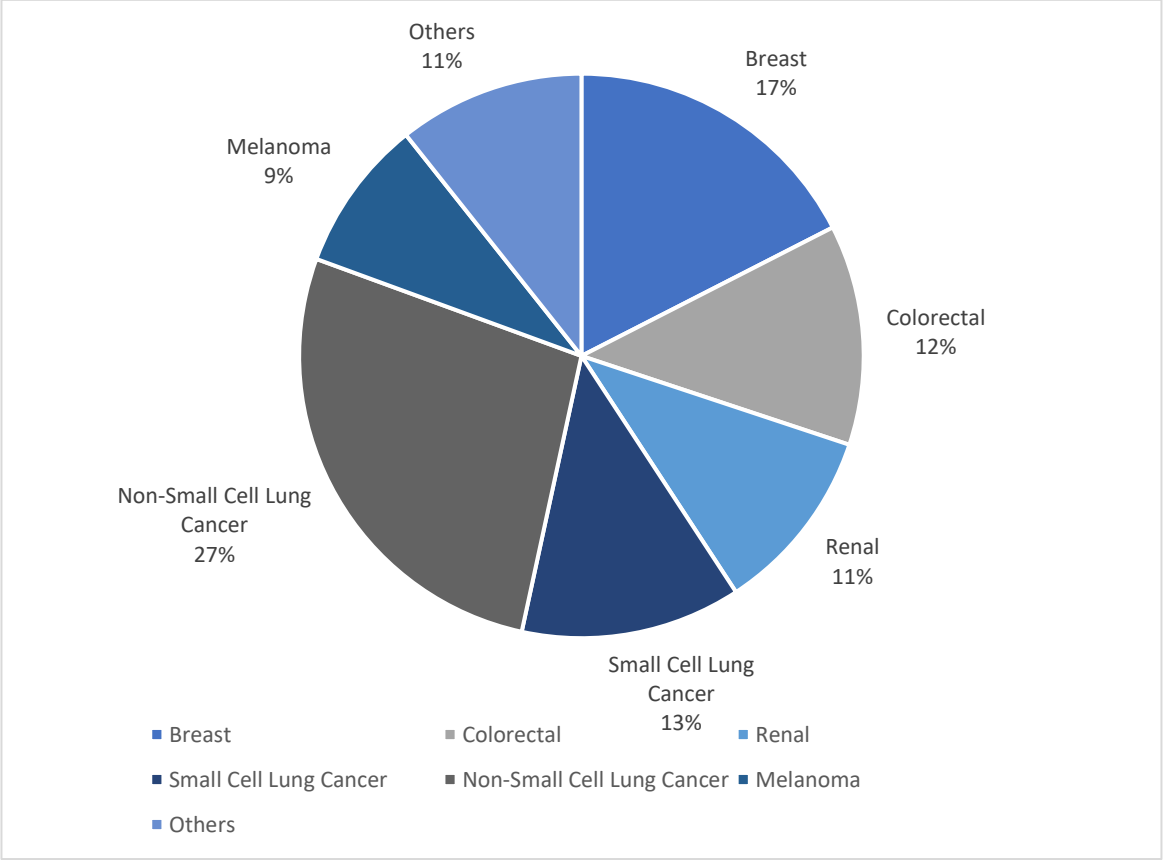

Figure 1.1 The proportion of primary site in patients with diagnosis of brain metastases. *Adapted from Nieder et al., 2011*

Incidence of BM varies greatly by primary cancer site. Lung cancer, breast cancer, melanoma, colorectal cancers, and renal cell carcinoma continue to be the leading cause of BM in adults. Brarnholtz *et al*. reported incidence according to primary site; in descending order primary sites included lung (19.9%), melanoma (6.9%), renal (6.5%), breast (5.1%) and colorectal cancer (1.8%). Another study by Nieder *et al*., demonstrated 40% of BM arise from lung cancers, followed by 17% from breast cancer and 9% from melanoma and 12% from CRC (Nieder *et al*., 2011) (Figure 1.1).

Globally, incidence of BM is believed to have increased during the last few decades. However, there are few studies which have examined time trends in epidemiology of BMs. Schouten *et al*., demonstrated that incidence of BM in a population-based study in Netherlands has remained static between 1986 and 1995 (Schouten *et al*., 2002). In contrast a more recent Swedish survey has shown that incidence rate of hospitalization because of BM has doubled from 7 to 14 per 100,000 population between 1987 and 2006 (Smedby *et al*., 2009). Increase in BM incidence could be due to improvements in the quality and frequency of neuroimaging, particularly more use of Magnetic Resonance Imaging (MRI) (Figure 1.2). Another explanation could be global increase in cancer incidence, increased use of surveillance imaging in groups of patients where cancer is highly likely to metastasise to the brain and improvement in SACT resulting in patients living longer with metastatic disease. Advancement in SACT is particularly applicable to non-small cell lung cancer, breast cancer and melanoma. In these tumour sites systemic treatment (targeted tyrosine kinase inhibitors, trastuzumab and programmed death-ligand one inhibitors respectively) advances offer effective treatment that have significantly improved survival. In some cases, e.g. trastuzumab, treatment for extra-cranial sites has limited efficacy for BM due to limitations in being able to cross the blood brain barrier, unmasking brain as a potential sanctuary metastatic site (Schouten *et al*., 2002).

Routine brain imaging of cancer patients in absence of neurological symptoms is not usually performed. Lung cancer and melanoma are exceptions where routine brain scans of patients diagnosed with high-risk disease. National Comprehensive Cancer Network (NCCN)

recommend annual surveillance Magnetic Resonance Imaging (MRI) scans of the brain for patients with Stage IIIB to IV melanoma (NCCN, 2016). Similarly, in lung cancer National Institute of Clinical Excellence (NICE) recommends imaging of the brain in patients with stage II & III disease being considered for radical treatment or patients with neurological symptoms with stage IV disease (NICE, 2019). One screening study has identified 15% of patients with lung cancer to have occult BM (Hochstenbag *et al*., 2000).

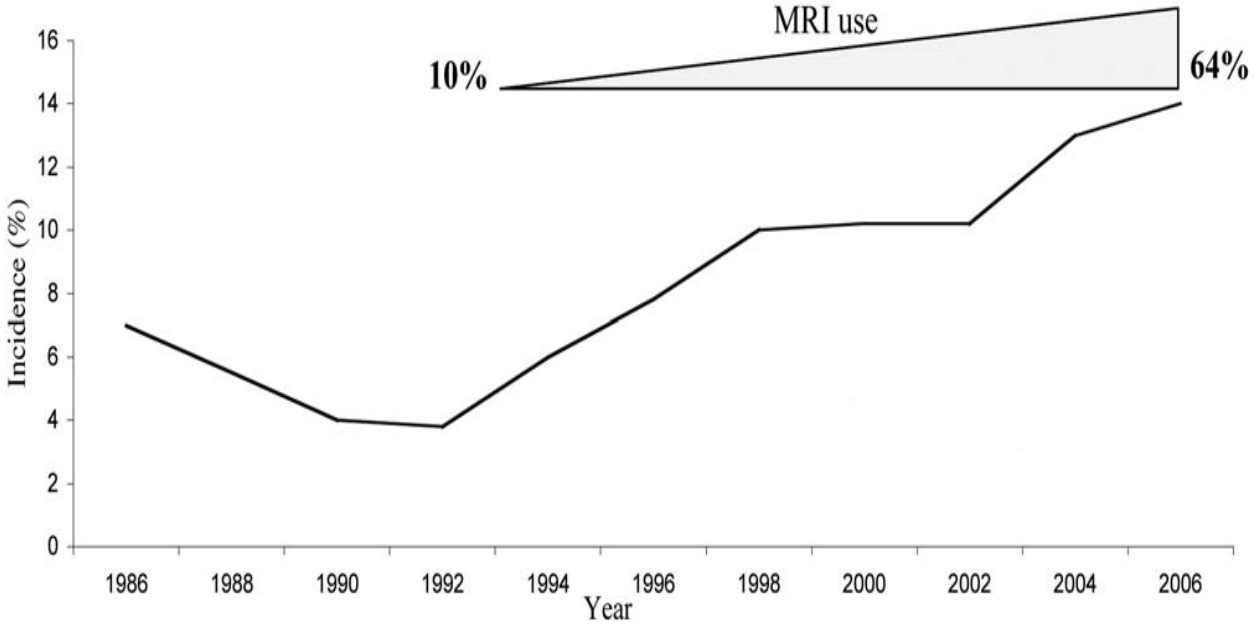

Figure 1.2 Trends in incidence of brain metastases over time in relation to use of Magnetic Resonance Imaging. Incidence of brain metastases in 2006 was 14% vs. 7% in 1986. Increase in incidence is proportional to use of 1.5 Tesla MRI over time. *Adapted from Smedby et al. and Neider et al.*

1.1.2 Pathophysiology of Brain Metastases

The exact sequence of events that lead to metastatic spread to the brain remain largely undetermined (Klos *et al.*, 2004). The most common mechanism hypothesised is haematogenous spread involving arterial blood supply leading to the most common pattern of grey-white matter junction contrast enhancing lesions (Klos and O'Neill, 2004 2001, Gavrilovic *et al*, Pruitt *et al*., 2017). This could be because of change in size of blood vessels that may act as a trap for the cancer cells (Pruitt *et al.*, 2017). Some subtypes of cancers are more likely to metastasise to the brain, for example, small cell lung cancer and adenocarcinoma of the lung are more likely to metastasise than squamous cell cancer of the

lung. Consequently, the "Seed and Soil" hypothesis was proposed by Paget. The hypothesis postulates that genetic changes in some cancer cells (the seed) promotes them to find the physiological and biochemical environment of the brain (the soil) a favourable place to grow (Paget *et al.,* 1889). Figure 1.3 presents a schematic diagram of pathophysiology of BM based on these hypotheses.

1.1.3 Diagnosis of Brain Metastases

An index of suspicion should be raised with any cancer patients presenting with neurological symptoms. Presenting symptoms in patients with BM are summarised in Table 1..1. Whilst these can depend on the location of the lesion, headache (42%) followed by confusion (31%) are the most common presenting symptoms (Klos *et al.,* 2004). Seizures are less frequent (20%) as a presenting symptom but may become more prevalent at the time of intracranial progression.

Nevertheless, approximately a third of the patients with BM are asymptomatic (Lalondrelle *et al.,* 2009). Where there is a high proportion of patients developing BM, e.g., NSCLC and melanoma, there is a role for surveillance imaging at presentation. As discussed in section 1.1.1, NICE recommends surveillance imaging for patients with stage II or III lung cancer undergoing radical treatment in the form of surgery or radiotherapy (NICE, 2019). Surveillance imaging may be one of the reasons for rising prevalence of BM.

Symptom	No. of patients	Percent
Headache	163	42
Weakness	107	27
Altered Mental State	121	31
Seizure	80	20
Ataxia	65	17
Sensory Disturbance	24	6
Speech Problems	40	10

Table 1.1 Symptoms of Brain Metastases in 392 patients. *Klos et al., 2004*

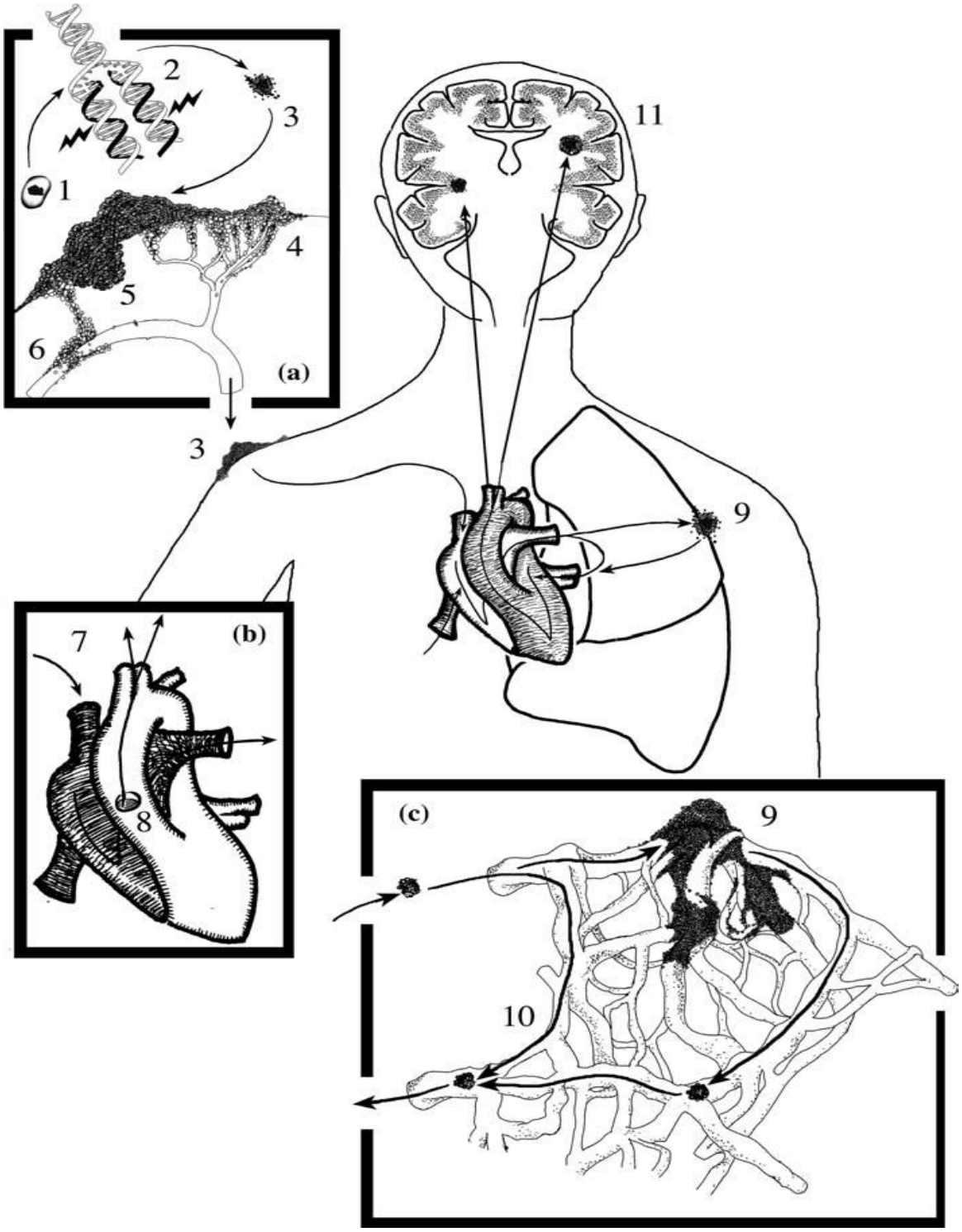

Figure 1.3 Pathophysiology of Brain Metastases. *(a) A normal cell (1) undergoes multiple genetic mutations or epigenetic changes (2) to become a cancer (a melanoma as shown here) (3). It then proliferates uncontrollably and develops its own feeding vessels (4) (angiogenesis), invades the normal tissue stroma (5) and enters blood vessels or lymph channels (6). (b) The tumour gains access to the right side of the heart via the venous circulation (7). The cancer cells may be shunted to the left side of the heart via a patent foramen ovale or septal defect (8) or: (c) More commonly, the cancer cells leave the heart via the pulmonary artery to reach the lung capillary bed (9), where they may either form a metastasis (9) or pass through that capillary bed to reach the left atrium (10), from which tumour cells enter the arterial circulation and seed the brain usually at the grey matter/white matter junction. If the ''soil'' (brain) is hospitable, the tumour may leave brain capillaries and become a brain metastasis (11). (Gavrilovic and Posner, 2005)*

The best imaging modality for defining distribution, size and number of BM is MRI because of its superior tissue contrast compared to Computed Tomography (CT) scan. When a CT demonstrates BM, an MRI should be performed when a limited number of BM are present and where surgical resection or SRS is appropriate. Characteristic features of BM on MRI are contrast enhancing lesions at the grey-white matter junction and a relatively smooth margin often with abundant oedema. Often, in patients with established diagnoses of cancer, in particular a cancer that is likely to metastasise to the brain, a radiological diagnosis of BM is formed without histological confirmation. For a single lesion in patients without a diagnosis of cancer, the differential diagnosis can include primary brain tumour e.g., glioma, lymphoma, abscess, infarct, and haemorrhage and in some cases, biopsy is warranted for definitive diagnosis. Advanced MRI techniques such as perfusion, MR spectroscopy and diffusion weighted imaging (DWI) have been used to help distinguish between these diagnoses.

1.1.4 Prognostic Factors in Brain Metastases

Several prognostic scores for BMs patients have been designed to guide the clinicians' treatment decisions (Table 1.2). In clinical practice and trials, the recursive partitioning analysis classes (RPA), the graded prognostic assessment index (GPA) and the diagnosis-specific GPA (DS-GPA) scores are largely used. Gaspar *et al*. described the prognostic index scoring model RPA, which was developed after evaluating 1,200 patients with BM. Patients were stratified into three classes and RPA classes were associated with different median OS rates: 7.1, 4.2, and 2.3 months for class I, II, and III, respectively.

Sperduto *et al*., 2008 proposed a disease specific graded prognostic assessment index (GPA), which considers four clinical criteria (age, Karnofsky Performance Status, number of BMs, and presence/absence of extracranial metastases) based on data from five randomised Radiation Therapy Oncology Group (RTOG) trials, including a total of 1,960 patients. A higher GPA score correlated to a better prognosis with a median OS of 11 months, while for GPA scores of 0–1, the OS was 2.6 months.

Factors	RPA	Rotterdam Score	SIR	BSBM	GPA
Basis	3 RTOG studies	Single institution	Single institution	Single Institution	5 RTOG Studies
Number of patients	1200	1292	65	110	1960
Age	<65 years	-	2 points: ≤ 50; 1 point: 51–59; 0 points: ≥ 60	-	1 point: <50 0.5 points: 50-59 0 point: >60
Performance Status	KPS <70 vs ≥70	ECOG 0-1 vs 2-3	2 points: KPS 80–100; 1 point: KPS 60–70; 0 point: KPS ≤ 50	1 point: KPS 80–100; 0 point: KPS ≤ 70	1 point: KPS 90-100 0.5 points: KPS 70-80 0 point: KPS <70
ECD	No vs yes	Limited vs extensive	2 points: none or complete remission 1 point: partial response of better	1 point: no 0 point: yes	1 point: none 0 points: present
Control of primary tumour	No vs yes	-	1 point: disease present 0 point: progressive disease	1 point: yes 0 point: no	-
Number of BM	-	-	2 points: 1; 1 point: 2; 0 point: ≥3	-	1 point: 1 0.5 points: 2-3 0 point: >3
Volume of BM	-	-	2 points: <5 cc; 1 point: 5-13 cc; 0 point: 13 cc	-	-
Interval to BM	-	-	-	-	-
Response to Steroids	-	Good, moderate, or little	-	-	-
Classes					
Class I	All 4 favourable factors	ECOG 0-1, limited ECD, good steroid response	8-10 points	3 points	3.5-4 points
Class II	All other patients	Other patients	4-7 points	2 points	3 points
Class III	KPS <70 regardless of other 3 factors	ECOG2-3, extensive ECD, little steroid response	1-3 points	1 point	1.5-2.5 points
Class IV	-	-	-	0 point	0-1 points

Table 1.2 Summary of prognostic factors in patients with brain metastases. *RPA: recursive partitioning analysis, SIR: score index for radiosurgery, BSBM: basic score for brain metastases, GPA: graded prognostic assessment, RTOG: Radiation Therapy Oncology Group, KPS: Karnofsky performance status, ECOG: Eastern Cooperative Oncology Group, ECD: Extracranial disease, BM: brain metastases, criteria not included in the index is marked '-'.*

Of all the scoring systems, GPA is used most widely as it is deemed most quantitative, least subjective, and easiest to apply clinically compared to the other prognostic indices. The same group developed a diagnosis specific GPA which stratifies GPA scores according to diagnosis and treatment of primary tumour. Retrospective analysis of data from eleven institutions comprising 4,259 patients was conducted. The group reported different GPA factors that influenced survival in patients according to their primary tumour. Patients with lung cancer had four prognostic factors: age, KPS, extracranial disease, and number of BM; patients with melanoma and renal cell carcinoma had two prognostic factors: KPS and number of BM; and patients with breast and colo-rectal cancers had one prognostic factor: KPS (See table 1.3 for details).

Primary Tumour	**Prognostic factors**	**GPA Scoring System**				
NSCLC/SCLC		0	0.5	1	-	-
	Age KPS ECD Number of BM	>60 <70 Present >3	50-60 70-80 - 2-3	<50 90-100 Absent 1	- - - -	- - - -
Melanoma/RCC		0	1	2	-	-
	KPS Number of BM	<70 >3	70-80 2-3	90-100 1	- -	- -
Breast/ Colo-rectal Cancer		0	1	2	3	4
	KPS	<70	70	80	90	100

Table 1.3 Criteria for Diagnosis-specific graded prognostic assessment indexes of patients with brain metastases. *GPA: graded prognostic assessment, NSCLC: non-small cell lung cancer, SCLC: small cell lung cancer, KPS: Karnofsky performance status, ECD: extracranial disease, BM: brain metastases, RCC: renal cell carcinoma. For all diagnoses GPA of 4 indicates the best prognosis and 0 indicates the worst. Sections not scored in a particular subgroup are marked as '-'. Adapted from Sperduto et al., 2010*

Median overall survival (OS) was determined by the diagnosis and GPA scores. Median OS was highest for patients with breast cancer (11.93 months) and lowest for those with small cell lung cancer (4.9 months). Range of OS for patients with GPA score of 0-1 was 2.79-6.11 months compared to 13.23 -18.74 months in patients with GPA score of 3.5-4. (Sperduto *et al*., 2010) This study offers further detailed understanding of prognostic factors in patients

with BM in a large sample size across multiple institutions. However, the main limitation is that it is a retrospective analysis and may be subject to selection bias.

All the prognostic scoring systems are focused on OS rather than neurological progression, neurological function, or quality of life. Incorporation of these additional factors will be beneficial in clinical decision making in patients with BM when assessing treatment outcomes with SRS.

1.2 Treatment options for brain metastases

1.2.1 General Considerations

The approach for treating BM is similar to that of patients with primary brain tumours. The key initial component is symptomatic management which includes control of peritumoural oedema and management of raised intracranial pressure with corticosteroids and treatment of seizures with anti-epileptics. Patients with poor PS (3 or more), large volume BM, or uncontrolled extracranial disease may not benefit from any form of radiotherapy and best supportive care approach with supportive corticosteroids and anti-epileptics is most appropriate.

Treatment aims in patients with good performance status are to achieve durable control of intracranial disease, minimise early and late adverse effects of treatment and maintain quality of life. The management of BM has become increasingly individualised with the advent of targeted SACT in certain cancer types. After the initial acute management, further assessment of patient fitness, number and volume of BM, extracranial disease status and treatment options for intra- and extra-cranial disease is needed.

Treatment options for BM include surgical resection of the metastases, SRS, WBRT or a combination of these treatments in addition to SACT. For certain subtypes of cancers, several forms of tyrosine kinase inhibitors (TKIs) have shown efficacy in patients with BM, e.g., BRAF-TKI inhibitors in melanoma, and epidermal growth factor receptor (EGFR)-TKI inhibitor and

anaplastic lymphoma kinase (ALK)-TKI inhibitors in patients with adenocarcinoma of the lung. Scheduling of SACT with respect to timing of radiotherapy treatment for BM needs to be considered. A retrospective analysis of patients with EGFR mutant NSCLC showed that upfront SRS followed by EGFR-TKI was associated with better OS compared to delayed SRS (46 months versus 25 months respectively) (Magnuson *et al*., 2017). NICE recommends consideration of SRS in patients with NSCLC with activating mutation who are suitable for treatment with a TKI (NICE, 2019).

Retrospective studies have often found prognosis to be correlated with treatment received for BM. Surgical candidates have sometimes been shown to have the best prognosis for all BM. However, a strong selection bias towards surgery exists for patients with limited disease burden and single or oligometastatic disease and presence of metastases in an accessible location. Those with a high burden of disease, recurrent chemotherapy-refractory disease, poor functional status, and diffuse BM are often only treated with palliative WBRT and excluded from surgical options.

1.2.2 Whole Brain Radiotherapy

Traditionally, whole brain radiotherapy (WBRT) has been the primary palliative treatment for patients with BM. WBRT can offer survival benefit for patients with BM compared with conservative treatment with high dose corticosteroid therapy (Arbit *et al*., 1995). The RTOG conducted RPA of 1200 patients from 3 RTOG trials (RTOG 79-16, RTOG 85-28 and RTOG 89-05) which showed survival advantage in patients who fulfilled the criteria for RPA Class I with OS of 7.1 months compared with 4.2 and 2.3 months for those is RPA Class II and III respectively (Gaspar *et al*., 1997). Similar survival advantage has been detected with using the newer GPA prognostic scoring with patients in Class I, II, III and IV having median OS of 11, 6.9, 3.8 and 2.6 months respectively (Sperduto *et al*., 2010).

However, the recently reported Quality of Life after Treatment for Brain Metastases (QUARTZ) trial, which randomised patients with NSCLC with BM to either WBRT plus supportive care or supportive care alone, showed no difference in median survival (9.2

weeks WBRT v 8.5 weeks) (Mulvenna *et al*., 2016). A considerable proportion of patients in this study had a poor performance status and further analysis demonstrated better prognostic subgroups who did benefit from WBRT, including patients younger than 60 years of age and patients with controlled primary disease.

Another predictive factor for treatment response is tumour type and its inherent radiosensitivity. Patients with small cell lung cancer and breast cancer show highest degree of complete response: 37% and 35% respectively, in contrast to patients with melanoma who have significantly lower response rates to WBRT and have a median OS of 2.3 months (Nieder *et al*., 2000). Various dose fractionation regimes have been used in randomised controlled trials (RCTs) for WBRT. None of which have any significant impact on OS. Summary of dose fractionation used in different trials is summarised in Table 1.4.

Trial	**Year of study**	**Number of participants**	**Randomisation Schedule***	**Median Overall Survival (months)****
Harwood *et al.*	1977	101	30 Gy/10# vs.10/1#	4.0-4.3
Kurtz *et al.*	1981	255	30 Gy/10# vs 50/20#	3.9-4.2
Borgelt *et al.*	1980	138	10 Gy/1# vs 30 Gy/10# vs 40 Gy/20#	4.2-4.8
Borgelt *et al.*	1981	64	12 Gy/2# vs 20 Gy/5#	2.8-3.0
Chatani *et al.*	1986	70	30 Gy/10# vs 50 Gy/20#	3.0-4.0
Haie-Meder *et al.*	1993	216	18 Gy/3# vs 36 Gy/6# or 43 Gy/13#	4.2-5.3
Chatani *et al.*	1994	72	30 Gy/10# vs 50 Gy/20# or 20 Gy/5#	2.4-4.3
Murray *et al.*	1997	445	54.4 Gy/34# vs 30 Gy/10#	4.5

Table 1.4 Randomised Trials of Whole Brain Radiotherapy Alone for Brain Metastases. ** Dose-fractionation schedule expressed as dose Gray (Gy)/ number of radiotherapy fractions (#). ** Survival difference between treat arms were not statistically significant in any study. (Shaw et al., 2003)*

Fractionation schedule, can however, have a significant impact on toxicities. It has been proposed that hypofractionated RT schedule of more than 3 Gy per fraction can be associated with greater toxicity, including NCF impairment (DeAngelis LM, 1989). Rates of symptomatic improvement with WBRT are generally less favourable, with approximately 25 to 40% of patients achieving stable or improved symptoms after WBRT.

Over the last two decades, management strategies for patients with BM have evolved significantly due to rationalising the use of WBRT and advances in modern technology and techniques in radiotherapy and neurosurgery. This has led to declining use of WBRT and increasing surveillance imaging following local treatment. Subsequent sections discuss approach to localised therapy for patients with limited number of BM.

1.2.3 Surgical Resection

Three trials have studied WBRT alone compared with surgery and WBRT. Surgery offers advantage in reduced local recurrence, better functional independence and improved overall survival. In 1990 a single centre randomised trial demonstrated an improvement in median survival of 40 weeks in the surgical group compared with 15 weeks in WBRT group ($p<0.01$) (Patchell *et al*., 1990). This study included a total of forty-eight patients with single BM. Patients had mean age of 60 years and mean KPS of 90. Local recurrence in the surgical group was 20% compared with 52% in the WBRT group. Functional independence was measured by KPS and patients in the surgery arm maintained KPS >70 in up to 38 weeks of follow up, whereas WBRT group maintained this KPS score for only 8 weeks.

Another similar trial by with 63 patients demonstrated improved survival in the surgical group (10 months) compared with the WBRT group (6 months), $p=0.04$. However, it did not show a significant difference in functional independence in the two groups (Vecht *et al*., 1993). A further retrospective review showed similar improvements in survival following resection of 1-3 metastases compared with whole brain radiotherapy (Bindal *et al*.,

1995). Survival advantage was more significant in patients with limited or controlled systemic disease and good performance status (KPS>70).

In contrast to these studies, a Canadian multi-centre trial in 1996 comparing surgical resection followed by WBRT compared with WBRT alone showed no significant difference in OS in the two groups: 5.62 months in the surgical group vs. 6.28 months in the WBRT group (p=0.24). This study also failed to show a difference in functional independence between the two groups. (Mintz *et al*., 1996)

In summary, these studies suggest surgery reduces the risk of local recurrence for patients with a single BM. Whilst the Patchell study demonstrated a survival benefit, this was not borne out in the Cochrane review. This Cochrane review conducted by Hart *et al*., 2005 examined the effectiveness of surgical resection and WBRT versus WBRT alone in the treatment of patients with single brain metastasis. The survival analysis in this review did not show a statistically significant difference between WBRT and surgery (RR = 0.72, 95CI 0.34-1.55, p=0.4). There was also a lack of statistical significance in reducing risk of neurological death (RR 0.68 95CI 0.43-1.09, p=0.5) (Hart *et al*.) (Figure 1.4). The lack of statistical significance could be due to the small number of patients in each of the trial.

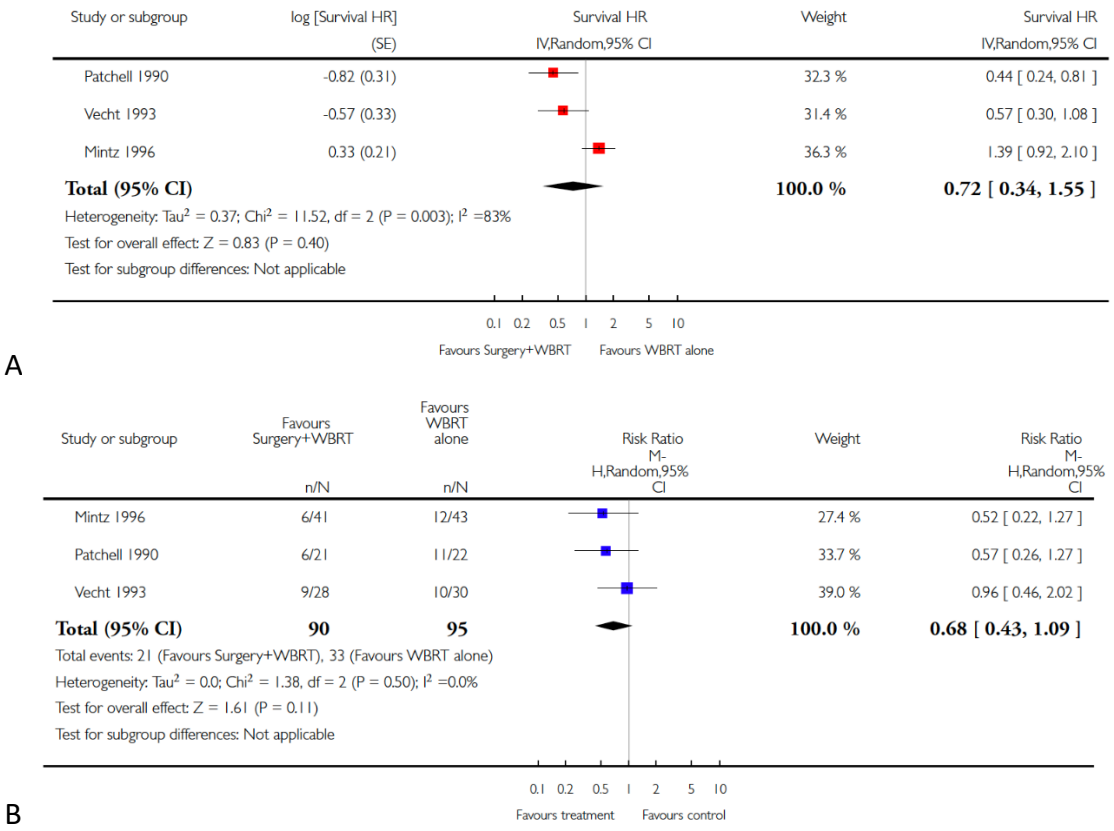

Figure 1.4 Forest plot demonstrating outcome in patients undergoing surgical resection for single brain metastases in addition to Whole Brain Radiotherapy compared with Whole Brain Radiotherapy alone. *A demonstrates Overall Survival, B demonstrates risk of neurological death (Hart et al., 2005 Cochrane Review**).***

1.2.4 Stereotactic Radiosurgery (SRS)

SRS is a highly conformal form of radiation therapy designed to deliver a high dose in a single treatment to the target volume while sparing adjacent normal tissues. Stereotactic guidance and precision immobilization ensure accurate tumour localization. When SRS was first described by Lars Leksell in the 1950s, the available imaging and radiation treatment delivery machines limited its application (Leksell, 1951). As imaging and treatment delivery systems have advanced, the utilization of SRS has increased. In collaboration with Borje Larrson, Leksell developed the first gamma knife unit, and clinical use of the gamma knife began in Sweden in 1967. Today, SRS can be delivered via three modalities: Robotic radiosurgery system, commonly known as CyberKnife, high dose gamma radiation also known as Gamma knife, or linear accelerator (LINAC).

1.2.4.1 Physics and Radiobiological Principles of SRS

SRS delivers single or a limited number of high doses to a radiographically discrete treatment volume by using multiple convergent beams. This results in a rapid fall-off of dose at the edge of the target volume and a clinically insignificant dose to adjacent normal tissue. High-energy x-rays produced by linear accelerators or gamma rays from the Gamma Knife unit are generally utilised.

The cellular processes triggered by single or a few high-dose radiation fractions are poorly understood but appear to differ from those of much smaller dose per fraction radiation schedules. DNA repair, redistribution, repopulation, and reoxygenation are less important with SRS than with fractionated radiotherapy. This is clinically illustrated by results of treating BM using either of the two methods. Where WBRT is only marginally effective for radioresistant tumours such as melanoma and renal cell carcinoma (Nieder *et al*., 1997), SRS is as effective for these tumours as it is for radiosensitive tumours such as breast and lung (Brown *et al*., 2002).

The relationship between malignant cell survival and radiotherapy dose is usually represented by the linear quadratic (LQ) model. The LQ model shows that initially there is a linear relationship between RT dose (D), surviving cell fraction (SCF) with a slope α.

$$SCF = e^{-\alpha D}$$

As the dose increases, SCF decreases more rapidly and at moderate doses SCF is dependent on dose and dose squared.

$$SCF = e^{-\alpha D - \beta D^2}$$

Tissue response to radiation is often characterised by (α/β) ratio, which is quoted to be 2-3 Gy for brain tissue and 10-15 Gy for vast majority of rapidly proliferating tumours. The concept of fractionated radiotherapy delivered consecutively over days rather than a large single fraction is to optimise the balance between tumour control and minimise late normal

tissue toxicity. Using the LQ model, biologically effective dose (BED) can be calculated for a particular (α/β) ratio, where D represents the total dose of radiation (Gy), and d is the dose per fraction (Gy).

$$BED = D\ (1 + \frac{d}{(\alpha/\beta)})$$

Consequently, BED for a tissue with low (α/β) will increase much more rapidly with high dose per fraction radiation schedule compared to those with high (α/β) tissue. However, for hypofractionated stereotactic radiosurgery or radiotherapy regimes, particularly for doses of above 10 Gy per fraction, the LQ model may not be representative of the radiobiological effect. LQ model has been well validated experimentally and theoretically up to 10 Gy and it has been perceived that it can be applied reasonably up to 18 Gy fraction size. Therefore, for doses above this, an adjusted LQ model is considered. Hypotheses exist around vascular damage effect and antigen expression stimulating the immune environment which is a different mechanism from the classical model of DNA damage. Hence, this may result in higher cell death than compared to in vitro observations (Figure 1.5).

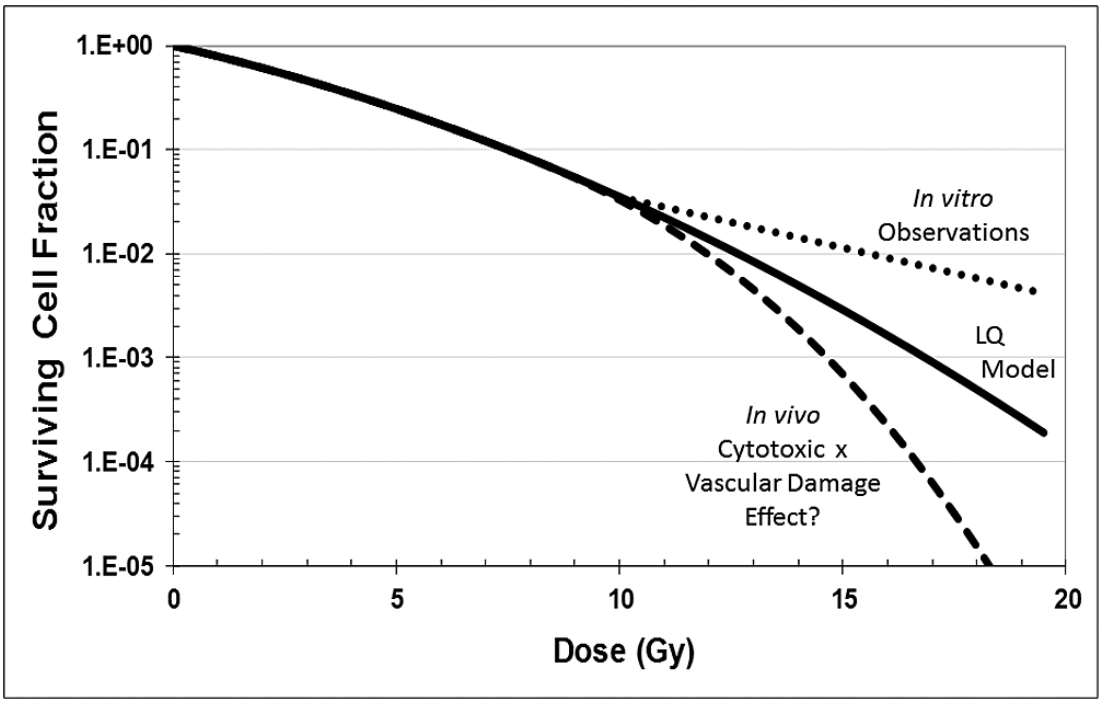

Figure 1.5 Hypothesis of surviving cell fraction when tumour cells radiation response when exposed to single dose radiation for the linear quadratic (LQ) model. *In vivo tumours and in vitro cell cultures cell surviving fraction determined by the product of direct cell kill and indirect vascular damage. (Held et al., 2006)*

BED of SRS and fractionated stereotactic radiotherapy doses used in clinical practice as applied to tumour cells and normal tissues is summarised in Table 1.5. Given the radiobiological modelling of (α/β) ratio of normal tissues, there is a discrepancy between BED of tumour tissue and normal tissue. Hence, risk of late toxicity is higher with SRS than with usual fractionation of 1.8 – 2 Gy per fraction regimens.

The current doses of SRS have been derived mainly from the RTOG 9005 study where re-irradiation with SRS was used for patients with brain tumours (primary gliomas and metastases). This study demonstrated maximum tolerable doses of single fraction SRS for patients with previously irradiated primary brain tumours and BM as 24 Gy, 18 Gy and 15 Gy for tumours <20 mm, 21-30 mm, and 31-40 mm, respectively. The maximum dose of 24 Gy was decided by the trial investigators as there was a reluctance to increase the dose to 27 Gy (Shaw *et al.*, 1996). Multivariate analysis in this cohort of patients showed that treated volumes > 8200 mm^3 was associated with unacceptable neurological toxicity (defined as grade 3 or more irreversible neurological symptoms requiring outpatient or inpatient medications e.g. corticosteroids) (Shaw *et al.*, 1996).

Total Dose of Radiation (Gy)/ Number of fractions	**BED_{15}**	**BED_{10}**	**BED_3**	**BED_2**
15/1	30	37.5	90	127.5
18/1	39.6	50.4	126	180
21/1	50.4	65.1	168	241.5
24/1	62.4	81.6	216	312
21/3	30.8	35.7	70	94.5

Table 1.5 Biologically Equivalent doses (BED) according to different α/β ratio of the tissues for different SRS dose fractionation regimen used in routine clinical practice. *All doses are in units of Gray. BED_{15} and BED_{10} represent α/β ratio of tumour tissue and BED_3 and BED_2 represent normal tissue within the brain.*

1.2.4.2 Stereotactic Radiosurgery Techniques

Precision in target localisation is a prerequisite for successful SRS treatment. Historically, this has been accomplished by the application of a stereotactic head frame using pins that attach to the outer table of the skull. The head frame placement is done with local anaesthesia, although sedation may be required. Modern Linac-based SRS systems now typically employ frameless, image-guided stereotactic systems for precision localization, which eliminates the need for skeletal fixation of the patient's head. These include the CyberKnife and the ExacTrac X-Ray systems, which avoid the need for cranial frames or fiducials. With these non-invasive systems, motion is minimized by application of an individualized frame or mask.

Both gamma rays and X-rays are photon radiation. As photons penetrate tissue, energy deposition decreases exponentially with depth below the surface and the radiation passes entirely through the tissue. Several different systems are available for photon-based SRS. The most widely used are the Gamma Knife and Linac, which have similar efficacy. This was illustrated in a multicentre clinical trial that combined SRS with WBRT for the treatment of BM; no differences were observed in either efficacy or toxicity in patients treated with the two systems (Aoyama *et al*., 2015, Brown *et al*., 2016a, Sahgal *et al*., 2015). However, subgroup analysis was not conducted to specifically look at different SRS treatment techniques.

Gamma Knife

The Gamma Knife system consists of an array of more than two hundred cobalt-60 sources surrounded by an 18,000 kg shield. The sources are oriented such that all the beams converge at a single point termed the isocentre. This array produces a target accuracy between 0.1 and 1 mm, which is at least as good as the best possible lesion delineation with current imaging technology. During treatment, the patient is positioned so that the target coincides with the isocentre of the Gamma Knife unit. Using techniques of beam blocking, multiple or overlapping isocentres, and differential isocentre weighting, the radiation volume is approximated to that of the target lesion (Figure 1.6).

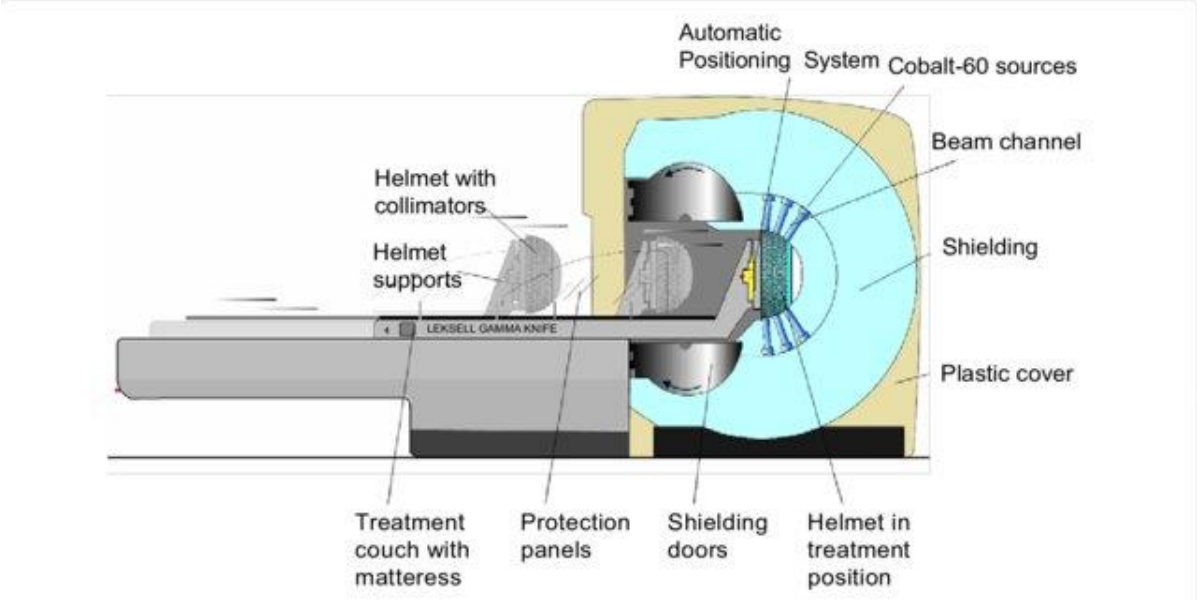

Figure 1.6 Schematic diagram of Gamma Knife. *Diagram shows the patient couch with head collimator helmet containing the beam collimation inserts for the individual Cobalt sources, all directed at a fixed point in space within the Gamma Knife. (Frederik Vernimmen, 2014)*

Linear Accelerator Based System (Linac)

The principles of a Linac are similar to those of the Gamma Knife. Instead of using an array of cobalt sources, multiple non-coplanar arcs of radiation are used that intersect at the target volume. As a result, radiation received by normal tissue in each beam path is minimal relative to the point of beam convergence. Linac-based devices also achieve target accuracy between 0.1 and 1 mm. The radiation volume is carefully matched to the lesion. The ExacTrac X-Ray system consists of two infrared cameras for patient tracking, two floor-mounted kilovolt X-ray tubes, and two ceiling-mounted detectors. X-ray images of the cranial skeletal anatomy are fused to the digital reconstructed radiographs derived from the treatment planning CT scan to facilitate patient positioning. Infrared fiducial markers attached to the patient allow precise tracking of patient's motion by the infrared camera. This information is transmitted to an integrated computer system that corrects for any motion by adjusting the position of the treatment couch prior to the radiation delivery. Target accuracy of approximately 1 mm is achieved. Prior to treatment, CT images are used to define the spatial relationship between the patient's bony anatomy and the target volume. During the actual treatment, patient movement is monitored with minimal time lag by the system's low dose X-ray cameras.

These images are compared with radiographs derived from the pre-treatment CT scan. Based upon these comparisons, the computer-controlled robotic arm adjusts the mobile linear accelerator in response to changes in patient position (Figure 1.7).

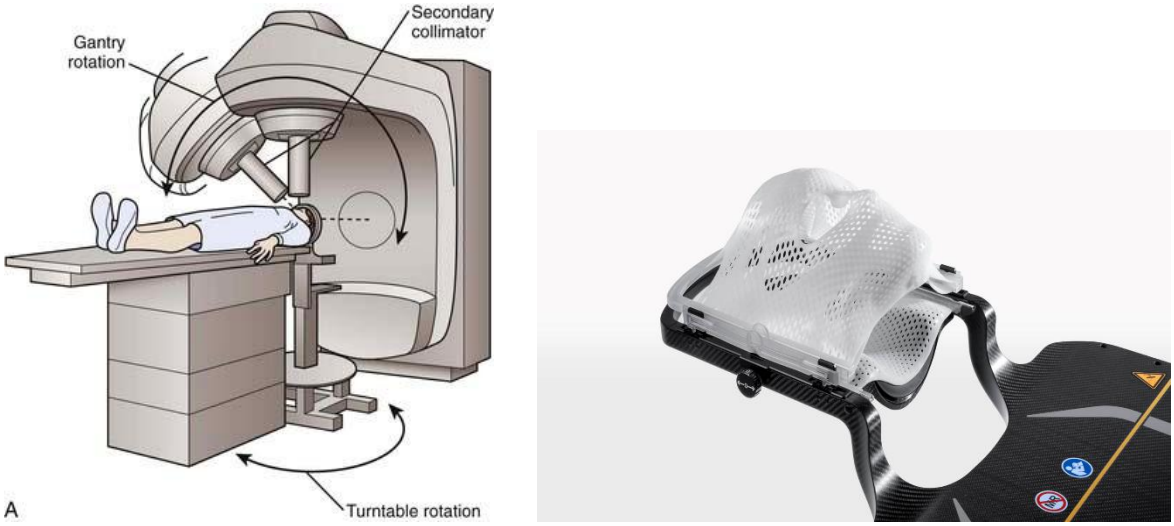

Figure 1.7 Schematic of linac isocentric set-up demonstrating patient position for radiosurgery on table extension. *Note rotation of table and gantry about isocenter. (Alexander and Loeffler, 1993 McGraw-Hill, 1993.)*

CyberKnife

The CyberKnife device combines a mobile linear accelerator with an image-guided robotic system with an x-ray imaging device capable of delivering high precision radiotherapy (Figure 1.8). The mobility of the device, combined with real-time imaging, eliminates the need for an invasive stereotactic head frame. The robotic arm allows a wide array of noncoplanar beam angles that can produce a highly conformal dose distribution, even for irregularly shaped targets.

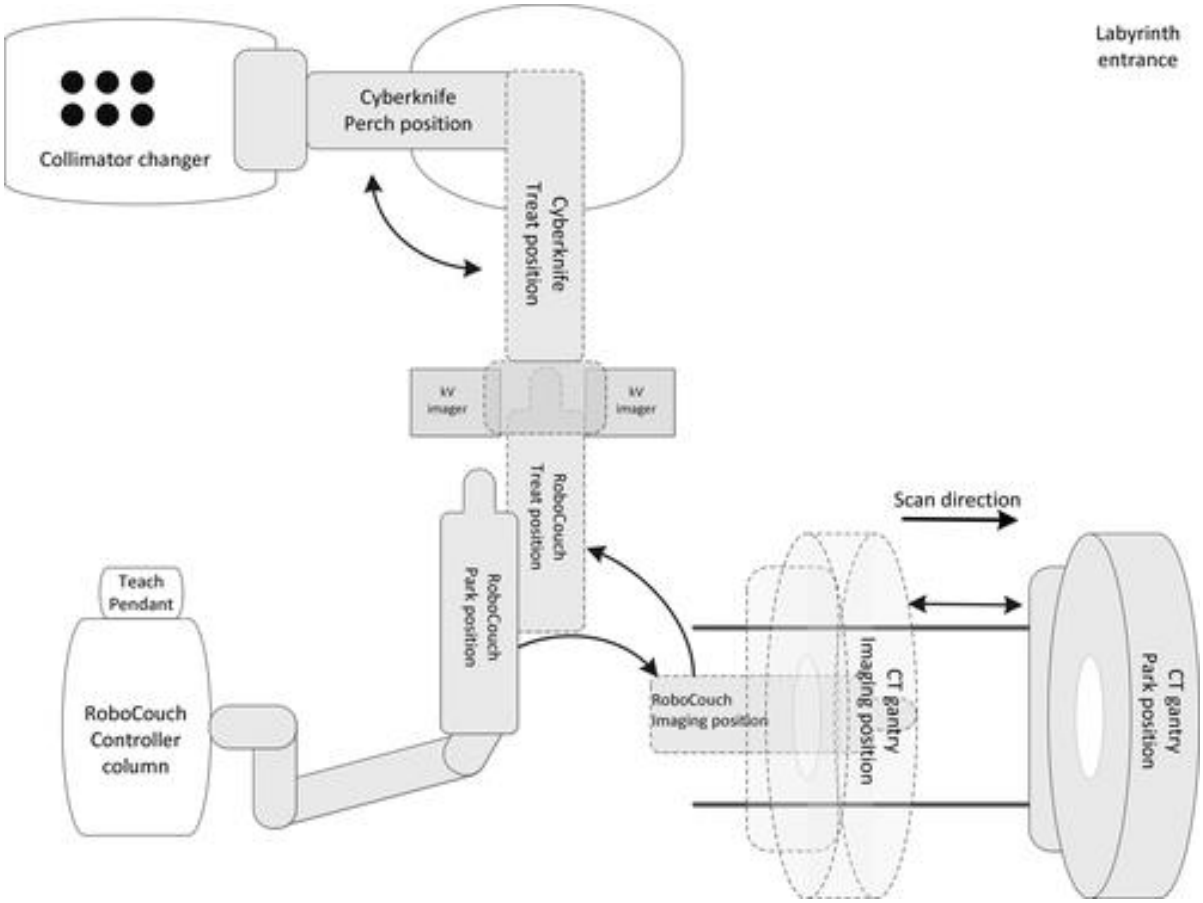

Figure 1.8 Schematic overview of the integrated CyberKnife/CT system (top view of treatment room). *Solid lines indicate the park positions of each component, while dashed lines indicate positions for imaging or treatment. The arrows indicate the motion direction of components between these positions. (Papalazarou et al., 2017)*

Tomotherapy

Tomotherapy is a form of intensity-modified RT where the radiation is delivered by a linear accelerator that rotates around the patient (Figure 1.9). Comparisons between tomotherapy and Gamma Knife or dedicated Linac SRS platforms as treatment for brain metastasis have shown that the latter platforms are superior in terms of conformal delivery and sparing of radiation to the normal brain tissue. Although this technique may provide improved tumour coverage and avoidance of OARs for BM in eloquent areas such as close to the brainstem or base of skull (Baisden *et al*., 2007). Currently, tomotherapy is not routinely used as a delivery platform for SRS.

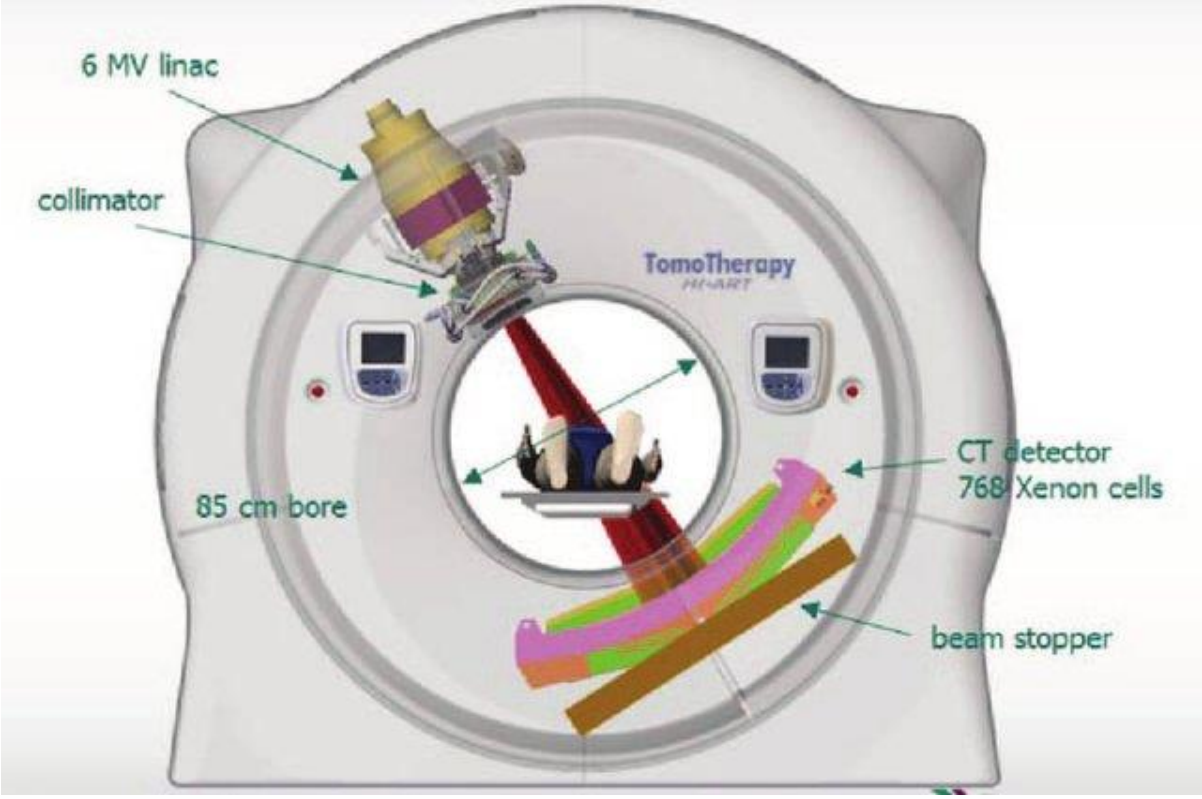

Figure 1.9 A schematic overview of the helical tomotherapy (HT) machine. *The HT machine looks and works like a spiral computed tomography scan: The patient moves into the machine while the radiation source continuously turns around the patient. (Van Gestel et al., 2013)*

1.2.4.3 Evidence for Stereotactic Radiosurgery

While initial trials supporting the efficacy and safety of SRS for up to four BM utilised WBRT in both treatment arms, subsequent trials studied SRS plus WBRT versus SRS alone in this patient group. A meta-analysis of multiple RCTs supports the use of SRS alone in the initial management of patients with a limited number of BM that are appropriate targets for SRS (i.e., <3 cm in diameter) (Sahgal *et al*., 2015). This meta-analysis included 5 RCTs including 663 patients and demonstrated that the addition of WBRT to SRS decreased the relative risk of intracranial disease progression at 1 year by 53% (RR 0.47, 95% CI 0.34-0.66) but did not improve overall survival (HR 1.11, 95% CI 0.83-1.48). These findings were further confirmed by a large RCT by Brown *et al*., 2016. In this trial, 213 patients with one to three BM (68% lung primary) were randomly assigned to SRS plus WBRT or SRS alone. Cognitive deterioration, defined as a decline >1 standard deviation from baseline in any of six cognitive tests at three months, was more likely in the WBRT plus SRS group 92% versus 64% in group

treated with SRS alone. Similar to other trials, the addition of WBRT improved intracranial tumour control rates compared with SRS alone (88% versus 65% at 6 months and 85% versus 50% at 12 months) but did not improve overall survival (HR 1.02, 95% CI 0.75-1.38). A subsequent trial in surgical patients also found worse cognitive outcomes with WBRT versus SRS and no difference in overall survival.

The lack of benefit on overall survival in these studies could be because of more effective salvage treatment options following SRS, namely, surgery, repeat SRS, or salvage WBRT or more effective systemic therapy that can cross the blood brain barrier. SRS alone in patients with limited numbers of BM with regular post-treatment MRI surveillance is now recommended over offering WBRT upfront (NICE 2018). In conclusion, the benefits from WBRT avoidance are therefore considered to be preserved NCF, and improved quality of life. This does come at the expense of increase rates of intracranial tumour relapse however, which highlights the need for routine surveillance brain imaging for all patients following treatment with SRS alone. A recent meta-analysis reports a survival advantage in young patients with good performance status treated with SRS alone vs SRS + WBRT which has again supported recommendations to not routinely add WBRT to SRS for limited BM (Sahgal *et al*., 2015) . Therefore, in patients with a limited number of BM, deferring adjunctive WBRT with close radiological surveillance is now advised for patients receiving SRS for a single brain metastasis, with the rationale of avoiding early and late side effects from WBRT. Recurrence of BM can often be treated effectively with repeat SRS, surgery or delayed WBRT (NICE, 2018).

Evidence for Post-Operative Stereotactic Radiosurgery

Patients who undergo surgical resection of a single brain metastasis have approximately 50% risk of local recurrence at the surgical site within 12 months (Patel *et al*., 2010). Postoperative WBRT reduces the risk of both local and distant failure at other sites in the brain by more than half but does not improve overall survival (Hart *et al*., 2005). SRS to the surgical cavity has become an alternative option to postoperative WBRT in patients who undergo resection of a BM and have either no other lesions or a limited number, which are all amenable to SRS. This practice is supported by observational studies as well as two RCTs

showing that postoperative SRS decreases the risk of neurocognitive decline compared with WBRT and improves local control compared with observation (Brown *et al*., 2017, Mahajan *et al*., 2017).

In the first of these RCTs, a multicentre RCT conducted by Brown *et al*., 2017 194 patients with resected BM were randomly assigned to postoperative SRS (12 to 20 Gy in a single fraction depending on cavity volume) or WBRT (30 Gy in 10 fractions or 37.5 Gy in 15 fractions). At 6 months, patients assigned to SRS had a lower risk of cognitive deterioration compared with those who were assigned to WBRT (52 versus 85 percent) and similar median overall survival (12.2 versus 11.6 months). Notably, SRS was associated with worse rates of surgical site control (80 versus 87 percent at 6 months and 61 versus 81 percent at 12 months) as well as overall intracranial control (55 versus 81 percent at 6 months) compared with WBRT (Brown *et al*., 2017). Use of salvage therapy in both arms was comparable and not statistically significant. One possible explanation for the relatively high rate of local recurrence after SRS seen in this trial is that 40 percent of cavities were wider than 3 cm and thereby received a lower single fraction dose, which may have been insufficient to control microscopic disease. Although SRS did not result in a difference in overall survival, surgical cavity SRS is an effective strategy to delay WBRT and the associated NCF impairment. (Brown *et al*., 2017)

The second RCT compared postoperative SRS (12 to 16 Gy in a single fraction) with observation in 132 patients who underwent complete resection of one to three BM. With a median follow-up of 11 months, local control rates were higher for SRS compared with observation (85% versus 66% at 6 months and 72% versus 43% at 12 months), and median overall survival was similar (17 versus 18 months). In patients treated with SRS, the most important risk factor for local recurrence was preoperative tumour diameter >2.5 cm (Mahajan *et al*., 2017). Given these mixed results at present there remains some debate about the role of post-operative SRS and, as such, its routine use is not currently recommended by NICE (NICE 2018).

Dose and fractionation of focal radiation is tailored based on factors such as size of the cavity and location. Single fraction SRS can be used for small cavities (<3 cm in diameter), whereas hypofractionated SRS may offer better local control rates for larger cavities and preoperative tumour size >2.5 cm.

1.2.5 Systemic Therapy

Historically, in patients with metastatic disease intra and extracranial disease has been treated as distinct compartments, particularly with respect to anticipated response rates with SACT. More recently, with the development of TKIs and immunotherapy in cancers, SACT drugs are now being developed that can overcome the blood brain barrier more effectively than traditional cytotoxic chemotherapeutic agents. Notably treatment for non-small cell lung cancer, melanoma, and breast cancer has evolved recently with newer systemic agents having greater ability to cross the blood brain barrier. In addition to this, BM often respond to drugs that have activity against the primary tumour. SACT can be broadly divided into three categories: cytotoxic chemotherapy, targeted therapy, and immunotherapy.

Incidence of CNS metastases in patients with breast cancer has reduced in the recent years with improved systemic therapy. Overall survival in this patient group was consistent with previously published randomised controlled trials (Brown *et al*., 2016a, Aoyama *et al*., 2015, Sahgal *et al*., 2015, Andrews *et al*., 2004). Median overall survival was higher in patients who were treated with SACT. There was a trend towards improved survival in patients treated with TKIs or immunotherapy. This may reflect favourable prognostic features, primary site, and tumour biology; however, the numbers are too small for further analysis. In a sub-group analysis of patients with melanoma having combination immunotherapy with Ipilimumab and Nivolumab, 12 month survival was reported to be 81.5% (Tawbi *et al*., 2018).

Cytotoxic Chemotherapy

Traditionally chemotherapy drugs are thought not to penetrate the blood brain barrier. However, there is a differential in intracranial response rates according to the primary

tumour. For a cancer such as small cell lung cancer, which is inherently sensitive to chemotherapy, intracranial response rates are as high as 65% as shown by a prospective real-world study conducted by Chen *et al*., 2008. In contrast to this, BM originating from non-small cell lung cancer exhibit a much lower response rate. Typically, response rate is reported to be approximately 30%

Targeted Therapy

In NSCLC, the use of targeted small molecule inhibitors has been rising with increasing recognition of genetic mutations and targeted agents. The first generation of these drugs are the epidermal growth factor receptor (EGFR) TKIs, erlotinib and gefitinib. Both agents produce a good, but short lived, intracranial response (6.6 - 11.7 months). Second generation EGFR-TKIs, such as afatinib, have been less well evaluated for treatment of BM as intracranial response was not objectively measured. A pooled analysis from LUXLUNG-3 and LUXLUNG-6 trials demonstrated improved PFS without improving OS in patients with BM undergoing treatment with afatinib versus chemotherapy (Schuler *et al*., 2016). The third generation EGFR-TKIs, e.g. Osimertinib, have been shown to have greater intracranial activity (Reungwetwattana *et al*., 2018, Goss *et al*., 2018).

In breast cancer, Lapatinib has been shown to have intracranial response rates of <10%, however, when combined with capecitabine chemotherapy, significantly higher response rates are observed, 57% objective response rate was reported with 5% complete response and 52% partial response (Bachelot *et al*., 2013).

Immune Check Point Inhibitors

Immune checkpoint inhibitors have shown intracranial activity in early clinical trials for patients with BM from melanoma and non–small cell lung cancer. Anti-programmed death ligand 1 (anti-PDL1) antibodies, e.g., nivolumab and pembrolizumab have been approved for advanced melanoma, kidney cancer, and NSCLC. Early trials of these agents excluded patients with BM. However, subsequent retrospective and prospective studies included patients with asymptomatic or controlled BM and the evidence is summarised in Table 1.6.

It has been reported that Pembrolizumab has varying intracranial control rate depending on the primary tumour, indicating inherent tumour heterogeneity in treatment response Table 1.6 (Goldberg *et al*., 2016). Moreover, combination immunotherapy may be more effective in achieving higher intracranial response rate (Long *et al*., 2018)

Mechanism of Action	Primary site	Drug	Outcomes	References
Cytotoxic Chemotherapy	Small Cell Lung Cancer	Carboplatin and Etoposide	CNS RR 65% OS 6 mo	(Chen *et al.*, 2008)
	Non-Small Cell Lung Cancer	Platinum doublet	1 year survival rate 30% PFS 3.6 mo	(Moro-Sibilot D, 2015)
EGFR TKI	Non- Small Cell Lung Cancer	Gefitinib	CNS RR 10% PFS 3 months CNS RR 88% PFS 14 mo	(Ceresoli *et al.*, 2004) (Iuchi *et al.*, 2013)
		Erlotinib	CNS RR 86% PFS 11.8 mo	(Koizumi *et al.*, 2013)
		Afatinib	CNS RR 60-80%; PFS 8.2 mo	(Schuler *et al.*, 2016)
		Osimertinib	CNS RR 91% Median PFS 15.2 Months	(Reungwetwattana *et al.*, 2018)
	Breast Cancer	Lapatinib and Capecitabine	CNS RR 65.9% Median OS 17 months	(Bachelot *et al.*, 2013)
ALK TKI	Non-Small Cell Lung Cancer	Crizotinib	CNS RR 15-39%, Median PFS 9 months	(Solomon *et al.*, 2014)
		Alectinib	CNS RR 64-81%,	(Hida *et al.*, 2017)
T-DM1 inhibitor	HER positive breast cancer	Ado-trastuzumab	CNS Progression - 22%, PFS 9 mo, OS 26.8 mo	(Verma *et al.*, 2012)
BRAF and MEK TKI	Melanoma	Dabrafenib and Trametinib	CNS RR 44-59%,	(Davies *et al.*, 2017)
Immune check point inhibitors	Small Cell Lung Cancer	Atezolizumab	CNS RR Not measured	(Horn *et al.*, 2018)
	Non-Small Cell Lung Cancer	Pembrolizumab	CNS RR 33%	(Goldberg *et al.*, 2016)
		Nivolumab	39%; median OS 8.6 mo	(Crinò *et al.*, 2019)
	Melanoma	Ipilimumab	CNS disease control 10-24%. Median OS 7 months	(Margolin *et al.*, 2012)
		Pembrolizumab	CNS RR 22%	(Goldberg *et al.*, 2016)
		Nivolumab	CNS RR 20%	(Long *et al.*, 2018)

Table 1.6 Summary of systemic anticancer therapy agents that are effective in brain metastases. *CNS: central nervous system, ALK: Anaplastic lymphoma kinase, BRAF: v-raf murine sarcoma viral oncogene homolog B1 , EGFR: epidermal growth factor receptor, HER-2: human epidermal growth factor receptor-2, MEK: mitogen-activated protein kinase, mo: Months, OS: overall survival, PFS: progression free survival, RR: response rate, T-DM1: transtuzumab emtansine, TKI: tyrosine kinase inhibitor.*

1.2.6 Toxicities of different treatment modalities

The major risks associated with surgical resection include postoperative neurologic worsening, infection, intracranial haemorrhage, and perioperative stroke. Nevertheless, hospitalization time tends to be relatively short (less than 5 days), and one-month neurological outcomes are either stable or improved in approximately 90 percent of patients. The risk of permanent paresis with surgery is estimated to be approximately 8 to 9%. Risk factors for postoperative weakness in one study included preoperative chemotherapy or radiation therapy and RPA class II. There are cerebral regions where surgical resection is associated with high risk of mortality, such as the brain stem. Therefore, most surgical series include patients with BM that are surgically accessible and not in an eloquent area such as the primary motor strip.

Acute neurological symptoms from SRS may be due to transient swelling that begins 12 to 48 hours after therapy. Symptoms can include mild nausea, dizziness or vertigo, seizures, or new headache. A short course of corticosteroids around the time of radiosurgery is usually administered to minimize acute SRS-related toxicity. Long term toxicities following radiation includes radionecrosis and NCF impairment. Radiation necrosis occurs in approximately 10 percent of treated tumours anywhere from six months to several years after treatment. Reported rates of radiation necrosis after postoperative SRS range from 4 to 18 percent. The two most important risk factors for radiation necrosis in patients with BM are prior radiation (either SRS or WBRT) to the same lesion and size of the lesion (with larger tumour volumes associated with higher risk). For tumours treated with prior SRS, the risk of symptomatic adverse radiation effects may be as high as 20 percent within 12 months of retreatment. Use of hypofractionated rather than single fraction SRS for tumours >2.5 cm may decrease the risk of radiation necrosis.

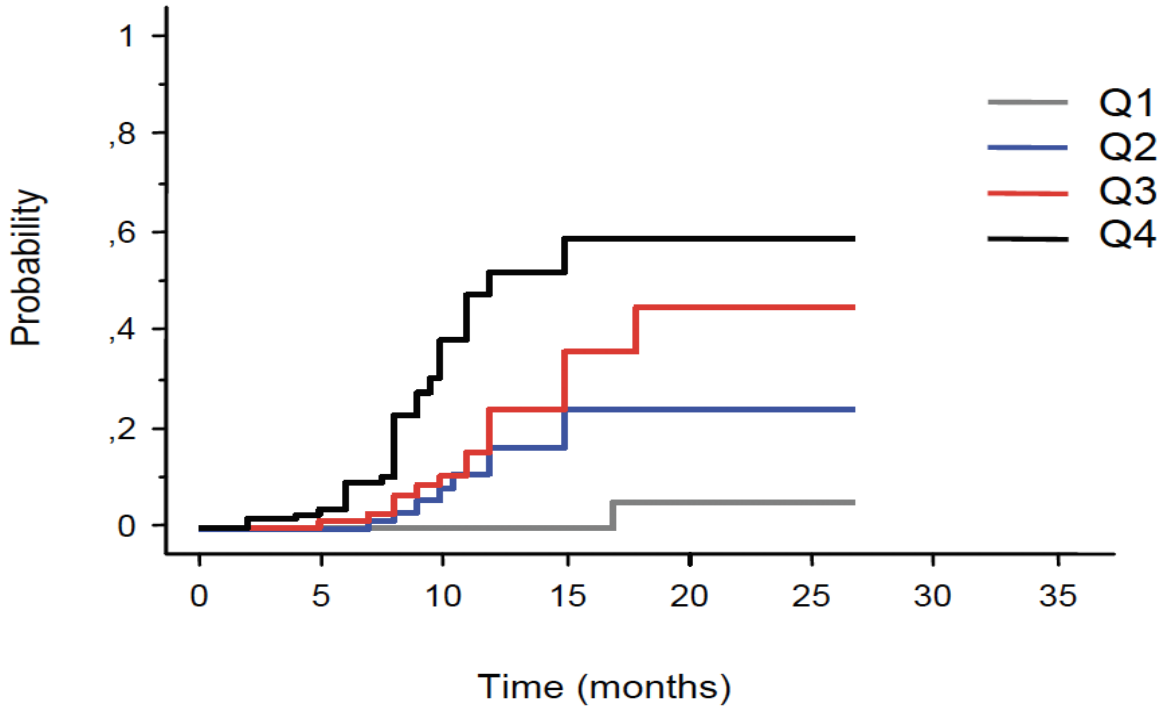

Figure 1.10 Risk of brain radionecrosis after stereotactic radiosurgery for brain metastases in relation to the brain volume receiving 12 Gy (V12 Gy) stratified into four quartiles. *The risk increased significantly as the volume receiving 12 Gy increased. Q1 - V12Gy <3.3 cm^3, Q2 - V12Gy 3.3-5.9 cm^3, Q3 – V12Gy 6-10.9 cm^3, Q4 – V12Gy >10.9 cm^3 (Minniti et al., 2011)*

Targeted therapy and immunotherapy may also increase the risk of radiation necrosis. Most of the evidence consists of case series and retrospective studies, and the role, if any, of sequence and timing of therapy in relation to SRS is not well understood. In a retrospective study of 180 patients who underwent SRS for BM over a six-year period, twenty two percent developed treatment-related imaging changes or biopsy-proven necrosis. The median time to necrosis was 9.5 months after SRS (Colaco *et al.,* 2016). The risk was higher in patients receiving immunotherapy (38%) or targeted therapy (25%) compared with cytotoxic chemotherapy (17%) (Colaco *et al.,* 2016). A larger observational study found that the risk of radiation necrosis after SRS was 2.5-fold higher in patients who had received immunotherapy. Patients undergoing immunotherapy treatment live longer and higher rate of radionecrosis could be due to longer follow up as it is considered to be a late toxicity. Patients with radiation necrosis may be asymptomatic or present with focal neurological signs and symptoms related to cerebral oedema. Imaging typically shows increased enhancement at the site of prior SRS accompanied by surrounding oedema. Treatment is largely symptomatic with corticosteroids. Resection may be required for resistant symptoms.

The long-term effects of SRS on NCF have not been well studied, but the available data are reassuring. Radiologically, periventricular, and subcortical white matter changes can accumulate in patients treated with SRS alone, although at a lower rate than is seen after WBRT. Additional risk factors for NCF impairment included higher number of treated tumours and higher integral SRS dose to the skull. The clinical significance of these changes is not yet known. RCTs studying effects of WBRT have shown that a considerable proportion of patients undergoing SRS alone may substantial NCF impairment. A recent RCT conducted by Brown *et al*., 2016 showed that up to 60% of patients can develop NCF impairment following SRS alone.

1.2.7 Choosing a treatment modality

Important factors to consider in choosing treatment modality for patients with BM are tumour size, location, number of metastases, degree of mass effect and oedema, presence, or absence of neurological symptoms, raised intracranial pressure (ICP), functional status, presence, extent and control of systemic disease, patient's preference, type of primary tumour and expected prognosis from primary tumour.

In most patients with a high intracranial tumour burden, including those with multiple, large BM, WBRT remains the standard approach to initial treatment. Initial systemic therapy with deferred radiation and close brain surveillance is increasingly an alternative to initial radiation therapy in carefully selected patients, especially those with melanoma and NSCLC with a targetable genetic mutation. The main goal of WBRT in patients with a good performance status who are not eligible for SRS or surgery is to improve neurological symptoms caused by the metastases and surrounding oedema. In RCTs composed primarily of patients with NSCLC and breast cancer, the median OS in patients treated with WBRT ranges from four to six months.

Aggressive treatment for BM in patients with a poor prognosis or poor performance status generally is not warranted. For most of these patients, overall survival is more likely to be determined by the activity and extent of extracranial disease than by the success of

treatment in controlling BM. WBRT has traditionally been the preferred approach if active treatment is indicated. Although WBRT is thought to improve survival by some months compared with use of corticosteroids based on observational studies, RCTs that directly compared WBRT with supportive care alone in patients with a poor prognosis are scarce. QUARTZ trial is the largest RCT which has looked at WBRT compared to supportive care in patients with NSCLC and it showed that patients who had WBRT lived on average 9.2 weeks compared to 8.5 weeks with supportive care (Mulvenna *et al*., 2016). Neider *et al*., analysed 113 patients who received supportive care or WBRT retrospectively. This group reported median overall survival of 2 months in the whole cohort. Patients who received WBRT lived for 15 days longer than patients who received supportive care alone, median overall survival was 2.2 and 1.7 months respectively (Nieder *et al*., 2013).

Based on the evidence from multiple RCTs demonstrating survival benefit of SRS, NICE recommends SRS for patients with overall BM volume <20 cc, with World Health Organisation Performance Status (WHO PS) of 2 or better, have controlled or controllable extra cranial disease and expected prognosis of longer than 6 months (NICE, 2018).

For patients with a single, surgically accessible BM that is large or associated with significant oedema, symptoms of raised ICP and mass effect, surgical resection achieves rapid symptom relief and local control. In carefully selected patients, resection has been shown to improve survival and decrease the risk of neurologic death compared with a radiation-alone approach. Surgery, or stereotactic biopsy for poorly accessible tumours, is also favoured for single lesions when there is uncertainty regarding the histologic diagnosis. For such lesions that are surgically inaccessible, stereotactic biopsy may be indicated to guide further therapy.

Advances in neurosurgery have significantly improved the safety of surgical resection of BM, making this approach applicable to a larger number of patients, including lesions in both eloquent and non-eloquent regions of the brain. Patients with absent extra cranial disease, better performance status (KPS >70) and younger age benefit the most from surgery as discussed in section 1.2.3.

SRS is a good alternative to surgery or WBRT for small BM. Neurotoxicity and local failure after SRS increase with increasing lesion size, and thus consideration of SRS rather than surgery should generally be limited to lesions with a diameter of 3 cm or less. For patients with single BM who are equally appropriate candidates for surgery and SRS, the choice should be individualized. No adequately powered randomized trials have been completed comparing SRS alone with surgery plus postoperative radiation.

1.3 Effect of radiation on neurocognitive function

Decline in NCF and quality of life (QoL) has been demonstrated in patients undergoing WBRT for BM with and without SRS with 90% of patients showing signs of decline in NCF scores and QoL (Li *et al*., 2008, Brown *et al*., 2016a, Chang *et al*., 2009). Thus, in patients with BM undergoing WBRT, hippocampal sparing radiotherapy techniques have been devised in order to maintain NCF post radiation. In a multicentre phase II study sponsored by RTOG, 113 patients with BM from a non-haematological cancer, other than small cell lung cancer, were treated with hippocampal-avoidance WBRT delivered to a dose of 30 Gy in 10 fractions. Patients with metastases within 5 mm of the hippocampus were excluded. The primary endpoint was decline in the Hopkin's verbal learning test – delayed recall (HVLT-R DR) at four months compared with baseline at the start of WBRT. The median overall survival was 6.8 months. In 42 evaluable patients, the mean relative decline in HVLT-R DR from baseline to four months was 7% (95% CI -4.7 to 18.7%). The probability of HVLT-R total recall (HVLT-R DR) deterioration at four months was 19%. This was favourable compared with a previous RCT of WBRT with or without SRS, in which the probability of HVLT-R TR deterioration at four months was 24% in those treated with SRS alone and 52% in those treated with WBRT plus SRS. Risk of progression in the hippocampal avoidance area was 4.5%. Although these findings are encouraging, they represent results of a single-arm trial, with all the limitations of a historic comparison. In particular, median OS in the trial was superior to prior trials, making it difficult to exclude improved survivorship as an explanation for the apparent improvement in NCF.

Based on these findings, HIPPO trial has been designed, which has closed to recruitment and results are awaited. The HIPPO trial is a UK randomised Phase II trial of hippocampal sparing vs conventional WBRT after surgical resection or radiosurgery in patients with favourable prognosis with 1–4 BM (Megias *et al*., 2017).

In patients with primary brain tumours, a study conducted by Gondi *et al*., 2012 showed that 40% of the bilateral hippocampi receiving > 7.3 Gy was associated with impairment in the Wechsler Memory Scale -III Word List and delayed recall. This was a small study which analysed the results of 18 patients and 6 controls who completed the 18-month NCF assessments (Gondi *et al*., 2012). Understanding of dose tolerance of the hippocampus is limited in patients undergoing either fractionated RT or SRS. Moreover, radiobiological effects of single high dose of radiation may differ from fractionated RT (Brown *et al*., 2014).

Despite the precision of SRS treatments, rate of NCF impairment in this patient cohort is not trivial. Recent RCTs have reported up to 60% of patients having NCF impairment following SRS alone (Brown *et al*., 2016a). With increasing incidence of BM, improved imaging techniques able to identify smaller lesions, greater effectiveness of systemic therapy, and patients with metastatic disease living longer, there is a great need to preserve quality of life and reduce the risk of NCF impairment in these patients. SRS is an alternative treatment to WBRT which, largely fulfils these requirements and indications for SRS are widening since publication of the NICE guidance in 2018 which removed the number of metastases as being a barrier. Instead, the advice is that overall volume of BM should be considered when treating with SRS.

Pharmacological measures, such as memantine, have been investigated in patients undergoing WBRT as a radioprotective agent. In a double blinded placebo controlled RCT, 508 patients with BM were randomised between WBRT and memantine vs WBRT and placebo. This study did not demonstrate a statistically significant difference in NCF impairment at 24 weeks between the two groups (Brown *et al*., 2013).

1.3.1 Anatomical Structures Implicated in NCF Impairment Post Radiation

There is increasing awareness from cancer and non-cancerous studies that several cortical and sub-cortical structures play a vital role in maintaining NCF. Among these the key structures that have been studied in some detail are the medial temporal lobe, the hippocampus, pre-frontal cortex and white matter tracts. Figure 1.11 demonstrates organisation of major cortical and subcortical structures involved in NCF.

The hippocampus is a paired sub-cortical brain structure located in the medial temporal lobes medial to the temporal horn of the lateral ventricle. The hippocampus is composed of the dentate gyrus and the cornu ammonis regions and forms an integral part of the limbic system. Its main purpose is formation of new memories, consolidation and retrieval of information and learning. Bilateral and unilateral radiation injury to the hippocampus is known to alter memory formation.

Mitotically active neural stem cells are in two different parts of the brain, namely subventricular zone, and the subgranular zone of the dentate gyrus. The granular layer of the hippocampus is formed by NSCs (neural stem cells) migrating into the hippocampus from the dentate gyrus. NSCs are capable of self-renewal and differentiating into different cell types, thus exhibiting typical features of stem cells. In QUANTEC analysis, the α/β value of the normal brain is taken to be 2.9 (Emami, 2013). For the hippocampus, mostly the α/β value used in studies ranges from 2 to 3. However, another school of thought is that the α/β value for NSCs compartment is closer to ten which is a general value established for all stem cells. Some authors use α/β value of 10 for the true hippocampus and α/β value of 2 for the whole hippocampus planning-at-risk volume illustrating the lack of consensus regarding the optimal model of radiation sensitivity.

Radiation effect on neurogenesis via NSCs in the hippocampus has been implicated following WBRT. Particular attention has been given to long-term NCF effects of radiation; however, recent studies show that altered NCF may occur much earlier following radiation leading to

long-term changes. Pathophysiological understanding of neurocognitive decline following radiotherapy is also limited although different hypotheses exist including vascular injury, white matter injury, loss of brain plasticity and functional network disruption. To understand these aspects, there is a need for advanced imaging in patients undergoing radiation.

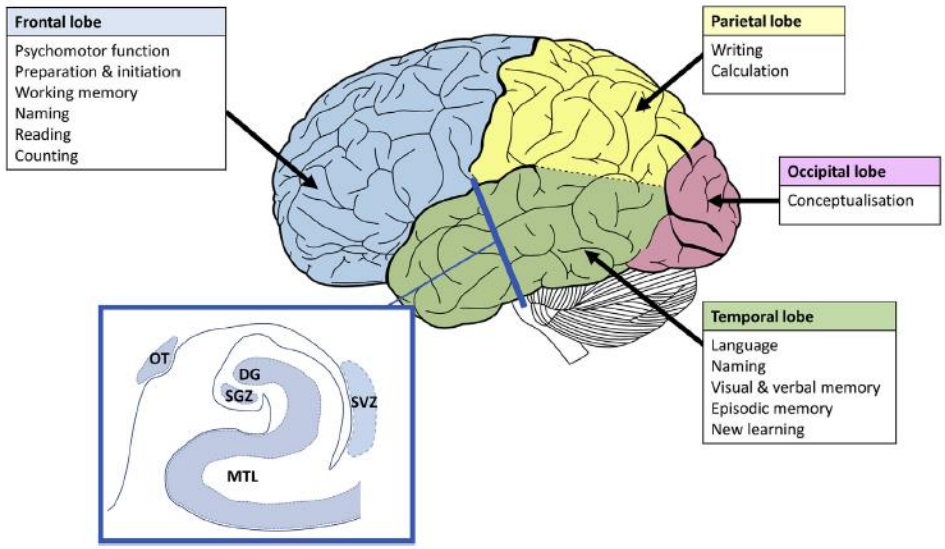

Figure 1.11 Organisation of major cognitive structures in the central nervous system. *The coronal section shows the location of neural stem cells where neurogenesis takes place. The hippocampus lies in the medial temporal lobe (MTL). Neurogenesis occurs within the subgranular zone (SGZ) of the dentate gyrus (DG) and just below the floor of the lateral ventricle in the subventricular zone (SVZ). OT represent the optic tracts (Pinkham et al., 2015)*

The pre-frontal cortex (PFC) plays a key role in executive functioning, information processing speed and sustaining attention. The latter two processes rely on a complex frontal-subcortical network involving both the white matter tracts and the cortical structures. There is evidence from animal studies of white matter degeneration, necrosis, and multifocal cerebrovascular injury consisting of perivascular oedema, abnormal angiogenesis and perivascular extracellular matrix deposition following WBRT in pre-frontal cortex and temporal lobes (Andrews *et al*., 2017). A prospective clinical trial in patients with primary brain tumour demonstrated association between executive functioning and changes in the white matter tracts of the PFC (Tringale *et al*., 2019). On the contrary, a radiotherapy dosimetric study of hippocampus and pre-frontal cortex in patients undergoing pituitary radiotherapy failed to illustrate a dose response relationship with NCF impairment. However,

this was a small study where patients were divided into four groups, hence statistical power was low (Brummelman *et al*., 2012)

White matter tracts form a complex network of neurons connecting cortical, subcortical, and cotico-cortical structures. Of these, the hippocampal white matter tracts have been studied most widely in other conditions affecting NCF, e.g., Alzheimer's dementia, schizophrenia, disorders of memory, and aging. Thus, there is increased awareness that the hippocampus alone being responsible for NCF impairment is a simplistic view. There is evidence of animal studies (Bracht *et al*., 2016), human autopsy studies (Lengyel *et al*., 2003, Vigliani *et al*., 1999) and MRI studies (Connor *et al*., 2016 *et al*., 2004, Burhan *et al*., 2013) that white matter tracts show pathophysiological changes following radiotherapy. Pathogenesis of these, will be discuss in section 1.3.3.

1.3.2 Time Course of NCF Impairment

NCF impairment following brain radiotherapy can follow a biphasic pattern. Acute effects of radiotherapy occur within days to weeks of treatment and present with symptoms such as fatigue, nausea, and vomiting. Early delayed effects on NCF can become apparent between 1 to 6 months after radiotherapy and often manifest as somnolence with a degree of resolution over time. Late effects of radiotherapy are observed 6 months or longer after radiotherapy, are irreversible, progressive, and manifest as changes in memory and executive functions. Thus late effects of radiotherapy is of greater relevance, particularly in patients with BM who have a typical reported median overall survival of around 12 -15 months in clinical trials (Brown *et al*., 2016a).Figure 1.12 illustrates the time course of NCF impairment following radiotherapy along with underlying pathophysiological signs that may be causing the relevant effects.

Tumour progression can also have an adverse impact on NCF and can be a confounding factor in studies of patients with BM and primary brain tumours. In treatment of patients with BM there is a trade-off between achieving optimum intracranial control and risk of NCF impairment. As discussed previously in section 1.2.4.3, several RCTs have demonstrated

improved intracranial control with the addition of WBRT to SRS, but without a survival benefit and with worsening NCF therefore routine use of WBRT is no longer recommended.

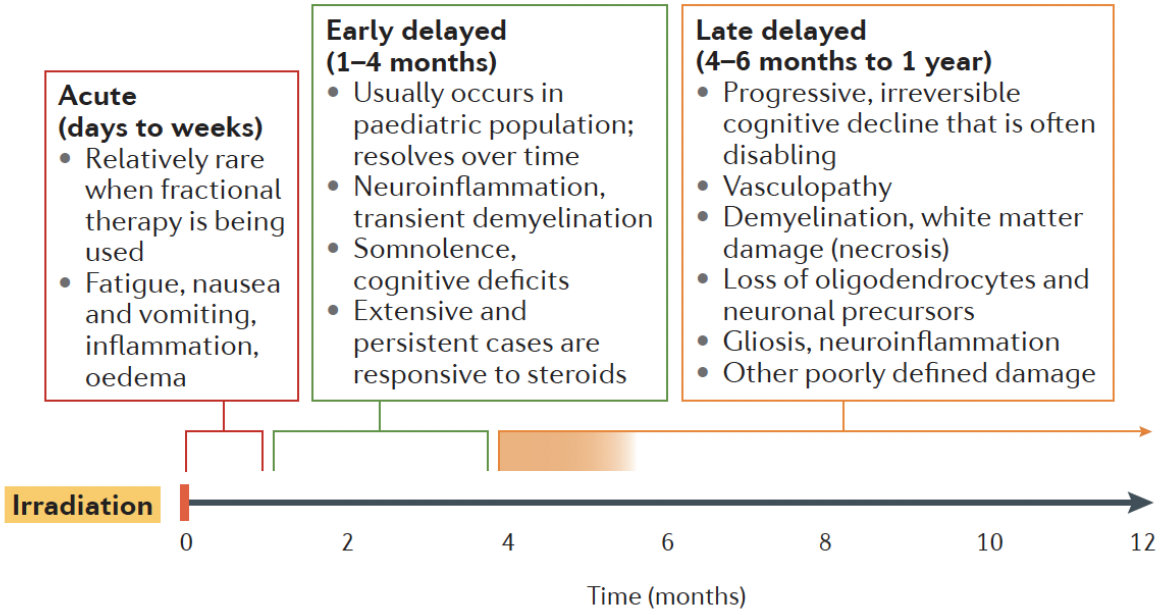

Figure 1.12 Symptoms and Pathological Manifestations of Radiotherapy Induced CNS Injury and NCF Impairment (*Makale et al., 2017)*

1.3.3 Pathogenesis of NCF Impairment Following Radiotherapy

Radiation injury can affect some or all the structures and pathways described in section 1.3.1, and is multi-factorial and complex. Pathogenesis of NCF impairment can be characterized by vascular abnormalities, inflammation, parenchymal damage, and myelopathy (Makale *et al*., 2017). Vascular damage and neuro-inflammation are often characterized as early changes that can occur after radiotherapy subsequently leading to metabolic changes, neuronal loss, and white matter necrosis (

Figure 1.13).

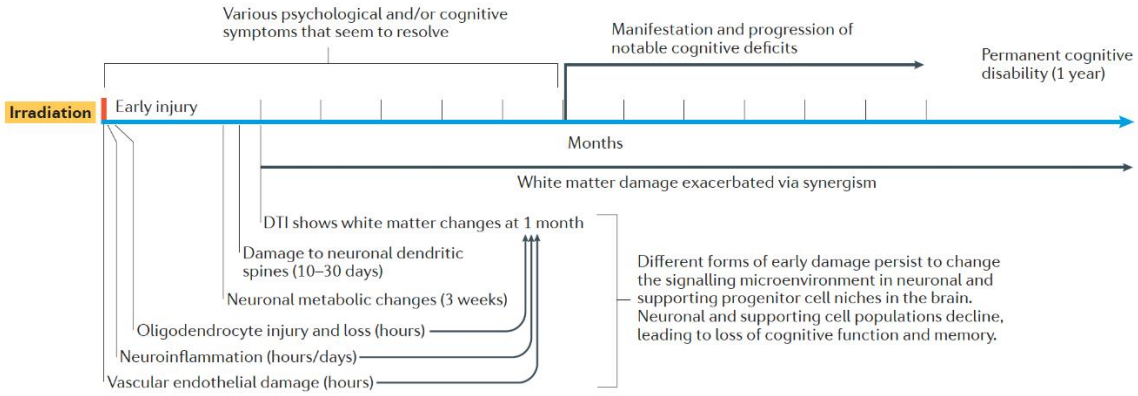

Figure 1.13 Mechanisms of early CNS injury in patients with brain tumours receiving radiotherapy. A schematic demonstration of mechanisms and interaction that underlie permanent NCF impairment. *(Makale et al., 2017)*

Vascular Hypothesis

Micro and macro-vascular sequelae of endothelial disruption can occur months to years after radiotherapy. Endothelial damage can occur months to years after radiotherapy and pathologically can present as microvascular dilatation and vessel wall thickening. Vascular sequelae can lead to poor perfusion of brain tissue, cause ischaemic stroke, secondary demyelination, and necrosis. Multiple animal studies have illustrated vascular structural changes following exposure to radiotherapy. Another animal study has illustrated presence of tissue hypoxia in the hippocampus following WBRT (Warrington *et al*., 2011). However, radiation induced necrosis has also been reported without vascular changes indicating that vascular damage is not solely responsible for effects of radiotherapy (Figure 1.14).

Inflammation

Astrocytes and microglial cells respond to radiotherapy by secreting factors that induce inflammation that can alter cell differentiation. Pro-inflammatory cytokines, e.g., interleukin (IL)-1β, tumour necrosis factor (TNF), IL-6 and IL-18 and inflammatory markers such as glial fibrillary acidic protein (GFAP), intercellular adhesion molecule-1 and NF-κB have been measured in specific regions of the brain following radiation exposure.

Examination of markers of neurogenesis and inflammation in the human hippocampus after intracranial radiation treatment for leukaemia and medulloblastoma showed increased expression consistent with inflammation, with virtually complete inhibition of neurogenesis (Monje *et al*., 2007). Inflammation in the hippocampal microenvironment causes microvascular damage, which also results in the release of signalling molecules, thereby changing the progenitor cell microenvironment in a way that suppresses differentiation to the neuronal phenotype. The levels of vascular endothelial growth factor in the hippocampus have been shown to affect hippocampal angiogenesis and neurogenesis, and to modulate hippocampal plasticity of mature neurons, thus vascular damage, and inflammation both contribute to late sequelae of radiotherapy.

Parenchymal Damage

Oligodendrocytes and astrocytes are two types of glial cells in the central nervous system. Oligodendrocytes are the glial cells that synthesise myelin sheath, provide axonal metabolic support and contribute to neuroplasticity. Astrocytes are the most abundant glial cells in the CNS and play essential functions in blood brain barrier maintenance, neuronal survival, synapse formation, strength, and turnover. This raises the possibility that radiotherapy affects may be more profound on the reproductive capacity of oligodendrocytes type-2 astrocytes progenitor cells which leads to demyelination and white matter necrosis. In animal studies oligodendrocyte cell depletion has been reported within 24 hours of radiotherapy in doses as low as 3 Gy (Figure 1.14). Although, it would be expected for acute damage such as this to recover, it is also consistent with late radiotherapy damage, therefore, the relationship between acute and late radiotherapy effects remains unclear.

Radiotherapy leads to gliosis by activating astrocytes proliferation and formation of scar tissue. Characteristic features of gliosis include hypertrophy of astrocytic processes, upregulation of intermediate filaments, and increased expression of GFA. A single dose of 15 Gy radiation to the rat brain has been reported to increase the levels of inflammatory markers in astrocytes at 30 minutes and GFAP levels at 6 hours, with a further increase at 24 hours. These changes have also been illustrated in the late phase of radiotherapy effects.

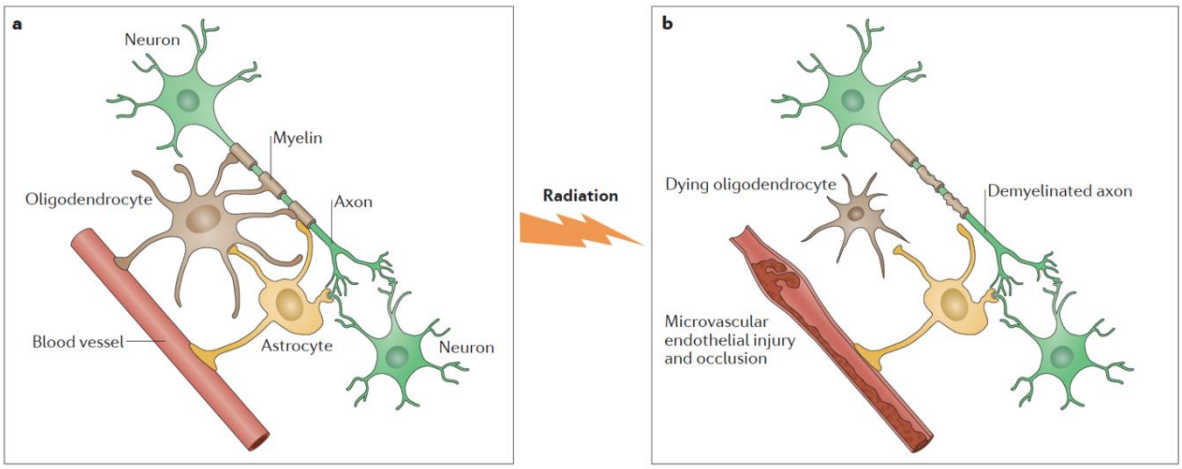

Figure 1.14 Vascular Damage and oligodendrocyte depletion underlying radiotherapy-induced white matter damage. *a - In the healthy brain, white matter provides essential connectivity for cortical and sub-cortical functions. Oligodendrocytes produce and maintain myelin around the axons. b - Radiotherapy-induced loss of oligodendrocytes results in a loss of myelin integrity. In addition, damage to the feeding microvessels not only compromises white matter but also has adverse effects on the perfusion of other key CNS elements, such as astrocytes, which provide metabolic and functional support to neurons. (Makale et al., 2017)*

Neurogenesis

NCF impairment following radiotherapy thought to derive from damage to differentiated neural cells, altered neurogenesis, and the resulting loss of hippocampal plasticity. Human NSCs transplantation has been reported to attenuate radiation-induced cognitive dysfunction in head-irradiated mice (Acharya *et al*., 2011). The hippocampus, entorhinal cortex, perirhinal cortex, and parahippocampal cortex are particularly sensitive to vascular injury, and radiation has been hypothesized to cause vascular rarefaction in the hippocampus and cognitive dysfunction that is reversible with hypoxia (Ashpole *et al*., 2014).

This theory gains interest of the radiobiological models as NSCs are thought to be inherently sensitive to radiotherapy as discussed in section 1.3.1. Pre-clinical models suggest doses as low as 2 Gy result in apoptosis of the NSCs indicating that NCF impairment can manifest at low doses (Acharya *et al*., 2010).

1.4 Structural and functional imaging modalities in neurocognitive impairment

Imaging is key to identifying and recording CNS damage in patients undergoing radiotherapy. Structural and functional changes to grey and white matter in the frontal lobe, temporal lobe and the hippocampus have been linked to NCF impairment in patients undergoing radiotherapy. Modern imaging, particularly with MRI, can provide intricate details of changes to structure by detailed structural MRI, perfusion by measuring cerebral blood flow, diffusion measures of white matter tracts by diffusion tensor imaging (DTI), and metabolic changes by MR spectroscopy (MRS). However, it remains a clinical challenge to differentiate between effects of radiotherapy and tumour progression.

1.4.1 Basics of Magnetic Resonance Imaging

Hydrogen is the most abundant atom found in the human body as 80% of it is composed of water. It is found in the form of water molecules which are arranged as one oxygen and two hydrogen atoms (H_20). Each hydrogen atom contains a nucleus and orbiting electrons, and MRI fundamentally relies on the spinning motion of hydrogen nuclei in the human body. In addition to protons being found in water, they are also present in lipid and other molecules which also contribute to the signal. In the absence of an applied magnetic field, the nuclei are randomly orientated. When placed in a strong static external magnetic field, nuclei of atoms act like tiny dipolar magnets that align parallel to (termed as spin-up nuclei) or against (termed as spin-down nuclei) the magnetic field (B_0) depending on their energy state as demonstrated in Figure 1.15.

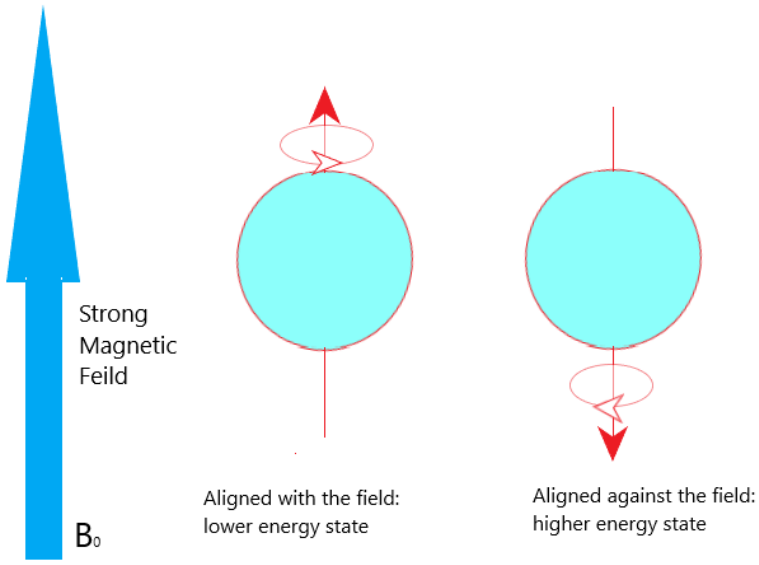

Figure 1.15 Schematic presentation of production of net magnetization of protons when a strong magnetic field (B_0) is applied.

B_0 field produces an additional motion of the hydrogen magnets around B_0 in a circular path, known as the precession. In this model, most nuclei are spin up with a smaller number of spin-down nuclei. The precessional frequency is demonstrated by Larmor equation which stipulates that precessional frequency directly proportional to the magnetic field strength, which is 128MHz at 3 Tesla.

$$\omega_0 = \gamma B_0$$

When radiofrequency (RF) coil is utilised to emit a RF pulse at the same frequency as precessional frequency. The application of this RF pulse leads to an increase in the number of high energy spins due to resonance. When resonance occurs, the net magnetization vector (NMV) moves out of alignment with B_0 into the transverse plane. This is called the B_1 field, orientated in a direction perpendicular to and rotating about B_0 field. The magnitude of B_1 is approximately 10^{-5} B_0.

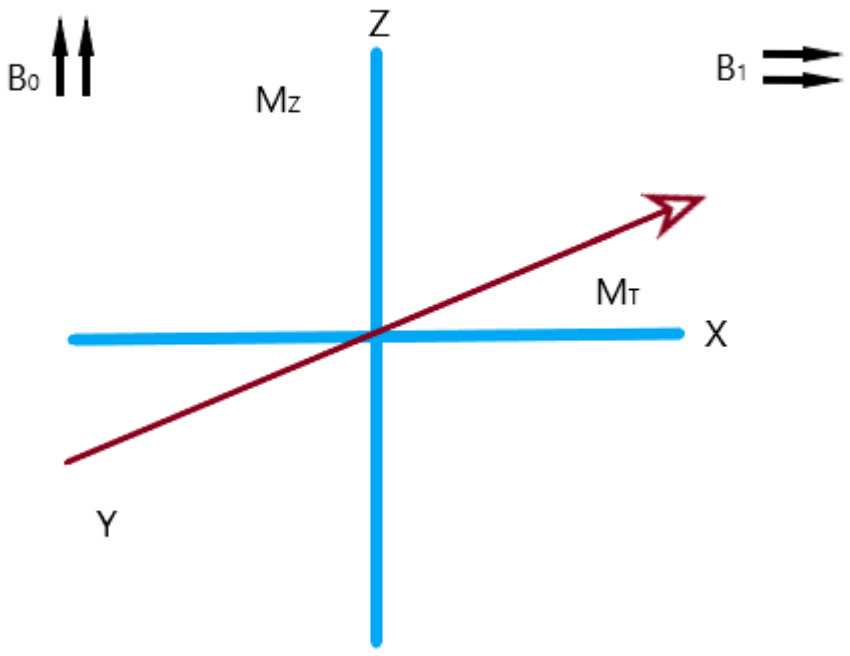

Figure 1.16 Schematic presentation of the net magnetisation vector (NMV). M_Z: longitudinal magnetisation, M_T: transverse magnetisation

Transverse magnetisation (M_T) is produced by the net magnetic movement of hydrogen and represents the balance between high and low energy nuclei. The NMV moving into B1 is caused by low energy spins joining the high-energy population. The NMV then lies at an angle to B_0 rather than parallel as it did before the RF pulse was applied to excite the tissue. This angle is referred to as the flip angle and its magnitude is dependent on the RF pulse amplitude and duration. Flip angle determines the signal intensity and image contrast. The transverse magnetisation is dictated by the x and y direction and rotates around the z axis. A spin echo (is produced by pairs of RF pulses, whereas a gradient echo is produced by a single RF pulse in conjunction with a gradient reversal.

When the RF pulse is switched off, relaxation occurs where the NMV realigns with B0 as the hydrogen nuclei lose the energy from RF pulse. As relaxation occurs, magnetisation in the longitudinal plane (Mz) recovers, this is called T1 recovery. At the same time, there is a loss of magnetisation in the transverse plane, this is called T2 decay.

T1 recovery is the process of hydrogen nuclei losing thermal energy to the surrounding environment or lattice, hence the term spin-lattice relaxation. Energy released to the lattice results in nuclei recovering their magnetisation in the longitudinal direction. This recovery time is an exponential with a recovery time constant; the T1 relaxation time. This is the time it takes 63% of the longitudinal magnetisation to recover i.e., realign to B_0 with most nuclei in a low energy state. The spin-lattice relaxation time determines what delay between pulses should be used. The nuclear spin system must be allowed to relax back to equilibrium before the next pulse is applied and this time is determined by T1 relaxation.

T2 decay is caused by the magnetic fields of proximal nuclei interacting with each other and deviating from the Larmor frequency, also called spin-spin relaxation. In addition, static magnetic field inhomogeneities, such as those found near the boundaries of different tissue types (e.g., water and bone) cause additional dephasing of hydrogen nuclei which mimics T2 decay. Like T1 recovery, T2 decay is exponential so the T2 recovery time constant is the time it takes 63% of the transverse magnetisation to decay.

Decay caused by field inhomogeneities can be reversed with 180° refocusing pulse. Following a RF pulse, a free induction decay (FID) curve is present, and the FID has an exponential T2* decay. The application of 180° pulse can reverse the T2* effects, however, signal decay still occurs due to irreversible T2 decay.

In order to image the region of interest, which for the purposes of this thesis is the brain, the relevant area is selected spatially within the magnetic field. MR scanners have additional gradient coils which manipulate static magnetic field and therefore creating a spatial variation of the Larmor frequency.

To image a slice of material requires a method of exciting only material within that slice. This is achieved by superimposing a small spatially varying magnetic field, called a gradient field which is created from the gradient coils, one for frequency encoding in the x plane and a second for phase encoding in the y plane. Normally a slice is localised in z plane and then a coil pair in x and y plane. The gradient field is applied in the same direction as while the RF

pulse is applied. These gradient coils make the frequency and phase of the signal relate to position within the image. Stronger gradients allow better spatial specificity and therefore resolution.

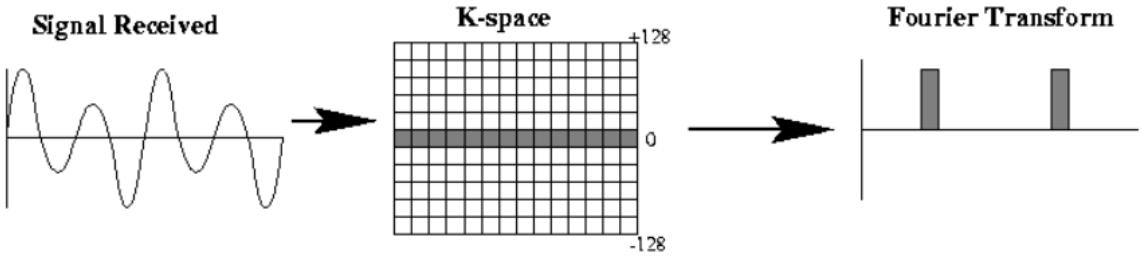

Figure 1.17 Presentation of Fourier Transformation converting data stored in k-space to frequencies and amplitude in the form of sinusoidal waves. [Image adapted from (Westbrook et al., 2008)]

When data of each signal position are collected, the information is stored as data points in the computer system as an array. This is referred to as K-space (Moratal *et al*., 2008). Each row of K-space contained the raw data received under a particular phase gradient, where the order in which the rows are recorded, depends on the imaging sequence used. Once all of K-space has been drawn together, it is processed using Fourier Transform (FT) to create a MR image. FT is a mathematical procedure with decomposes signals into frequencies and amplitudes of its component sinusoidal waves (Figure 1.17 and 1.18)

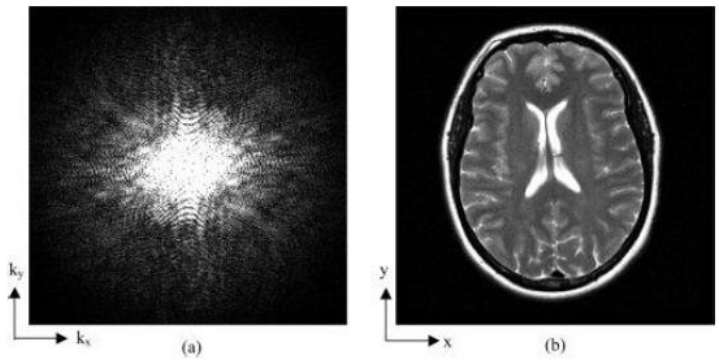

Figure 1.18 Transformation of spatial information in k-space (a) into conventional MR image space (b) via Fourier Transform. [Image adapted from (Paschal and Morris, 2004)]

1.4.2 Structural imaging

Historically, pathological studies of post-mortem showed the greatest neurodegenerative changes in the hippocampus (Bobinski *et al*., 1999). In accordance with this, MRI studies first started to examine structural changes within the hippocampus with particular regards to the volume and shape. In addition to this, generalised grey matter cortical loss has also been associated with NCF decline (Gress *et al.*, 2001). With improving MR technology, total volume and sub-hippocampal volumes can be defined well using automated software such as Freesurfer (Henschel *et al*., 2020) . In a study by Schuff *et al*., hippocampus volumes of forty participants with normal cognition were compared to thirty-six patients with mild cognitive impairment and twenty-nine patients with Alzheimer's dementia. Total hippocampal volume of patients with normal NCF was 6327 mm^3. This was significantly reduced by 11% to 5657 mm^3 in patients with mild cognitive impairment ($p<0.05$) and by 27% to 4595 mm^3 in those with Alzheimer's dementia ($p<0.01$). When Alzheimer's dementia was compared with mild cognitive impairment, hippocampus was 19% significantly smaller in Alzheimer's ($p<0.01$) (Schuff *et al*., 1999).

Volumetric studies of the pre-frontal cortex, amygdala and hippocampus have been conducted in ageing patients and in patients with other disorders such as schizophrenia and depression. Two studies looking at volume of various subcortical regions found an association with depressive symptoms and volume of the amygdala; however, no such correlation was found with hippocampal volumes (Vasilopoulou *et al*., 2011, Hastings *et al*., 2004).

1.4.3 Perfusion Imaging

Generalised cerebral perfusion and more specifically hippocampus perfusion has been studied in conditions affecting cognition such as Alzheimer's dementia, mild cognitive impairment, and some psychiatric disorders. In a study looking at healthy older and young adults comparing memory tests score and hippocampal perfusion, older adults with no history of cerebrovascular disease, cognitive impairment, or mental illness, hippocampal

perfusion was found to be inversely correlated with memory performance while controlling for hippocampal atrophy (Rane *et al*., 2013). This contrasts with another study examining patients with known diagnosis of different forms of dementia, where perfusion measurements in the bilateral parietal cortices and hippocampus were lower in dementia of Alzheimer type and multi-infarct dementia patients than in controls. Hypoperfusion in the hippocampus was a more sensitive marker than hypoperfusion in the parietal cortex in diagnosing dementia of Alzheimer type (Ohnishi *et al*., 1995). Although it remains unknown whether hypoperfusion is the cause or effect of Alzheimer's disease, it shows promise as a potential biomarker for identifying this condition (Austin *et al*., 2011).

In another study by Rodriguez *et al*., 2000 a positive correlation was reported between score of mini-mental status examination and hippocampal perfusion (Rodrigueza, 2000). The group also reported a statistically significant difference in perfusion of both of the hippocampi between controls and patients ($p<0.001$). In summary, most studies show a positive correlation between hippocampal blood flow and cognition.

1.4.4 Metabolic measurements

MRS detects cerebral metabolites in-vivo within a defined region of interest, most commonly N-acetyl aspartate (NAA), choline (Cho) and Creatine (Cr) containing compounds. The values are usually expressed as a ratio relative to Cr as it is considered to be relatively stable. Several other metabolites have also been identified and studied in disorders of the brain such as epilepsy, namely glutamate metabolites. There is an advantage to performing MRS at 3 T as metabolites often grouped together (glutamate, glutamine, and GABA) separate out and these are inseparable at lower strength MRI. MRS studies of the hippocampus are somewhat less frequent due to their technical challenges. Such challenges mainly relate to anatomical location of the hippocampi being close to the petrous bone and ventricles, which causes poor homogeneity of the B_0 magnetic field resulting in low spectral resolution relative to other regions within the brain. Despite these challenges, MRS has been increasingly studied in neurodegenerative and psychiatric disorders. A feasibility study of 20 healthy volunteers illustrated reliable and reproducible neurochemical profile of the hippocampi using MRS at 3 T (Allaili *et al*., 2015)

In a study of twenty patients undergoing WBRT, ten patients underwent neurocognitive assessments and MRS of bilateral hippocampi pre-treatment and at 4 months post treatment. Weak to moderate correlations were observed between left hippocampi NAA and auditory verbal learning tests and brief visuospatial memory tests. It is important to note that this study had a small number of patients and half of the patients did not complete the protocol (Pospisil *et al*., 2015)

There is ongoing research to identify a non-invasive biomarker that may precede symptomatic presentation of diseases such as Alzheimer's dementia (AD) and help distinguish AD from other neurodegenerative disease. It is considered to be more sensitive than physical structural changes. A study of 31 patients, 6 with Alzheimer's disease, 8 with mild memory impairment and 17 healthy controls demonstrated reduction of 15% in the hippocampal NAA/Cr within the group with mild memory impairment and 18% reduction in the group with Alzheimer's disease (Caserta *et al*., 2008). Schuff *et al*., 1999 demonstrated a reduction in NAA/Cho and NAA/Cr with ageing (Schuff *et al*., 1999). A systematic review by Wang *et al*., 2015 concluded that NAA, myo-inositol, and the NAA/Cr ratio may act as potential biomarkers of brain dysfunction in patients with Alzheimer's disease and have the potential of contributing towards diagnostic processes of the condition (Wang *et al*., 2015).

1.4.5 Diffusion Weighted Imaging

Diffusion weighted imaging (DWI) is a non-invasive method which measures diffusion of water at cellular level. Diffusion Tensor Imaging (DTI) is an extension of DWI that represents the overall movement of water molecules as an ellipse using a mathematical model, with quantitative DTI metrics allowing objective study of white matter (Assaf and Pasternak, 2008). DTI has been widely studied in various brain disorders including Alzheimer's disease, schizophrenia, multiple sclerosis, autism, stroke, and Parkinson's disease.

A study of 32 patients with high grade glioma undergoing fractionated brain radiotherapy demonstrated a linear dose-dependent decrease in fractional anisotropy (FA) and increase in

median diffusivity at 1, 4-6 and 9-11 months post radiotherapy indicating dose-dependent irreversible progressive changes to white matter (Connor *et al*., 2016). Another study in patients undergoing WBRT demonstrated significant decrease in FA values of the cingulum, fornix, and corpus callosum from pre-radiotherapy to the end of radiotherapy (-14%, -12.5%, and -5.2% respectively), and from pre-radiotherapy to 1 month post radiotherapy (-11.9%, -12.8%, and -6.4% respectively) (Nazem-Zadeh *et al*., 2012). This study demonstrated early changes in diffusion metrics as well as a differential sensitivity to radiation with cingulum and fornix tract being affected more than the corpus callosum. The reduction in FA may be attributed to a number of pathophysiological processes comprising of oedema, demyelination, gliosis, and inflammation, therefore it may be considered to be non-specific (Assaf and Pasternak, 2008). Thus, it is important to consider other metrics such as median and radial diffusivity alongside FA.

DTI has been utilised in surgical planning of low grade glioma resection and there is increasing interest in utilising DTI to map out tracts and tumour infiltration in order to inform high dose volume for radiotherapy planning (Bulakasi, 2009, Jena *et al*., 2005). Identifying the relationships of tumour edge to critical white matter pathways and eloquent areas of cerebral cortex could lead to reduced normal tissue complications (Whitfield *et al*., 2014).

Multiple studies have investigated pathophysiology of Alzheimer's disease with DTI. In particular, the fornix tract has been investigated most widely and reduced FA has been associated with patients with Alzheimer's disease compared to patients with mild cognitive impairment and healthy controls (Liu *et al*., 2011, Huang *et al*., 2012 Choo *et al*., Elahi *et al*., and Madhovan *et al*, Choo *et al*., 2010, Elahi *et al*., 2017). Other tracts have also been investigated, namely corpus collosum, cingulum, parahippocampal, uncinate fasciculus, superior longitudinal fasciculus, and cerebellar tracts (Acosta-Cabronero and Nestor, 2014, Leyden *et al*., 2015, Bracht *et al*., 2016). Significantly reduced FA has been demonstrated in each of these tracts, in particular the cingulum, however, lower FA in the fornix was associated with early stage of pathology and the degeneration of this tract was more severely impaired along the progression of Alzheimer's disease.

1.5 Summary

The management of BM poses a great challenge and remains a complex and highly individualized subspecialty within clinical oncology. As cancer prognoses continue to improve with the development of systemic therapy that can penetrate the blood brain barrier, offering improved intracranial control of disease and survival, neurocognitive sequelae of treatment have become more important. NCF reporting in patients undertaking trial activity for glioma and BM is strongly advised internationally and has become a key feature of some of the recently reported RCTs.

I have described the impact of radiotherapy on NCF in detail with different treatments that are offered to patients with BM, the underlying pathophysiological hypothesis that led to NCF impairment and potential use of MRI techniques which may help improve the understanding of radiotherapy effects on brain tissue.

SRS has become the standard of care for many patients with oligometastatic BM, partly due to its effectiveness in providing tumour control and its reduced impact on NCF. There is, however, ongoing interest in the effect of radiation on neurocognitive function and in the role of the hippocampus in this. There remains the potential for radiotherapy to be optimised to spare the hippocampus Because of its precision, SRS offers an attractive way of tailoring radiotherapy dose, reducing the radiation dose to critical structures such as the hippocampus and its effects on these structures. Modern MRI techniques then also offer the opportunity to non-invasively monitor the effects of treatment on patients.

1.6 Thesis Aims

In this thesis, I study factors that impact on NCF at presentation and following treatment with stereotactic radiosurgery for patients with a limited number of BM. I conduct a local review of our outcomes with SRS and perform a radiotherapy planning study to evaluate different RT planning methods and will present this work in chapters 2 and 3, respectively. I lead the design and conduct of a prospective clinical study that has successfully recruited thirty-one

patients having SRS. I present work from this observational study relating to baseline and follow-up clinical and neurocognitive measures as well as structural, functional, and metabolic MRI measures of normal brain tissue and structures in chapters 5, 6 and 7. Chapter 8 reports functional and structural MRI findings of tumour tissue of the BM and assessment of treatment response and Chapter 9 will focus on future work and hypotheses.

Chapter 2 - Clinical outcome and hippocampal dosimetry in patients undergoing stereotactic radiosurgery for brain metastases.

2.1 Introduction

RT remains the standard treatment for the majority of patients with BM. However, concerns for NCF impairment post RT have led to decreasing use of WBRT where more focal treatment such as SRS is feasible and appropriate. For patients with BM, concern for recurrence of intracranial metastases resulted in initial clinical trials testing WBRT + SRS compared to WBRT alone (Andrews *et al*., 2004). However, recent trials have randomised patients with limited BM to having SRS alone versus SRS and WBRT (Sahgal *et al*., 2015, Brown *et al*., 2016a, Aoyama *et al*., 2015). Most recent of these trials conducted by Brown *et al*., showed that rates of NCF impairment was significantly lower in the group having SRS alone than those patients who had SRS and WBRT (60% vs 90% respectively) (Brown *et al*., 2016a). This highlights that, whilst the rate NCF impairment is less following SRS, that despite the precision of SRS, patients are still at risk of developing NCF impairment post treatment.

NCF impairment is a well-recognised toxicity of cranial radiotherapy (Greene-Schloesser *et al*., 2012). The underlying aetiology of NCF impairment following SRS is not fully understood (Makale *et al*., 2017). It is possible that radiation dose to key structures may play a role. The hippocampi are a pair of subcortical structures located in bilateral medial temporal lobes and are thought to play a crucial role in memory formation and irradiation of the hippocampi has been implicated as one underlying pathological mechanism (Chang *et al*., 2016, Okoukoni *et al*., 2017). Anatomy of main cortical structures and hippocampi in a T1 weighted MRI is presented in Figure 2.1. Conventionally, the brain is considered a radioresistant organ probably due to expected lack of mitosis in adults. However, recent evidence suggests that mitotically active neural stem cells are present in certain areas of adult mammalian brains. One of these areas is the hippocampus.

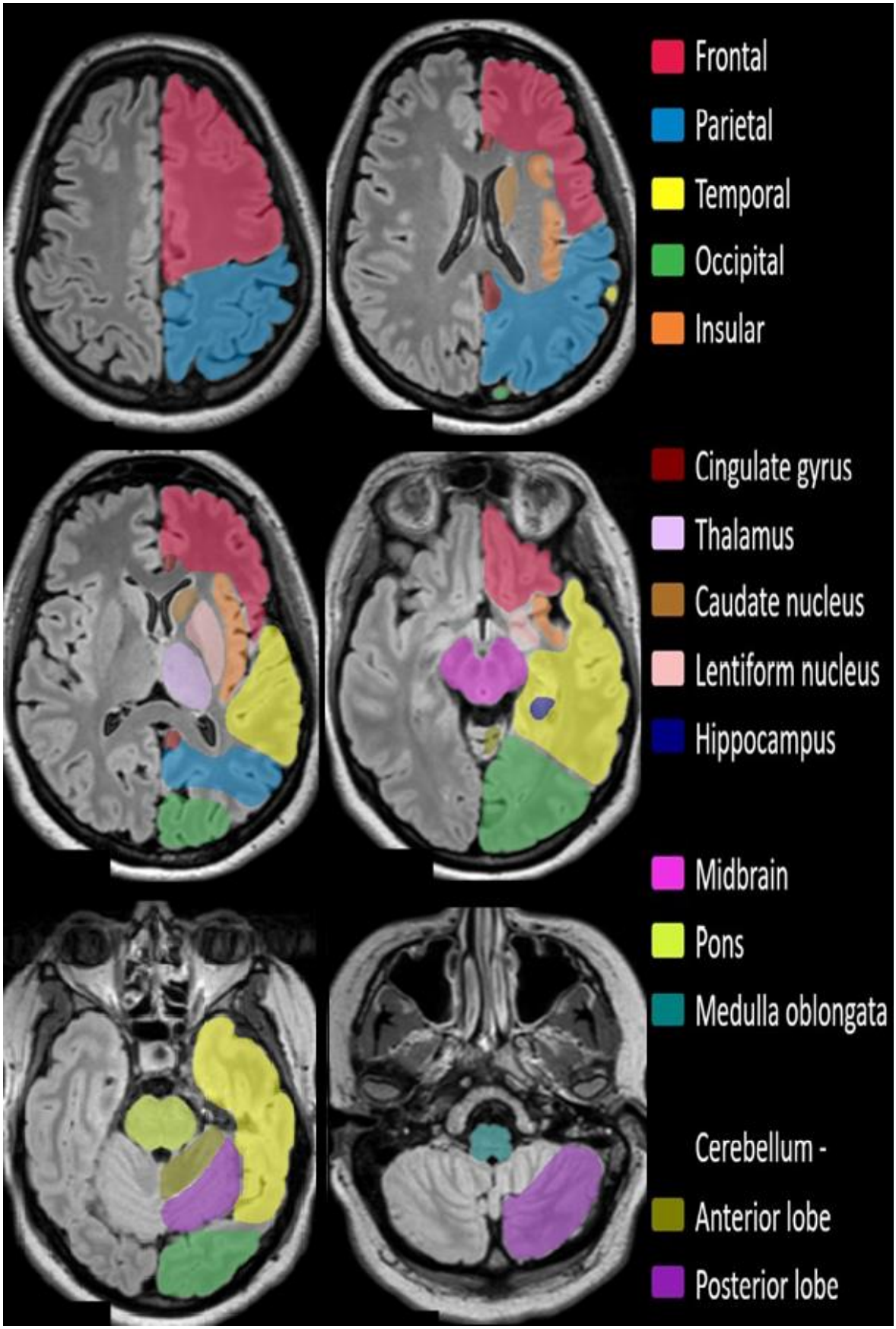

Figure 2.1 T1-weighted MRI of a healthy volunteer demonstrating anatomical location of the intracranial structures in relation to the hippocampus. Case courtesy of Maciej Debowski, Radiopaedia.org, rID: 61691 (Debowski M, 2018)

Clinically, NCF impairment can follow a biphasic pattern that can occur acutely within a few weeks of radiotherapy followed by a phase of recovery and then long term NCF impairment which may occur after many months. Therefore, giving rise to the hypothesis that neurogenesis within the hippocampus may have an acute and late reaction to radiotherapy.

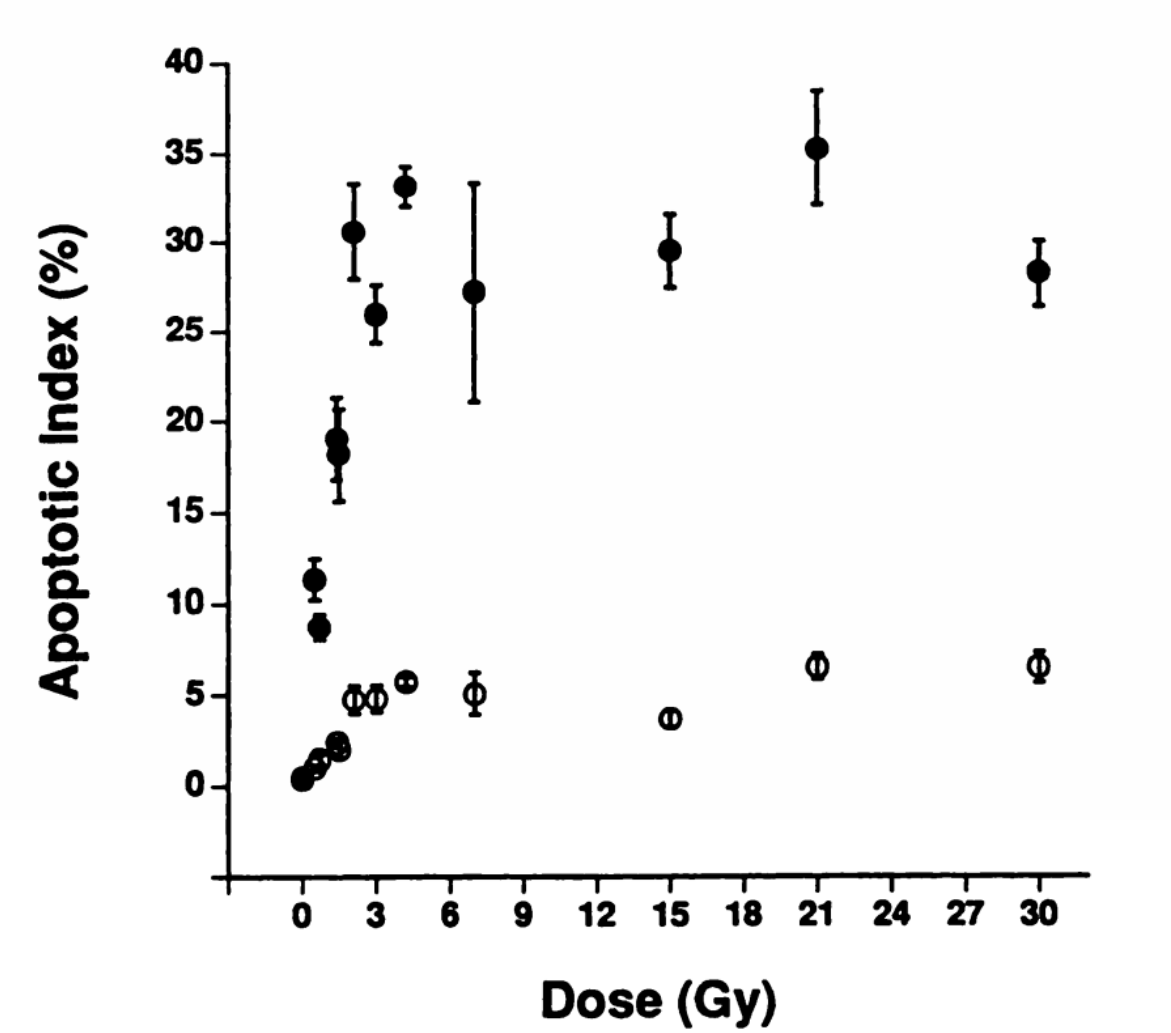

Figure 2.2 Apoptotic index as a function of radiation dose to the whole brain of adult rats in the subependymal zone (•) and corpus collosum (o).*Each symbol represents a mean of 3-6 rats; bars represent SE. (Shinohara et al., 1997)*

Historically, the hypothesis of hippocampus induced NCF impairment was supported mainly by pre-clinical models. Apoptosis of neural stem cells was first described by Shinohara *et al*., where the group demonstrated differential cell death in different regions of the brain following exposure to radiation. Figure 2.2 shows apoptotic index as a measure of cell death following exposure to different radiotherapy fractionation in the subependymal zone and corpus collosum. Corpus collosum appears to be more

radioresistant compared to the subependymal zone where neuronal stem cells lie. In vivo animal studies demonstrated sensitivity of hippocampus to radiation (Shinohara *et al*., 1997). A study by Acharya *et al*., demonstrated that doses as low as 1 and 2 Gy can induce apoptosis in the neural stem cells within the hippocampus of adult rats (Acharya *et al*., 2010) (Figure 2.3).

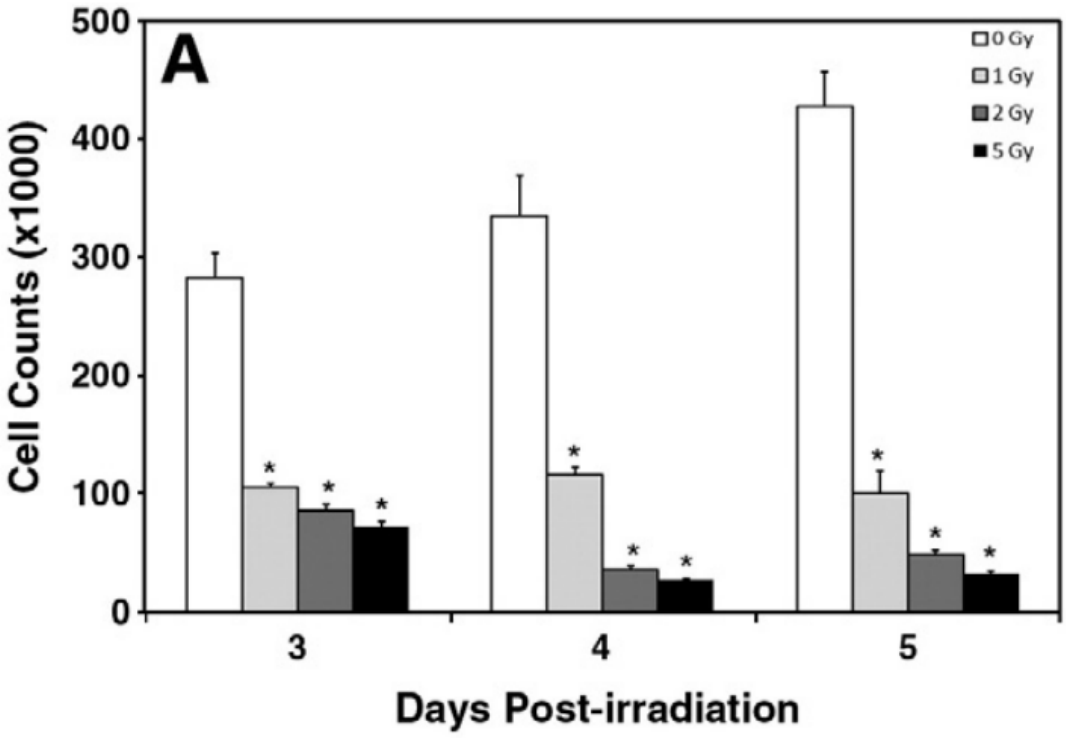

Figure 2.3: Cell survival parameters in irradiated hippocampal neural stem cells. *Exponentially growing cells were seeded at a density of 50,000 cells/well and cell counts were quantified by green-based fluorescence. Data show that the number of cells exhibits a dose-dependent decline at days 3, 4, and 5 post radiation. (Acharya et al., 2010)*

Although significant pre-clinical data supports loss of NSCs in the hippocampus and changes in neuronal architecture following radiation, more recently, clinical studies have also provided dose response data in humans. A prospective study showed a dose response relationship between the hippocampus and objective NCF scores in patients with low grade glioma who were treated with fractionated radiotherapy, further consolidating the theory that hippocampal dose may be responsible for NCF impairment in humans (Gondi *et al*., 2012). With the development of modern RT techniques such as intensity modulated radiation therapy (IMRT) and volumetric modulated arc therapy (VMAT) it has become possible to avoid structures such as the hippocampus (Figure 2.4). More recently, results of the first prospective phase II study (RTOG 0933) of hippocampal

sparing in BM patients suggest a reduction in risk of NCF in patients undergoing hippocampal sparing WBRT. Primary cognitive outcome was delayed recall at 4 months as measured by the Hopkins Verbal Learning Test. Results were compared to historical control group and they showed 7% of patients experienced decline in memory compared to 30% of patients in the historical cohort (p = 0.0003) (Gondi *et al*., 2014a).

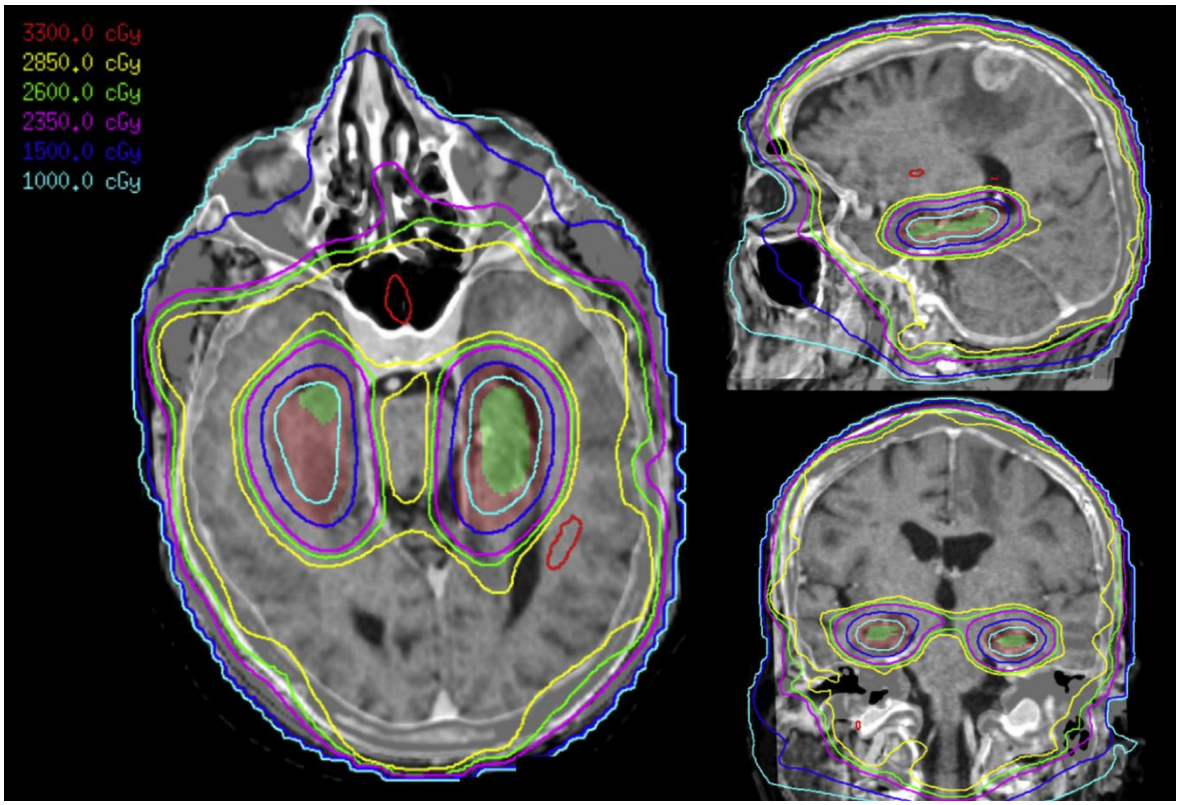

Figure 2.4 Hippocampal-sparing whole brain radiotherapy can restrict dose to bilateral hippocampi while maintaining homogenous dose to the rest of the brain. *Hippocampus has been shaded in green, and hippocampus planning risk volume in pink. Isodose line representing 10 Gy in light blue shows sparing the hippocampus bilaterally while delivering 28.5 Gy (yellow isodose line) to the whole brain. (Pinkham et al., 2015)*

Hippocampal dosimetry has been studied to some extent in patients with primary brain tumours and in patients with BM undergoing fractionated radiotherapy. However, this remains uncharacterised for patients undergoing SRS. An organ at risk (OAR) can be defined as a serial or parallel organ. In a serial organ, dose to 0.1 cc (D0.1 cc) is critical as the complication probability depends on a high dose received in a small volume; in contrast, in a parallel organ, the complication probability depends on the dose bath received by the whole organ, i.e., mean dose or dose to a certain volume of the organ of interest (Burman *et al*., 1991). Examples of serial organs include the spinal cord, optic

chiasm and brain stem and parallel organs include lungs, heart, and kidney (Burman *et al.*, 1991, Yorke, 2001). This remains unknown for the hippocampus.

2.2 Hypothesis

I hypothesise that dose to the hippocampus will be high in the following group of patients:

- Location of metastases in the temporal lobe as hippocampus is in the medial temporal lobe;
- Large planning target volume (PTV);
- Metastases in close proximity of the hippocampus; and
- Patients with multiple metastases due to increased number of beams and dose deposition in different areas.

2.3 Materials and Methods

To test this hypothesis, I conducted a detailed retrospective analysis of the SRS treatment plans at Velindre Cancer Centre and measured dose received by the hippocampus during SRS treatment.

2.3.1 Patients

Case notes and radiotherapy treatment plans were reviewed for all patients treated with SRS alone without WBRT at Velindre Cancer Centre (VCC) between January 2015 and January 2016. At VCC patients included were those with 1-3 BM with a maximum tumour volume of 20 cc, WHO performance status 0-2 and controlled or controllable extracranial disease.

2.3.2 Radiotherapy Planning

SRS treatment was planned using a forward planned, dynamic conformal arc technique using the iPlan Treatment Planning System (TPS) (BrainLAB, Germany). Immobilisation was achieved using the BrainLab Frameless Radiosurgery immobilisation system. All patients underwent a CT planning scan without contrast (0.6mm slice thickness) and MRI

planning scan with intravenous contrast 1 mm isotropic spoiled gradient echo sequence. The planning images were localised and fused using the Brainlab CT localiser and target volumes were defined. PTV was created by adding a 1 mm margin to gross tumour volume (GTV). Organs at risk (OARs) including eyes, lenses, optic nerves, optic chiasm, brainstem, and cochlea were delineated with 1mm planning organ at risk volume (PRV) margin as standard. The treatment was planned without the knowledge of hippocampal location as hippocampus is not a standard OAR included in SRS planning. Typically, 3 - 5 non-coplanar arcs were used to plan the treatment with objectives for conformity index and homogeneity index of <1.32 and <1.5, respectively. For plans containing multiple PTV volumes separate isocentres were used for each PTV. Treatment was prescribed to 80% isodose and the prescription dose for SRS is volume dependent as summarised in Table 2.1.

Volume of PTV (cc)	Dose Prescription
< 7	21 Gy
7-13	18 Gy
> 13	15 Gy

Table 2.1 Dose Prescription used for cerebral metastases. *Gy represents unit of radiotherapy dose in Gray. Cc: cubic centimeteres, PTV: Planning target volume*

2.3.3 Hippocampal Delineation and Dosimetry

For each case hippocampal segmentation was carried out retrospectively using the spoiled gradient 3-dimensional T1 weighted MRI images, according to the RTOG 0933 atlas (Gondi *et al*., 2014b). The outlining protocol states outlining the subgranular zone of the hippocampus where neural stem cells are located (Figure 2.5). The volumes were peer reviewed by one other clinical oncology consultant specialising in Neuro-Oncology. 1 mm margin was added to create the PRV as applied to other organs at risk. Dose volume histograms were created using the iPlan RT Dose 4.5 treatment planning system. The following doses delivered to individual and combined hippocampi PRVs were recorded: dose to 0.1 cc of the hippocampus (D0.1 cc), dose to 50% of the hippocampus (D50), dose to 10% of the hippocampus (D10), dose to 40% of the hippocampus (D40), dose to 70% of the hippocampus (D70) and mean dose. A range of doses were chosen as it has not been

determined by normal tissue complication probability (NTCP) modelling whether hippocampus is a serial or a parallel organ.

The distance between the PTV and the following volumes was calculated as the minimum distance from the edge of PTV to the edge of volume of interest: right and left hippocampus, brainstem, optic chiasm. The reason for choosing the minimum distance was that this is likely to have the biggest dosimetric impact. In patients with more than one PTV, the smallest distance between the PTV and the relevant OAR was recorded.

2.3.4 Statistics

Data was also collected on patient demographics, anatomical factors of the metastases, primary site and its treatment, use of steroids and survival. Dosimetric analysis was performed using CERR (Computational Environment for Radiotherapy Research) (Deasy *et al*., 2003). Statistical analysis was conducted using SPSS software. Spearman rank correlation coefficient was calculated to examine factors influencing hippocampal dose. Factors included location of the metastases, i.e., metastases in temporal lobe and distance from PTV.

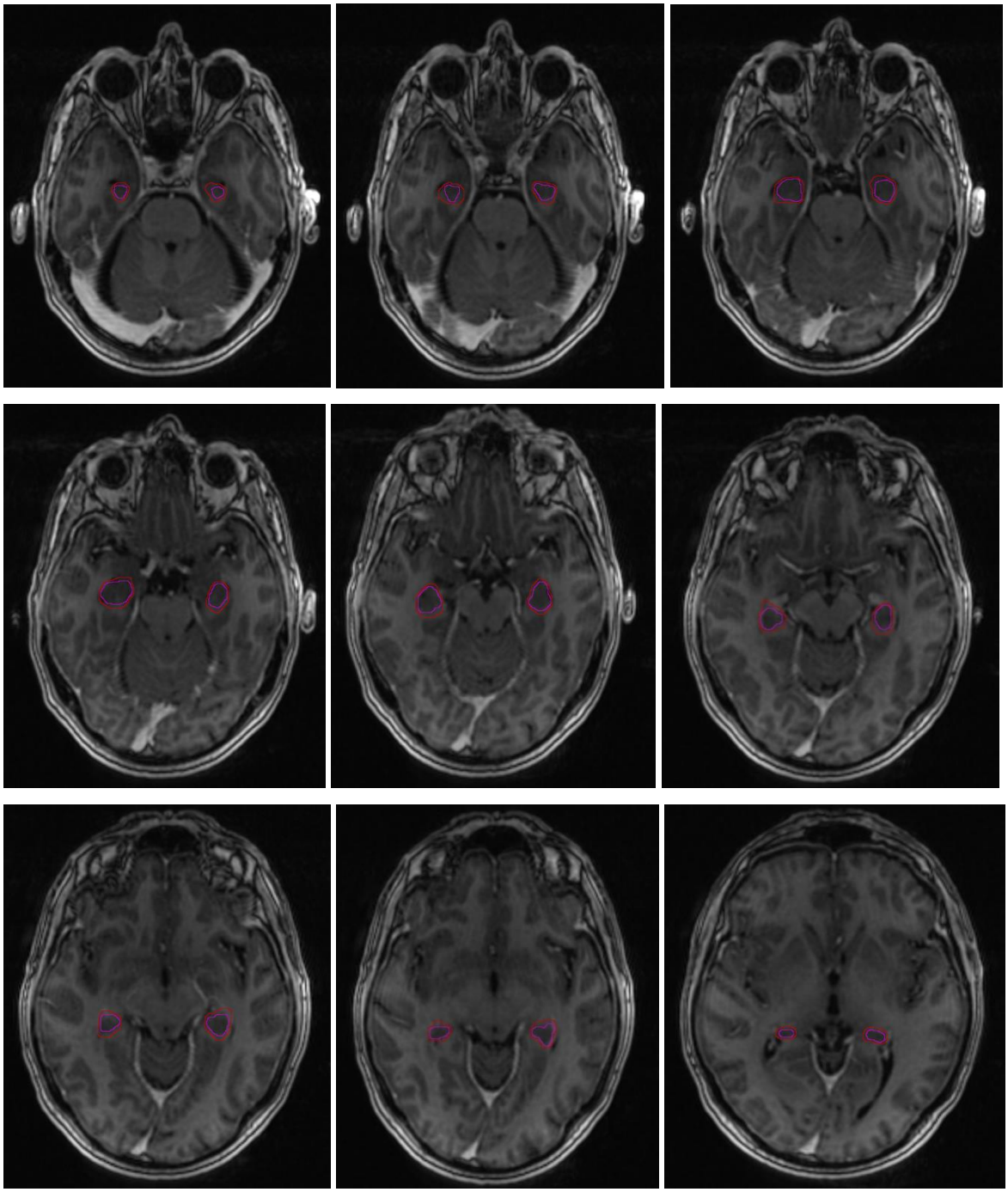

Figure 2.5 Delineation of Subgranular Zone of the Hippocampus on T1-weighted spoiled gradient recalled echo (SPGR). *Axial Slices are displayed starting the most caudal slice in top left position and bottom right being most cranial. Purple line represents the hippocampus and red line represents planning organ at risk volume (PRV) with 1mm margin applied to the hippocampus. As per contouring atlas for RTOG 0933 (Gondi et al., 2014b).*

2.4 Results

2.4.1 Patients' demographics

Thirty patients were treated with SRS alone during this time period. A total of forty-seven metastases were treated: eighteen patients had a single metastasis, seven patients had 2 and 5 patients had three metastases. Fifty-three percent of patients had neurological symptoms and seizure was prevalent in 10% of patients based on case note review. Thirty percent patients presented with synchronous BM. The most common primary malignancies were lung, melanoma, and renal cell carcinoma. Extracranial disease was present in nineteen patients, out of whom seventeen patients had controlled extracranial disease at the time of SRS and two had controllable disease. Most patients presented with metachronous BM (n.21) and median time from diagnosis of primary cancer to diagnosis of BM was 24.5 months with a range of 0-171 months. Patient characteristics are summarised in Table 2.2.

2.4.2 Anatomy of the metastases

Most metastases were located in the frontal lobe (15), followed by parietal lobe (13) and cerebellum (9). Less common sites were temporal lobe (5), occipital lobe (3), and brain stem (2). Of these, two metastases were located close to the lateral ventricle.

2.4.3 Confounding factors

All patients received 12 mg of dexamethasone daily to be taken on day 2 and 3 following SRS. However, seventeen patients had a longer course of steroids prescribed than the standard 2-day regimen. Eleven patients did not receive any extra steroids. Medical records were incomplete for the remaining patients. The reason for prolonged course of steroids was presence of neurological symptoms. For patients receiving concurrent SACT, TKIs were withheld for a total of 5 days, 2 days before, the day of and 2 days after SRS. Patients who were on immunotherapy or chemotherapy, a gap for minimum of 1 week was advised between SRS and treatment.

Characteristic	No. (%)
Sex	
Male	14 (47)
Female	16 (53)
Age, mean	61 years
Performance status, median	1
Neurological symptoms	16 (53)
Seizures	3 (10)
Synchronous Brain Metastases	9 (30)
Median time: diagnosis of brain metastases and first diagnosis of cancer	24.5 Months
Presence of extracranial disease	19 (63)
Extracranial Disease controlled	17/19
Primary Cancer	
Breast	1 (3.3)
Lung	12 (40)
Melanoma	4 (13.3)
Renal	7 (23.3)
Others (colo-rectal, bladder, CUP, angiosarcoma)	6 (20)
Number of brain metastases	
1 metastasis	18 (60)
2 metastases	7 (23)
3 metastases	5 (17)
Total number of metastases	47
Location of metastases	
Frontal	15 (30)
Parietal	13 (28)
Temporal	5 (11)
Cerebellar	9 (20)
Occipital	3 (7)
Brainstem	2 (4)
Patients receiving SACT	18 (60)
Types of SACT	
Chemotherapy	11/30 (37)
Oral targeted SACT (e.g., TKI)	5/ 30 (17)
Immunotherapy	2/ 30 (7)

Table 2.2 Demographics of patients who received stereotactic radiosurgery (SRS) in 1 year. *WHO: World Health Organisation, CUP: Carcinoma of unknown primary, SACT: systemic anticancer therapy, TKI: Tyrosine kinase inhibitor*

2.4.4 Survival

Median time from date of treatment to the progression of intracranial disease was 5 months. Median overall survival (OS) was 11 months which is comparable with previously published studies (Figure 2.6) (Brown *et al*., 2016b, Tsao *et al*., 2012). Improved survival was observed in patients who received systemic anti-cancer therapy (SACT) before or after SRS treatment compared to patients who did not receive systemic treatment. Median survival in these groups was 11 and 1 months, respectively. Further analysis of patients who received SACT showed greater survival in patients who received targeted agents or immunotherapy with a medial overall survival of 12 months. Statistical significance was not performed due to the small number in each group.

There was no statistically significant difference in the median OS between patients who had synchronous or metachronous presentation (median OS 14 versus 9 months respectively, p-value 0.15). The presence of extracranial disease was associated with improved median OS (12 months in group with extracranial disease versus 7 months in group with no extracranial disease).

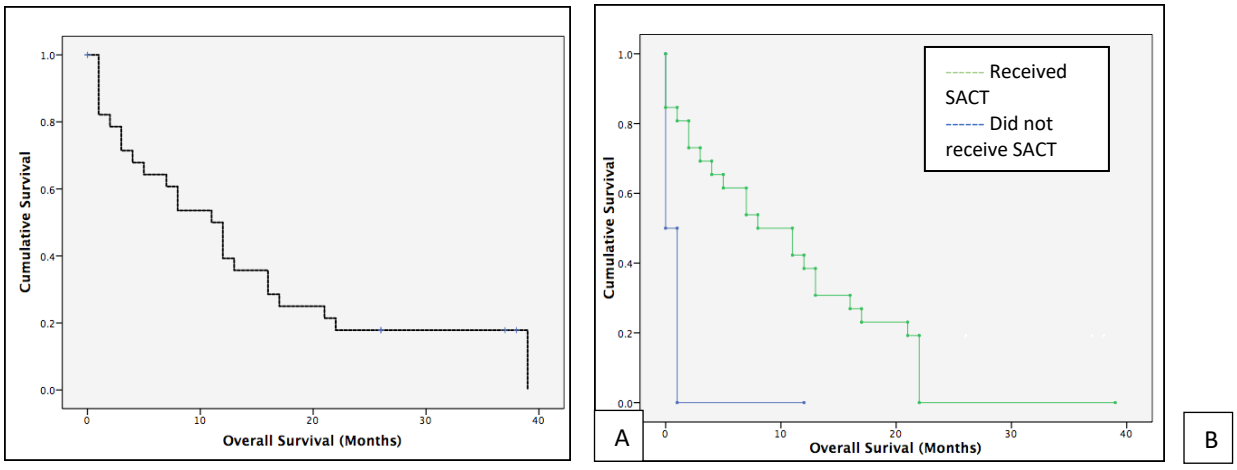

Figure 2.6 Overall survival of patients undergoing stereotactic radiosurgery in 1 year. *Figure A demonstrated OS for all patients and Figure B demonstrated OS stratified according to whether patients received systemic anticancer therapy (SACT)*

2.4.5 Hippocampal Dosimetry

Location of the metastases according to lobar location had an impact on dose delivered to the hippocampus. Metastases in temporal lobe were associated with a higher dose deposition in the hippocampus. This is likely due to the location of the hippocampus being in the medial temporal lobe. Tables 2.3 and 2.4 summarizes structural aspects of the planning volumes and organs at risk. Distance between the hippocampi and PTV is similar to distance between PTV and brainstem. However, distance from the optic chiasm was higher which could be due to its location being anterior to the brainstem (Figure 2.1).

Volume	Volume (cc)
GTV	1.98 (0.05-20.04)
PTV	6.56 (0.66-30.73)
Left Hippocampus	2.15 (1.23-3.68)
Right Hippocampus	2.37 (1.51-3.87)
Composite hippocampus	4.49 (2.75-7.15)

Table 2.3 Volumetric analysis of planning volumes of all 47 metastases and each hippocampus in 30 participants. *Figures presented are median with range in brackets. GTV: gross tumour volume, PTV: planning target volume*

OARs	Distance from PTV (cm)
Left hippocampus	2.36 (0-6.52)
Right hippocampus	3.85 (0-6.72)
Brainstem	2.38 (0-4.95)
Optic chiasm	5.11 (0.9-8.89)

Table 2.4 Distance between Planning Target Volume (PTV) and Organs and Risk (OARs)*. Figures presented are median with range in brackets*

A range of radiotherapy doses were recorded in the hippocampi. D0.1 cc of the ipsilateral hippocampus was > 5 Gy in 7 patients and 2 - 4.9 Gy in 8 patients. Figure 2.7 demonstrates dose to 0.1 cc, D40, D50, D70 and mean dose received by the hippocampus

in this patient population. Each of these dose metrics were highly correlated with each other and one dose constraint was not discriminatory, r_s = 0.806-0.866 (p <0.001). In all the patients, ipsilateral hippocampus received a higher dose, this is due to the presence of metastases in close proximity to one of the hippocampi and ability of SRS to allow sharp dose fall off and reduce dose to surrounding structures. Distance between PTV and the ipsilateral hippocampus was <1 cm in those who received >5 Gy to D0.1 cc and between 1-2 cm for those who received 2-4.9 Gy. Figure 2.8 demonstrates the difference in doses to 0.1 cc from the left and right hippocampus for each case. Correlation analysis between left and right hippocampus showed that there was no statistically significant correlation between the doses r_s = 0.273, p-value 0.144.

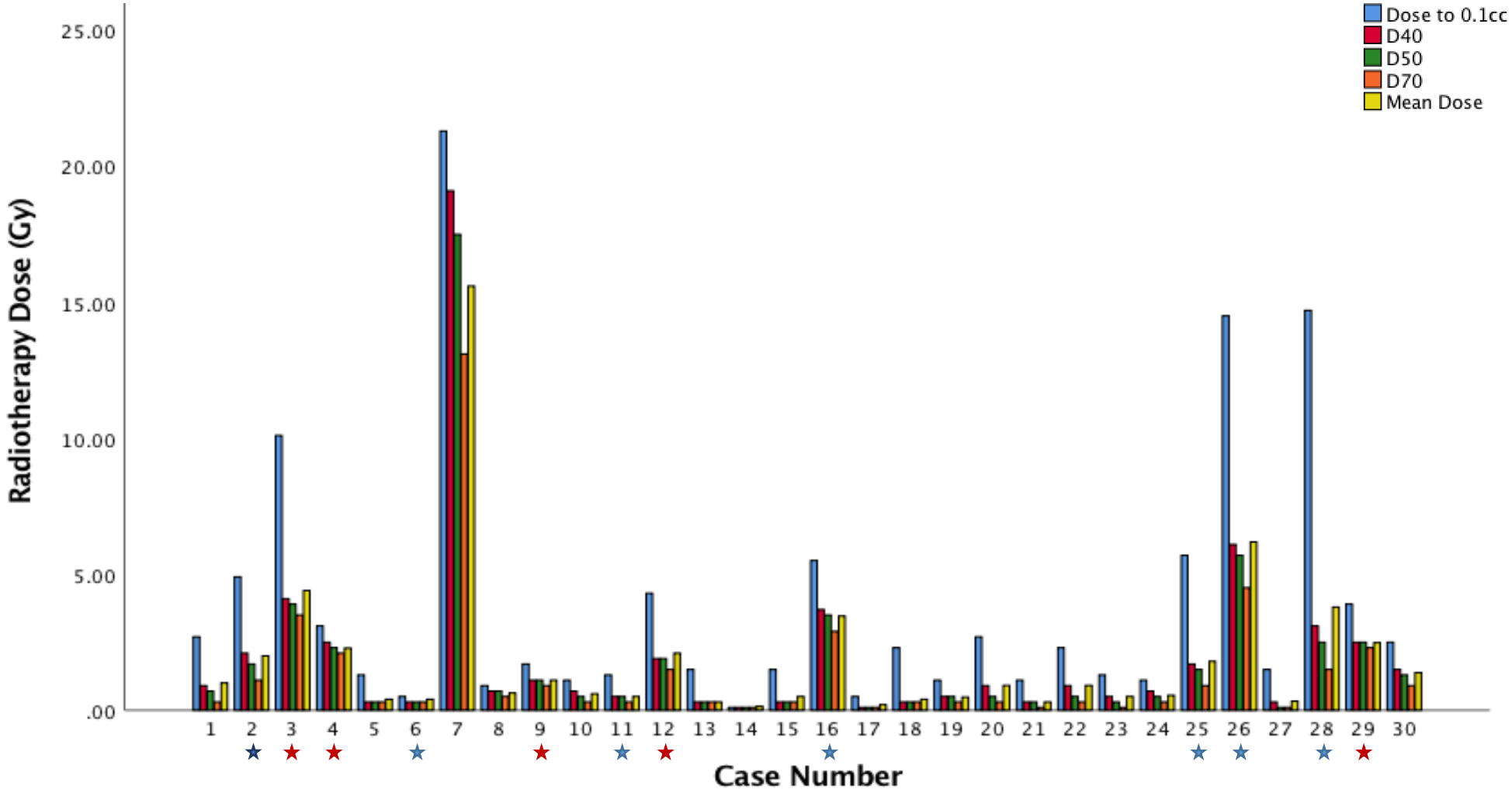

Figure 2.7 Range of ipsilateral hippocampal dose received in individual patients. D40, D50 and D50 represent dose received by 40%, 50% and 70% of the hippocampus respectively. Gy: unit of radiotherapy dose in Gray. ★ *Patients with 2 metastases,* ★ *Patients with 3 metastases. Patient 7 had metastases within 1 mm of the hippocampus.*

ADD Figure 2.7b – waterfall for D0.1cc

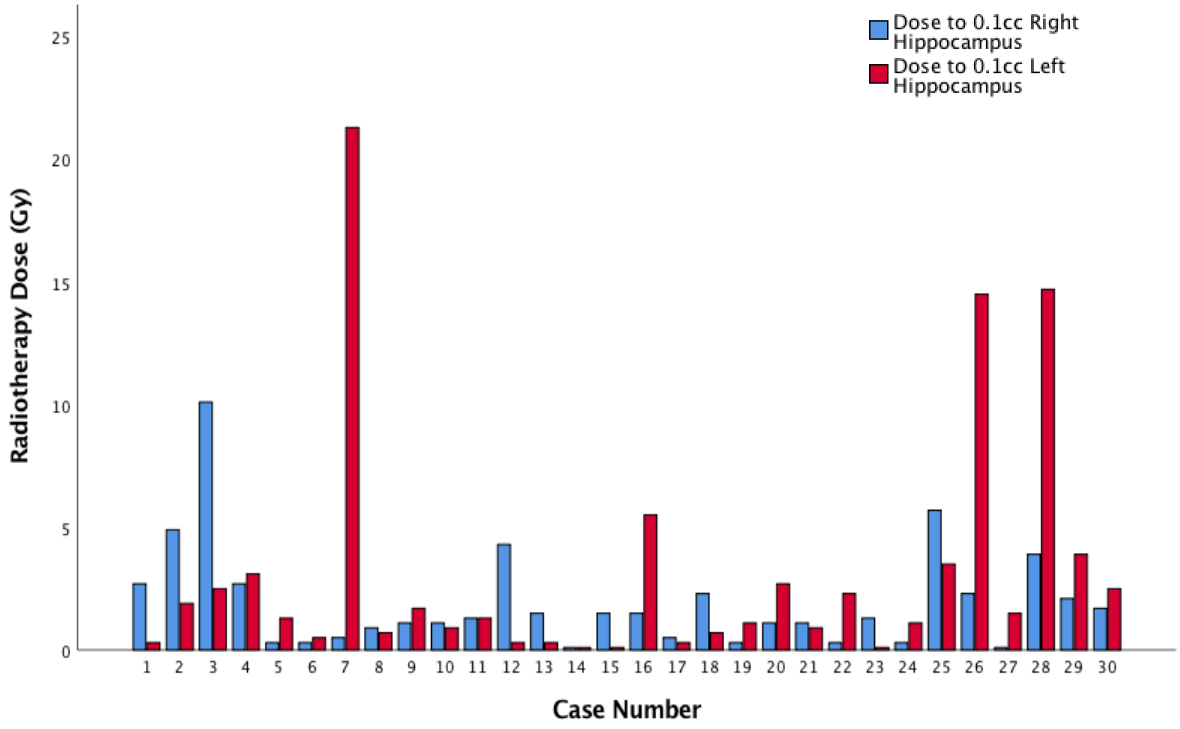

Figure 2.8 Bar chart representing the difference in the radiotherapy dose delivered to individual hippocampus in each case.

There was a positive correlation between D0.1 cc to the ipsilateral hippocampus and the planning target volume (PTV) with r_s = 0.38, (p <0.05). There was a negative correlation between D0.1 cc to the ipsilateral hippocampus and distance between PTV and hippocampus, correlation coefficient for right and left hippocampus was -0.637 and -0.814 (p-value <0.05). Another interesting finding was that dose received by the hippocampus was higher where the metastases were located close to critical intracranial structures such as brainstem and optic chiasm, correlation coefficient was -0.562 and -0.612 respectively, p-value <0.05. Figure 2.9 describes the relationship between the doses received by the hippocampus in respect to these different factors.

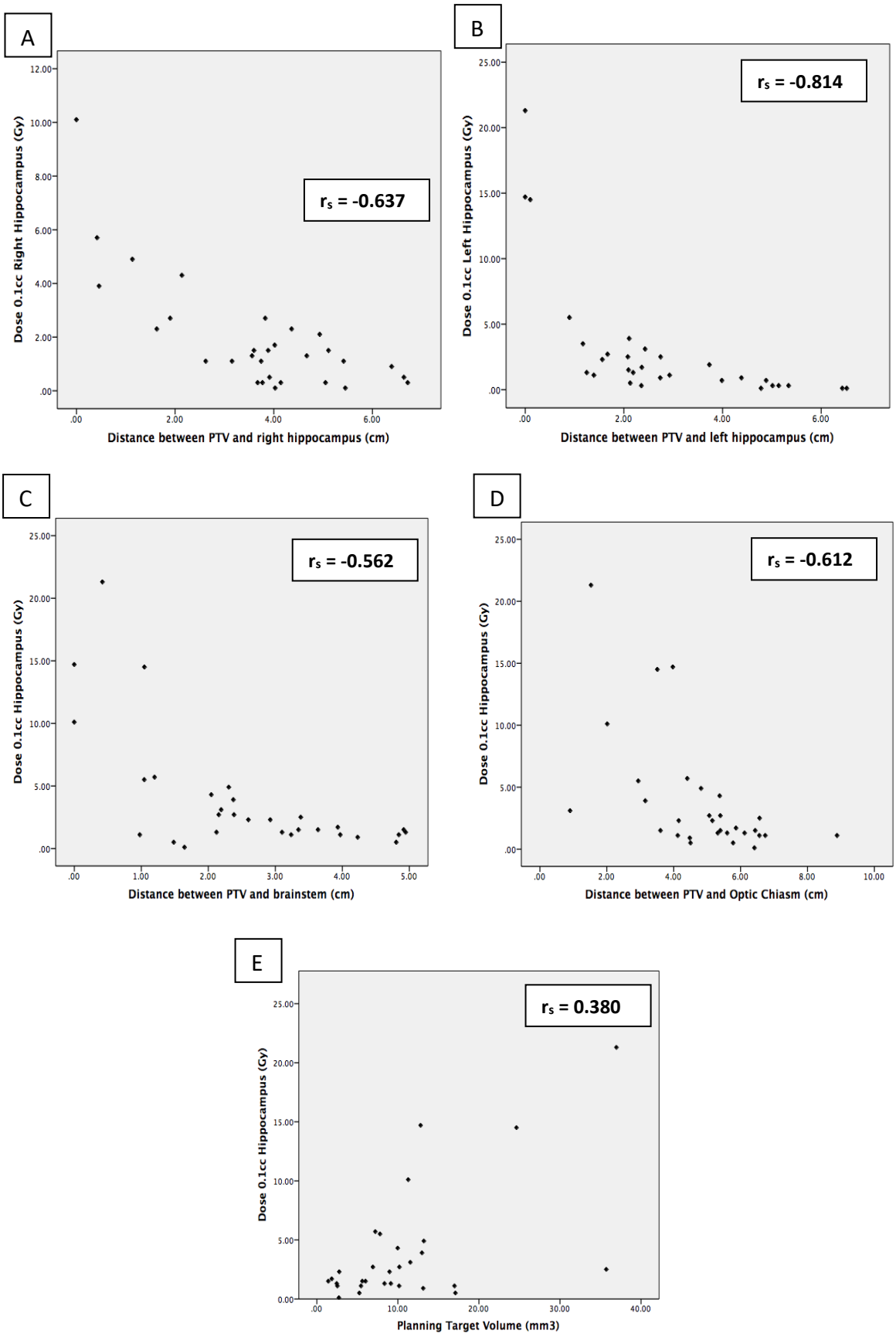

Figure 2.9 Scatter plots demonstrating correlation between Dose to 0.1 cc of the Hippocampus and its influencing factors. *A - Dose to 0.1 cc to the right hippocampus and distance between PTV and right hippocampus. B - Dose to 0.1 cc of the left hippocampus and distance between PTV and left hippocampus. C, D and E represent dose to 0.1 cc of the composite hippocampus and distance between brainstem, optic chiasm and planning target volume (PTV) respectively.*

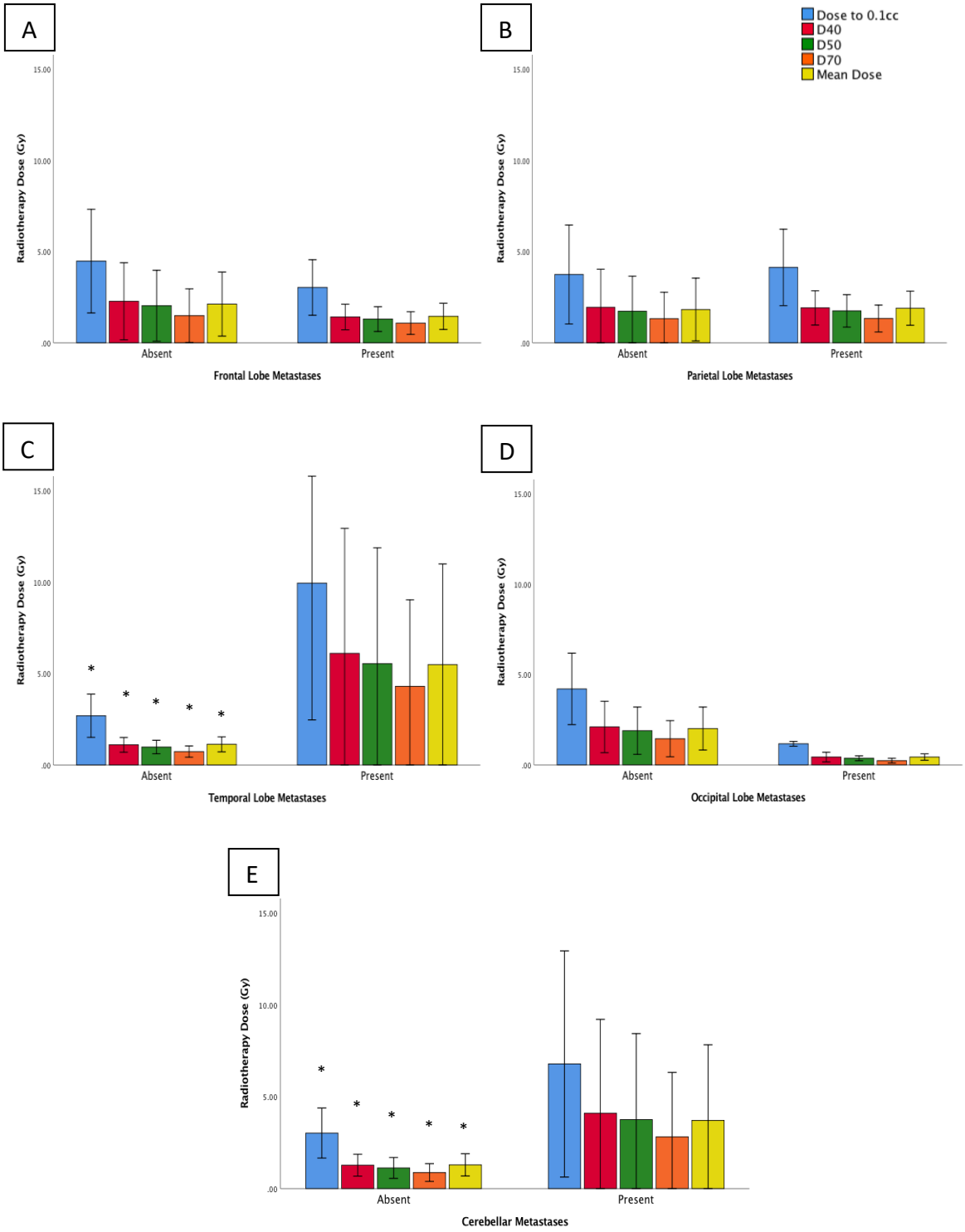

Figure 2.10 Range of doses delivered to the composite hippocampus according to the location of metastases in different lobes of the brain. *Each graph represents metastases present in a different lobe within the brain: A – Frontal Lobe, B – Parietal Lobe, C – Temporal Lobe, D – Occipital Lobe, E – Cerebellum. Bars marked with symbol * represents where the different in doses were statistically significant (p-value <0.05).*

Hippocampus dose was significantly higher in those patients who had a metastasis within the temporal lobe or cerebellum, whereas presence of metastases in other regions of the brain did not impact on hippocampal dose significantly. There was also a larger variation in dose between patients who had metastases present in temporal lobe and cerebellum, although this may be due to low numbers of patients. These data are displayed in Figure 2.10.

Number of metastases did not influence the dose to the hippocampus significantly. However, the seven patients with two metastases received higher dose to the hippocampus compared with the eighteen patients with single metastasis, this was not seen in the five patients with three metastases (Figure 2.11). The outliers on this diagram are the patients who had metastases located within the medial temporal lobe.

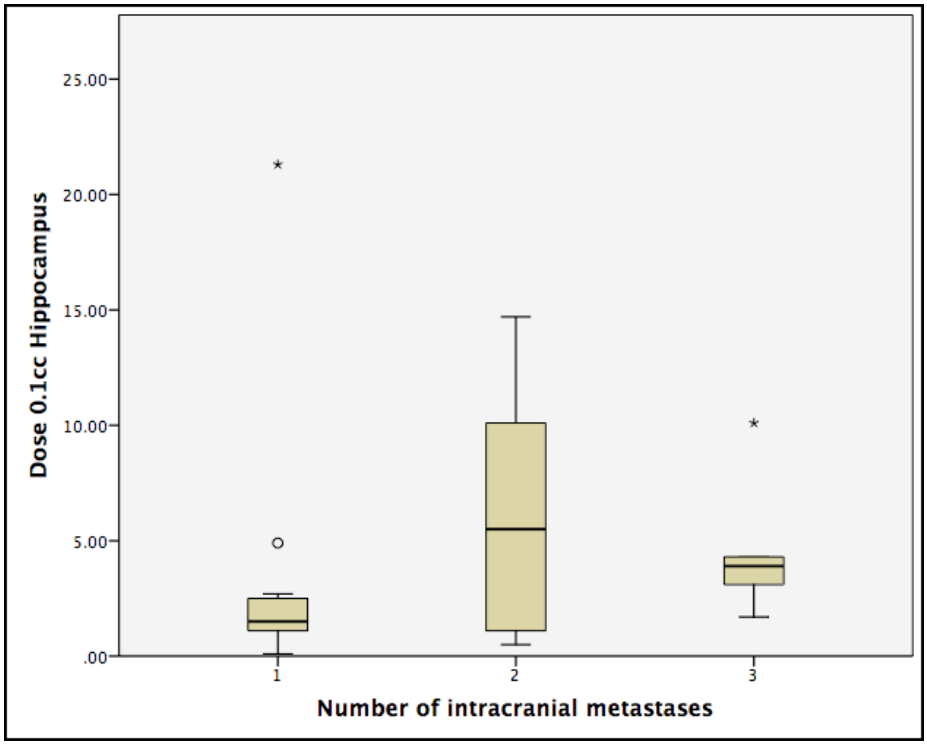

Figure 2.11 Box Plot demonstrating Dose to 0.1 cc of the ipsilateral hippocampus grouped by number of metastases present. *The outliers on the diagram are patients who had metastases located within the medial temporal lobe*

2.5 Discussion

The hippocampus has been implicated in developing neurocognitive dysfunction following radiation and here it has been demonstrated that even with the precision of SRS there is a considerable proportion of patients receiving >5 Gy to D0.1 cc of the hippocampus. Radiotherapy dose constraints to the hippocampus vary considerably in the literature and these have rarely been correlated with neurocognitive outcome. Most groups advocate minimising dose to the bilateral hippocampi (Gondi *et al*., 2012, Marsh *et al*., 2011). Hippocampus dosimetry and neurocognitive decline have previously been studied in primary brain tumours where patients undergo fractionated radiotherapy and, in this study, greater than 7.3 Gy delivered to 40% of the bilateral hippocampi was associated with significant NCF decline (Gondi *et al*., 2012). Such correlation and dose-response relationships have not been studied in SRS. However, radiobiology of single fraction RT is poorly understood as it defies the principles of repopulation and repair in radiobiology (Brown *et al*., 2014). In addition, there is evidence from animal studies that endothelial cell apoptosis (Garcia-Barros *et al*., 2003) and vascular damage (Park *et al*., 2012) with fraction dose of more than 10 Gy may play an important role in enhanced tumour control with SRS.

Anatomical position of the metastases with respect to the hippocampus appears to be the main factor that influences the dose delivered to the hippocampus. This was shown by demonstrating a strong negative correlation between dose and distance of PTV from the ipsilateral hippocampus. We have also observed a negative correlation between hippocampal dose and distance of PTV from organs at risk (OAR) such as the brainstem and the optic chiasm. This may be due to use of unconventional beam entry points in order to reduce radiotherapy dose to these OARs and raises the question of whether radiotherapy planners can reduce dose to the hippocampi without impacting on other planning metrics. If BED of 7.3 Gy is considered to be a significant dose, then the dose constraint for hippocampus will be considered to be much more stringent than that applied to other OARs as described in SABR Consortium guidelines, e.g., mandatory dose constraint for brainstem and optic pathway has a maximum tolerance of less than 15 and 8 Gy respectively (Consortium, 2019). Therefore, dose constraint to the hippocampus is likely to be an optimal constraint to be met in an ideal circumstance, e.g., BM more than

2 cm away from the hippocampus, to achieve a balance between NCF impairment and tumour control. Currently, as there is not a dose tolerance defined for SRS nationally or internationally, the practice of hippocampal delineation as an OAR is likely to vary between centres.

There was a positive correlation with PTV volume, therefore larger volume was associated with higher dose received by the hippocampus. In contrast, number of metastases alone did not affect the hippocampus dose significantly. Therefore, we can extrapolate that distance from the PTV plays a pivotal role in dose received by the hippocampus. Number of metastases has also been removed as a constraint for SRS treatment by NICE and the overall volume is more important; regardless of number of metastases, BM with volume of less than 20 cc are eligible for SRS (NICE, 2018).

The main limitations of the retrospective review are that it is a retrospective data, there is a lack of NCF clinical data, and small number of patients. NCF data was not collected prospectively in this patient cohort, and we decided not to perform a retrospective review of medical notes due to the low-quality data assurance and substantial risk of bias. Multi-test correction was not performed in this pilot dataset due to small number of patients. For future studies that examine NCF in patients receiving SRS we would propose correlating NCF outcomes collected prospectively with detailed hippocampal dosimetry to help define appropriate dose volume constraints. It may also be beneficial to correlate these data with structural or physiological changes seen on MRI imaging to try and identify potential causes of neurocognitive decline.

2.6 Conclusions

It has been demonstrated that there is a large inter-individual variation in hippocampal dosimetry in patients undergoing SRS, which is mainly caused by the physical position of the metastases. Hippocampal dose may lead to differences in neurocognitive sequelae to patients. Therefore, I propose to study this in further detail by correlating dosimetric information combined with objective neurocognitive function tests in a prospective observational clinical study.

Initially, I will explore how the hippocampal dose may be reduced in SRS planning. In order to do this, I will conduct a radiotherapy replanning study with dynamic conformal arc therapy and VMAT planning techniques to examine whether it is practically feasible to reduce the dose to hippocampus while maintaining the quality of rest of radiotherapy plan and its clinical acceptability.

Chapter 3 – Dosimetric impact of hippocampal avoidance during treatment planning of stereotactic radiosurgery for patients with brain metastases

3.1 Introduction

Despite the precision of SRS, NCF impairment following treatment is not negligible and despite the complexities of RT induced NCF impairment, hippocampal radiation dose has been implicated in animal and human studies. As demonstrated in Chapter 2, there is a significant proportion of patients receiving high dose radiation to the hippocampus as it is not routinely delineated and, to date, dose constraints for the hippocampus in single fraction SRS are not routinely used (Consortium, 2019). There have been few studies examining hippocampal dose received during SRS. A retrospective analysis by Riina *et al*., demonstrated that in patients treated with the gamma knife SRS technique, those with 10 or more BM received significantly higher dose to the hippocampus compared to patients with 4-9 BM (Riina *et al*., 2020). Understanding is increasing of the effects of avoidance of the hippocampus during planning of SRS treatment, however this is less appreciated for patients undergoing treatment for less than 4 BM (Chang *et al*., 2016, Zhang *et al*., 2017).

Feasibility and clinical significance of hippocampal sparing has been studied in WBRT, primary brain tumours, patients with >4 BM and fractionated SRS (Daniela Falco *et al*., 2018, Di Carlo *et al*., 2018, Awad *et al*., 2013, Popp *et al*., 2020, Susko *et al*., 2020). However, for patients with limited BM undergoing single fraction SRS, it is less well understood and there is a need for detailed radiotherapy planning studies using the different platforms used to deliver SRS to define the optimal way of delivering SRS while preserving NCF.

Three main SRS delivery platforms are used clinically for treatment as discussed in section 1.2.4.2. The practicality of delivering SRS using linear accelerators (Linacs) is appealing due to the wide availability of Linacs. In Velindre Cancer Centre, SRS treatment is planned using dynamic conformal arc technique using the iPlan TPS (BrainLAB, Germany).

Alternative method of treating on a Linac is volumetric modulated arc therapy (VMAT) which is a form of intensity modulated radiotherapy (IMRT) that uses arc-based therapy to deliver radiation from continuous rotation of the gantry, allowing treatment of the target with a full or partial arc. Treatments are typically delivered with a reduced number of monitor units (MUs) and beam-on time compared with conventional static field IMRT (Salkeld *et al*., 2014). As VMAT is widely available, interest has developed in studying VMAT in comparison with standard SRS techniques. A dosimetric study comparing gamma knife and VMAT rapid arc showed that VMAT was able to achieve an equivalent conformal plan with Paddick's conformity index (PCI) being significantly higher in VMAT plans compared to gamma knife plans (0.76 vs 0.46 respectively, p-value <0.001). Moreover, normal brain tissue volumes were higher in gamma knife plans: 28%, 31%, and 81% higher than VMAT plans for V4, V8 and V12 Gy respectively (Vance Keeling, 2016).

Another radiotherapy planning study conducted by Yidong *et al*., 2010 compared dosimetry and treatment efficacy between VMAT and IMRT. This study showed that VMAT with single or double arcs has the ability to produce highly conformal plans for hypofractionated SRS. VMAT with double rapid arc technique was able to achieve improvement in conformality of PTV coverage, and reduction in OAR doses (Figure 3.1). VMAT was also a more efficient treatment with shorter treatment delivery time and using less monitor units (Yidong Ma, 2010).

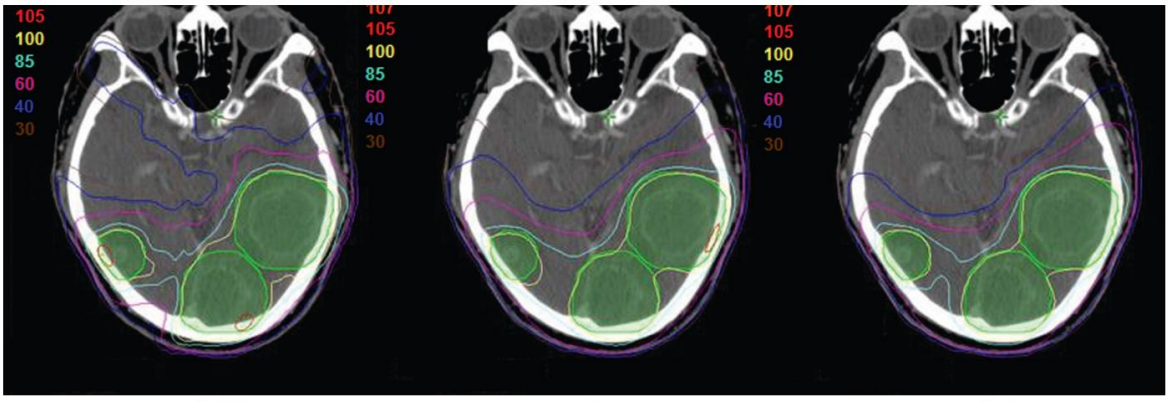

Figure 3.1 Isodose distribution on axial views of a representative case from (Yidong Ma, 2010)*. From left to right, IMRT plan, VMAT plan with single rapid arc, VMAT plan with dual rapid arc respectively. Red line = 105%, yellow = 100%, light blue = 85%, pink = 60% and dark blue 40% of the prescribed dose. PTV contours are indicated in green.*

VMAT has also been shown to be equivalent to CyberKnife and Linac based SRS in patients with multiple BM ranging from 3-8 metastases and 1-4 metastases respectively

(Slosarek *et al*., 2018, Salkeld *et al*., 2014). VMAT was demonstrated to have equivalence in dose conformality, homogeneity and minimized the volume of brain receiving 4 Gy and 12 Gy compared with CyberKnife when treating patients with BM (Slosarek *et al*., 2018). When compared to LINAC based SRS, there was equivalence in conformity indices and volume receiving 12 Gy was lower in VMAT plans (13.3 cm^3 vs 23.3 cm^3) compared with LINAC SRS plans in patients with 1-4 BM. (Salkeld *et al*., 2014).

Despite multiple studies testing equivalence of VMAT delivery platforms for SRS, hippocampal sparing for single fraction SRS has not been widely studied. In addition, hippocampal avoidance is possible during WBRT and fractionated SRS, thus its evaluation in single fraction SRS is required. This is of potential clinical importance as I have demonstrated a number of patients receiving high dose to the hippocampus in Chapter 2. At Velindre Cancer Centre the Linac based dynamic conformal arc technique is used for SRS delivery and so in this chapter, I set out to compare two different planning techniques for Linac based SRS delivery to test the following hypotheses:

- Using the dynamic conformal arc technique, can hippocampal dose be reduced once identified as an OAR?
- Can the VMAT technique produce radiotherapy plans of clinical equivalence and reduced hippocampus dose compared to the dynamic conformal arc technique?

3.2 Methods

3.2.1 Patient Selection

Ten patients with 18 BM ranging from 1-3 BM previously treated with single fraction SRS alone were selected for the study. The patients receiving more than 2 Gy to one hippocampus were selected for this planning study from those identified from the retrospective review conducted in Chapter 2. Table 3.1 shows patients' characteristics.

Patient Number	Number of Metastases	Total GTV volume (cc)	Total PTV volume (cc)
2	1	2.0565	3.419502
6	2	2.9471	4.880648
1	1	3.5763	5.289468
3	1	3.9048	6.838111
7	2	4.2846	7.35451
5	2	5.5791	8.46829
10	3	6.5648	10.57856
8	2	7.9262	11.01803
9	2	10.55	14.95406
4	2	13.159	17.12528

Table 3.1 Patients characteristics ordered in ascending GTV volume ordered in ascending PTV volume measured in cubic centimeters (cc). *GTV: Gross Tumour Volume, PTV: Planning Target Volume,*

3.2.2 Radiotherapy Planning

CT planning was performed on a Siemens Somatom Sensation Open CT simulator in the treatment position, using a Brainlab Head and Neck Localiser box and Frameless SRS Mask System, with 0.6 mm slices. These images were localised using the 'Localisation' module on iPlan RT Image Treatment Planning System (TPS) (BrainLAB, Germany). The RTOG Image localisation defined the stereotactic frame of reference. T1 weighted spoilt gradient echo and T2 weighted MR images with contrast are also acquired on 1.5 Tesla Siemens in the treatment position and subsequently rigidly fused to the localised CT set. The GTV encompassing the metastasis was outlined by the treating clinical oncologist; 1 mm margin is applied to create the PTV. Organs at risk (OAR) that were delineated are eyes, lens, optic nerves, chiasm, brainstem, and remainder of the normal brain. Hippocampus was outlined manually using the RTOG 0933 manual as described in Chapter 2. A 1 mm PRV is added to all OAR volumes.

Prescription doses for the PTV were dependent on its volume as follows; 21 Gy to 80% isodose for PTV < 7 cc, 18 Gy to 80% isodose for PTV 7-13 cc and 15 Gy to 80% isodose for PTV > 13 cc. OAR dose constraints were followed according to SABR Consortium

guidelines v6.1.0 (Table 3.2) (Consortium, 2019). All radiotherapy plans were reviewed by a physicist with minimum 3 years of experience and a clinical neuro-oncologist for quality and safety.

OAR	Constraint	Optimal (Gy)	Mandatory (Gy)
Optic Pathway	DMax (0.1 cc)	-	<8
Brainstem	DMax (0.1 cc)	<10	<15
Normal Brain	D10 cc	<12	-
	D50%	<5	-
Lens	DMax (0.1 cc)	<1.5	-
Orbit	DMax (0.1 cc)	<8	-

Table 3.2 Central Nervous System Dose Constraints as mandated by SABR Consortium (Consortium, 2019). *OAR: Organs at Risk, Gy: Gray, unit of radiotherapy dose, Dmax: dose received by 0.1 cc of the organ.*

Dynamic Conformal Arc Technique

The current planning protocol involves a forward planned, dynamic conformal arc technique using the iPlan RT Dose treatment planning software (BrainLAB, Germany). For control, initial radiotherapy plans that were used to treat the patients were utilised. Re-planning was conducted with the hippocampus visible and was done such that the hippocampal dose was reduced as much as reasonably practicable without compromising plan quality. Plan quality was checked by experienced physicist and measured by conformity, homogeneity, and gradient indices. Dynamic conformal arc plans were created in the iPlan TPS with multiple non-coplanar arcs with angles manually chosen to avoid OARs.

Volumetric Modulated Arc Technique

VMAT plans were generated using Raystation treatment planning software (RaySearch Laboratories, Sweden). This utilised a standard three arc technique that consisted of one 360^{o} coplanar arc and two non-coplanar half-arcs in sagittal oblique plane but avoiding exit through the entire patient. Hippocampus was given equal weighting as other OARs to

achieve lowest possible dose while maintaining dose to PTV and plan quality. Optimisation objectives were applied using a class solution to ensure consistency of plan quality and complexity across all VMAT plans.

Radiotherapy Plan Metrics

Dosimetric plan comparison was performed using a range of plan metrics including PTV coverage (D99%), point maximum in each PTV (D0.1 cc) and OAR doses. In addition, plan quality was assessed using the following indices. These were calculated using Matlab based package called CERR which was independent of all TPS.

Firstly, the Radiation Therapy Oncology Group conformity index (RTOG CI) was used which is a widely used metric employed to describe the quality of SRS plans. This is defined as

$$RTOG\ CI = \frac{\mathrm{PIV}_{100\%}}{\mathrm{TV}}$$

where $PIV_{100\%}$ is the volume covered by prescription isodose and TV is the target volume, which is a standard metric for assessing conformity as recommended by the ICRU (Feuvret *et al.*, 2006). RTOG CI of one represents ideal conformity, a value of greater than one indicates that the irradiated volume is greater than the target volume and includes healthy tissues, while a value of less than one suggests partial irradiation of target volume. An acceptable RTOG CI is between one and two.

Paddick's conformity index (PCI) (Paddick, 2000) builds on RTOG conformity index and is defined as

$$PCI = \frac{(\mathrm{TV}_{\mathrm{PIV}})^2}{\mathrm{TV} \times \mathrm{PIV}_{100\%}}$$

Where TV_{PIV} is the target volume covered by the prescription isodose, $PIV_{100\%}$. This index attempts to give further clarity on the conformity of the prescription isodose through estimation of under- or over-treatment. This index has an ideal value of one and plan quality decreases with decreasing index value. A value of less than one does not

differentiate between under or over treatment, therefore using PCI in conjunction with RTOG CI is more informative.

The dose gradient index (GI) complements the PCI and is defined as

$$GI = \frac{\mathrm{PIV}_{50\%}}{\mathrm{PIV}_{100\%}}$$

where $PIV_{50\%}$ is the volume covered by half the prescription isodose. This metric provides a distinction between plans with similar conformity by examining the dose gradient (Paddick, 2006). In the paper by Paddick, it ranged from 2.4 to 3.3 with a mean value of 2.83 for fifty-eight targets treated using Gamma Knife (Paddick, 2006).

Homogeneity Index (Feuvret *et al.*, 2006) was also calculated to quantify dose homogeneity within the PTV:

$$HI = \frac{Dmax}{RI}$$

where Dmax is the maximum isodose within the target and RI is the prescription isodose. A value of two or less is acceptable. Greater than two but less than 2.5 is considered to be a minor deviation and value of greater than 2.5 is a major deviation.

3.2.3 Statistics

Radiotherapy plan data from TPS was exported in DICOM format into Matlab. For consistency, the aforementioned metrics were analysed using the Matlab based package CERR independent of both planning systems. The spreadsheet was exported to SPSS for statistical analysis and graphs.

3.3 Results

Ten patients were identified who had received a dose of greater than 2 Gy to the ipsilateral hippocampus. A total of 18 BM were treated, three patients with one

metastasis, six patients with two metastases and one patient with three metastases. Prescribed radiotherapy dose varied from 15 Gy to 21 Gy depending on the PTV volume. Mean GTV and PTV was 3.36 cc and 4.996 cc respectively (Table 3.1). Analysis of plan metrics and RT doses was compared in the three groups: original RT plan, RT re-plan using dynamic conformal arc with hippocampus volume, and RT re-plan using VMAT techniques.

All iPlan and VMAT plans were clinically judged and met accepted quality criteria for RTOG and ICRU. When comparing the VMAT and the two iPlan SRS plans, there were no significant differences in the homogeneity indices across the three groups, see table 3.3 for statistical values. PCI was significantly better in both re-planned groups compared to the original RT plan. There was a non-significant trend towards higher gradient index in both re-planned groups, owing to reducing the dose deposition in the hippocampus where PTV was in close proximity with the hippocampus (Table 3.3, Figure 3.2).

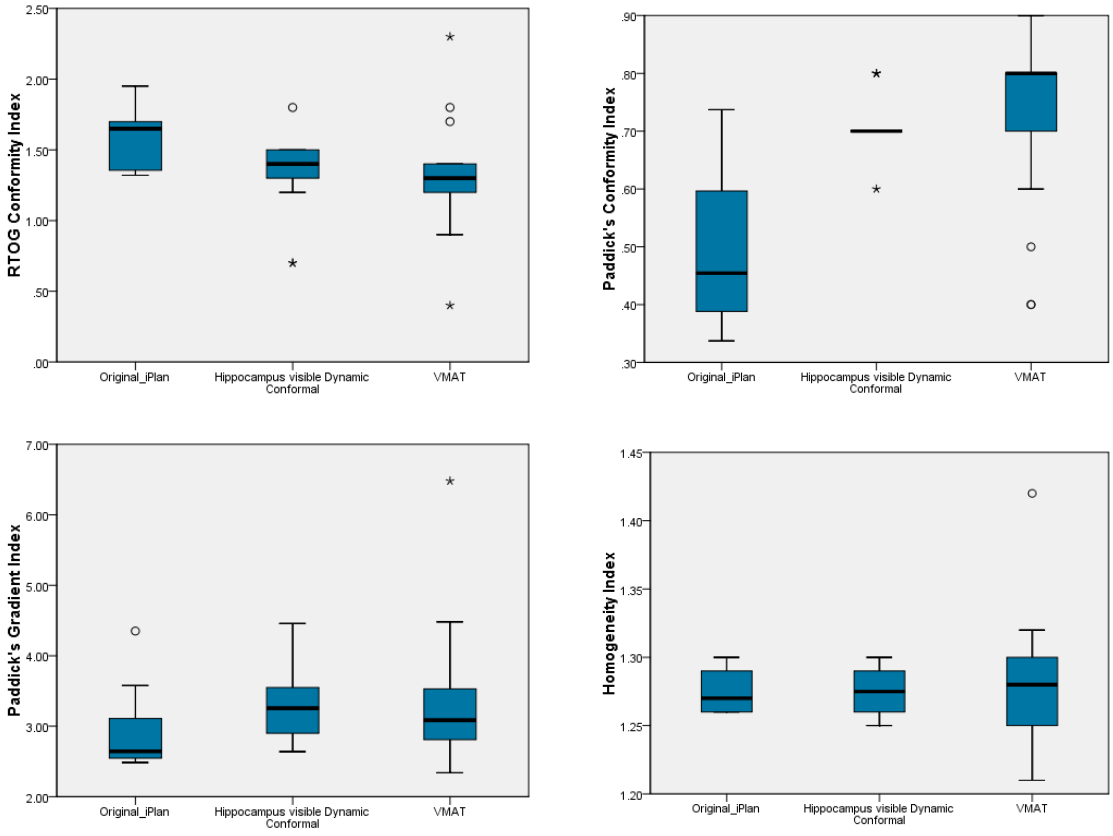

Figure 3.2 Box Plot demonstrating RTOG Conformity Index, Paddick's Conformity Index, Paddick's Gradient Index and Homogeneity Index in the 3 groups*. Values > 1.5 box lengths are outliers, marked with °, and values > 3 box lengths are marked with **.*

Dose delivered to the PTV across the three groups were comparable: dose delivered to the 99% of the PTV (D99%) and dose delivered to 2% of the PTV (D2%) were not significantly different statistically (p-value >0.05). Therefore, all three techniques were able to deliver similar doses to the PTV that were accepted clinically. Although with PTV 1 and 16, replans were able to achieve a higher dose to PTV, compared to others, there was no striking difference about the size and location of these PTVs. See Figure 3.3.

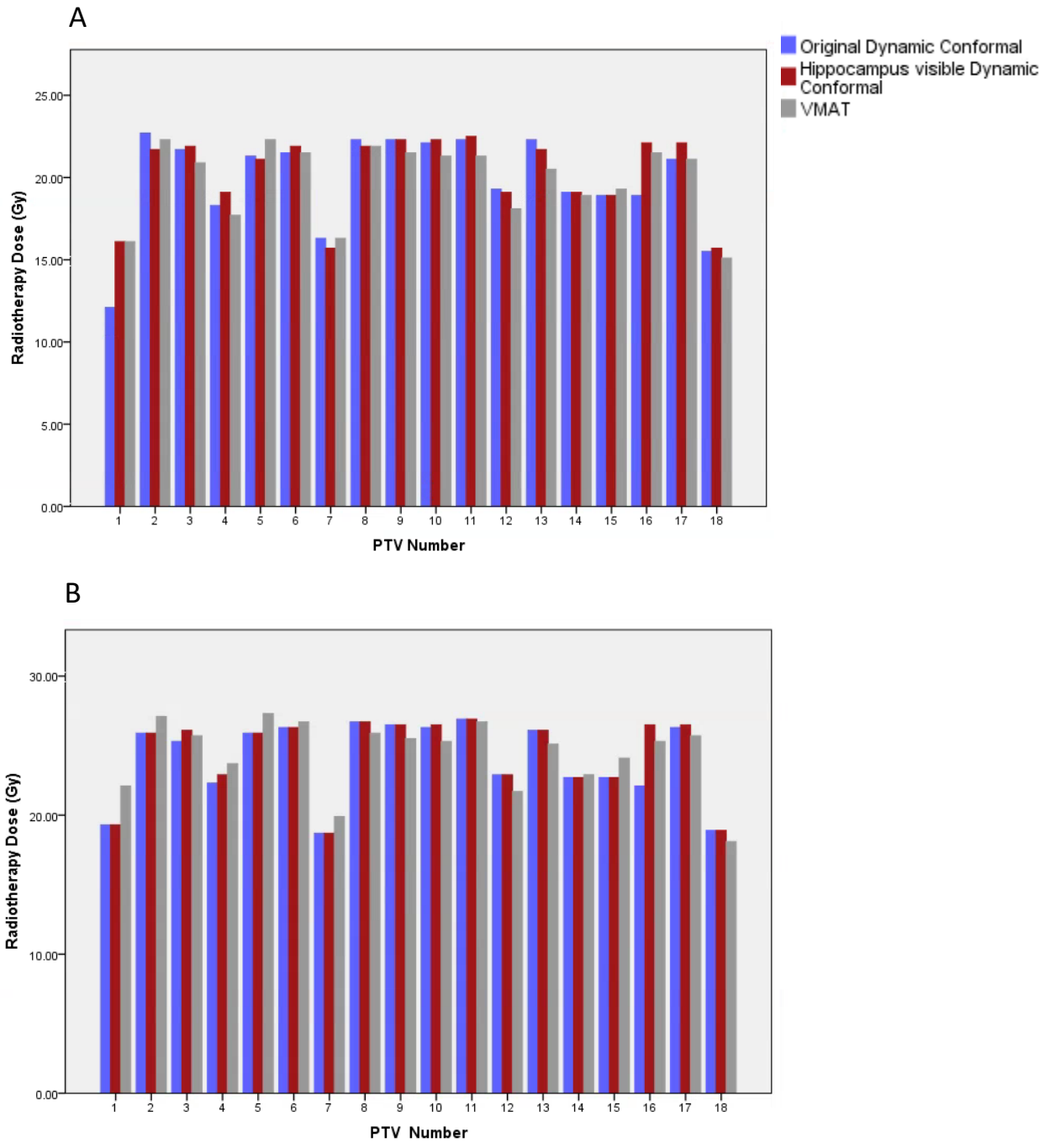

Figure 3.3 Dose delivered to the Planning Target Volume (PTV) in all 3 groups. *Graph A Dose received by 99% of PTV, Graph B represents Dose received by 2% of PTV*

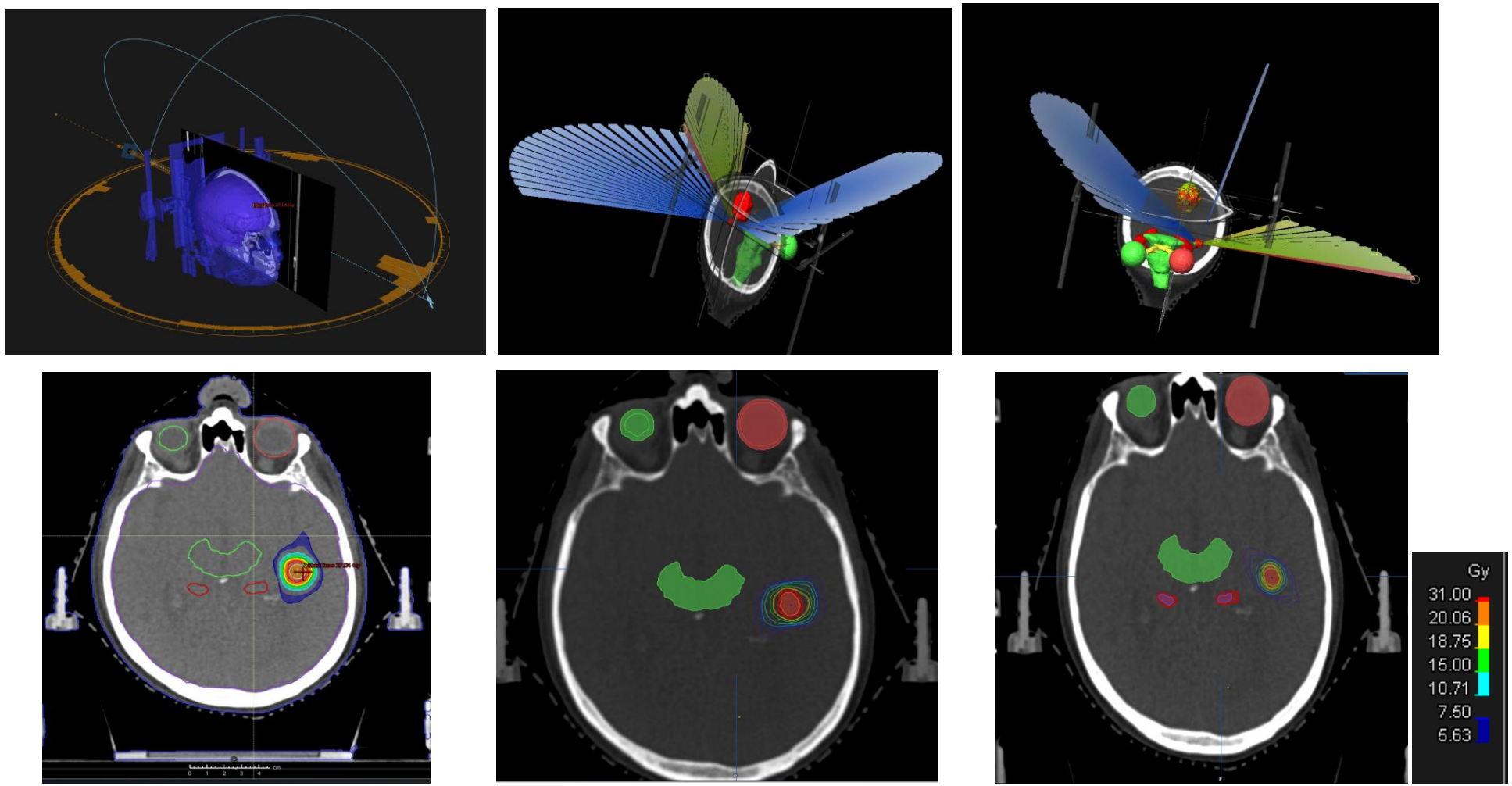

Figure 3.4 Radiotherapy Plans of brain metastases in a 64 year old male with renal cell carcinoma. *Top row represents (left to right) VMAT plan with 1 full arc and 2 partial arcs, original DCA plan with 3 arcs and re-plan with DCA using 3 arcs minimizing dose to the hippocampus. Bottom row represents the respective axial slice of CT showing dose distributions. Hippocampus is outlines in red and brainstem is outlined in green. Respective isodoses colour are displayed.*

Figure 3.4 demonstrates a representative case of the impact of hippocampal avoidance on the dose gradients. The middle plan in this figure is the original plan that used the DCA technique without the knowledge of hippocampus presence. In order to avoid the hippocampus, the dose is shifted to other areas of the brain, which in turn has an impact on the gradient index as discussed above.

3.3.1 Hippocampal Dosimetry

Using DCA and VMAT techniques hippocampus doses were significantly reduced without significant impact on plan conformity and other OAR doses (See Table 3.3). There was higher volume receiving 1 Gy (V1 Gy) in left and right hippocampi with VMAT plans compared to the re-plan DCA plans. The majority of the other dose constraints for the hippocampus were comparable between the DCA re-plan and VMAT plans. The length of arc and continuous radiation from the full arc being used in VMAT plans can potentially lead to increased low dose bath compared to DCA techniques. Figure 3.4 demonstrates the location and length of arcs being used in the three groups. The significance of low dose delivered to radiosensitive structures such as the hippocampus is unknown.

Figure 3.5 demonstrates dose to 0.1 cc of the individual hippocampi in all three groups and dose received during each of the radiotherapy plans for each individual case. Overall, there was a non-significant trend towards DCA technique achieving lower doses to the hippocampus compared with VMAT. The limited sample size might have resulted in an underpowered study leading to a false negative. In most cases there was an increase in the dose received by the contralateral hippocampus with VMAT technique when compared to the original and hippocampus visible DCA technique. All cases except case three illustrate this: whilst VMAT technique has demonstrated a dose reduction within the left hippocampus, right hippocampal dose has increased slightly which may prove to be clinically non-significant.

Dose Statistic	Original Plan		Dynamic Conformal Arc		VMAT		p-value		
	Mean	Range	Mean	Range	Mean	Range	Original vs DCA	Original vs VMAT	DCA vs VMAT
Hippocampus									
Left, D 0.1 cc	4.02	0.30-7.90	2.64	0.3-6.7	3.15	1.00-6.6	**0.035**	**0.028**	0.463
Left, D 40%	2.00	0.10-5.10	0.87	0.0-2.7	1.53	0.5-2.5	**0.044**	**0.049**	0.105
Left, D 70%	1.12	0.10-2.50	0.55	0.0-2.1	0.85	0.3-1.7	**0.049**	**0.027**	0.243
Left, V 1 Gy	0.50	0.00-2.23	0.49	0.0-2.22	1.15	0.15-2.30	0.977	0.448	**0.041**
Right, D 0.1 cc	3.24	0.3-9.1	1.41	0.0-3.9	2.63	0.9-4.9	0.097	0.191	0.130
Right, D 40%	1.56	0.3-4.5	0.55	0.0-2.1	1.13	0.0-2.3	**0.03**	0.260	**0.045**
Right, D 70%	0.96	0.1-3.1	0.35	0.0-1.1	0.67	0.0-1.5	**0.03**	0.228	**0.035**
Right, V 1 Gy	2.00	0.00-4.13	0.71	0.0-4.24	1.17	0.02-2.3	**0.04**	**0.024**	0.667
Whole Brain									
Whole Brain D10 cc	13.74	6.5-18.7	14.64	10.1-18,7	14.35	8.0-17.9	0.201	0.514	0.476
Whole Brain V 12 Gy	15.26	6.15-24.37	15.96	7.73-24.39	15.22	5.72-21.44	0.789	0.978	0.836
Whole Brain V 5 Gy	71.87	14.89-138.16	82.69	35.05-138.52	69.83	18.37-103.72	0.555	0.584	0.329
Whole Brain V 3 Gy	185.08	21.46-324.45	195.14	88.24-311.63	176.32	46.79-267.39	0.805	0.582	0.606
Whole Brain V 1 Gy	533.45	71.06-853.31	524.80	197.17-804.95	585.17	295.29-821.51	0.932	0.920	0.525
Other Brain Structures									
Brainstem D0.1 cc	6.48	1.7-18.1	5.94	0.5-18.1	6.80	2.0-19.0	0.839	0.867	0.744
Optic Chiasm D0.1 cc	0.66	0.1-3.9	0.78	0.1-4.3	0.79	0.0-2.1	0.781	0.667	0.452
Eye, Right D0.1 cc	0.22	0.1-0.5	0.30	0.1-0.9	0.97	0.0-3.5	0.388	**0.001**	**0.003**
Eye, Left D0.1 cc	0.18	0.1-0.3	0.24	0.1-0.3	0.71	0.0-2.0	0.196	**0.028**	**0.023**
Lens, Right D0.1 cc	0.16	0.1-0.3	0.16	0.0-0.3	0.31	0.0-1.7	0.830	**0.036**	**0.040**
Lens, Left D0.1 cc	0.14	0.1-0.3	0.15	0.0-0.3	0.25	0.0-1.0	0.820	**0.084**	0.164
Optic Nerve, Right D0.1 cc	0.62	0.1-3.7	1.11	0.0-4.9	0.63	0.0-2.3	0.471	0.985	0.066
Optic Nerve, Left D0.1 cc	0.44	0.1-2.3	0.51	0.0-2.5	0.43	0.0-1.1	0.822	0.982	0.909
PTV									
RTOG CI	1.60	1.1-2.0	1.35	0.7-1.8	1.31	0.4-2.3	**0.011**	**0.021**	0.727
PCI	0.49	0.3-0.6	0.71	0.6-0.8	0.72	0.4-0.8	**<0.0001**	**<0.0001**	0.879
GI	2.89	2.49-4.35	3.30	2.63-4.45	3.33	2.34-6.48	0.120	0.123	0.233
HI	1.27	1.26-1.30	1.27	1.25-1.30	1.28	1.21-1.42	0.895	0.662	0.624
PTV D 99	19.83	16.0-22.0	20.28	16.0-22.0	19.83	16.0-22.0	0.610	0.519	0.567

Table 3.3 Dose Statistics for original SRS plan without hippocampus, Dynamic Conformal Arc (DCA) plan with hippocampus visible, and Volumetric Arc Therapy (VMAT) for all 10 cases. *Statistically significant results are highlighted in bold.*

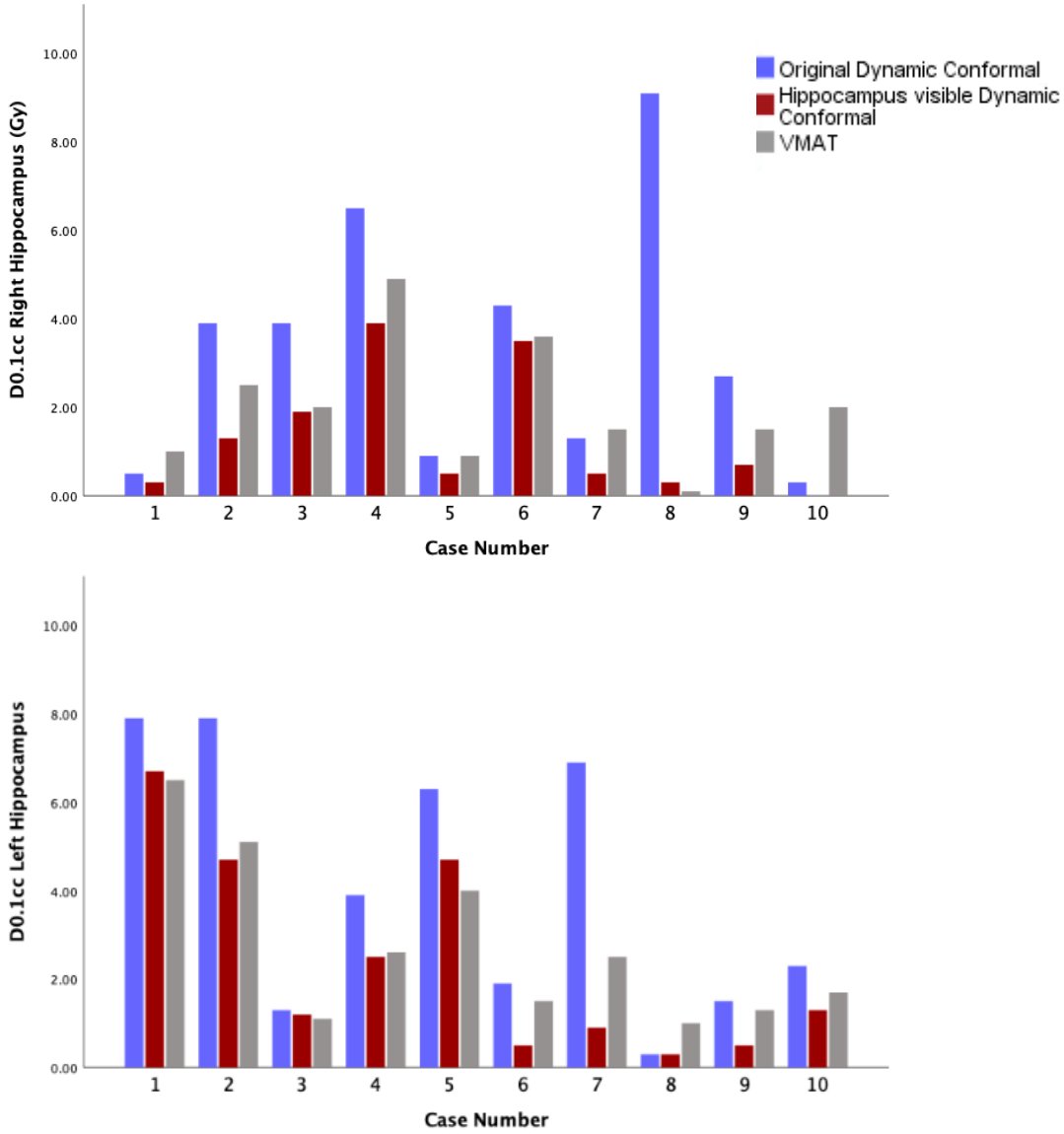

Figure 3.5 Bar graph representing dose delivered to left and right hippocampi for each plan. *D0.1 cc: Dose received by 0.1 cc of respective hippocampi*

In cases where the hippocampus was within 1 cm of the metastases, the dose reduction was still achievable, but not a degree that might be considered clinically relevant (e.g., case 1 and 2 left hippocampus and case four of the right hippocampus). Dose to the left hippocampus in seven and right hippocampus of case 1 and 8, a significant reduction in hippocampal dose was apparent. This is likely to be related to the position of the metastases. If the metastases are abutting or in close proximity to the hippocampus, i.e., within 1 cm, it may be more challenging to reduce the dose delivered to the hippocampus down to a clinically relevant reduction. However, if the metastases were further away, e.g. in Case 8 there was 2.4 cm distance between the PTV and metastases, it was possible to reduce the dose significantly (See Figure 3.6).

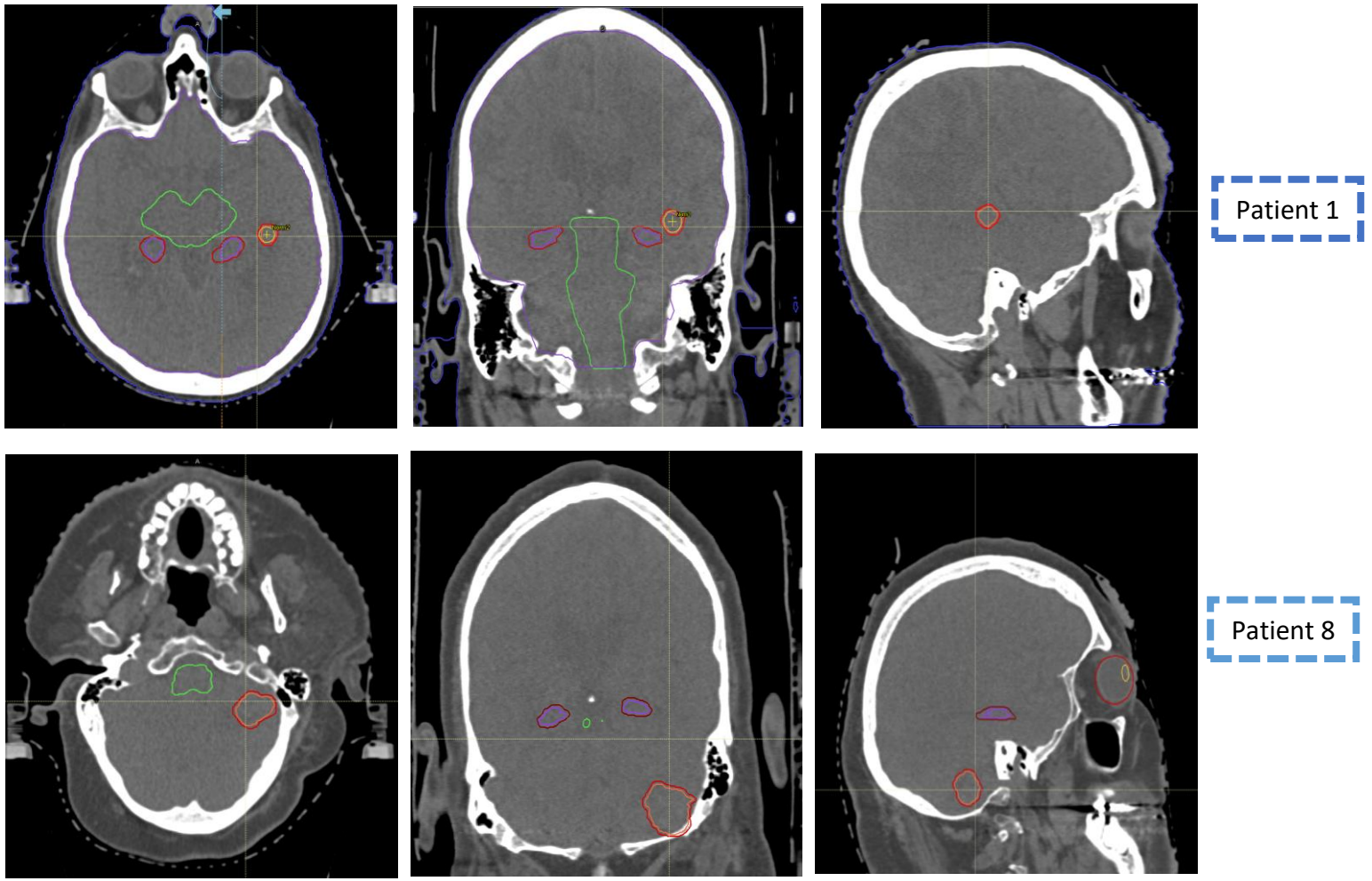

Figure 3.6 Axial, Coronal and Sagittal planes of patient 1(top) and patient 8(bottom) illustrating the position of metastases (GTV in orange and PTV in red) in relation to the hippocampus (in purple). *Brainstem is delineated in green. Patient 1, a 64 year old male with renal cell carcinoma, is where dose was reduced by 1 Gy and Patient 8, a 48 year old female with NSCLC, is where the dose was reduced by 7 Gy during the radiotherapy replanning process*

3.3.2 Other Organs at Risk

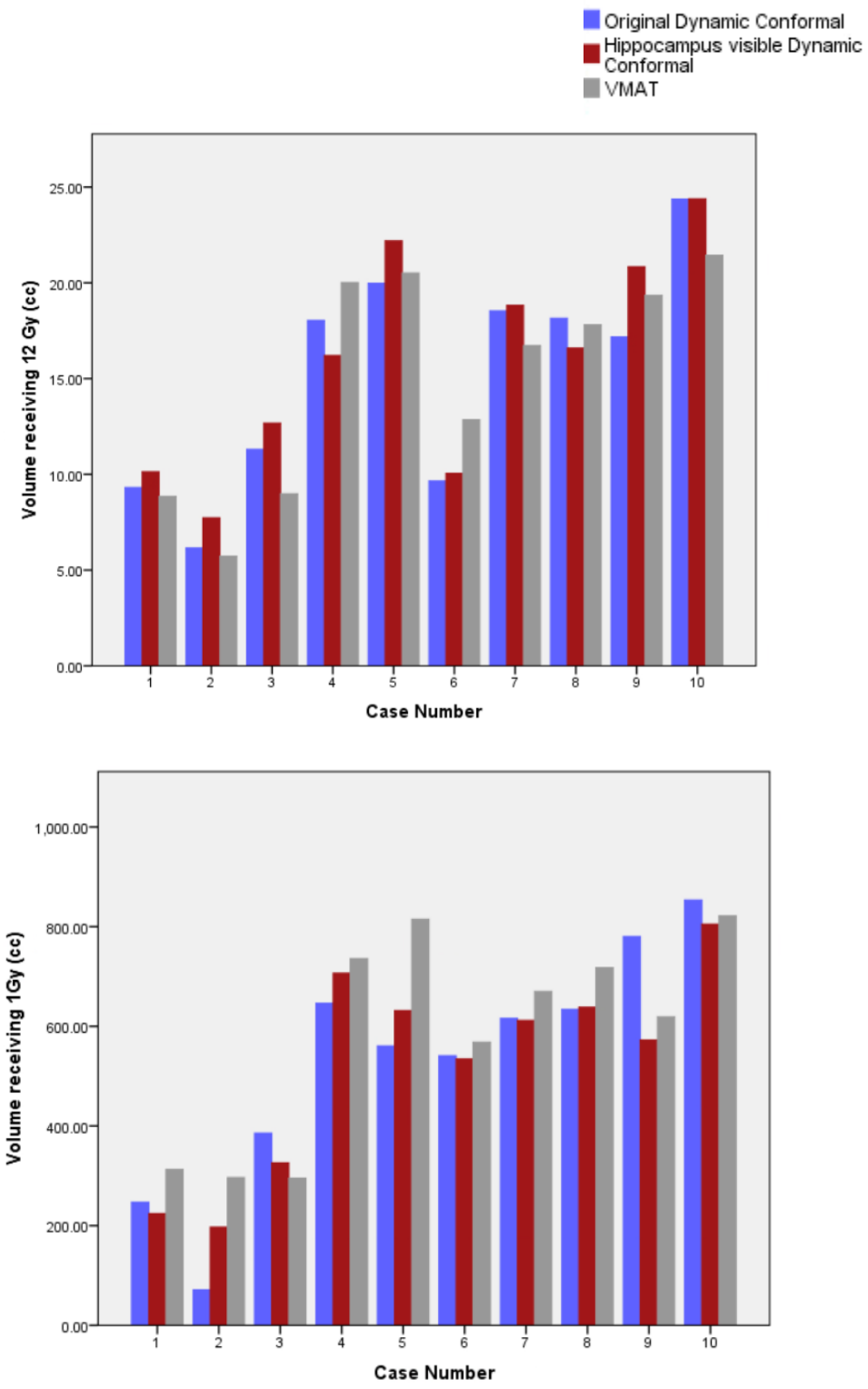

Figure 3.7 Bar graph demonstrating total brain volume receiving 12 Gy and 1 Gy dose for each plan.

VMAT led to higher volumes of brain receiving 1 Gy, however the volume of brain receiving 3 Gy and 5 Gy was lower in VMAT planned treatment than DCA plans. Dose received by 10 cc and volume receiving 12 Gy were equivalent. There was no statistical significance in the whole brain doses in the individual cases or in the mean across the three groups (See table 3.3 & figure 3.7).

There was no statistically significant difference in dose received by the brainstem or optic chiasm, this was because these organs at risk were given similar objectives to hippocampus during the planning process.

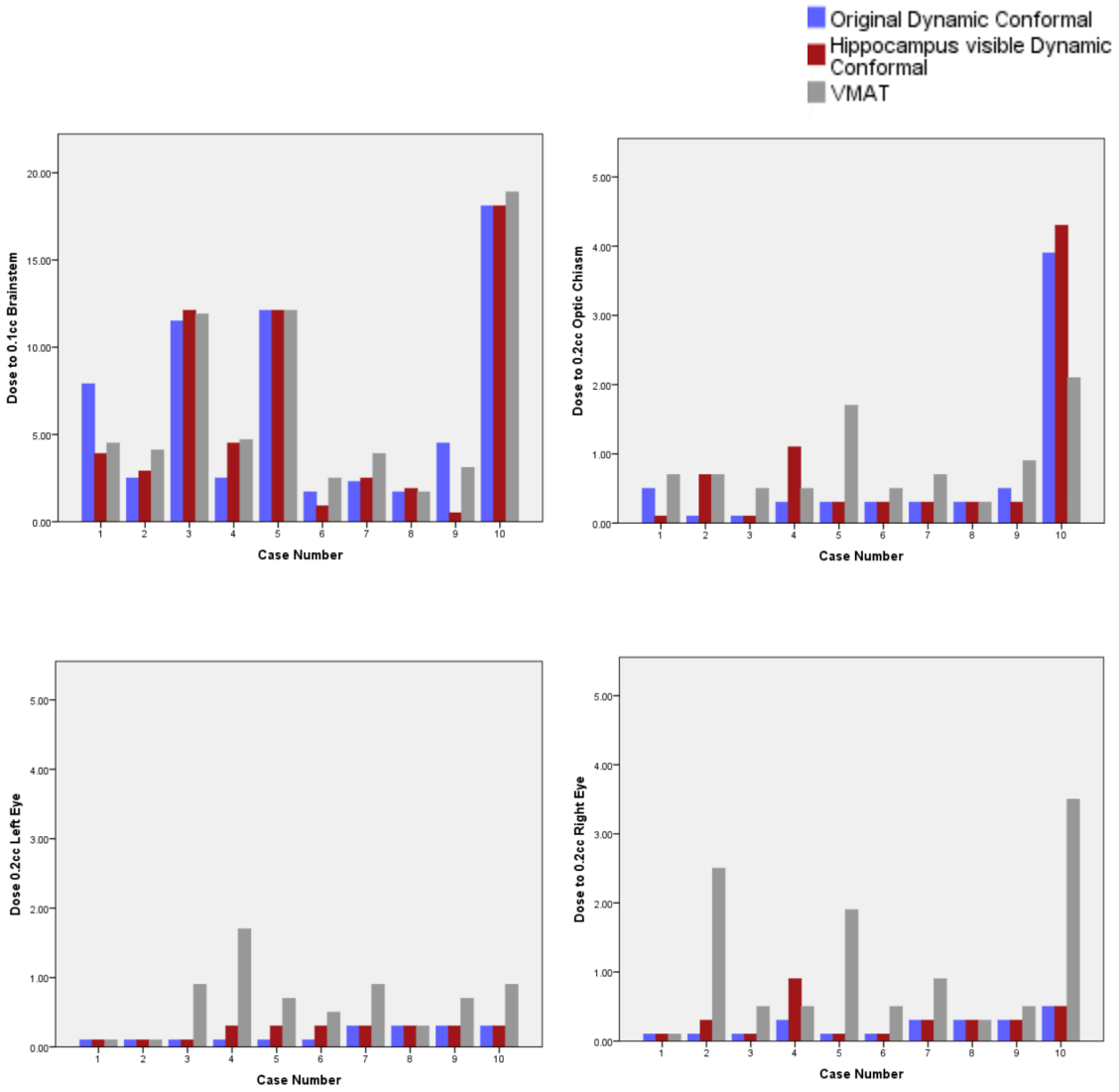

Figure 3.8 Dose constraints for organs at risk for each plan: Brainstem, Optic Chiasm, left and right eye.
All doses are displayed in radiotherapy Gy units.

Slightly higher doses, but within the tolerance of SABR consortium guidance, were delivered to the orbital structures. When radiotherapy dose is being pushed away from one organ, it is deposited elsewhere and as a trade-off, slightly higher dose to other OARs while maintaining the dose tolerance as per national guidance would lead to a more acceptable plan with respect to hippocampal dosing. VMAT led to statistically significant higher doses in other organs at risk in comparison to DCA (See table 3.3, Figure 3.8).

3.4 Discussion

This planning study has demonstrated that both VMAT and DCA techniques can achieve overall radiotherapy plan equivalence in achieving lower doses to the hippocampus while maintaining plan conformity, dose to the PTV and other OARs. Both VMAT and DCA techniques were capable of achieving SRS quality treatment plans for patients with 1-3 BM with accepted levels of conformity and homogeneity.

Hippocampus dose was significantly reduced using DCA and VMAT techniques, more so with DCA technique than VMAT, although both techniques were not significantly different in the hippocampal avoidance group. We have demonstrated here that it is feasible to reduce the dose to the hippocampus and treating it like other OARs can lead to significant reduction in radiotherapy dose. As hippocampus is implicated in NCF decline, and SRS use is increasing, it is important to consider outlining the hippocampus and reducing the dose where feasible in the radiotherapy planning process. Hippocampal avoidance has been studied more widely in patients undergoing WBRT and multiple BM usually >4. However, we have demonstrated here that it is an important factor to consider in any patient undergoing SRS.

Plan quality was evaluated for conformity and homogeneity using RTOG CI, RTOG HI, Paddick CI and Paddick GI. There are limitations of these indices, and it remains debatable as to which indices should be used in routine clinical practice. For example RTOG CI does not account for the degree of spatial intersection of the two volumes of their shapes (Feuvret *et al*., 2006). Therefore, a conformity index on its own does not provide meaningful practical information and should be assessed by visualization and dose volume histograms.

There were no differences observed in homogeneity indices within the three groups. However, the replanning exercise using DCA and VMAT both led to an increasingly conformal plan compared to the original radiotherapy plan. Gradient index showed a non-significant trend of higher dose gradient in the hippocampal avoidance RT plans, likely due to avoiding dose deposition in close proximity to hippocampi.

The normal brain V12 Gy (volume of brain receiving 12 Gy) isodose, which includes the healthy brain surrounding the BM is an important metric for development of symptomatic radionecrosis. VMAT and DCA plans led to equivalent values of V12 Gy. VMAT led to increased delivery of low doses e.g., 1 Gy to the hippocampus and normal brain. It is possible that use of 360° arc led to this and future replanning studies should investigate advantages and disadvantages of using partial arcs vs full arcs. Whilst 1 Gy may not be significant for the normal brain, the significance of this for radiosensitive structures such as the hippocampus is unknown.

During the radiotherapy plan optimization process, dose being reduced in one area leads to higher doses in other areas. However, there is often a trade off between significance of the dose deposition depending on the organ. For example, in this planning study, reducing the hippocampal dose led to slightly increased doses, albeit within the tolerance, to the orbital structures. In addition to this in all cases except case three, contralateral hippocampus dose was increased slightly whilst reducing the dose to the ipsilateral hippocampus. These plans were clinically acceptable as despite the slight increase in dose, they were still within the optimal radiotherapy tolerance.

Time taken to delineate hippocampus was not measured, however, if this becomes a standard OAR to delineate it would be crucial to measure this in future studies. A number of planning systems also have the tool for auto delineation of OARs which may not be too cumbersome on the planners.

3.5 Conclusions

DCA and VMAT both techniques have proven to produce plans that are deliverable clinically and meet the dose constraints and plan quality described by RTOG and the UK

SABR Consortium whilst reducing the dose delivered to the hippocampal region. I have demonstrated so far that there is a considerable proportion of patients undergoing SRS in whom hippocampus received a significant dose and it is possible to reduce the dose the hippocampus by outlining this as an OAR like others OARs such as brain stem, chiasm, optic nerves, and the optic apparatus. However, the dose tolerance of hippocampi and its significance in contribution to NCF impairment followed SRS remains largely unknown. The next chapter focuses on developing a prospective study of patients undergoing SRS for BM to study NCF impairment, hippocampal dosimetry and functional MRI assessment of the hippocampi and other brain regions involved in NCF.

Chapter 4- Designing a prospective study for patients undergoing stereotactic radiosurgery – A clinical observational study to measure neurocognitive function before and after treatment with a translational imaging component to study the accompanying hippocampal changes following radiotherapy

4.1 Introduction

SRS and WBRT has demonstrated a survival benefit over WBRT alone, establishing SRS treatment for 1-3 BM (Andrews *et al*., 2004, Aoyama *et al*., 2015). This improved outcome has put greater emphasis on quality of life (QoL) following treatment and particularly on the deleterious effect on NCF of WBRT. Consequently, SRS is recommended without WBRT, in favour of close surveillance, as a strategy to preserve NCF (NICE, 2018). Nevertheless, even in patients treated with SRS alone a sizeable proportion of patients (24% of patients reported in randomised trials) suffer NCF impairment, with memory the most commonly affected neurocognitive domain (Chang *et al*., 2009). In the most recent randomised trial, NCF impairment has been reported to be 60% (Brown *et al*). The RANO group advocate use of standardised NCF tests in patients with brain tumour and BM to examine different aspects of NCF (Lin *et al*., 2013).

Neurosurgical experience has described eloquent brain regions to be carefully avoided, however, understanding of regional vulnerability for radiotherapy is limited. Current clinical practice for SRS is to consider and minimise dose to the brain stem, optic pathway, eye apparatus, cochlea, and spinal canal and the remaining brain parenchyma is treated homogeneously in terms of risk of radiotherapy exposure (Consortium, 2019). There is increasing evidence that radiosensitivity varies within the brain from human and animal studies as discussed in Section 2.1.

The effect of radiation on neurogenesis in the hippocampus has been implicated in NCF impairment (Gondi *et al*., 2012, Makale *et al*., 2017) - evident following WBRT and techniques such as hippocampal–sparing radiotherapy which have been evaluated to limit hippocampal radiation dose during WBRT (Konopka-Filippow, 2019, Awad *et al*., 2013). However, limited information exists to define radiation dose tolerance constraints for the hippocampus either for standard radiotherapy fractionation or for SRS. Equally, other structures exist within the brain that are likely to be important for NCF, including the amygdala, and prefrontal cortex, which have not been as extensively evaluated for the effect of radiation on NCF and only limited studies have correlated neurocognitive outcomes with radiation dose and neurophysiological change in these structures. Mechanistic understanding of neurocognitive decline following radiotherapy is also limited although different hypotheses exist including vascular injury, white matter injury, loss of brain plasticity, functional network disruption and cortical loss (Makale *et al*., 2017).

One hypothesis is that synergistic effects of vascular endothelial injury, glial cell destruction and inflammatory effects of radiotherapy lead to its acute adverse effects. MRI is the most widely available non-invasive method with a potential to detect biologically diverse radiotherapy-induced changes. White matter injury may be a result of vascular damage, therefore vascular changes may precede detectable changes in diffusion metrics of white matter change. Likewise, metabolic changes identified by spectroscopy may occur ahead of structural changes such as reduction in volume (Schuff *et al*., 1999). Schuff *et al*., demonstrated that reduction in metabolites such as N-acetyl aspartate (NAA) provides stronger support for neuronal loss in the aging hippocampus than volume measurements alone (Schuff *et al*., 1999).

Seibert *et al*., demonstrated increased sensitivity of 9 cortical regions (entorhinal cortex, inferior parietal, inferior, middle, and superior temporal, temporal pole, isthmus cingulate, parahippocampal and superior frontal) to radiation in patients with brain tumour undergoing fractionated radiotherapy compared to other cortical regions defined in the

Desikan-Killany atlas (Seibert *et al*., 2017b). There was a significant reduction in cortical thickness 1 year post radiation in the aforementioned regions. As it was a retrospective study, there were several limitations and impact of other concomitant treatments such as surgery and chemotherapy (Seibert *et al*., 2017b). Another study conducted by the same group showed dose dependent hippocampal atrophy in patients who received high dose to the hippocampi (>40 Gy) vs those who received low dose (<10 Gy). Hippocampal volume decreased by 6% at 1 year in the high dose group (Seibert *et al*., 2017a). This was also a retrospective study and analysis of the group in which doses between 10 and 40 Gy would have been received by the hippocampus was not presented. This degree of reduction in hippocampal volume is considered to be significant and is thought to be related to radiation rather than normal ageing processes as , typically, reduction of less than 1% is expected in the population as a result of ageing (Chincarini *et al*., 2016). Increased sensitivity of certain regions in the brain, in particular frontal and temporal regions, has also been demonstrated in imaging studies of paediatric populations (Ajithkumar *et al*., 2017). Another hypothesis is that atrophy over time may not be a true finding if it was caused by resolution of oedema (Armstrong *et al*., 2005). These studies highlight the importance of matching imaging findings to radiotherapy doses and measures of NCF.

This chapter will focus on the MRI protocol development and healthy volunteer scans performed at CUBRIC to assess the tolerance of scans and robustness of the MRI analysis pathways. Chapter 5 and 6 will examine baseline clinical and MRI data respectively and identify potential confounding factors. Chapter 7 will describe NCF and MRI changes at follow up. Chapter 8 will study multiparametric MRI imaging of the BM and its response to treatment.

4.2 Clinical Design

In order to study neurocognitive impairment following SRS a clinical observational study was designed with the aim of measuring NCF in patients prospectively before and after SRS treatment. We aimed to recruit forty patients from Velindre Cancer Centre (VCC) and

perform detailed NCF testing before SRS and at 3 time points following treatment: 1 month, 3 months and 6 months. To measure structural and physiological changes before and after treatment a translational MRI study was also performed with Cardiff University Brain Research Imaging Centre (CUBRIC) in a subset of thirty patients, whereby patients underwent MR imaging at CUBRIC before and at 2 time points following SRS: 1 month and 3 months.

4.2.1 Sample Size

An observational study was designed to recruit forty patients undergoing SRS only for one to three BM over a 2-year period (April 2017 till April2019). Recruitment of forty patients was based on feasibility and analysis of patients treated with SRS at Velindre Cancer Centre. As evident from my retrospective study, approximately thirty patients are treated with SRS in VCC in 1 year, thus by recruiting forty patients in 2 years we aimed to recruit 66% of the potential eligible patient population. Imaging sub-study was limited to thirty patients due to funding limitations and cost of research MRI scans. For the purposes of this study, patients were included who were recruited from April 2017 till December 2018. All comers presenting to Velindre Cancer Centre undergoing SRS and fulfilling the inclusion criteria were approached for the study.

4.2.2 Inclusion and Exclusion Criteria

Inclusion criteria

- Patients ≥ 18 years of age
- WHO Performance status 0 - 2
- All patients must have undergone prior assessment by the South Wales Neuro-Oncology MDT and SRS must be the recommended treatment with the collective agreement of the MDT.

- Patients will have one to three cranial metastases undergoing stereotactic radiosurgery.
- Patients will have established diagnosis of cancer and absent or controllable primary disease with an estimated prognosis of ≥ 6 months.
- Pre-treatment scans must not show a tumour volume of more than 20 cc. This will usually mean that no individual tumour has a diameter in excess of 3 cm.
- A brain magnetic resonance imaging (MRI) scan (may be the MRI planning scan) will be required within 1 month of recruitment to the study.

Exclusion criteria

- Contra-indication to MRI
- Patients presenting with pressure symptoms best relieved by neurosurgery
- Prior history of neurosurgery, SRS or WBRT
- Histological diagnosis of leukaemia, lymphoma, germ cell tumour or small cell carcinoma.
- Presence of leptomeningeal disease.
- Pregnancy
- Patients with pre-existing diagnosed neurocognitive dysfunction

4.2.3 Objectives of the Study

The objectives of this study were:

1) To measure changes in NCF in patients receiving SRS at VCC for one to three BM at 1-, 3-, and 6-months following treatment.
2) To correlate radiation dose received by the hippocampus with changes in NCF and identify if radiation dose parameters to these structures correlate with NCF decline at 1-, 3-, and 6- months following treatment.
3) To measure structural, physiological, metabolic and diffusion changes in the hippocampus following SRS using MRI and correlate these with NCF change at 1-, and 3- months.

Moreover, I used this opportunity to perform multi-parametric MRI imaging of the metastases. The objectives were:

1) Measure change in perfusion of the metastases at baseline and 1-, and 3 months interval and correlate with response and progression
2) Assess feasibility of microstructure MRI in patients with BM
3) Changes in brain tissue in close vicinity of the metastases

4.2.4 Timing of Assessments

Patients were screened at the South Wales Neuro-Oncology multi-disciplinary team (MDT) meeting that occurred on a weekly basis. Patients fulfilling the inclusion and exclusion criteria were approached and provided with a patient information leaflet (Appendix A). Patients were given at least 24 hours to read the information provided and before considering participating in the study. Once written consent was given patients underwent baseline NCF testing and completed questionnaires regarding QoL. This was done at one of the visits for SRS treatment planning appointments. If patients also gave consent for the translational MRI study, baseline research MRI was organised at CUBRIC prior to SRS treatment. Subsequent assessments were done between 20-40 days, 80-100 and 160-200 days for 1 month, 3 month, and 6 months, respectively. MRI, NCF and QoL assessments were done at 1 and 3 months, whilst NCF and QoL assessments were performed at 6 months only. Figure 4.1 demonstrates the timeline of assessments performed in this study. Details of the NCF testing battery and MRI scanning protocol used in our study are discussed in section 4.3 and 4.4, respectively.

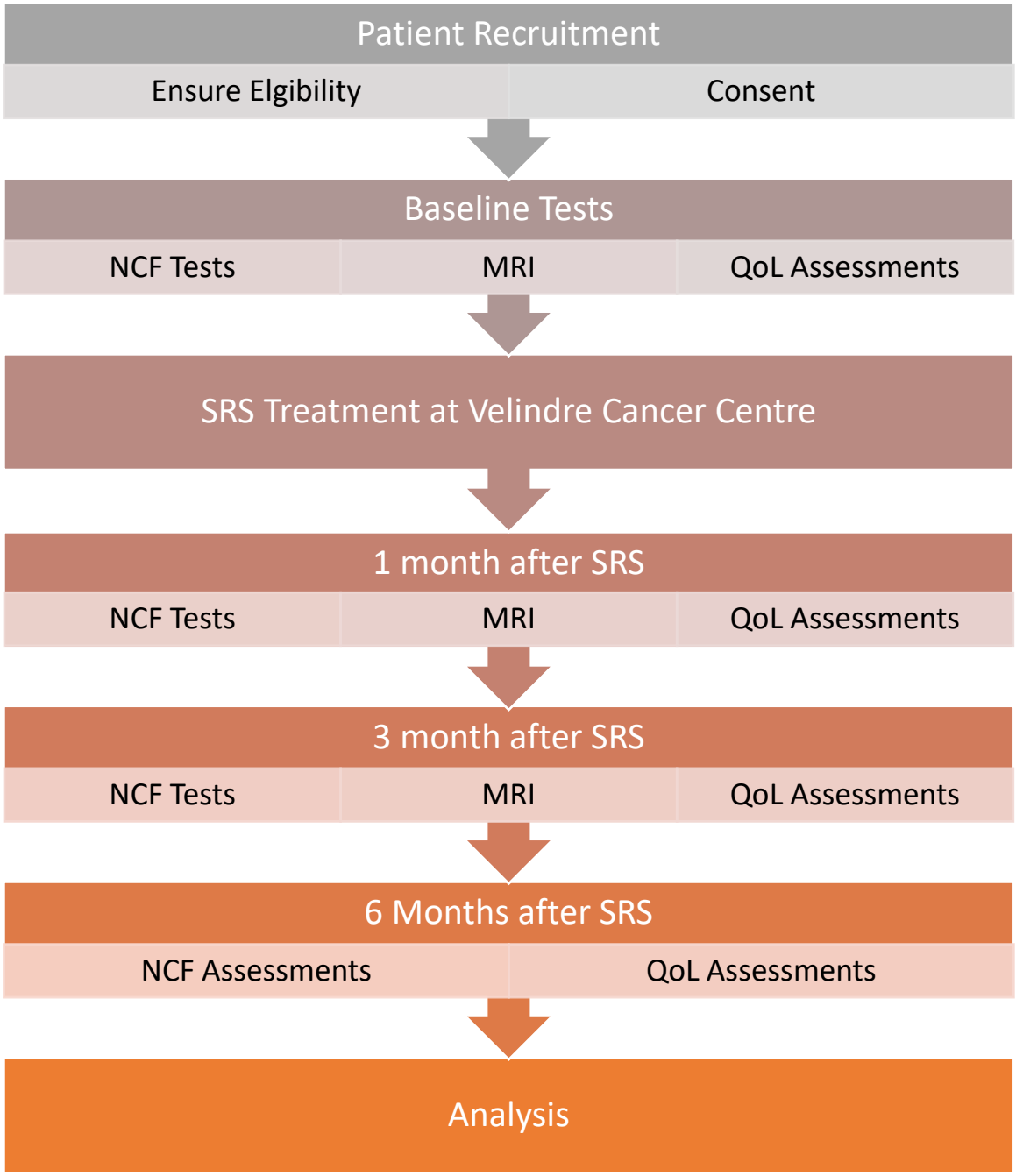

Figure 4.1 Flow diagram showing timing of NCF and MRI assessments done in the study at different time points. NCF: Neurocognitive Function, MRI: Magnetic resonance imaging, QoL: Quality of Life, SRS: Stereotactic Radiosurgery. Not all patients had MRI scans, they were given the option to participate in NCF only or NCF and MRI.

4.3 Neurocognitive Function Testing

4.3.1 Neurocognitive testing – Background

The response Assessment in Neuro-Oncology (RANO) working group recommend inclusion of survival, radiological response, objective, and subjective patient related outcomes. Objective patient related outcomes can be measured using a battery of NCF testing whereas subjective outcomes can be measured using health related quality of life (Lin *et al*., 2013).

The selection of NCF tests in an assessment battery should be guided by the specific questions posed in the relevant clinical context. McDuff *et al*., states that domains that may be involved in radiation induced injury following WBRT include global NCF impairment, memory, executive function, attention, and motor speed (McDuff *et al*., 2013). NCF tests utilised in this study measured performance in the following domains: memory, processing, executive function, verbal fluency, attention span, verbal memory, and learning. A review conducted by University of Netherlands analysed fourteen studies examining NCF impairment following SRS: seven of there were single-group or observational studies, five randomised clinical trials and two pilot studies. Mini-mental State Examination (MMSE) was utilised in earlier studies (n=8); however, the majority of the studies did not find a significant change in MMSE score (Andrews *et al*., 2004, Aoyama *et al*., 2015, Schimmel *et al*., 2018). This is likely to reflect that the MMSE is thought to be a crude measure of memory and NCF, and whilst it may have its place in screening for NCF impairment, it is not considered sensitive enough to identify subtle and precise changes in NCF (Schimmel *et al*., 2018). Findings of the six studies that utilised objective NCF testing are summarised in Table 4.1.

Study	Design	NCF Tests	NCF Outcome
Chang *et al.*, 2007	Single-group (pilot) – SRS alone	HVLT-R, COWAT, TMT A & B, WAIS Digit Span and Digit Symbol, GP	Cognitive decline at 1 month (n Z 13): 100% on ≥ 1 test, 54% on ≥ 2 tests; In a subgroup (n Z 5) alive after 7 months, 80% had stable/ improved scores on memory,
Chang *et al.*, 2009	Randomised controlled trial – SRS vs SRS + WBRT	HVLT-R, COWAT, TMT A & B, WAIS Digit Span and Digit Symbol, GP	Trial stopped prematurely due to significantly larger probability of decline on HVLT-R total recall at 4 months : 7/ 11 (SRS + WBRT) vs 4/20 (SRS) Significant probabilities of decline (SRS vs SRS + WBRT): At 4 months: total recall: 24% vs 52%, delayed recall: 6% vs 22%, delayed recognition: 0% vs 11%
Onodera *et al.*, 2014	Pilot study (non-randomized): treated with SRS (1-2 metastases) and WBRT ≥ 3	RBANS list learning, RBANS semantic fluency, TMT A & B, MMSE	SRS group: no change in any test at any time point during FU; WBRT group: sig decline of delayed mem at 4 months (n = 17), sig improvement in immediate mem at 8 months (n = 14)
Kirkpatrick *et al.*, 2015	Single Group – SRS alone	TMT A & B, MMSE	No significant changes in MMSE or TMT A & B scores at 3 months
Habets *et al.*, 2016	Single Group – treated with SRS alone	Auditory Verbal Learning, Rey Complex figure, Stroop, Letter digit modalities, Digit Span, Concept shifting, Word fluency, BADS	No significant changes in domain scores at 3 (n = 39) and 6 months (n = 29) Non-significant trend toward improvement in verbal memory
Brown *et al.*, 2016	Randomised Controlled Trial: SRS + WBRT vs SRS alone	HVLT-R, COWAT, TMT A&B and GP	At 3 months: significantly more decline WBRT +SRS vs SRS (91.7% vs 63.5%) in immediate recall (30% vs 8%), delayed recall (51% vs 20%), verbal fluency (19% vs 2%)

Table 4.1 Studies that assessed NCF effects of SRS using formal testing methods. *BADS: Behavioral Assessment of the Dysexecutive Syndrome; COWAT: Controlled Oral Word Association Test; FU: follow-up; GP: grooved pegboard; HVLT-R: Hopkins Verbal Learning Test- Revised; RBANS: Repeatable Battery for the Assessment of Neuropsychological Status; SRS: stereotactic radiation surgery; TMT: trail-making test; WAIS: Wechsler Adult Intelligence Scale; WBRT: whole brain radiation therapy. Adapted from (Schimmel et al., 2018)*

4.3.2 Neurocognitive function testing battery used in the clinical study

NCF tests, the domains tested and method of testing for each test we used in our study are summarised in Table 4.2. Tests were administered by a member of clinical psychology team at VCC. HVLT, COWAT, TMT-A and TMT-B have been recommended by the Response Assessment in Neuro-Oncology (RANO) Group as a minimum set of assessments to be included in clinical studies involving patients with BM (Lin *et al*., 2013). Clinical trials and studies have often included Digital Symbol and Digit Span as a second measure of working memory (Dwan *et al*., 2015). Complete NCF testing took approximately 60 minutes to deliver at each time point.

In addition to NCF testing, we formally measured quality of life using the QLQ-C30 with BN20 questionnaires and supplementary questions. BN20 has been designed by the EORTC group specifically for patients undergoing treatment for neurological malignancy. NCF and treatment for cancer can also impact on functional well-being of the patients and in order to collect this data objectively, the Functional Assessment of Cancer Therapy - General (FACT-G) questionnaire was also utilised. This test measured four aspects of well-being: physical, social, emotional, and functional.

There are simpler and well-known tests to measure NCF such as Mini-mental state examination (MMSE) and Montreal cognitive assessment (MoCA), however they have poor sensitivity and specificity in identifying subtle NCF changes as detailed NCF tests and have not been recommended by the RANO group. These tests are a valuable tool for screening and are used widely in patients with cognitive impairment, however, there is a lack of psychometric data to detect changes over time in patients with BM and therefore these were not included in our study.

Test	Domain	Administration
Trail Making Test A (TMT-A)	Visual-motor processing speed	Consecutively connect the dots of twenty-five circles numbered 1 to 25. Scored as number of seconds to complete (0-300).
Trail Making Test B (TMT-B)	Executive function	Consecutively connect the dots of twenty-five targets, but now alternately numbered and lettered (1, A, 2, B, etc). Scored as number of seconds to complete (0-300).
Controlled Oral Word Association Test (COWAT)	Verbal fluency and executive function	Subject is asked to produce as many words as possible, excluding proper nouns, beginning with a given letter within 1 minute. Repeated three times with different letters. Age and sex adjusted raw score (0 – no upper limit).
Hopkins Verbal Learning Test – Revised (HVLT-R): Immediate recall, Delayed Recall, Recognition	Verbal memory and learning	Immediate memory of word list rehearsed 3 times (max score = 36). After 20-30 min delay, number of words correctly recalled (max score = 12). Recognition of words from a longer list (max score = 12). There are six alternative versions available to avoid recall effects.
Wechsler digit span (Digit Symbol and Digit Span)	Attention span and verbal working memory	Subject has to repeat sequences of numbers both forwards and backwards. Scored by adding total number of correct sequences.
Test of premorbid function (TOPF)	Premorbid IQ and memory	Reading of a list of seventy words which get progressively harder (atypical grapheme to phoneme translations). Scored by software (regression equation).

Table 4.2 Summary of Neurocognitive function Battery

4.4 Magnetic Resonance Imaging

The translational MRI study was designed to study changes in hippocampus at 1- and 3-months following SRS to gain an insight into effects of SRS on normal tissue at Cardiff University Brain Research Imaging Centre (CUBRIC). CUBRIC is equipped with four research MRI scans, two of which were used in this study: the 3 Tesla (3 T) Siemens Prisma System and the Siemens 3 Tesla Connectom system. The latter facility is unique in the UK as this is one of only four such systems in the world. This is the first time, as far as we are aware, that this scanner is being used to scan patients with BM. The connectome scanner features three hundred milli Tesla/metre gradient coils which are at least four times stronger than those found in conventional MR systems. This allows probing tissue microstructure to much finer detail than standard MRI systems (Jones *et al.*, 2018).

During July 2016 and April 2017, I wrote the study protocol, participant information leaflet, applied for research ethics committee approval and research and development approvals with Velindre University NHS Trust and Cardiff University. During this time, I developed a comprehensive MRI protocol to study structural, physiological, metabolic and diffusion changes of the hippocampus using the 3 T MRI scanner. For purposes of protocol development, MRI scans were performed in healthy volunteers. There are established ethical agreements in place to conduct such MRI scans in CUBRIC with an aim to develop a study protocol.

In this section, I have described method of MRI analysis presented in subsequent chapters in sections 4.4.1 (structural MRI), 4.4.2 (perfusion MRI), 4.4.3 (functional MRI), 4.4.4 (MR Spectroscopy), and 4.4.5 (diffusion MRI). The MRI data presented in this chapter is of the healthy volunteers acquired at CUBRIC. I have analysed all the data presented in this and subsequent chapter. The connectome scanner sequences are described in Section 4.4.6.

4.4.1 MRI Contrast and Structural Measurements

An MR image has contrast if there are areas of varying signal, high signal appears white and low signal appears dark on the image. Areas of intermediate signal appear grey. The two molecules contributing to extreme of contrast in MRI are fat and water. Due to their molecular structure, fat molecules are affected to a lesser extent compared to water molecules from B_0. Therefore, Larmor frequency of hydrogen in water is higher than that of hydrogen in fat. Hence, hydrogen in fat recovers more rapidly along the longitudinal axis and loses transverse magnetisation faster than water. Given the inherent magnetic properties of these two molecules, T1 recovery time and T2 decay is short in fat and long in water.

A T1 weighted image is where the contrast is largely dependent on the differences in T1 times between fat and water and all other tissues possess intermediate signal. To achieve this, repetition time (TR) must be short enough so that fat and water do not fully return to B_0. T2 weighted image is where the contrast is largely dependent on differences in T2 times between fat and water. The echo time (TE) control the amount of T2 decay and therefore it must be long enough to allow sufficient time for fat and water to decay. The T1 and T2 relaxation times of tissue are dependent on the type of tissue and field strength of the magnet. As field strength increases, the relaxation time of brain tissue also rises. The relevant relaxation times and proton density for different tissue compartments within the brain are listed in Table 4.3.

Compartment	T1 (ms)	T2 (ms)	T2* (ms)	PD
Grey Matter	1820	100	50	0.69
White Matter	1080	70	50	0.61
CSF	3817	1442	n/a	1.00
Arterial Blood	1932	275	46	0.72

Table 4.3 Relaxation Times and Proton Density (PD) at 3 T for tissue compartments. (Stanisz et al., 2005, Macintosh and Graham, 2013)

Generalized Auto-calibrating Partially Parallel Acquisition (GRAPPA) is a parallel imaging technique to speed up MRI pulse sequences. The Fourier plane of the image is

reconstructed from the frequency signals of each coil reconstruction in the frequency domain. This technique uses k-space under sampling: A model from the centre of k-space is acquired and the missing intermediary lines are reconstructed (Griswold *et al*., 2002). Initially this technique was described by Griswold *et al*., in 2002 and is used widely to reduce acquisition time without significant effect on SNR and image quality. Figure 4.2 demonstrates images acquired with and without GRAPPA in a healthy volunteer in 3 T MRI. Although this can be a useful technique to be used in structural images, it may reduce SNR significantly in functional imaging. Therefore, GRAPPA was only utilised in imaging T1 and T2 weighted images in this study.

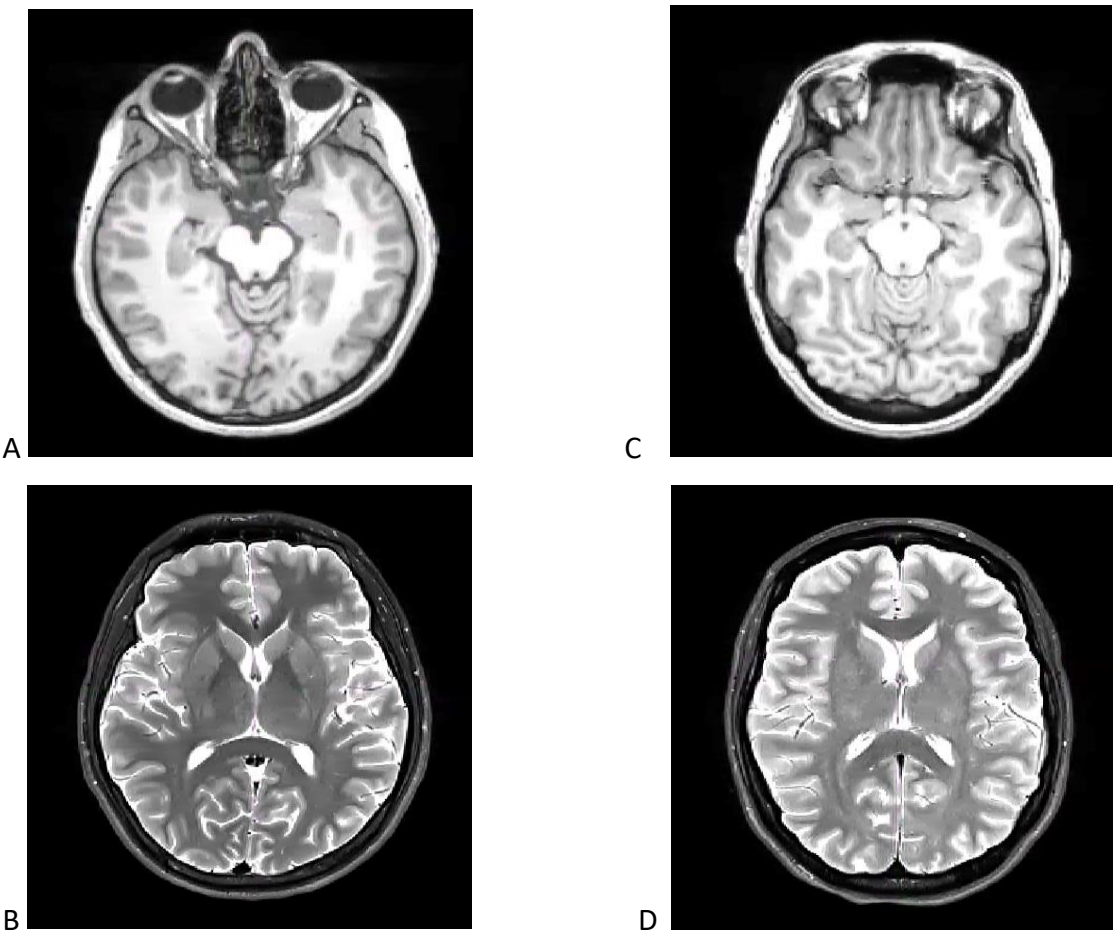

Figure 4.2 T1 weighted (top) and T2 weighted (bottom) images acquired without GRAPPA (A & B) and with GRAPPA (C&D). Acquisition time for T1 and T2 was 7:23 and 4:12 minutes without GRAPPA and 5:19 and 2:45 minutes with GRAPPA respectively. GRAPPA: Generalised Autocalibrating Partially Parallel Acquisition.

T1 Fast Spoiled Gradient Echo (T1 FSPGR) improves the anatomical display of the sulcal structure of the hemispheric convexities compared to standard T1 spin echo sequences. It is the imaging of choice for delineating the hippocampus (Gondi *et al*., 2014b). T1 FSPGR

allows volumetric imaging and with gadolinium-based contrast agent is the sequence of choice of delineating BM for SRS. Research MRI scans were performed without gadolinium-based contrast to avoid risks of repeated contrast agents and to avoid contamination with ASL sequences.

To perform structural measurements, the T1 FSPGR images were skull stripped using the brain extraction tool (BET) which deletes non-brain tissue from an image of the whole head (Smith, 2002). Following this, cortical reconstruction and volumetric segmentation of the subcortical white matter and deep grey matter volumetric structures was performed with the Freesurfer image analysis suite (Henschel *et al*., 2020). The technical details of these procedures have been described in prior publications (Dale *et al*., 1999, Fischl *et al*., 2002).

4.4.2 Physiological Measurements

An important physiological parameter of cerebral function is measurement of blood flow. Cerebral blood flow can be quantified using two main methods: Dynamic susceptibility weighted (DSC) MRI and arterial spin labelling (ASL).

DSC-MRI is a commonly used perfusion sequence that is based on use of intravenous contrast agent. Images are acquired using rapid T2* imaging while the contrast agent passes the brain tissue. Various relative perfusion measures can be extracted by measuring signal intensity as a function of time and fitting to a mathematical model. The main limitation of this method is use of intravenous contrast, and it can be problematic in patient who might have allergic reactions or impaired renal function.

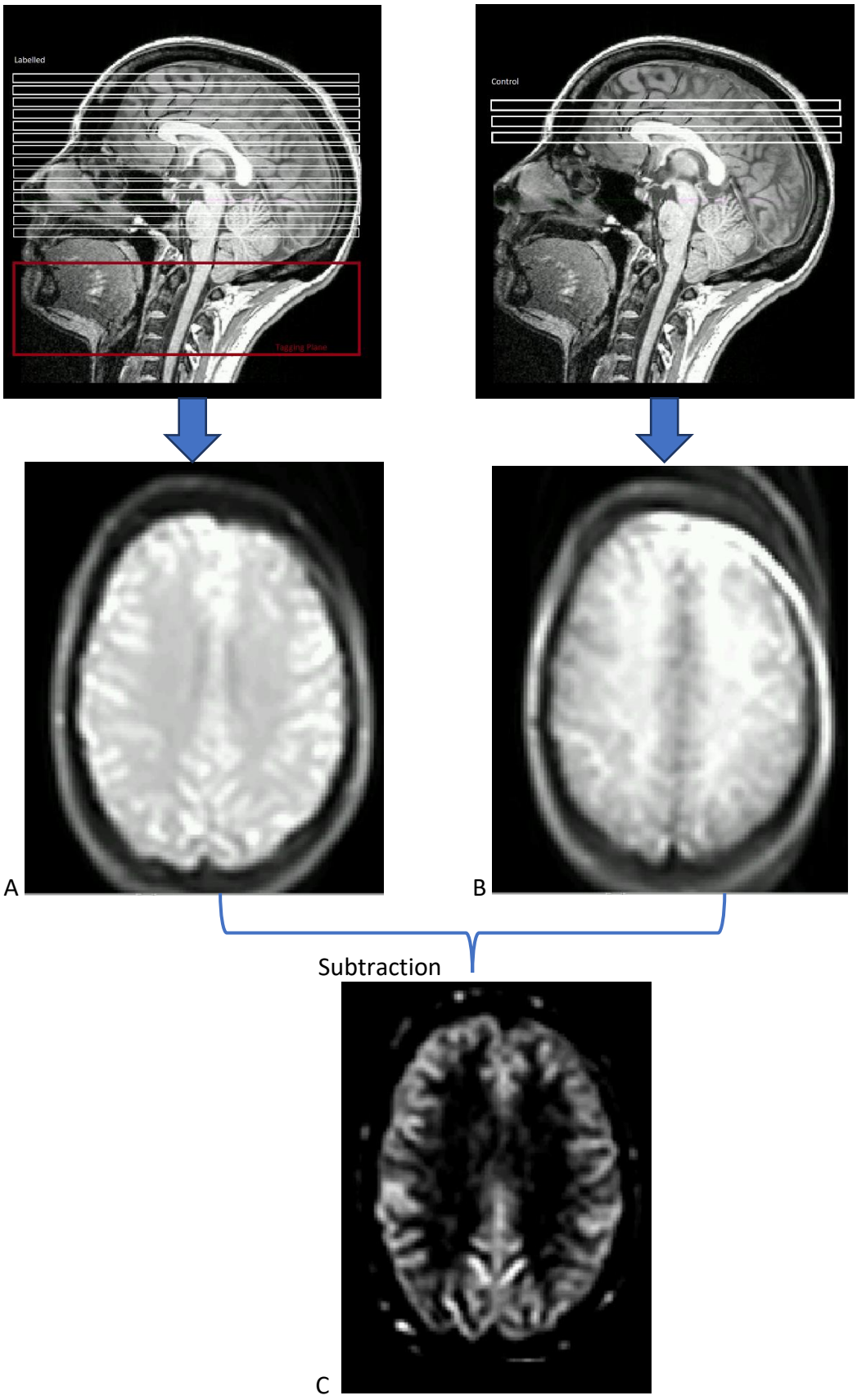

Figure 4.3 Theory of how Arterial Spin Labelling works. Images are acquired with and without labelling called the labelled (A) and controlled images (B) respectively. Following imaging, these images are subtracted to produce perfusion weighted imaging (C).

Alternatively, ASL does not require the administration of a contrast agent. In this technique patient's own water molecules serve as an endogenous diffusible tracer. This is achieved by magnetically labelling water molecules in proximal blood vessels with radiofrequency pulses. After a time-delay to allow magnetically labelled arterial blood to reach tissue capillary bed, the labelled hydrogen atoms exchange with the hydrogen atoms in the tissue which is identified as a signal change. A pulse sequence is used to acquire an image data at the slice location. Same pulse sequence is then used to acquire an image without the previous tagging. These two images are then subtracted to produce a map of perfusion (See Figure 4.3). By applying a mathematical model, various perfusion measures can be obtained. The main measure is absolute value of cerebral blood flow (CBF) which is measured in units of millilitres per minute per hundred-gram brain tissue. CBF is coupled with regional brain metabolism (Raichle, 1998, Alsop *et al*., 2015). CBF within the grey matter is thought to be approximately 60 ml/100g/min, ranging between 40 to 100 (Chappell *et al*., 2017). This is one of the major advantages of using ASL technique in research. ASL was the chosen method in this study due to its ability to calculate absolute CBF. As this method does not utilise gadolinium-based contrast agent, it also gave flexibility of performing research MRI alongside imaging that would be conducted as a standard in patient's care. Otherwise, if gadolinium-based contrast agents were utilised for research MRI, it would require a minimum 48-hour gap between research and standard MRI scans. Table 4.4 summarizes key characteristics of the two sequences.

	DSC	ASL
Contrast Agent	Yes	No
Data Acquisition	First pass of IV contrast through regional circulation	Continuous or Pulsed arrival of diffusion of labelled water
Relaxation mechanism	T2* susceptibility from IV contrast	Magnetization exchange from labelled water
Imaging sequence	T2* weighted rapid GRE or EPI	2D/3D EPI read out
Acquisition Time	1-2 minutes	3-5 minutes

Table 4.4 Comparison of Dynamic Susceptibility Weighting (DSC) and Arterial Spin Labelling (ASL) sequences. *GRE: gradient echo, EPI: echo planar imaging.*

Two main aspects need to be considered relating to ASL implementation: labelling techniques and readout approaches. There are two main methods of labelling used in clinical and research environments. First is referred to as continuous ASL (CASL), which continuously inverts blood flowing into an imaging slice; and second is pulsed ASL (PASL) which periodically inverts a block of arterial blood and measures arrival of that blood into the imaging slice (Chappell *et al*., 2017, Wong *et al*., 1998). CASL is implemented by applying many RF pulses to achieve pseudo-continuous ASL (PCASL). The overall SNR and labelling efficiency is thought to be higher of PCASL than PASL (Alsop *et al*., 2015). However, using modified PASL labelling techniques such as quantitative imaging of perfusion using a single subtraction (QUIPSS) which is comparable to PCASL techniques in terms of SNR and labelling efficiency (Wong *et al*., 1998).

Read out approaches can be two or three dimensional. Two dimensional approaches such as multi-slice or single shot echo planar imaging (EPI). Although Single shot 2D imaging is less sensitive to motion artefacts than multi-slice acquisition, there can be loss of signal in medial temporal lobe (See figure 4.8). 3D readout approaches of gradient and spin echo (GRASE) and Flow-sensitive alternating inversion recovery (FAIR) are considered to be superior and are recommended by the IMSRM perfusion study group and the European Consortium for ASL in Dementia (Alsop *et al*., 2015). FAIR creates perfusion imaging by frequency-selective inversion pulse with (tagged image) and without (control image) an accompanying slice selection gradient, with same carrier frequency. In the tagged image pulse is played with the slice-selection gradient inversion of the spins within the imaging slice – spins outside the slice leaving unaffected. In the control image the slice-selection gradient can be either played with zero amplitude or at a different time. Advantages of FAIR readout is tagging of the arterial blood feeding the tissue from both proximal and distal sides of the imaging slice. If the flow direction is unknown or the feeding arteries have tortuous paths, FAIR reduces underestimation of perfusion, because inflows from both directions are registered and contribute to the difference image.

Trials of PASL, PCASL with 2D and 3D readout approaches were conducted on healthy volunteers. Summary of these results are demonstrated in Table 4.5 and Figure 4.4. This demonstrates loss of signal particularly in the medial temporal lobe with 2D read out approaches. Following this experiment, FAIR-QUIPSS II 3D ASL was the chosen method for

the study going forward. Final experiment looked at slice thickness for this sequence to decide the optimal slice thickness. Following acquisition, CBF in units of ml/100g/min is calculated using the following equation.

$$CBF = \frac{600.\lambda.(SI_{control} - SI_{label}).e^{\frac{T1}{T_{1,blood}}}}{2.\propto.TI_1.SI_{PD}}$$

Where λ is the brain/blood partition coefficient in ml/g, $SI_{control}$ and SI_{label} are the time-averaged signal intensities in the control and label images respectively, $T_{1,\ blood}$ is the longitudinal relaxation time of the blood in seconds and α is the labelling efficiency. SI_{PD} is the signal intensity of a proton density weighted image and TI is the inversion time (Alsop *et al*., 2015, Wong *et al*., 2008).

Sequence	Scan Parameters	Cerebral Blood Flow (ml/min/100g)		
		GM	Left HC	Right HC
2D PASL EPISTAR	TR/TE 2500/12, TI 1800, flip angle 90, BW 2365, Slice thickness 8 mm, FoV 256 x 256	38.85	39.34	36.45
2D PASL EPISTAR	TR/TE 2500/12, TI 1800, flip angle 90, BW 2365, Slice thickness 8 mm, FoV 256 x 256, with hamming filter	39.02	37.64	37.25
2D PASL EPISTAR	TR/TE 2500/10, TI 1800, flip angle 90, BW 3005, Slice thickness 8 mm, FoV 256 x 256	41.62	40.32	30.96
2D PASL EPISTAR	TR/TE 2500/10, TI 1800, flip angle 90, BW 3005, Slice thickness 8 mm, FoV 256 x 256 with hamming filter	41.42	40.95	41.28
2D PCASL	TR/TE 3700/10, flip angle 90, BW 2300, slice thickness 7 mm, FOV 256 x 256	45.23	32.65	33.87
3D PASL FAIR-QUIPPS II - 3 mm	TR/TE 3300/13.48, TI 1990, flip angle 180, slice thickness 3 mm, FoV 192 x 192	67.34	72.97	73.89
3D PASL FAIR-QUIPPS II - 4 mm	TR/TE 4600/16, TI 1990, flip angle 180, slice thickness 4 mm, FoV 192 x 192	56.89	48.29	45.56
3D PASL FAIR-QUIPPS II 5.25	TR/TE 3300/25.38, TI 1990, flip angle 180, slice thickness 5.25 mm, FoV 256 x 256	54.25	46.32	47.43

Table 4.5 Measurement of Cerebral Blood Flow in the Grey Matter (GM) and bilateral hippocampi using different ASL sequences. *EPISTAR: Echo-Planar Imaging-based Signal Targeting by Alternating Radiofrequency pulses, FAIR: Flow-sensitive alternating inversion recovery, FoV: Field of view, PASL: Pulsed aterial spin labelling, PCASL: Pulsed continuous arterial spin labellig, QUIPSS: Quantitative imaging of perfusion using a single subtraction, TE: Echo time, TI: Inversion time, TR: Repition time,*

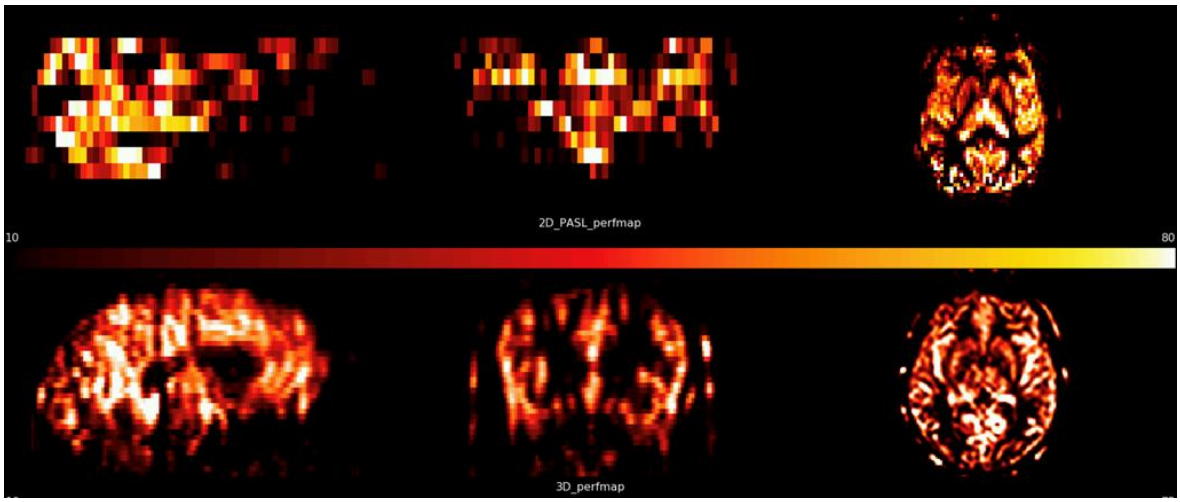

Figure 4.4 2D PASL (top) vs 3D PASL GRASE readout (bottom). This demonstrates cerebral blood flow for the same participant with 2 different acquisitions

4.4.3 Functional Measurements

Functional activity can be measured non-invasively by blood oxygen level dependent (BOLD) functional MRI (fMRI). Principle of BOLD is based on increased oxygen consumption leading to relative increase in deoxyhaemoglobin concentration to oxyhaemoglobin concentration in regions of high neuronal activity (Spitzer *et al*., 1995, Posner and Raichle, 1994). Due to paramagnetic quality of deoxyhaemoglobin, the relative decrease in its concentration can be detected by MRI as increased signal in T2* weighted images (Kroll *et al*., 2017). Traditionally this technique has been used to localise brain function by presenting a certain stimulus or performing a task to elicit neuronal responses (Biswal *et al*., 1995). However, there is increasing interest in spontaneous fluctuations in BOLD signal in the resting state. These fluctuations are thought to reflect functional organisation in the brain (Greicius *et al*., 2003). A number of resting state networks (RSNs) have been identified, which can be divided into three groups: default mode network (DMN), somatomotor RSN, and attention and RSN. In addition to these networks, there are visual, auditory and language networks that are mainly utilised in task-based analysis by providing the participant with the relevant stimuli (Kamran *et al*., 2014).

The DMN is perhaps regarded as the most fundamental RSN. A distinguishing property of this network to others is that it is more active at rest than during performance of a

stimulus driven task. Greicius, *et al*., 2003 first described this network in 2003 and since then it has been replicated using a variety of processing methods (Smith *et al*., 2009, Beckmann *et al*., 2005, De Luca *et al*., 2006, Power *et al*., 2011, Yeo *et al*., 2011, Damoiseaux *et al*., 2006, van den Heuvel *et al*., 2008, Lee *et al*., 2012, Fox *et al*., 2005) .The initial study of 14 healthy individuals hypothesised that certain regions in the brain, including posterior cingulate cortex and ventral anterior cingulate cortex consistently show greater activity during the resting states than during cognitive stimuli. Therefore these regions constitute a default mode of brain function, subsequently named as DMN (Greicius *et al*., 2003). The DMN has suggested to be associated with retrieving memory and internal processing of self at rest. Therefore it is speculated that DMN may be a key network showing early disruption in cognitive impairment associated with Alzheimer's disease (Zhang *et al*., 2020a).

The somatomotor network, first identified by Biswal eta al., encompasses primary sensory and motor networks. Although this can be visualised in the resting state, this is more active when the participant is exposed to a stimulus, therefore is more widely studied in task-based studies (Biswal *et al*., 1995). This is also true for visual, auditory and language networks (Smith *et al*., 2009, Tomasi and Volkow, 2012).

RSNs involved in cognition and attention include dorsal attention network, which is responsible for tasks requiring spatial attention, ventral attention network, which is involved in the detection of environmentally salient events, frontoparietal control network, associated with working memory and control of goal directed behaviour, and cingulo-opercular network, which is thought to be responsible for executive function.

There has been increased use of rsfMRI and task-based fMRI imaging in patients pre-surgical planning in patients with primary brain tumour. Use of fMRI may lead to reduced morbidity while maximising complete resection of the tumour. This can also stratify patients in whom awake craniotomy may be an important consideration (Kamran *et al*., 2014).

Resting state fMRI is analysed using two main techniques, independent components analysis (ICA) and seed-based correlation mapping. Both methods yield highly producible

results and depend on the basic concept that spontaneous neural activity is correlated within widely distributed regions of the brain. Seed- based method relies on prior knowledge and assumptions about network connections, whereas ICA technique makes no prior assumptions regarding the topography of the obtained components. Therefore, this technique was used for the purposes of this study. In recent years, a new method of graph theory has emerged in analysing rsfMRI which exploits topological properties of ROIs rather than simply seed based correlations.

ICA decomposes a four-dimensional functional data matrix into a set of spatial maps, each with an associated time course. This is a method of separating the original data in a way which does not require a specific experimental paradigm and separates out signals of interest from noise or artefacts (Beckmann *et al.*, 2005). MELODIC (multivariate exploratory linear optimized decomposition into independent components) is a tool which has been incorporated in FSL (FMRIB software library). FSL is a software package used for analysing MRI-based neuroimaging data. It is widely used around the world and covers analysis of structural, diffusion, task-based and resting-state fMRI data (Jenkinson *et al.*, 2012b). As example of healthy volunteer RSN identification is demonstrated in Figure 4.5.

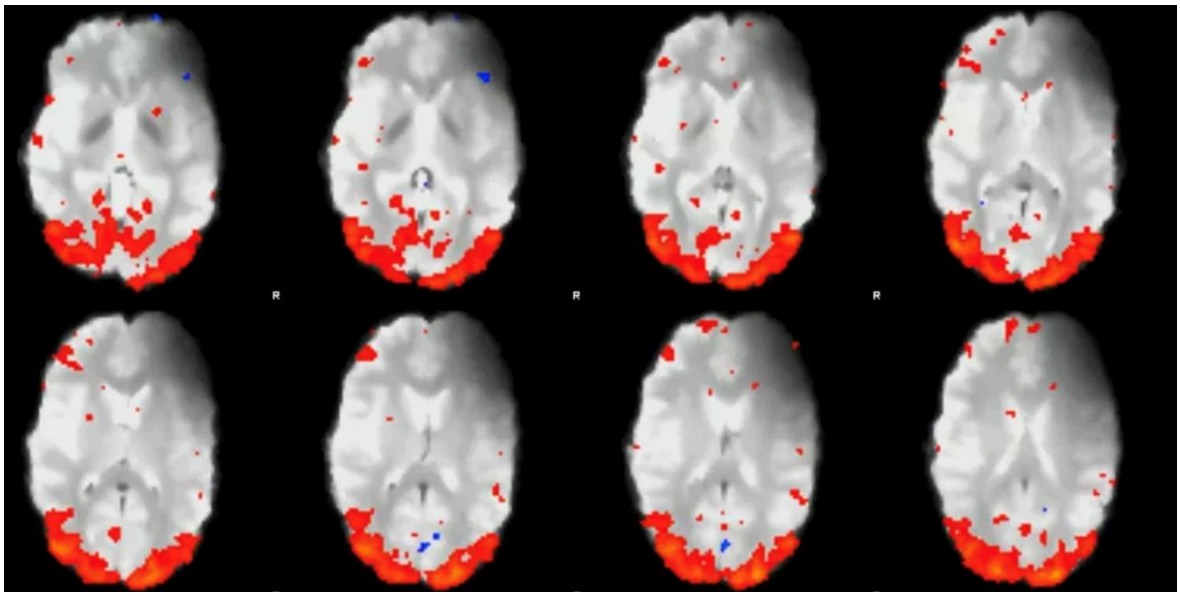

Figure 4.5 Activation of visual resting state network in a healthy individual acquired by resting state fMRI. Red statistically higher correlation among the highlighted voxels with blue areas representing anticorrelation.

4.4.4 Metabolic Measurements

MR Spectroscopy (MRS) produces a spectrum instead of an MR image (Westbrook *et al*., 2008). It analyses signal of hydrogen protons attached to other molecules and allows detection and quantification of brain metabolites in vivo (Allaili *et al*., 2015, Blüml, 2013). A spectrum plot is produced of signal intensity vs frequency that displays the chemical shift. Chemical shift is measured in parts per million in frequency (ppm). MRS is restricted to the analysis of regions of interest (ROI) due to low concentration of MR-detectable chemicals (Hashemi *et al*., 2010). Therefore, it requires a trained person to place the voxel on the ROI accurately. Once the voxel is placed, 2 processes are performed to increase SNR and identification of the metabolites: shimming and water suppression (Westbrook *et al*., 2008, Hashemi *et al*., 2010).

Shimming refers to the process of adjusting field gradient to optimise the magnetic homogeneity within the voxel (McRobbie *et al*., 2007). Voxel homogeneity is quantified by line width (full width at half height) of the water resonance (Hashemi *et al*., 2010). This is particularly important when conducting MRS of the hippocampus as its close proximity to ventricles and petrous bone can lead to significant inhomogeneity within the voxel. Signal from water is 100,000 more than that of metabolites, because of abundance of water molecules within the human brain as discussed in section 1.4.1. Therefore, in order to identify metabolites, present at much lower concentration, water suppression is performed. This is achieved by exposing the voxel to an RF pulse that is 4.7 ppm from the universal standard (Hashemi *et al*., 2010).

Peaks on the spectrum are referred to as resonance. Some metabolites do not harbour a simple resonance and may be split into two, three or even more sub-peaks. Each metabolite has its own diagnostic pattern on the chemical shift spectrum depending on the number of protons present in the molecule. An area under a given peak is directly proportional to the number of protons contributing the peak.

MRS studies of the hippocampus are somewhat less frequent due to its technical challenges. Such challenges mainly relate to anatomical location of the hippocampi being close to the petrous bone and ventricles, which causes poor homogeneity of the B_0

magnetic field resulting in low spectral resolution relative to other regions within the brain. Despite these challenges, MRS of the hippocampus has been increasingly studied in neurodegenerative, epilepsy, and psychiatric disorders. There is research to identify a non-invasive biomarker that may precede symptomatic presentation of diseases such as Alzheimer's dementia (AD) and help distinguish AD from other neurodegenerative disease.

Spectra are read from right (0 ppm) to left (4 ppm). In the normal brain, the first peak is the main peak of N-acetyl aspartate (NAA) at 2ppm, followed by small peaks on the left of NAA peak between 2-2.5 ppm which consists of glutamate complexes. The next peak is of Creatine (Cr) at 3 ppm, followed by Choline (Cho) at 3.2 ppm. Myo-Inositol peak occurs at 3.5 ppm. A secondary Cr peak occurs at 3.9. If the baseline on the left side is risen, it signifies incomplete water suppression, as water peak resides at 4.7 ppm (Hashemi *et al*., 2010, Westbrook *et al*., 2008, McRobbie *et al*., 2007). Table 4.6 summarises metabolites detected and their clinical applications in pathology.

Metabolite	Peak (ppm)	Pathophysiological Correlation	Clinical Significance	Association with Conditions
N-acetyl aspartate (NAA)	2.0-2.5	Largest peak in the spectra; surrogate marker for neuronal density and integrity.	Reduced in white matter disease	Multiple sclerosis, hypoxic encephalopathy Low in tumours
Choline (Ch)	3.2-3.5	Metabolic marker of membrane density and integrity	High levels in increased cell membrane synthesis and cellularity	Malignant tumour, Inflammation, non-specific
Creatine (Cr)	3.03	Marker for intracellular energy	Not originated in the brain, assumed to be stable and used for calculating ratios.	Reduced in tumours
Myo-inositol (mI)	3.55	Involved in osmoregulation and volume regulation/ Increased levels believed to reflect increased numbers of glial cells	Increase in inflammatory conditions	Alzheimer's dementia
Glutamate, Glutamine & Gamma - aminobutyric acid(GABA) (Glx)	2.0-2.46	Most abundant neurotransmitters in the CNS.	Levels increase with underlying demyelination and neuronal loss	Increased in peri-tumoural brain oedema
Lactate	1.3	Increases as a result of hypoxia and poor vascularity.	Usually present in minute amounts and not detectable.	Important for tumours and usually detectable levels signify high grade tumour
Lipids	0.9, 1.3, 2.0	Rise of lipids is detected in various cellular processes such as necrosis, growth arrest, inflammation, malignancy, and apoptosis	Presence of lipids may indicate voxel contamination by lipidic space, scalp and subcutaneous tissues	None

Table 4.6 Summary of metabolites detected in MRS at 3 T and their clinical implications. *Adapted from (Mikkelsen and Hearshen, 2008)*

Single voxel MRS using Point Resolved Spectroscopy (PRESS) was the chosen method to measure chemical shift pattern in left and right hippocampus. T1 spoiled gradient echo images were obtained first and a 4.8 cc voxel was angulated along the anterior-posterior hippocampal axis and was positioned accordingly measuring 15 mm x 40 mm x 8 mm in left-right, anterior-posterior, and superior-inferior direction, respectively. Figure 4.6 represents position of left and right sided voxel. Although there are automated voxel placement tools, it was not used due to potential for anatomical changes due to oedema/hydrocephalus and so manual placement was sued each visit.

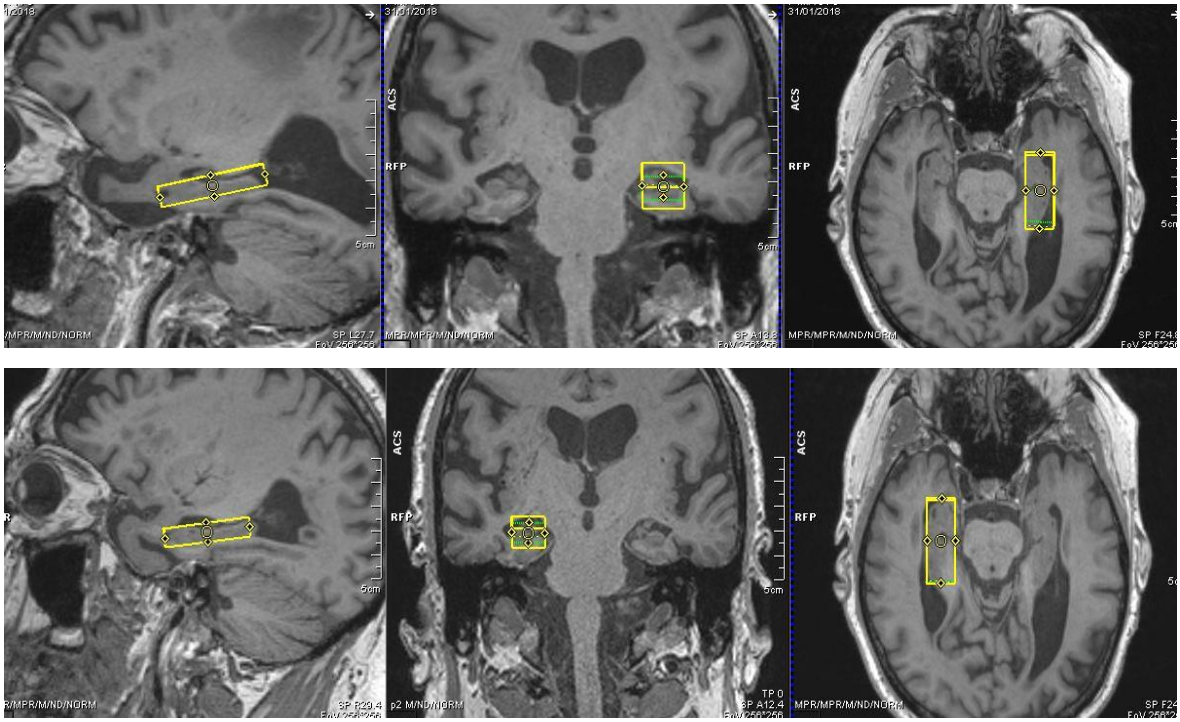

Figure 4.6 Voxel placement for left (top) and right (bottom) hippocampi. Voxel size is 15 x 8 x 40 mm = 4.8 cc

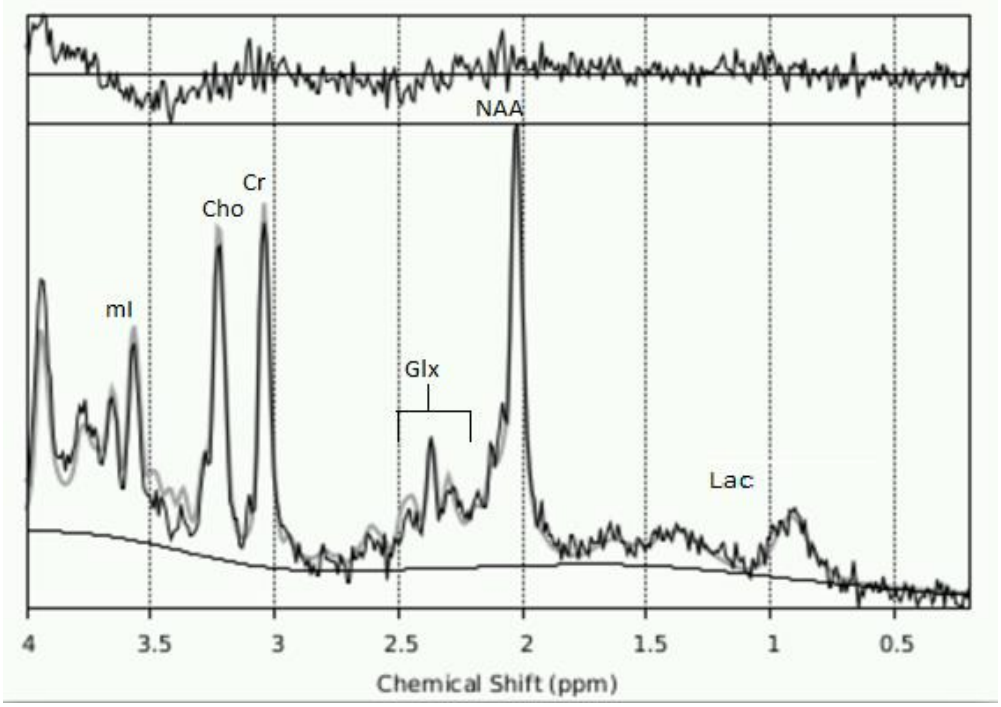

Figure 4.7 Chemical Shift Pattern from MR Spectroscopy of the hippocampus of a healthy volunteer acquired at 3 T MRI. *Cho: Choline, Cr: Creatine, Glx: glutamate complexes, Lac: Lactate, mI: myo-Inositol, NAA: N-acetyl aspartate*

MRS of bilateral hippocampi was performed on four healthy volunteers to test reliability and reproducibility of shimming, test objective measurements of metabolite concentrations, with and without water reference acquisition. Metabolites are largely presented as a ratio to Cr as this is thought to be the most stable metabolite in the brain (Sundgren *et al.*, 2009). However, it is unknown whether radiation injury may affect Cr as well, therefore, a separate water acquisition was acquired so that metabolites concentration can be calculated accurately. Final PRESS MRS Parameters used were TR = 2000 ms, TE = 35 ms, averages = 256, flip angle 90°. Prior to measuring the spectra shimming was performed to homogenize the B_0 field. For purposes of water reference, water free water spectra were obtained with four averages for each participant. Figure 4.7 represents a typical spectrum of metabolites in the hippocampus of a healthy volunteer acquired with 3 T MRI at CUBRIC.

The raw spectrum data acquired on the scanner were frequency and phase corrected. All the data underwent eddy current correction and were analysed using the linear combination model (LC Model) (Provencher, 2013). Simulated spectra of the LC Model fitting was performed over the spectral range from 0.5 to 4 ppm. For the calculation of

absolute concentration of metabolite two steps were done: calculating values with water peak and correction for CSF content.

Correction for CSF content was done by combining imaging and spectroscopy data. Automated delineating was performed of the 3 compartments using 3D T1 FSPGR images which were segmented into grey matter (GM), white matter (WM) and CSF using FSL software (Jenkinson *et al*., 2012a) (Figure 4.8). The relative tissue densities were assumed as per Gussew, *et al*. 2012 (see Table 4.7) (Gussew *et al*., 2012). This was performed to calculate the attenuation factor that needs to be applied to obtain milliMolal (mM) absolute concentration units which accounts for changes in the size of the water reference peak due to differences in T1 and T2 for grey and white matter and CSF. It also corrects for the fact that metabolites only appear in GM/WM and not in CSF.

Figure 4.8 Automated maps of white matter, grey matter, and cerebrospinal fluid (left, middle and right retrospectively) created within FSL software

Contrast/Compartment	Value
T1 white matter	1080
T2 white matter	70
T1 grey matter	1820
T2 grey matter	100
T1 CSF	4160
T2 CSF	500

Table 4.7 The relative tissue density of white matter, grey matter and CSF in T1 and T2 image (Gussew et al., 2012).

There are different approaches to MRS analysis, mainly Tarquin and LC Model, and I compared them to find the optimal approach. FWHM was 9.23 +/- 1.1 SD and SNR was 56 +/- 11.2 SD for pre-processed Tarquin method while with the LC Model, FWHM was 9.51 +/- 0.92 SD and SNR was 60.75 +/- 12.01 SD (p-value > 0.05). Although the quality control of both methods was similar, the concentration of metabolites using the LC Model was more reliable and consistent with the published literature (Table 4.8). This is because of excluding voxel that may have taken signal from CSF and white matter compartment and application of eddy current correction (Lin *et al.*, 1994). Therefore, this was the chosen method of data analysis for MRS going forward.

Metabolite	Pre-processed Tarquin Method	LC Model	p-value
RHC NAA	4.88 +/- 0.69	16.69 +/- 0.12	<0.001
LHC NAA	4.81 +/- 0.46	17.45 +/- 0.87	<0.001
RHC Choline	1.12 +/- 0.095	3.7 +/- 0.16	<0.001
LHC Choline	1.15 +/- 0.65	4 +/- 0.14	<0.001
RHC Creatine	4.31 +/- 0.54	14.16 +/- 0.55	<0.001
LHC Creatine	3.56 +/- 0.42	13.29 +/- 0.2	<0.001
RHC mI	4.63 +/- 0.67	7.77 +/- 0.67	<0.001
LHC mI	3.21 +/- 0.3	7.95 +/- 0.78	<0.001

Table 4.8 Metabolite concentration in bilateral hippocampi of 3 healthy individuals. The absolute concentration was more reliable with LC Model then with the pre-processed Tarquin method. *NAA: N-Acetyl Aspartate, mI: Myo Inositol.*

4.4.5 Diffusion MRI

Diffusion weighted imaging (DWI) is a form of MR imaging based on measuring the random Brownian motion of water molecules within a voxel of tissue (Bammer *et al.,* 2003). Thus, areas of high cellularity, e.g., tumour demonstrate restricted diffusion parameters. Diffusion tensor imaging (DTI) is a special case of DWI where there is sufficient diffusion directions to model underlying tissue microstructure beyond the basic orthogonal three direction approach used to calculate an apparent water diffusion coefficient. Since FA is standard deviation of eigenvalues it is rotationally invariant, while

other metrics invoking the eigenvectors permit directionality to be assessed, which is the basis of the directionally encoded colour maps. DTI can measure diffusion of water along an axon in many directions (O'Donnell *et al.,* 2011). Principal application of DTI is imaging of white matter, where orientation, location and anisotropy of the white matter tracts can be measured. DTI offers quantitative measures which provide information regarding the tract functionality, namely fractional anisotropy (FA), mean diffusivity (MD), radial diffusivity (RD) and axial diffusivity (AD). Table 4.9 summarises the clinical significance of each measure. These measures are ratios of the eigenvalues that are used to quantify the shape of the diffusion. FA is the most widely used anisotropy measure, it is a standard deviation of the eigenvalues. It is thought to represent white matter integrity, although many factors can cause a variation in its measure. MD is the simplest measure of diffusion, and it represents mean of the tensor's eigenvalues. MD is also referred to as apparent diffusion co-efficient, or ADC.

DTI measure	Clinical Significance
Fractional Anisotropy (FA)	Quantified directionality of diffusion in a summative manner FA can be low due to crossing fibres and the definition of abnormal varies. Transient vasogenic oedema might reduce FA while not damaging axons Most widely used measure
Mean Diffusivity (MD)	Measure of overall diffusion Increase in MD consistent with increased water content e.g., oedema or inflammation
Radial Diffusivity (RD)	Perpendicular to the white matter tract Predictor of demyelination
Axial Diffusivity (AD)	Parallel to the white matter tract Predictor of axonal loss

Table 4.9 Summary of the mathematical measured of axonal function and its clinical significance.

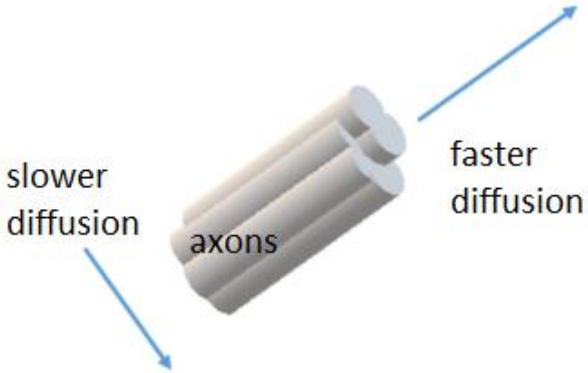

Figure 4.9 Illustration of anisotropic diffusion along the axons. This illustrates that diffusion measured parallel to the axons is faster than that of perpendicular to the axons in a white matter tract.

AD and RD are measures of diffusion in specific directions. AD is a measure of parallel diffusivity in relation to the axon and is equal to the largest eigenvalue, whereas RD is a measure of perpendicular diffusivity, and is equal to the average of two smaller eigenvalues (Figure 4.9).

In order to process the raw data, a number of pre-processing steps are involved: distortion correction (Glasser *et al*., 2013), gibbs ringing correction (Kellner *et al*., 2016), eddy current corrections (Andersson *et al.*, 2016), and geometric distortion correction using Top-up (Andersson *et al*., 2003). These methods are established and already published widely in the literature. Once the relevant corrections have been carried out, tractography was performed using the modified damped Richardson-Lucy (dRL) algorithm (Dell'Acqua *et al*., 2010). This method has been used in multiple studies and is able to provide a relatively accurate description of white matter organisation, estimation of fibre orientation with a short computational time. This creates an image that represents the major eigenvector field using a colour map (Figure 4.10). The colour scheme most commonly used to represent the orientation is as follows:

- Blue – superior-inferior
- Red – left-right
- Green – anterior-posterior

Tractography can produce false positive and false negative results. This is because the tensor model represents one major fibre direction in a voxel, thus tractography method can be confounded by regions of crossing fibres. Editing these fibres requires neuroanatomy knowledge. Figure 4.15 demonstrates an example of fornix tract in a healthy volunteer which has been edited following the Explore DTI manual (Leemans *et al*., 2009).

Tractography of the fornix and bilateral cingulum tracts was performed as they are both seen as critical parts of the limbic system (Bubb *et al*., 2018, Thomas *et al*., 2011) (Figure 4.11). The fornix tract originates in the hippocampus where it emerges from a collection of nerve fibres called the fimbria. It arches around the thalamus towards the front of the brain (Thomas *et al*., 2011). The cingulum tracts are prominent white matter tracts present in both cerebral hemispheres which interconnects frontal, parietal, and medial temporal regions with links to the cingulate gyrus (Bubb *et al*., 2018).

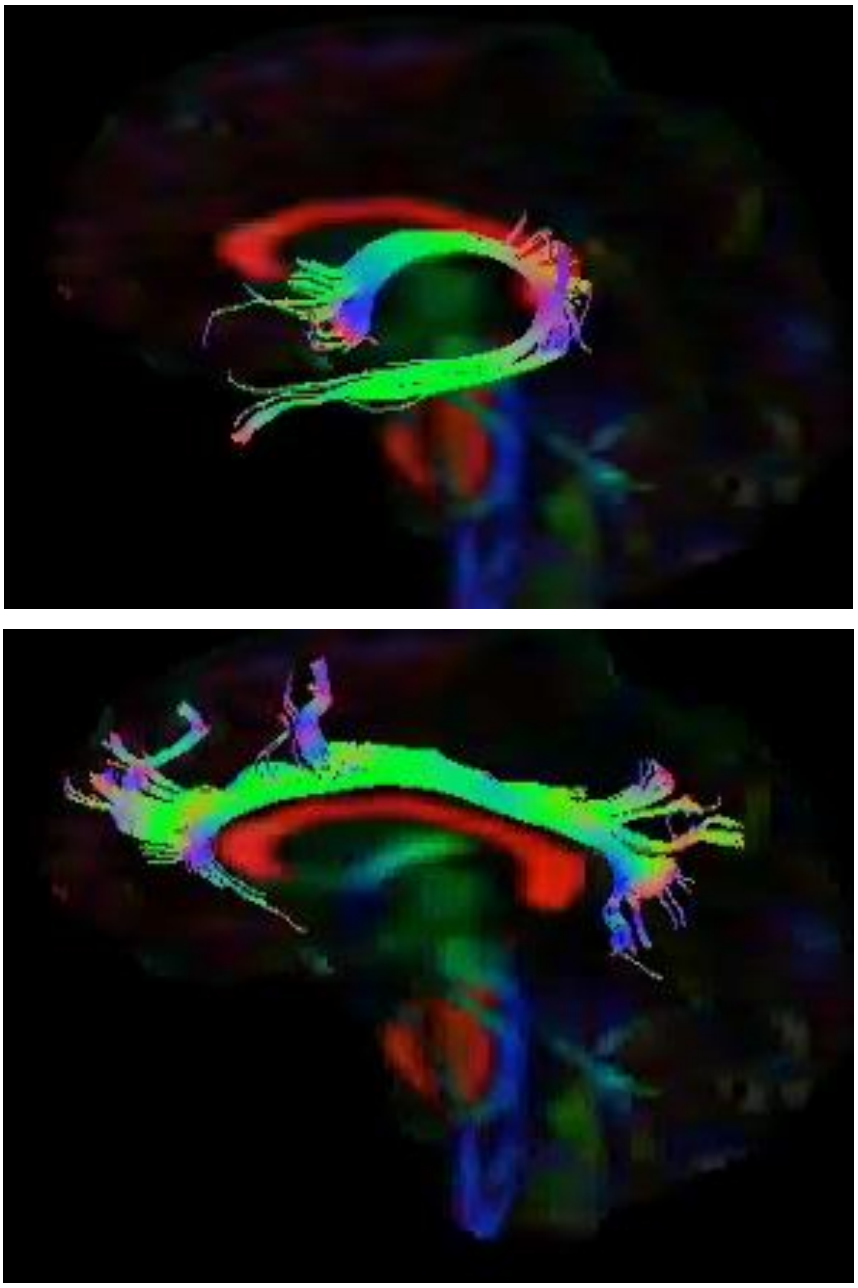

Figure 4.10 The Fornix tract (top) and the Cingulum Tract (bottom) in a healthy volunteer. *The green fibres indicate anterior-posterior direction of trajectory, blue fibres indicate superior -inferior direction of trajectory and red fibres indicate right-left direction of trajectory.*

4.4.6 Microstructure MRI

This is the first time in the world when patients with BM have been scanned using the Connectome scanner. This scanner is capable of producing a higher gradient strength compared to MRI scanners that are used in usual clinical practice, 300mT/m, and 40mT/m, respectively. This is a specially adapted scanner which can be used to probe microstructural detail in much finer detail. At the time of this research, there was only one other scanner in the world at Harvard University in United States of America.

The MRI scans performed using the connectome scanner focused on assessment of the BM and surrounding normal brain tissue. Two sequences performed were vascular, extracellular, and restricted diffusion for cytometry in Tumours (VERDICT) and composite hindered and restricted model of diffusion (CHARMED). Both sequences were based on DTI sequences and obtained multi-shell DTI images in sixty directions to allow probing of the microstructure of the brain. The high gradient strength of the scanner allows faster acquisition and ability to utilise higher b-values compared to standard 3 T scanner. VERDICT utilises low *b*-values and uses a mathematical model to estimate water content in three spaces intracellular, intravascular, and extracellular extravascular volumes and cell radius. CHARMED utilises higher *b*-values and provides estimation of directionality of nerve fibre tracts which may be multidirectional. These sequences have not been studied in patients with BM before, therefore we performed standard imaging parameters defined in the literature for human brain.

4.4.8 Final MRI Protocol

Final imaging protocol performed on the participants at CUBRIC is defined below.

3 Tesla Prisma	Parameters	Acquisition Time	Function	Parts of the brain studied
T1 FSPGR	TR 2300 ms, TE 2.98 ms, Flip angle 9°, FOV 256 mm, slice thickness 1 mm	5:19	Structural Image	Metastases & Organ at risk
T2 TSE	TR 4800 ms, TE 86 ms, Flip angle 150°, FOV 256 mm, slice thickness 3 mm	2:45	Structural Image	Metastases
T2 FLAIR	TR 11090 ms, TE 81 ms, Flip angle 155°, FOV 256 mm, slice thickness 2.5 mm	3:30	Structural Image	Metastases
ASL	TR 3300 ms, TE 13.48 ms, FOV 192 mm, Bolus duration 700 ms, TI 1990 ms, Slice thickness 3 mm	8:13	Perfusion	Metastases & Organ at risk
Single Shell DTI	TR 10000 ms, TE 56 ms, FOV 256 mm, b-value 1200 s/mm^2, 64 directions, slice thickness 2 mm	12:32	Tractography	Organ at risk
PRESS MR Spectroscopy – Left and Right Hippocampus	TR 2000 ms, TE 35 ms, Flip angle 90°, Water suppression bandwidth 50 Hz, 256 averages, Voxel size 40 x 15 x 8 mm	18:48	Metabolite Measurements	Organ at risk
BOLD	TR 3000 ms, TE 30 ms, Flip angle 89°, FOV 192 mm, slice thickness 2 mm.	6:11	Functional mapping/Oxygenation	Metastases & Organ at risk

Connectome Scanner	Parameters	Acquisition Time	Function	Parts of the brain studied
CHARMED	TR 3000 ms, TE 59 ms, FOV 220 mm, b-values = 0, 1000, 2000, 4000, 6000 s/mm2, 60 directions per shell, d/D 7.0, 23.3 ms, number of slices 66.	11:52	Multi-Shell DTI	Organ at risk
VERDICT	TR 3500 ms, TE 73 ms, FOV 220 mm, b-values = 0, 100, 200, 400, 800, 1000, 1500, 2000, 2500, 3000, 60 directions per shell, Delta 17.3, 25, 35 and 45 ms, number of slices 66.	8:06	Microstructure Imaging	Metastases

Table 4.10. Final MRI Protocol performed in the study. *ASL: Arterial Spin Labelling; BOLD: Blood oxygen level dependent; CHARMED: ; DTI: Diffusion Tensor Imaging; FSPGR: Fast spoiled gradient echo; FLAIR: ;FOV: Field of view; TE: Echo time; TR: Repition time; VERDICT: Vascular*

4.5 Conclusion

The trial protocol was completed with all neurocognitive and imaging parameters and approved by research ethics committee on 21st December 2016 (Wales REC reference number 16/WA/0374) and by Velindre University NHS Trust research and development department on 31st January 2017 (IRAS reference 209129). Service level agreement between Velindre University NHS Trust and CUBRIC was finalised on 7th April 2017. Velindre University NHS Trust was opened as the only recruiting site on and recruited its first patient on 4th May 2017. Subsequent chapters present clinical, NCF and MRI results at baseline and 1, 3, and 6-month follow up time points. First, I will present the results at baseline in Chapters 5 & 6, followed by NCF and MRI changes related to hippocampal dosimetry in Chapter 7. Chapter 8 will focus on functional and microstructure MRI of the metastases and surrounding normal brain tissue.

Chapter 5 - Clinical and Neurocognitive factors in Participants with Brain Metastases at presentation and their impact on outcome

5.1 Introduction

Although NCF impairment following treatment has been studied for primary and secondary brain tumours, baseline NCF at presentation of BM has not been investigated widely. As discussed in Chapter 1 and 4 BM themselves can cause substantial neurocognitive disability, hence, we used this opportunity to study NCF changes at baseline in this patient population. Adverse effects of radiotherapy treatment to the brain are commonly associated with impairment in memory, executive function, and attention (Platta *et al*., 2010). Approximately 90% of participants with BM enrolled in a randomised phase III trial exhibited impairment in at least 1 NCF domain (Mehta *et al*., 2003). Another study led by Herman *et al*., 2003, showed NCF impairment in 70% of the enrolled participants. Performance in neurocognitive tests is related to patient's ability to manage on a day-to-day basis and can have an impact on their ability to function independently (Herman *et al*., 2003).

A study conducted by Gerstenecker *et al*., analysed thirty-two participants with BM at baseline with demographically matched controls. Despite the aim of this study, in the patient group 26 out of thirty-two participants were tested within a week of commencing radiotherapy (11 whole brain and 15 focal radiotherapy). Six participants had undergone previous neurosurgery. Therefore, it is difficult to determine the contribution of acute radiotherapy treatment toxicity and post-surgical effects on NCF (Gerstenecker *et al*., 2014). Both groups undertook NCF tests in different domains: Hopkins Verbal Learning Test – Revised (HVLT-R), Digit Span subset from the Wechsler Adult Intelligence Scale third edition (WAIS-III), Digital Symbol subset from the WAIS-II, verbal fluency, The Trail Making Test A and B (TMTA and TMTB respectively), and Grooved Pegboard Test. Symptoms of depression were assessed using the Beck Depression Inventory and Karnofsky Performance Status was used for measure of functional status. Over 80% of participants

with BM displayed NCF impairment in at least one domain. BM participants performed significantly worse than their matched healthy controls in tests addressing memory (HVLT-R immediate) and language (verbal fluency and executive function (TMTB and Digit Symbol)). Digit Span, HVLT-recognition and TMTA were not worse in the patient group. A large proportion of participants exhibited neurocognitive dysfunction at or below 5th percentile: 46% in verbal fluency and 31% in executive functioning (Gerstenecker *et al.*, 2014). Figure 5.1 demonstrates the proportion of participants scoring at fifth percentile or below according to number of NCF tests impaired. Fifty-six percent of the participants displayed NCF impairment in three more tests at fifth percentile or below and 19% exhibited intact NCF in all domains (Figure 5.1). These data suggest that the majority of participants exhibit NCF impairment at presentation.

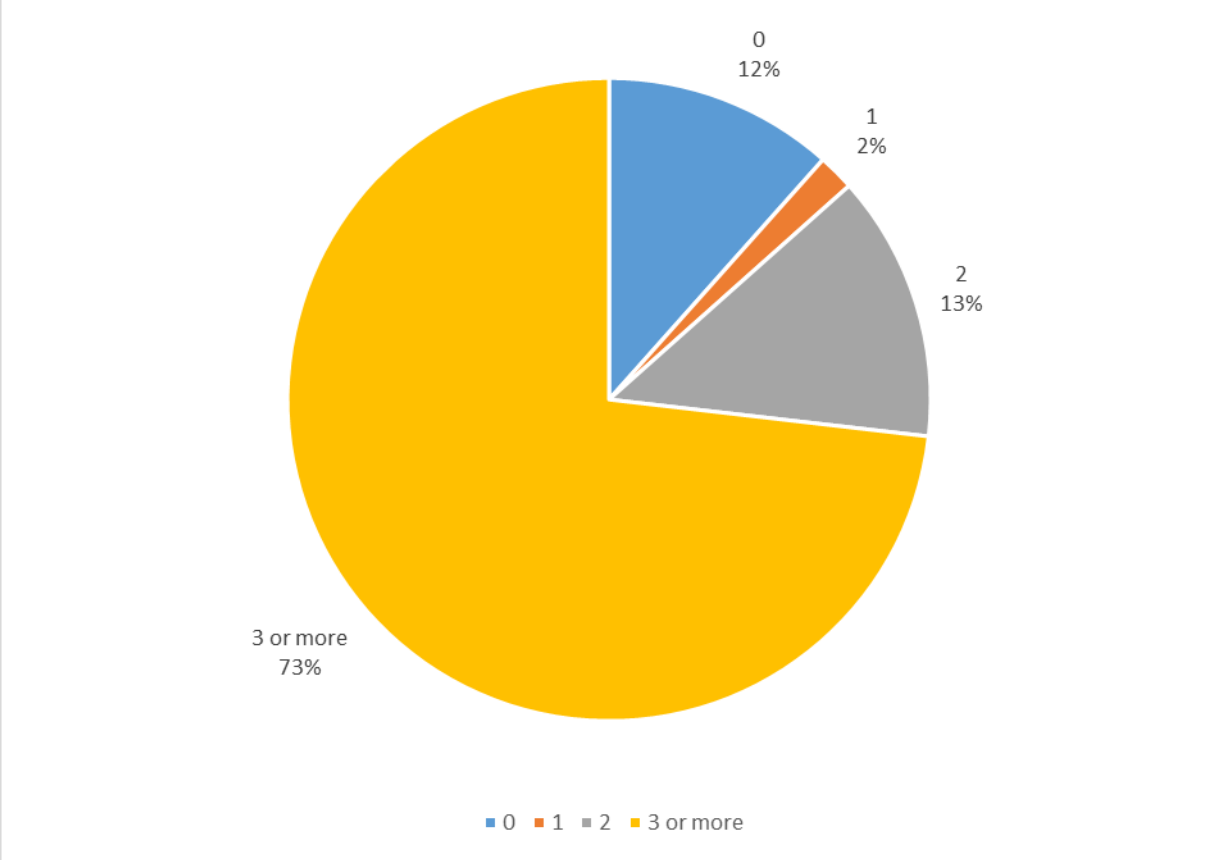

Figure 5.1 Percentage of participants scoring at 5th percentile or below divided according to number of neurocognitive tests. *Adapted from (Gerstenecker et al., 2014)*

Table 5.1 demonstrates that participants with BM scored significantly lower in memory, verbal fluency, and executive function domains, and significantly better in domains examining attention and processing speed (Gerstenecker *et al*., 2014). However, there are major limiting factor of this study is that they did not record important clinical factors that can influence NCF in this patient group, i.e., tumour location, tumour size, presence of oedema, number of lesions, burden of extracranial disease and concurrent use of steroids and systemic anti-cancer therapy. These participants are an extremely heterogeneous population where neurological and non-neurological factors can impact on NCF and quality of life greatly.

NCF Measure	Controls Mean percentile (SD)	BM Participants Mean percentile (SD)	p-value
HVLT-R immediate	25.8 (4.3)	9.0 (17.3)	<0.001
HVLT-R recognition	11.0 (1.1)	32.9	<0.001
Digit Span	18.1 (3.3)	42.6 (27.9)	0.005
Verbal Fluency	41.5 (10.4)	24.8 (29)	<0.001
TMTA	26.4 (7.7)	41.7 (29.4)	0.012
TMTB	66.3 (31)	26.5 (26.8)	<0.001
Digit Symbol	69.5 (16.6)	36.8 (32.9)	0.012

Table 5.1 Summary of NCF Tests Scores in participants with brain metastases compared with matched controls. *Scores normatively corrected. NCF: Neurocognitive function, SD: standard deviation, HVLT-R: Hopkins Verbal Learning Test – revised, TMTA: Trail Making Test A, TMTB: Trail Making Test B. (Table adapted from Gerstenecker et al., 2014).*

Another study conducted by Mehta *et al*., testing Motexafin gadolinium and WBRT in participants with BM showed significant NCF impairment at baseline: more than 65% of participants exhibited impairment in at least one test at baseline. NCF impairment was most prevalent in grooved PEG board test followed by HVLT tests (Mehta *et al*., 2003). They concluded that NCF outcome post treatment was unreliable because of impairment

caused by tumour growth and treatment. Although the group recorded NCF at baseline, factors contributing to NCF were not studied as it was not an endpoint of the study.

Several prognostic models have been designed for participants with BM namely RPA, GPA and DS-GPA, however these do not advocate incorporation of NCF testing. Although impact of NCF on survival has not been shown in participants with BM, NCF has been shown to be predictive of survival in recurrent primary brain tumours. A study conducted by Meyers *et al*., in participants with glioma revealed that except for Digit Span and grooved pegboard test, all other NCF tests (HVLT, COWAT, TMTA and B and Digital Symbol) were statistically related to worse overall survival (Meyers *et al*., 2000). In this study other factors that demonstrated statistically worse survival were diagnosis of glioblastoma multiforme, second recurrence episode, and three or more prior neurosurgeries. Performance on a test of verbal memory (HVLT) was independently and strongly related to survival after conducting multivariate analysis accounting for age, KPS score, histology, extent of resection, number of recurrences, and time since diagnosis. Participants with recurrent primary brain tumour have poor survival outcome, however, this study explored the reasons behind poorer survival in this group.

To investigate neurocognitive function in participants with BM we designed a prospective observational study, as described in chapter 4, in participants measuring neurocognitive function at baseline and following treatment with stereotactic radiosurgery. Before we analyse NCF changes following SRS treatment, it is important to understand burden of the NCF impairment at baseline and factors contributing to this. Therefore, I used this opportunity to study NCF impairment at baseline in participants undergoing SRS for BM.

5.2 Hypothesis

- Participants with BM will demonstrate impaired NCF in one or more domain at presentation.

- Participants with BM in the temporal lobe will exhibit NCF impairment in memory domain i.e., HVLT tests.
- Participants with BM in the frontal lobe will exhibit NCF impairment in executive function domain i.e., COWAT and TMTB.
- Participants with greater tumour volume will have lower NCF score.
- Participants having steroids and systemic anti-cancer treatment (SACT) at the time of testing will exhibit low NCF scores.

5.3 Methods

5.3.1 Study Design

The clinical design including inclusion and exclusion criteria and sample size has been described in section 4.2. In this chapter, I studied baseline clinical characteristics and NCF scores to identify factors which may influence outcome in this patient cohort, i.e., overall survival. Baseline data was collected on each participant: age, gender, primary cancer, location, number of total volumes of BM, timing of BM diagnosis, synchronous or metachronous, presence and sites of extracranial disease, control of extracranial disease, use of steroids and its dose, concurrent use of SACT, type of SACT, presence of seizure and neurological symptoms, date of intracranial progression, location of intracranial progression, and date of death.

5.3.2 NCF Testing

Section 4.3 describes the evidence for NCF tests used and summary of the NCF tests. A range of NCF testing was conducted by the same clinical psychologist at each time interval (Table 4.2) encompassing immediate recall, delayed recall, executive function, verbal fluency, and concentration. The tests included in the study have been recommended by the RANO group for trials in participants with BM (Lin *et al*., 2013).

Raw NCF test scores were calculated as standardised T scores (Iverson, 2011). Equation for T-score is expressed as:

$$T = 10 \times (\frac{x - M}{SD}) + 50$$

Where T is a T-score, x is a raw score, M is the mean of the normative sample and SD is that standard deviation of the normative sample. The T-score has a mean of fifty and standard deviation of ten. A T-score of less than 40 represents significant cognitive impairment, which is defined as below one standard deviation of the mean of the normalised population. Therefore, for the purposes of this study, those with a T-score of ≥40 were defined as having normal NCF scores and those with a T-score of <40 were defined as having impaired NCF (Benedict *et al*., 1998).

5.3.3 Statistical Analysis

Participants were dichotomised into NCF impaired or NCF retained group according to their T scores. Those with a score of <40 were considered to have impaired NCF and those with ≥40 were considered to have retained NCF. In the group comparisons between clinical factors and NCF were assessed using independent sample t-tests. Correlation analysis was conducted using Pearson correlation. Overall survival was defined as the time from diagnosis of BM until death due to any cause. Overall survival was calculated using Kaplan Meier survival calculations and comparison between the groups was performed using stratified log-rank tests. Planned subgroup analysis, specified by the stratification factors, were conducted. Bonferroni correction was used for multiple testing correction to assess for a discriminatory factor. Data were analysed using IBM SPSS Statistics Software version 28 (IBM Corp. Released 2021. IBM SPSS Statistics for Windows, Version 28.0. Armonk, NY: IBM Corp)

5.4 Results

Thirty-six participants were recruited between May 2017 and December 2018. Five participants were excluded following consent: one was due to absence of BM on the planning MRI brain; three participants deteriorated between planning process and treatment date and as a result did not undergo SRS; one patient decided not to participate after consenting due to commitment required for other oncological treatments.

5.4.1 Patient Characteristics

Mean age of all participants was 64 years. Median WHO performance status was one. Over a third of participants did not exhibit any neurological symptoms at presentation and all the participants without neurological symptoms had underlying primary cancer of NSCLC or melanoma. This is likely to be a consequence of surveillance brain imaging due to higher risk of CNS involvement and current NICE guidance (NICE, 2019, NICE, 2015).

Characteristic	n. (%)
Gender	
Male	17 (55)
Female	14 (45)
Age, mean (range)	64 (24-85) years
WHO Performance status, median	1
0	8 (26)
1	12 (39)
2	11 (35)
Handedness	
Right	26 (84)
Left	5 (16)
Level of Education, mean (range)	12.9 (10-22) years

Table 5.2 Demographics of Participants in the study. *WHO: World Health Organisation*

The most prevalent neurological symptom was seizure (16%) followed by cognitive symptoms (13%). Most common primary malignancy in this patient cohort was lung cancer: 39% of participants' primary diagnosis was non-small cell lung cancer. Extracranial

malignancy was present in the majority of participants and the most common site of extracranial metastases was lung. Primary tumour controlled based on recent imaging for 61% participants. For remainder of the participants, presentation with BM occurred simultaneously with extracranial disease progression and they underwent treatment for BM with SRS first followed by systemic therapy for primary malignancy. Thirty-two percent participants presented with synchronous BM. Median time between diagnosis of primary malignancy and BM diagnosis was 9 months ranging from 0 to 230 Months (Table 5.3).

Features of Malignancy and BM	n. (%)

Primary Cancer	
Lung	12 (39)
Melanoma	7 (22)
Renal	4 (13)
Breast	2 (6)
Colo-rectal	3 (10)
Others (oesophagus, bladder, and nasopharynx)	3 (10)
Extracranial disease present	26 (84)
Extracranial disease sites	
Lung	20
Bone	3
Liver	2
Lymph node	8
Soft Tissue	1
Adrenal	1
Extracranial Malignancy controlled	19 (61)
Synchronous Brain Metastases	10 (32)
Median time to diagnosis of Brain Metastases	9 Months
Number of brain metastases	
1 metastasis	23 (74)
2 metastases	7 (23)
3 metastases	1 (3)
Total number of metastases	40
Volume of Metastases, mean (range)	3.99 (0.75-15.91) cc
Location of metastases	
Frontal	14
Parietal	8
Temporal	5
Cerebellar	8
Occipital	2
Subcortical	3
Neurological symptoms	
None	11 (35)
Headache	3 (10)
Seizures	6 (16)
Motor	3 (10)
Ataxia	3 (10)
Cognition	4 (13)
Personality	1 (3)
Speech	1 (3)

Table 5.3 Baseline clinical features of primary malignancy and brain metastases.

Seventy-four percent of participants had a single intracranial metastasis at presentation and the most common site was frontal lobe followed by parietal lobe and cerebellum. Least common intracranial site was occipital lobe. Forty metastases were treated in total. Mean volume of BM was 3.99 cc ranging from 0.75 cc to 15.91 cc. There was no statistically significant correlation between number and volume of BM (p=0.632). One patient with three BM had small volume intracranial disease and total volume of BM for this patient was 1.07 cc. Figure 5.2 demonstrates the relationship between number and volume of BM.

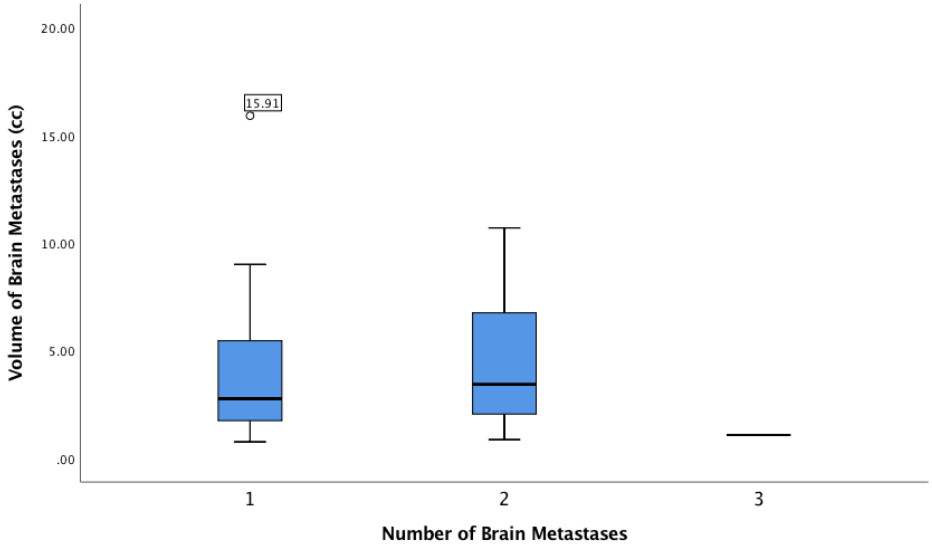

Figure 5.2 Boxplot representing relationship between number and total volume of brain metastases

Higher volume of BM was associated with presence of seizure with a mean total volume of BM in participants who did not have seizures of 3.56 cc compared with a volume of 5.78 cc in participants who had seizures (p-value <0.05).

Twenty-four (77%) participants were treated with systemic anticancer therapy. Fourteen participants (45%) had more than one modality of treatment (radiotherapy, surgery or SACT) for their primary cancer. Half of these participants were treated with cytotoxic chemotherapy. Fifteen participants had a course of dexamethasone in addition to short course of steroids administered following SRS treatment. Dose of dexamethasone varied from 0.5mg - 16mg.

Other Treatments	n.
Treatment for primary malignancy	
Radical Radiotherapy	8
Surgery	14
SACT	24
Participants receiving SACT	24
Types of SACT	
Chemotherapy	12
Oral targeted SACT (e.g., TKI)	8
Immunotherapy	4
Participants receiving Steroids	15
Dose of Steroids (mean, range)	6, 0.5-16mg

Table 5.4 Treatment for Primary Malignancy and Use of Steroids. *SACT: Systemic Anti-Cancer Therapy; TKI: Tyrosine kinase inhibitor.*

5.4.2 NCF Tests Results

Participation in NCF tests was tolerated well in this patient cohort and most participants adhered to the protocol without any impediments and completed all the assessments. Three participants were not able to complete TMT-B, one of the domains of NCF testing, and one was unable to complete delayed recall and recognition domains of HVLT. All other participants completed all the domains of NCF tests. Eleven, 35% participants did not exhibit significant NCF impairment in any domain whilst twenty, 65% of participants displayed NCF impairment in at least 1 NCF domain (Figure 5.3).

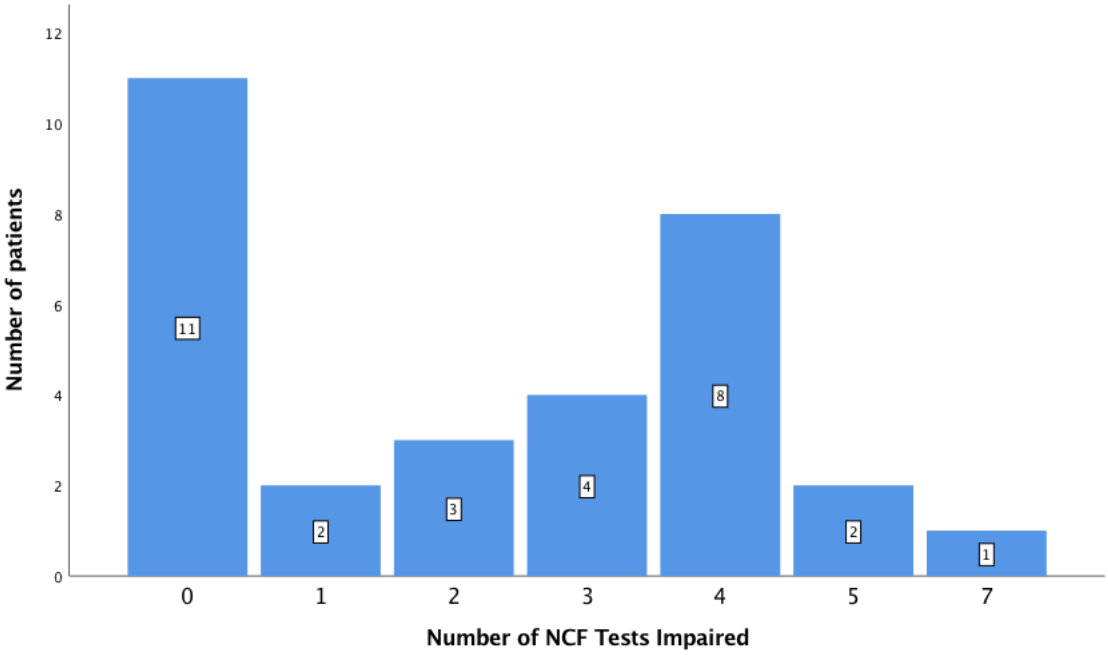

Figure 5.3 Number of NCF tests impaired in all the participants. 35.5% patients did not exhibit any NCF impairment; 6.5%, 9.6%, 12.9%, 25.8%, 6.5%, 3.2% demonstrated NCF impairments in 1, 2, 3, 4, 5, 7 domain on NCF tests.

HVLT scores for each domain, total recall, delayed recall, retention, and recognition, are illustrated in figure 5.4. Out of thirty-one participants 15 (48%) showed impaired NCF in total recall domain, 13 (42%) in delayed recall, 8 (26%) in retention and 6 (19%) in recognition. All except one patient (participant 8) completed the tests.

The scores of TMT A and B, COWAT and digit span are demonstrated in figure 5.5. Of the thirty-one patients, 4 (13%) showed impairments in TMT-A, 9 (29%) in TMT-B, 8 in COWAT (26%) and 6 (19%) in digit span. Three participants were unable to complete TMTB, therefore score has not been calculated for these. This is a key factor for those participants as this could have been due to impairment of executive function.

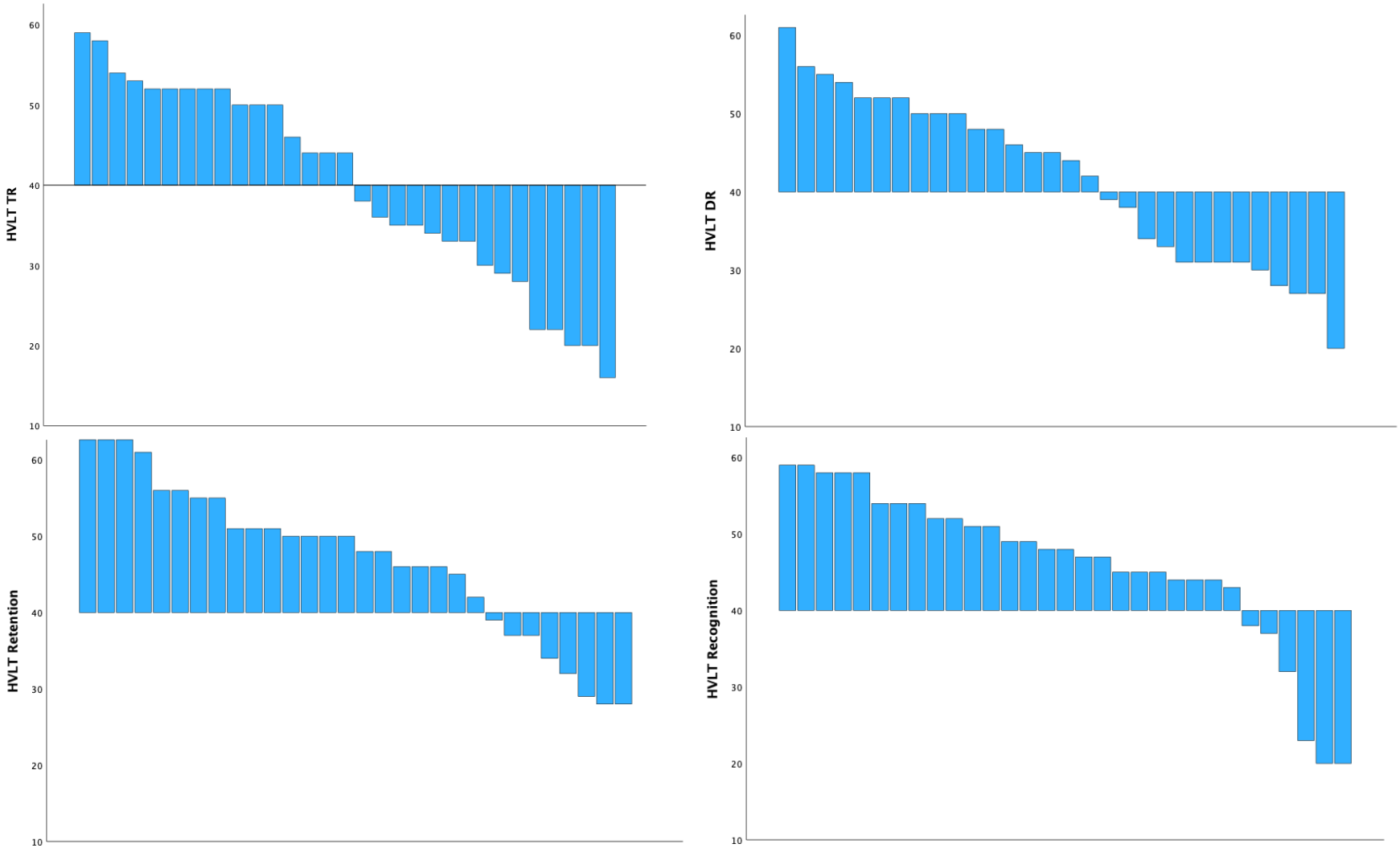

Figure 5.4 Waterfall chart demonstraing T score of each participant in the four domains of HVLT-R. *HVLT-R: Hopkins Verbal Learning Test – Revised; TR: Total Recall, DR: Delayed Recall*

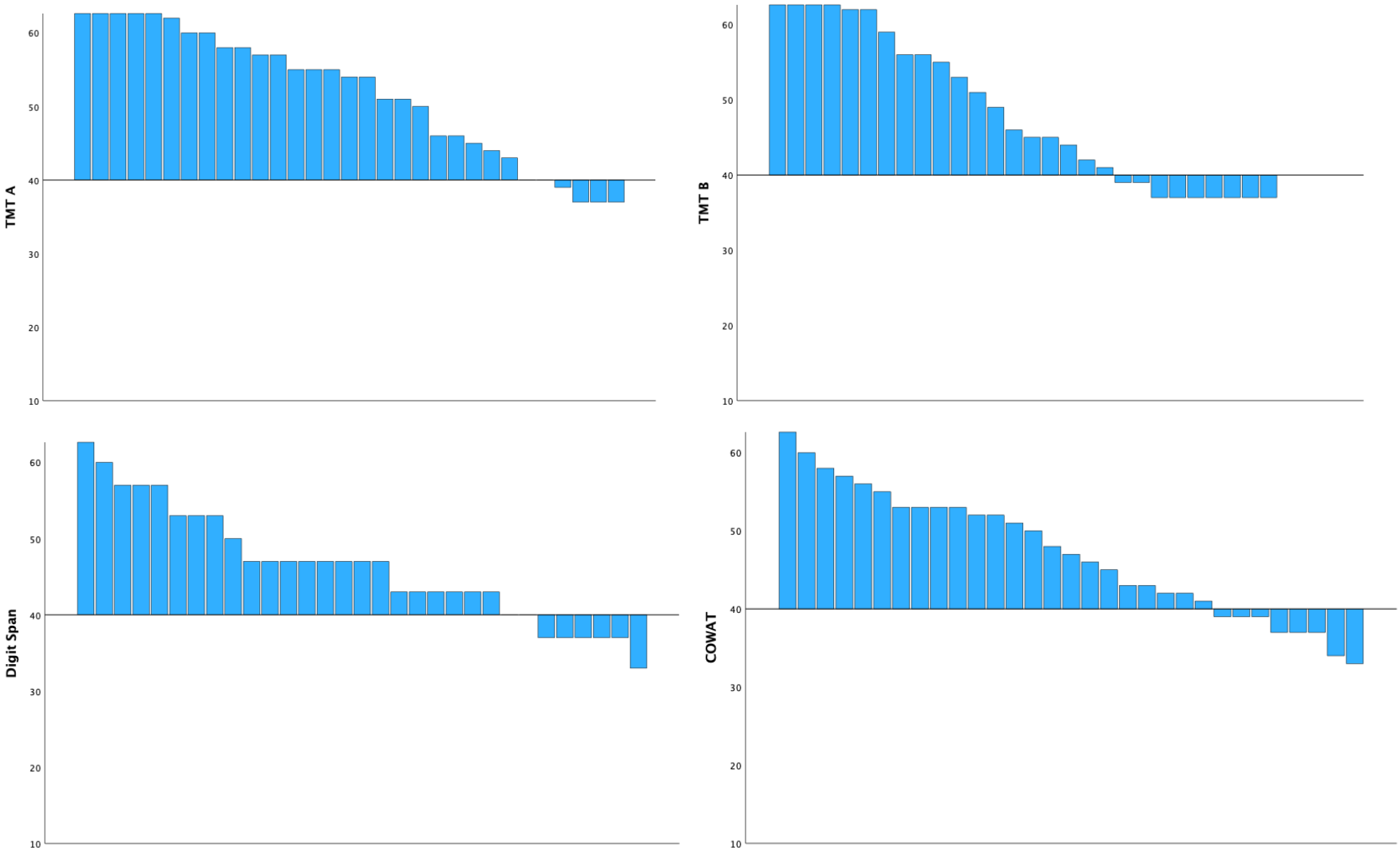

Figure 5.5 Waterfall chart demonstraing T score of each participant in Trail Making Test A&B, Controlled Oral Word Associal Test and Digit Span. *TMT A: Trail Making test A; TMT B: Trail Making test B; COWAT: Conrolled Oral Word Association Test*

5.4.3 Clinical and Tumour Factors Affecting NCF Scores

There was no significant correlation between scores in the different NCF domains and years of education (r=-0.06 - 0.06, p-value >0.05) or age (r=-0.061 - 0.343, p-value >0.05). Females scored statistically significantly higher than males in total and delayed recall. Tests investigating executive function can be associated with levels of education, however this correlation did not exist in this dataset. Table 5.5 summarises the scores for each NCF domain for males and females.

Test	Female (mean, SD)	Male (mean, SD)	p-value
HVLT-Total Recall	46.07 (10.85)	35.18 (12.00)	0.013
HVLT-Delayed Recall	45.93 (10.10)	37.94 (10.31)	0.041
HVLT-Retention	49.07 (9.12)	46.44 (13.51)	0.532
HVLT-Recognition	49.57 (9.04)	43.18 (11.13)	0.088
Digit Span	45.64 (9.09)	46.82 (6.29)	0.684
Trail Making Test A	52.71 (9.16)	51.06 (8.95)	0.617
Trail Making Test B	49.00 (12.34)	47.94 (8.45)	0.8
COWAT	46.79 (9.35)	47.24 (7.3)	0.855

Table 5.5 NCF Scores according to gender. *HVLT: Hopkins Verbal Learning Test, COWAT: Controlled Oral Word Association Test*

Number of BM did not adversely impact on NCF in any domain. There was no statistical significance between participants who had 1, 2 or 3 BM (Figure 5.6).

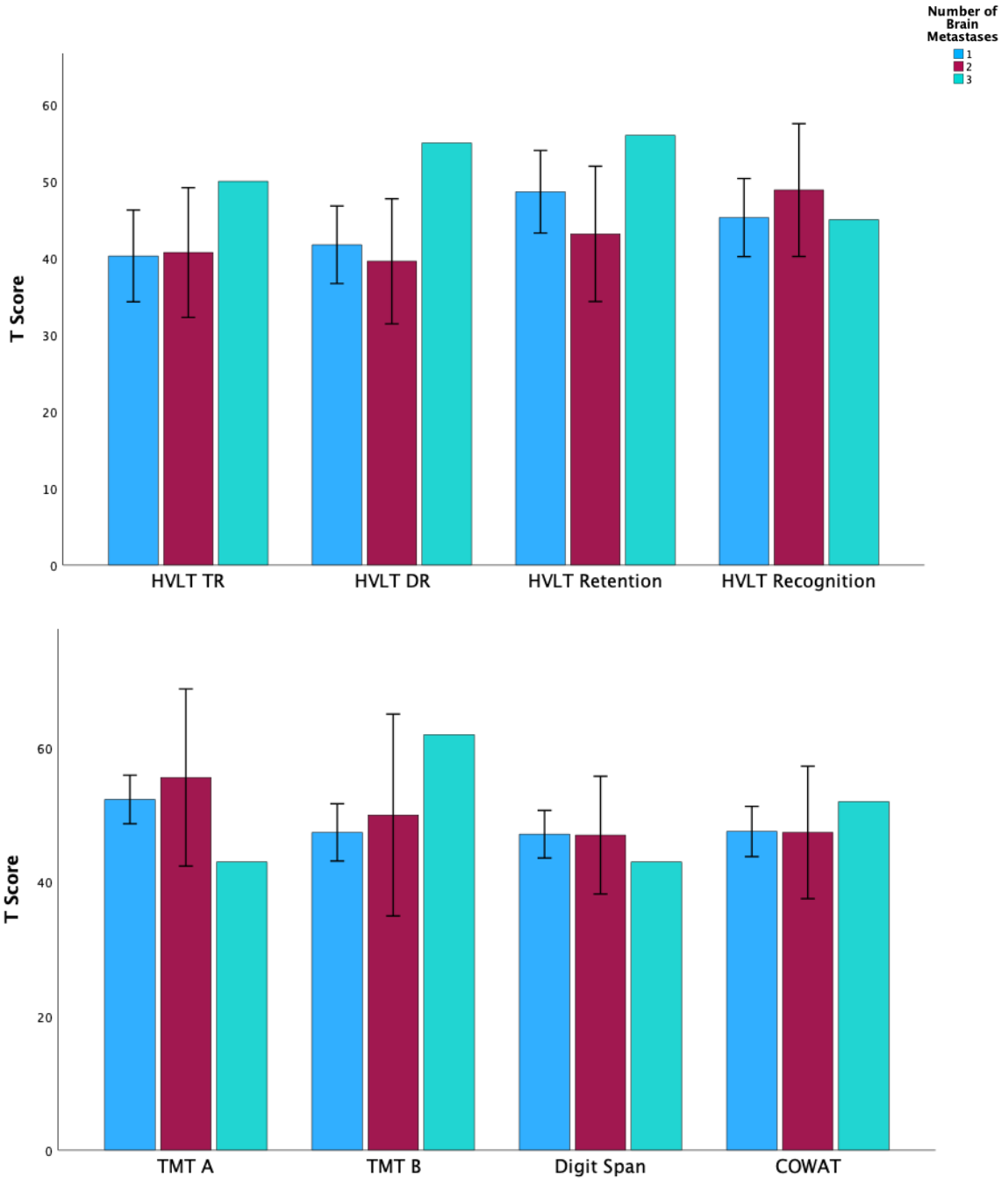

Figure 5.6 T-scores of NCF tests according to number of brain metastases. *HVLT TR: Hopkins verbal learning test total recall; HVLT DR: Hopkins verbal learning test delayed recall; HVLT Retention: Hopkins verbal learning test retention; HVLT Recognition: Hopkins verbal learning test recognition; TMT A: trail making test A, TMT B: trail making test B; COWAT: controlled oral word association test. Error bars represent 95% confidence interval. No error bars on patient with 3 metastases as there was 1 paricipant in this group.*

Analysing NCF scores according to tumour volume, did not demonstrate a statistically significant correlation between NCF scores and metastases volume in any domain. TMT-B scores were negatively correlated with metastases volume (r=-0.436, p-value 0.02). COWAT (r =-0.301), HVLT-TR (r = -0.264) and HVLT-DR (r = -0.204) were all weakly negatively correlated with metastases volume; however, statistical significance was not reached.

There was no significant difference in the NCF scores depending on the location of metastases within a certain lobe of the brain (Table 5.7).

Test	Frontal	Parietal	Temporal
HVLT-Total Recall	39.38 (+/-13.7) 40.61 (+/-12.08)	42.75 (+/-12.33) 39.17 (+/-12.81)	37.2 (+/-10/43) 40.65 (+/-13.06)
HVLT-Delayed Recall	43.46 (+/-9.63) 40.29 (+/-11.75)	47.14 (+/-8.17) 40 (+/-11.12)	35 (+/-9.513) 43 (+/-10.74)
HVLT-Retention	51.08 (+/-11.69) 45.06 (+/-11.07)	52.71 (+/-6.34) 46.13 (+/-12.42)	39.8 (+/-9.86) 49.24 (+/-11.38)
HVLT-Recognition	47 (+/-10.91) 45.39 (+/-10.6)	49.75 (+/-4.62) 44.78 (+/-11.8)	42.2 (+/-14.29) 46.81 (+/-9.9)
Digit Span	45.54 (+/-4.56) 46.83 (+/-9.25)	44.5 (+/-8.54) 46.91 (+/-7.3)	50.8 (+/-45.42) 45.42 (+/-7.11)
Trail Making Test A	52.85 (+/-9.14) 51.06 (+/-8.97)	50.25 (+/-9.65) 52.35 (+/-8.83)	52.8 (+/-9.86) 51.62 (+/-8.94)
Trail Making Test B	47.36 (+/- 10.01) 49.06 (+/-10.4)	52.14 (+/-10.04) 47.14 (+/-10.04)	49.6 (+/-11.91) 48.13 (+/-9.95)
COWAT	44.69 (+/-8.27) 48.72 (+/-7.85)	47.75 (+/-7.09) 46.78 (+/-8.62)	51 (+/-8.52) 42.27 (+/-8.02)

Table 5.6 T-scores of NCF tests in relation to Location of Metastases Data is mean +/- SD for each group. Top row is the value where metastases is present in that lobe, bottom row is where metastases is absent in that lobe. *HVLT: Hopkins Verbal Learning Test, COWAT: Controlled Oral Word Association Test*

Participants treated with SACT at the time of testing, particularly with chemotherapy, displayed lower NCF scores in most NCF domains, however this did not reach statistical significance. Figure 5.7 summarises NCF scores in all domains according to participants receiving SACT.

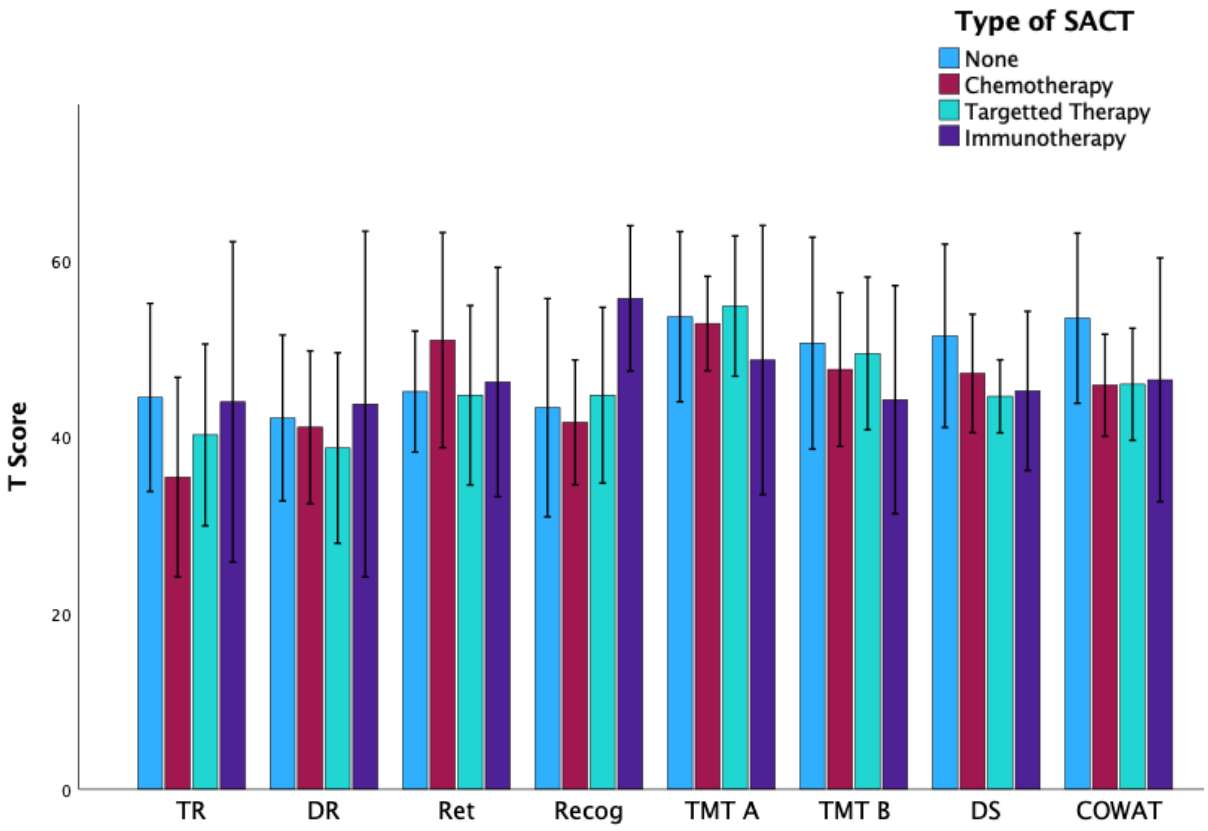

Figure 5.7 T-scores of all NCF tests according to different types of systemic anti-cancer therapies on different domains of NCF testing. *TR: Hopkins verbal learning test total recall; DR: Hopkins verbal learning test delayed recall; Ret: Hopkins verbal learning test retention; Recog: Hopkins verbal learning test recognition; TMTA: trail making test A, TMT B: trail making test B; DS: digit span; COWAT: controlled oral word association test. . Error bars represent 95% confidence interval.*

There was no statistically significant difference in the groups stratified according to receipt of steroids (Figure 5.8). If participants received steroids and SACT at baseline compared with receiving either one of the treatments, they were much more likely to have NCF impairment in HVLT-TR (mean T score 30 +/-8.77 vs 46.18 +/-11.04, p-value 0.03).

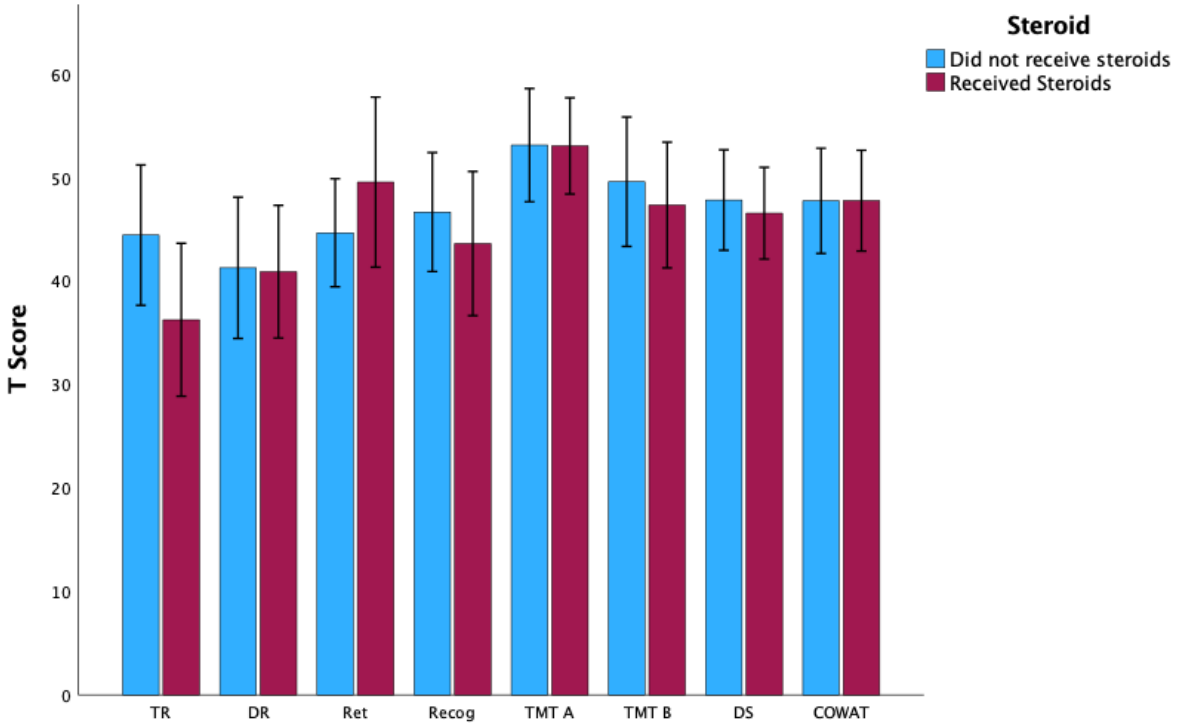

Figure 5.8 Bar chart representing NCF scores according to receipt of steroids. *TR: Hopkins verbal learning test total recall; DR: Hopkins verbal learning test delayed recall; Ret: Hopkins verbal learning test retention; Recog: Hopkins verbal learning test recognition; TMT A: trail making test A, TMT B: trail making test B; DS: Digit Span; COWAT: controlled oral word association test. . Error bars represent 95% confidence interval.*

5.4.4 Survival

Median overall survival was 11 months (Figure 5.9). Twelve (42%) of the participants were alive at 12 months and six were alive at 24 months. Nine participants were alive at the time of data analysis (November 2019). Half of all deaths were due to neurological causes. Thirteen participants had intracranial progression, four of these were disease progression at the SRS treatment site. Of those who had recurrence at the site of SRS, three

participants had surgical resection after SRS treatment. Five participants were treated with further SRS, one was treated with whole brain radiotherapy, two received systemic therapy and two were not well enough to receive further active oncological treatment, hence best supportive care was advised (Table 5.7). Three participants deteriorated rapidly following SRS and did not have any post treatment imaging to assess for intracranial relapse.

Treatment for Intracranial progression	n.
Surgical resection	3
Further SRS	5
Whole brain radiotherapy	1
Systemic Anti-Cancer Therapy	2
Best supportive care	2

Table 5.7 Treatment given for intracranial disease progression for all 13 participants who had intracranial progression.

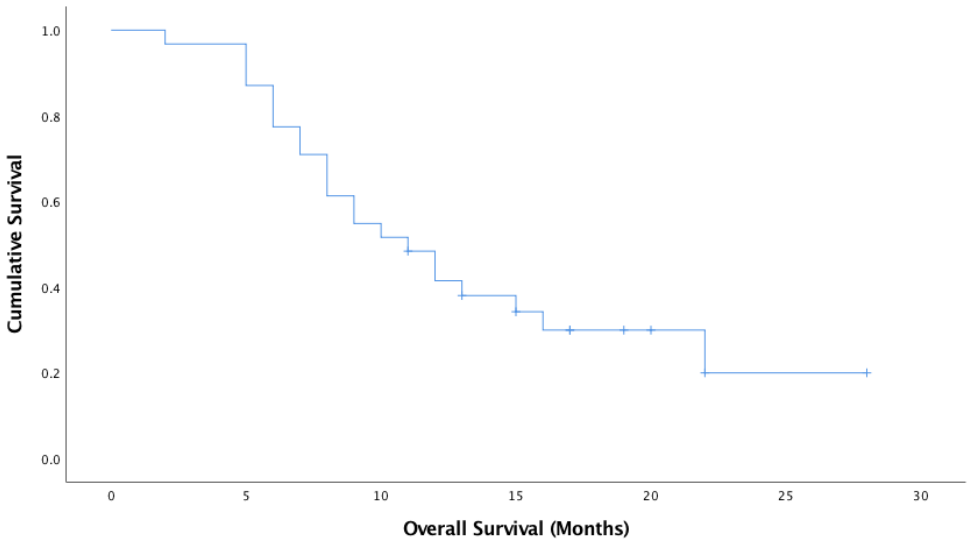

Figure 5.9 Overall Survival of all participants recruited to the study

Several clinical factors were shown to be associated with patient survival in our cohort. Participants with WHO PS 0 had significantly improved overall survival compared to participants with WHO PS 2 at presentation. Median overall survival was 15 months versus 7 months, p=0.043 (Figure 5.10).

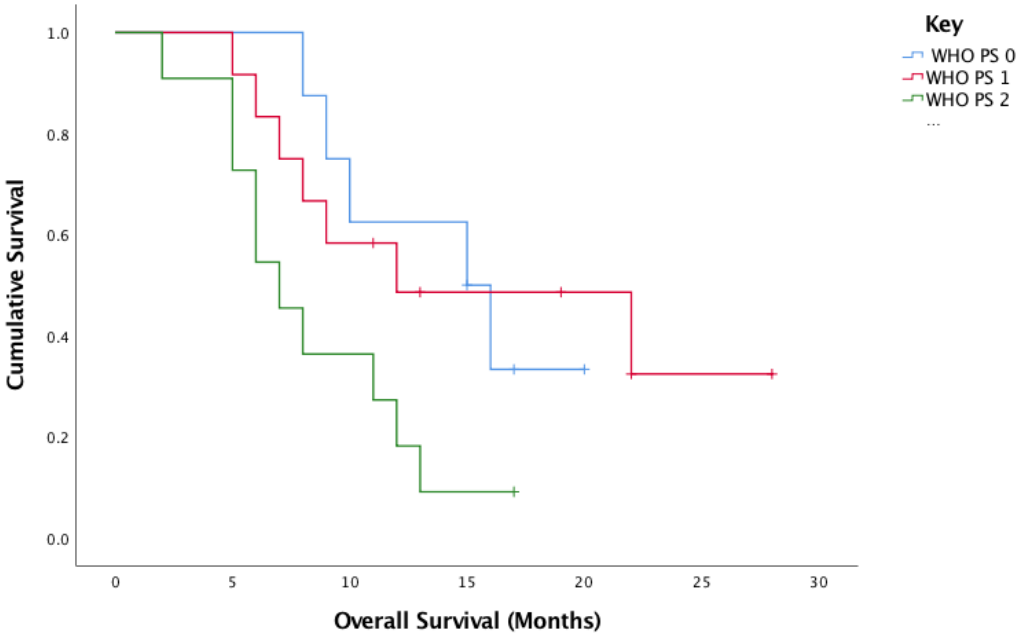

Figure 5.10 Overall Survival according to patient's WHO performance status at presentation. *WHO PS: World Health Organisation Performance Status.*

Absence of neurological symptoms was associated with better overall survival compared to those who had symptomatic BM, median OS 14 months vs 7 months respectively, p-value 0.479. Median survival was 12 months in participants who did not have seizures compared to 6 months in participants who had seizures (Figure 5.11). This difference was not statistically significant (p-value = 0.072).

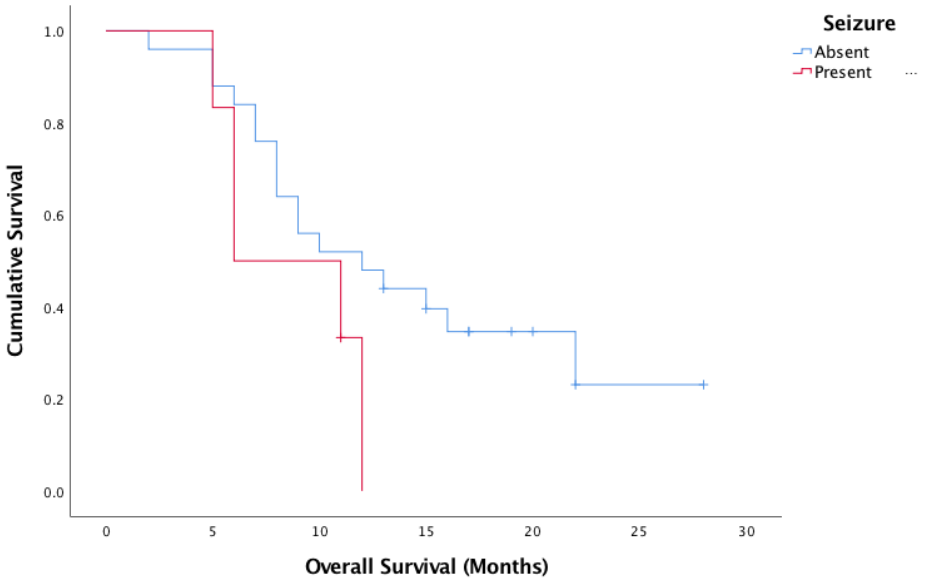

Figure 5.11 Overall Survival according to presence of seizure pretreatment for Brain Metastases

Participants with primary diagnoses of non-small lung cancer (NSCLC), renal cell cancer and melanoma showed the highest median survival, 15, 13 and 10 months, respectively. Whereas breast cancer was associated with lowest median overall survival (5 months) in this patient cohort. There was no statistically significant difference in survival in patients who received SACT or not (Figure 5.12).

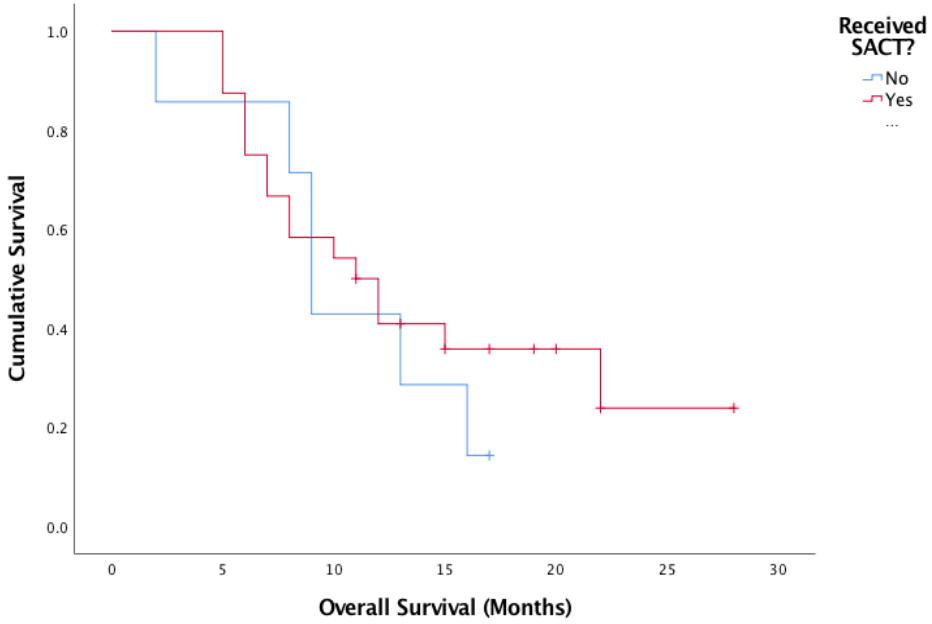

Figure 5.12 Overall Survival according to administration of SACT. *SACT: Systemic anti-cancer therapy*

Participants with NCF impairment in any domain have worse median survival compared to participants who had retained NCF 6 months vs 17 months respectively, however, this did not reach statistical significance (HR 2.084, p=0.094) (Figure 5.13). On investigating whether one NCF domain had greater impact on survival than another our data demonstrated a trend toward improved survival in the patient group with retained NCF in all NCF domains, which did not reach statistical significance (figure 5.14, table 5.8).

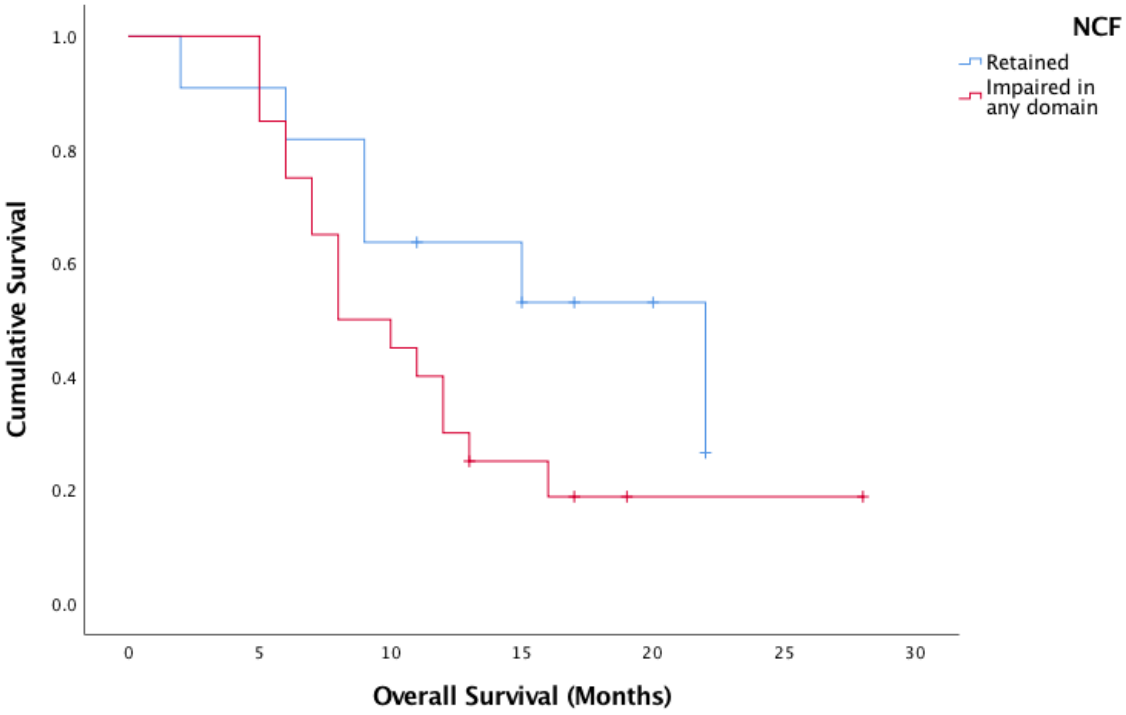

Figure 5.13 Overall survival in months according to Neurocognitive Impairment in any domain *NCF: Neurocognitive Function*

Test	Hazard Ratio	95% Confidence Interval
HVLT-TR	1.765	0.17 - 18.28
HVLT-DR	1.128	0.086 - 14.718
HVLT- Retention	0.822	0.132 - 5.112
HVLT-Recognition	0.271	0.041 - 1.772
Digit Span	3.658	0.284 - 47.191
TMT-A	0.349	0.032 - 3.849
TMT-B	3.182	0.464 - 21.838
COWAT	0.345	0.038 - 3.105

Table 5.8 Hazard Ratio and 95% confidence interval for all NCF tests represented in Figure 5.15. *As the hazard ratio crosses 1, it did not reach statistical significance.*

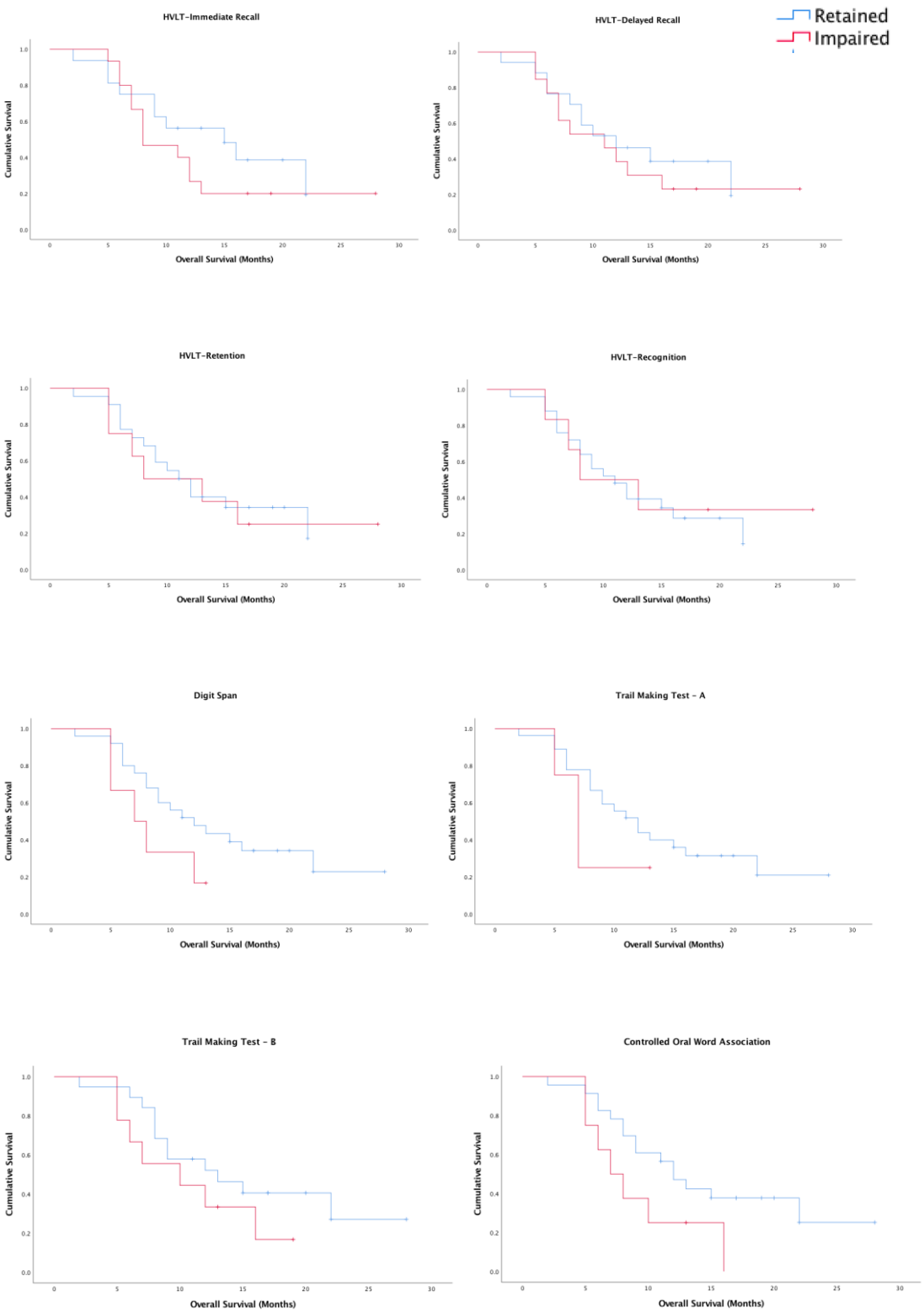

Figure 5.14 Overall survival in participants according to different NCF tests performed. *HVLT: Hopkins Verbal Learning Test*

5.5 Discussion

The focus of much of previous studies examining neurocognition in participants with BM has been on NCF impairment after treatment, particularly radiotherapy. This has supported the role of SRS alone, sparing participants of the neurocognitive impact of WBRT (NICE, 2018, Brown *et al*., 2016a, Chang *et al*., 2009, Sahgal *et al*., 2015). Studies have also examined baseline NCF impairment at baseline in all patients with BM (Gerstenecker *et al*., 2014, Herman *et al*., 2003). However, this has not been studied in patients undergoing SRS alone. Possible reasons for this could be that this cohort of patients present with limited volume of intracranial disease with favourable prognosis.

In this cohort, the most common primary cancer was NSCLC followed by melanoma, which is consistent with published literature. The Majority of participants had WHO performance status of one and had controlled extracranial disease at the time of SRS. Ten participants were asymptomatic. All of these participants had an underlying diagnosis of melanoma or NSCLC. This is likely attributable to established use of surveillance brain imaging at diagnosis in lung cancer and regular surveillance imaging in melanoma. This also translated in better survival in participants with BM who had an underlying diagnosis of lung cancer and melanoma, however we did not demonstrate statistical significance, possibly due to low number of participants. Another group of participants who had better survival outcome was participants with renal cell carcinoma. It is important to note that role of immunotherapy is established in these cancer sites and recent studies have demonstrated synergistic effect of immunotherapy and radiation (Turgeon *et al*., 2019). Combination of immunotherapy and radiotherapy continues to be an evolving treatment paradigm – a recent phase III trial has established role of adjuvant immunotherapy following chemoradiotherapy for stage III NSCLC as standard of care in UK (Antonia *et al*., 2018).

SRS without WBRT can lead to increased risk of intracranial relapse which has been demonstrated in previously published clinical trials (Brown *et al*., 2016a). Hence, 3

monthly surveillance MRI is advised by NICE following SRS (NICE, 2018). Limited intracranial relapse can often be managed with salvage therapy with either further SRS or neurosurgical resection. This has been demonstrated in our study as 9 out of 15 participants who relapsed had either further SRS or surgical resection.

I have demonstrated that a considerable proportion of participants with BM present with impaired NCF at baseline. Sixty four percent of all participants with newly diagnosed BM undergoing SRS exhibited cognitive impairment in at least one cognitive domain and all domains can be affected: memory, attention, processing information and executive function. When exploring further into specific NCF domains, impairment in memory was observed most frequently; half of the participants were impaired on two measures of verbal memory: 48% impaired in HVLT-TR and 42% impaired in HVLT-DR. This was followed by deficiency in retention, executive function, and verbal fluency: 25% impaired in retention, 29% impaired in TMT-B and 25% impaired in COWAT. Three participants were unable to complete TMT-B, which is a significant consideration as all these three participants displayed NCF impairment in several other domains. Impairment in the recognition arm of the HVLT test, as well as processing speed and attention was less frequent.

Most participants exhibited impairment in immediate and delayed recall domain on HVLT-R. It is easy to administer, well tolerated and has been validated in participants with brain disorders. High test–retest reliability and discriminatory validity has been established (Byrne, 2000). It has been shown to have high sensitivity and specificity for detecting mild dementia in older people (Hogervorst *et al*., 2002). It has been used extensively in research with diverse populations including the elderly, individuals with mild cognitive impairment, dementia, HIV, traumatic brain injury, Huntington's disease, Parkinson's disease, schizophrenia, and multiple sclerosis (Belkonen, 2011).

A small number of studies have looked at NCF impairment at baseline in this patient group. There are several potential reasons for this in this cohort of participants: location

of the tumour, volume of tumour, concurrent delivery of SACT, chemotherapy and concurrent use of dexamethasone. The location of metastases did not impact significantly as there was no significant difference in NCF test scores stratified according to the location of metastases. It was noteworthy that in participants who received steroids and SACT, NCF impairment was more significant than those who did not receive either treatment, however the differences were not statistically significant. NCF impairment following treatment with steroids and SACT is well recognised as two separate entities, however both factors that can impact on NCF independently may have synergistic effect on NCF when given concurrently.

Steroids have associated with NCF impairment particularly with regards to executive function. Steroid-induced psychosis is a well-recognised side effect which may be due to effect on the pathways involved in executive function of the brain (Moore and O'Keeffe, 1999). Lower NCF has been associated with chemotherapy in participants with breast cancer hence giving rise to the term "chemo brain" (Staat and Segatore, 2005). There is limited understanding of pathogenesis of NCF impairment due to chemotherapy and one hypothesis suggests disruption in cerebral blood flow which may give rise to cognitive impairment in the short term. Long term effects of chemotherapy on NCF are not known. It is important to note that fatigue due to disease or other cancer treatments can also impact on NCF. This will be discussed more in detail in Chapter 7.

Factors associated with improved survival were absence of seizure, performance status 0, participants receiving SACT and with retained NCF. Individually these factors did not demonstrate statistical significance. Presence of seizure has been shown to be associated with improved survival in primary brain tumour (Lu *et al*., 2018). The presence of seizures is thought to indicate a low-grade glioma which has transformed into high grade tumour. However, in patients with BM it is associated with higher BM burden and therefore may represent advanced disease.

Impaired NCF was associated with worse overall survival in this patient cohort. We did not demonstrate statistical significance, likely because of small number of participants. Worse NCF has been associated with worse survival in participants with recurrent glioma (Meyers *et al*., 2000), however, this has not been demonstrated in participants with BM before. Multivariate analysis considering WHO PS, presence of seizure, presence of neurological symptoms, treatment with concurrent SACT, BM volume and numbers, demonstrated that NCF impairment was not discriminatory and therefore, could be a surrogate marker for disease burden in this patient population.

I have demonstrated that two thirds of patients undergoing SRS exhibit NCF impairment at baseline, there is a need to develop robust prognostic tools for this cohort to guide their management. In order to show to address all the hypotheses thoroughly in a prospective study you will need to have enough participants to address expected confounding factors which can be challenging. This is a heterogenous population with multiple primary cancer diagnoses on variable treatments which can have an impact on patient's survival and response to treatment. With small number of patients and multiple measurements, it is challenging to demonstrate statistical significance.

5.6 Conclusion

In this chapter I have demonstrated that two-thirds of participants have NCF impairment at presentation prior to receiving oncological treatment that offers local control for BM. This reinforces the clinical importance of preserving NCF as much as possible in this patient cohort as acute and long term NCF impairment will have a significant impact on patient's quality of life. We also demonstrate that NCF at baseline may also have an impact on overall survival. The next chapter will examine role of baseline functional MRI in correlating NCF with physiological, functional, structural, and metabolic components of the MRI scans at baseline.

Chapter 6 – Baseline MRI results of normal tissue and its correlation with NCF prior to having treatment with SRS.

6.1 Introduction

The previous chapter demonstrated significant morbidity of NCF impairment in patients with BM prior to SRS treatment. Before studying the impact of SRS, it is important to study the results of baseline MRI and its relation to NCF. In this chapter I will study correlation of neurocognitive scores with MRI parameters of participants before undergoing treatment with SRS. Four aspects of MRI will be addressed in detail: hippocampal volume, cerebral blood flow and perfusion measured by arterial spin labelling, spectroscopy of the hippocampus and diffusion parameters of the relevant tracts.

NCF impairment is prevalent in patients with BM before and after treatment (Herman *et al*., 2003, Gerstenecker *et al*., 2014, Chang *et al*., 2009, Brown *et al*., 2016a) and we demonstrated NCF impairment at baseline in the data from patients in our study presented in chapter 5. The treatment of BM includes a variety of modalities including whole brain radiotherapy (WBRT), stereotactic radiosurgery (SRS), systemic anti-cancer therapy (SACT) and neurosurgery and, as discussed in previous chapters. Several randomised controlled trials and observational studies have reported worsening neurocognitive outcomes following treatment with WBRT and SRS (Brown *et al*., 2016a, Chang *et al*., 2009, Aoyama *et al*., 2015).

Although, there are studies looking at NCF changes after treatment, it is also important to understand the pathophysiology of NCF impairment in patients presenting with BM. As discussed in section 5.1 and 5.5, there are several clinical factors in these patients which can impact on NCF. Nevertheless, better understanding of the baseline function of normal tissue in the brain and the potential impact of the tumour and SACT on the function of normal tissue is important. Using MRI imaging at baseline is a vital component of improving this understanding of normal tissue function.

MRI has been used to study the response of treatment and identifying difference in patients who show signs of progression vs. pseudoprogression vs. response (Walker *et al*., 2014, Galldiks *et al*., 2020), however, there is a lack of data correlating imaging findings with NCF at baseline in this group.

Each one of the MRI modalities mentioned above have been shown in the literature to be associated with NCF impairment as discussed in sections 1.4 and 4.4 in patients with conditions such as Alzheimer's disease, mild cognitive impairment, and schizophrenia. However, they have not been examined in detail in patients with BM. Studies have not previously been performed evaluating these four brain parameters (blood flow, spectroscopy, diffusion, and structural changes) together and comparing these with neurocognitive function in patients with BM.

In addition, often only 1 or 2 parameters of MR imaging modality are tested**.** For example, in a study looking at progression from mild cognitive impairment to dementia, hippocampal volume and diffusion parameters of the fornix tracts were compared as a non-invasive predictive biomarker for identifying patients at increased risk of progressing to dementia. It was found that hippocampal volume was highly correlated with integrity of the fornix tract and an increase risk of developing dementia (Mielke *et al*., 2012). Spectroscopic measures of hippocampal metabolites and hippocampal volume have been studied separately in patients with dementia (Schuff *et al*., 1999). However, cross study comparisons present their own challenges and reservations, and it is currently uncertain which modality may be more sensitive to a clinical change in NCF.

In this chapter we present data from multi-parametric MRI measurements of the hippocampus prior to treatment in patients with BM using the following MRI modalities:

- Structural MRI
- Perfusion
- MR Spectroscopy
- Diffusion Tensor Imaging

6.1.1 Structural MRI

Historically, post-mortem studies of patients with dementia showed that the greatest neurodegenerative changes were evident in the hippocampus (Bobinski *et al*., 1999). In accordance with this, MRI studies first examined structural changes within the hippocampus with particular regards to the volume and shape. In addition to this generalised grey matter cortical loss has also been associated with NCF decline (Gress, 2001). With improving MR technology, total volume and sub-hippocampal volumes can be defined well using automated software such as Freesurfer (Henschel *et al*., 2020). In a study by Schuff *et al*., hippocampus volumes of forty participants with normal cognition were compared to thirty-six patients with mild cognitive impairment and twenty-nine patients with Alzheimer's dementia. Total hippocampal volume of patients with retained NCF was 6327 mm^3. This was significantly reduced by 11% to 5657 mm^3 in patients with mild cognitive impairment ($p<0.05$) and 27% to 4595 mm^3 in those with Alzheimer's dementia ($p<0.01$). When Alzheimer's dementia was compared with mild cognitive impairment, hippocampus was 19% significantly smaller in AD ($p<0.01$) (Schuff *et al*., 1999).

Volumetric studies of pre-frontal cortex, amygdala, hippocampus have been conducted in aging patients and in patients with other disorders such as schizophrenia, major depression. One study looking at volume of various subcortical regions found an association with depressive symptoms and volume of the amygdala, however no correlation was found with hippocampal volumes (Vasilopoulou *et al*., 2011).

6.1.2 Perfusion

Generalised cerebral perfusion and more specifically hippocampus perfusion has been studied in conditions affecting cognition such as Alzheimer's dementia, mild cognitive impairment, and some psychiatric disorders. In a study looking at healthy older and young adults comparing memory tests score and hippocampal perfusion, older adults with no history of cerebrovascular disease, cognitive impairment, or mental illness, hippocampal perfusion was found to be inversely correlated with memory performance (Rane *et al*.,

2013). In another study examining patients with known diagnoses of different forms of dementia CBF measurements in the bilateral parietal cortices and hippocampus were lower in dementia of Alzheimer type and multi-infarct dementia patients than in controls. Hypoperfusion in the hippocampus was a more sensitive marker than hypoperfusion in the parietal cortex in diagnosing dementia of Alzheimer type (Ohnishi *et al*., 1995). In another study by Rodriguez *et al*., a positive correlation was reported between score of mini-mental status examination and hippocampal perfusion. The group also reported a statistically significant difference in CBF of both hippocampi between controls and patients ($p<0.001$) (Rodrigueza, 2000).

6.1.3 Spectroscopy

MR Spectroscopy (MRS) studies of the hippocampus are somewhat less frequent due to its technical challenges. Such challenges mainly relate to anatomical location of the hippocampi being close to the petrous bone and ventricles, which causes poor homogeneity of the B_0 magnetic field resulting in low spectral resolution relative to other regions within the brain (Allaili *et al*., 2015). Despite these challenges, MRS has been increasingly utilised in neurodegenerative and psychiatric disorders (Block *et al*., 2009). There is ongoing research to identify a non-invasive biomarker that may precede symptomatic presentation of diseases such as Alzheimer's dementia (AD) and help distinguish AD from other neurodegenerative disease (Caserta *et al*., 2008). Significance of the metabolites detected by MR Spec have been listed in Table 4.6.

6.1.4 Diffusion Tensor Imaging

White matter tracts have been studied in many conditions, e.g., multiple sclerosis, epilepsy and disorders affecting cognition (Fields, 2008, Acosta-Cabronero and Nestor, 2014). As we develop increased understanding of NCF decline following radiotherapy treatment, there is increasing understanding of pathophysiology of radiation induced damage (Makale *et al*., 2017). However, as noted in Chapter 5, this cohort of patients are presenting with baseline

neurocognitive impairment, and little is understood regarding pathophysiology of NCF impairment in patients presenting with BM.

In studies examining the fornix tract (major white matter tract linking the hippocampus to other regions within the brain), in patients with dementia DTI imaging demonstrated low value of fractional anisotropy and high level of median and radial diffusivity suggesting that white matter tracts are affected, however, these markers need further validation (Metzler-Baddeley *et al*., 2019, Oishi *et al*., 2011). In this study we examine the fornix and cingulum tract as they are considered to be critical tracts in the limbic system as discussed in section 4.4.6 (Thomas *et al*., 2011, Bubb *et al*., 2018).

6.2 Hypothesis

The overarching hypothesis is that patients with NCF impairment at baseline will exhibit functional and structural changes that may be detected by MRI. The rationale for the specific MRI parameters I have investigated are summarised below:

- Patients with baseline NCF impairment will have reduced volume of the hippocampus.
- Cerebral blood flow (CBF) will vary with age and older patients with show lower blood flow in the hippocampus and grey matter.
- Patients with baseline NCF impairment will exhibit lower CBF in the hippocampus than those with retained NCF.
- Patients with baseline NCF impairment will show evidence of low concentrations of metabolites which represent markers of neuronal health such as NAA.
- Patients with baseline NCF impairment will exhibit lower fractional anisotropy values and higher median and radial diffusivity in the fornix tract.

6.3 Methods

The overall inclusion and exclusion criteria of participants has been described in section 4.2. The details of MRI acquisition parameters, pre-processing of the data for each MR sequence and calculation of the mathematical values of hippocampal volume, blood flow, metabolite measurements, diffusion metric measurements have been described in section 4.4. NCF scores calculation and definition of impairment has been described in section 5.3.2.

Statistical analysis was performed using IBM SPSS Statistics Software version 28 (IBM Corp. Released 2021. IBM SPSS Statistics for Windows, Version 28.0. Armonk, NY: IBM Corp). T-tests was performed to look at differences in two groups (NCF impaired and NCF retained) as MRI data was normally distributed. The data was checked for normality using normal population distribution.

The following MR measures were considered:

- Hippocampal Volume
- Hippocampal Blood Flow
- Hippocampal Metabolite concentration
- Diffusion Measure of the Fornix Tract and Cingulum

For correlation testing of two continuous variables e.g., age and blood flow, spearman correlation coefficient was computed as age was not normally distributed.

6.4 Results

Twenty out of thirty-one patients described in Chapter 5 underwent MRI scans in CUBRIC at baseline prior to commencing SRS. In order to increase the overall recruitment, patients were given the choice to participate in the translational MRI arm of the study. Reasons for exclusion from the MRI component of the study are summarised in Table 6.1. Clinical data of the patients is presented in Chapter 5 which has described the patients' baseline demographics, presenting symptoms, volume of metastases and overall survival.

Reason for exclusion from MRI arm	Number
Treatment date brought forward	2
Patient's choice	4
Separate travel for MRI	3
Contraindication for 3 T MRI	2

Table 6.1 Reasons for exclusion from MRI arm of the study. A total of 11 patients did not participate

6.4.1 Structural MRI Results

Figure 6.1 demonstrates colour coded regional identification of different structures processed using FreeSurfer software (Henschel *et al*., 2020).

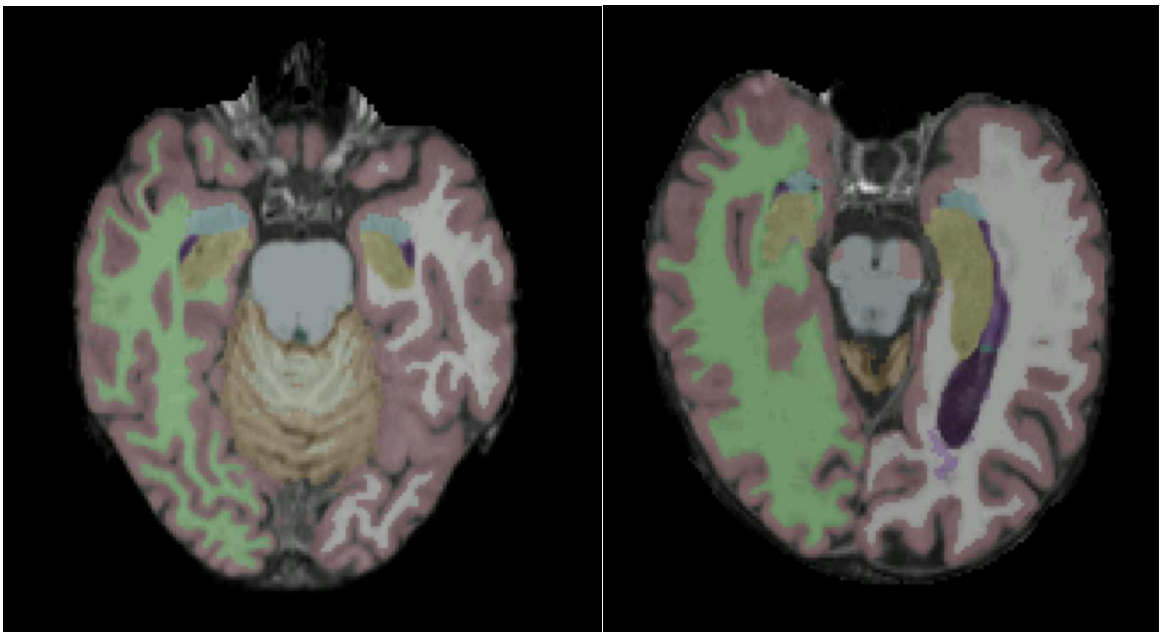

Figure 6.1 Example of cerebral cortical and subcortical structures delineation from Freesurfer software in 2 patients*. Visual comparison of a patient with reduced hippocampal volumes (left) who was a 84 year old man with renal cell carcinoma and a patient with normal hippocampal volumes (right) who was a 24 year old man with melanoma. Hippocampus is marked as the yellow structure medial to the lateral ventricles. Green: right cerebral hemisphere, White: Left cerebral hemisphere, Amygdala: light blue anterior to the hippocampus, grey matter: purple.*

Mean volume of left and right hippocampi were highly correlated, r = 0.438, p-value = 0.037, (Figure 6.2). There were two outliers identified, both of whom had a BM in left medial temporal lobe.

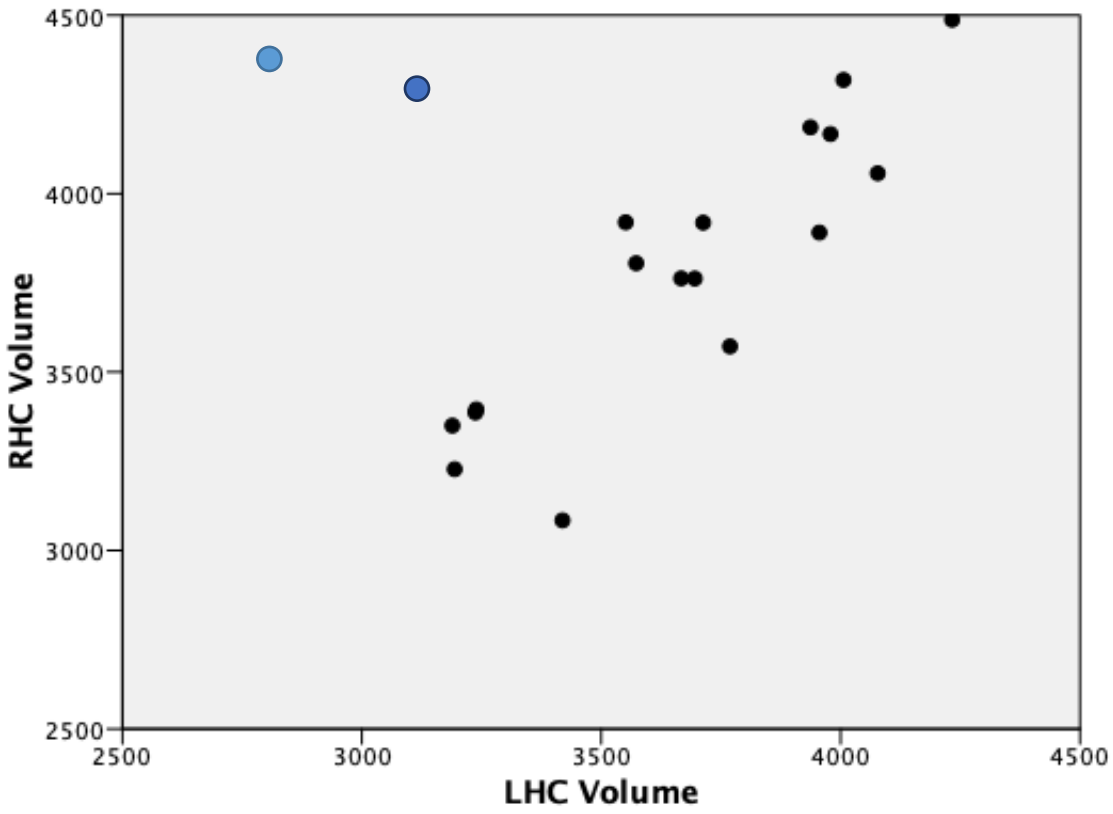

Figure 6.2 Scatter plot demonstrating relationship between volumes of the left and right hippocampi in mm^3 (r = 0.438, p-value <0.05). *Each point on the chart represents RHC volume on y-axis and LHC volume on the x-axis. LHC: Left Hippocampus; RHC: Right Hippocampus. Outliers are marked*

Left and right hippocampal volumes were strongly correlated with age, correlation coefficient, r= -0.43, p-value <0.05 and r = -0.38, p-value <0.05, respectively. However, there was no statistically significant difference between the mean volume of hippocampus in the group of patients taking steroids or receiving systemic anti-cancer therapy (SACT). This is illustrated in table 6.2.

	Steroids	No Steroids	p-value
LHC Volume (mm^3)	3562 (365)	3650 (436)	0.32
RHC Volume (mm^3)	3861 (316)	3894 (466)	0.42

	SACT	No SACT	p-value
LHC Volume (mm^3)	3668 (376)	3495 (383)	0.16
RHC Volume (mm^3)	3866 (380)	3797 (453)	0.35

Table 6.2 Mean +/- 2SD left and right hippocampus volumes in patients receiving steroids prior to SRS treatment (top) and for patients receiving concurrent SACT within 6 weeks of SRS treatment (bottom). *LHC: Left Hippocampus; RHC: Right Hippocampus. SACT: Systemic Anti-Cancer Therapy.*

Figure 6.3 demonstrates variability in the mean left and right hippocampal volumes in each of the NCF domains. There was no statistically significant difference between the patients who had retained NCF versus those with impaired NCF in each of the domains. Although, in the domains which test memory, namely, in the four domains of Hopkins Verbal Learning Test (HVLT), there was a non-significant trend towards reduced volume of the bilateral hippocampi. Whereas this was not found in the NCF domains testing executive function and attention, i.e., TMT, COWAT and digit span.

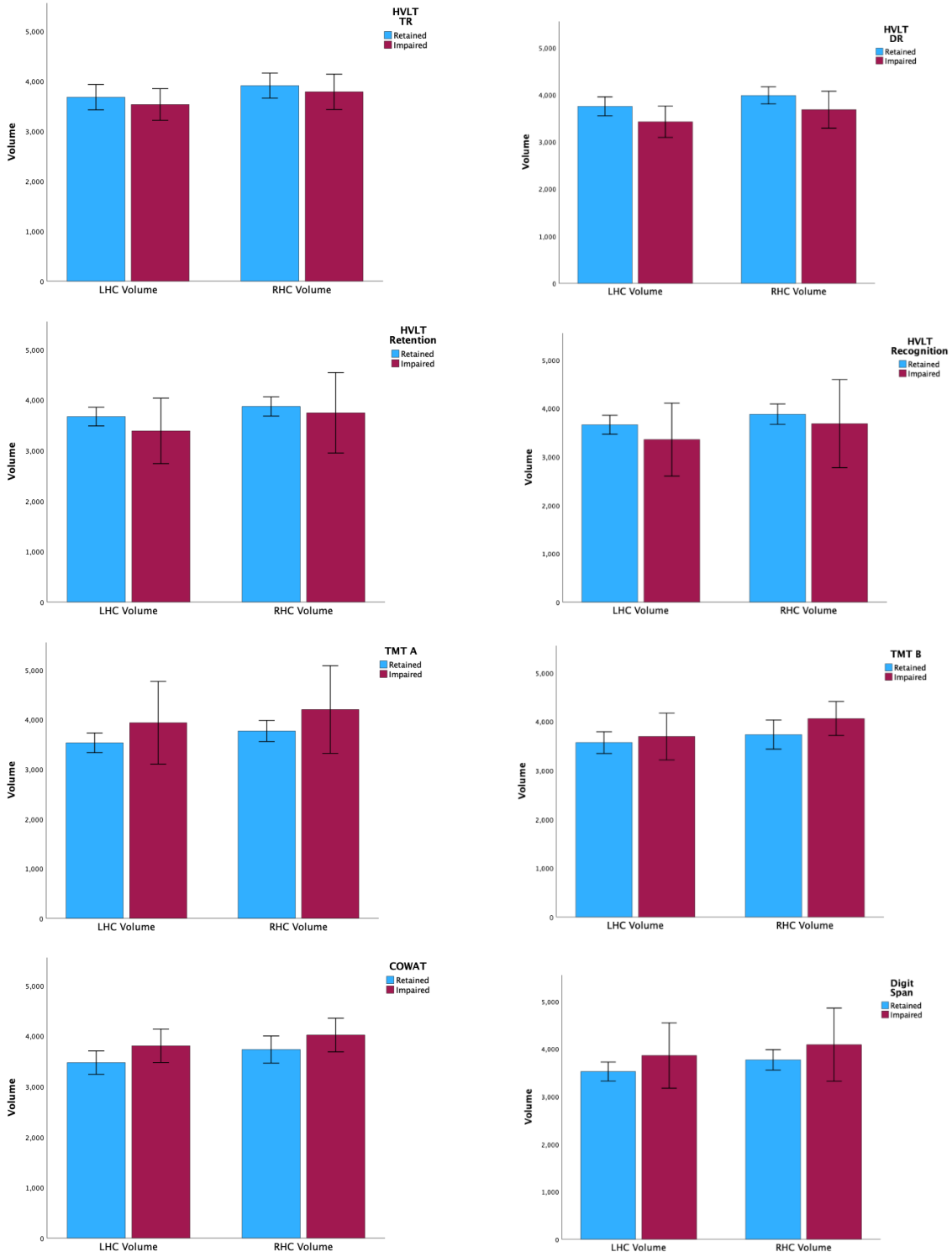

Figure 6.3 Variation in the mean left and right hippocampus volume for each of the NCF domains. *Error bars represent 95% confidence interval of the mean. HVLT: Hopkin's verbal learning test-revised, TR: Total Recall, DR: Delayed recall. TMTA: trail making test A, TMTB: trail making test B, COWAT: Controlled oral word association test, LHC: Left hippocampus, RHC: right hippocampus.*

6.4.2 Cerebral Blood Flow

Out of twenty patients scanned at baseline, eighteen patient's data were analysed. Two patients were excluded. The reason for exclusion was lack of signal of cerebral blood flow in the grey matter which resulted in negative values, and therefore was a false negative. One of the patients had a history of cerebrovascular disease and due to this, transit time was slow resulting in lack of signal. Another patient had previous radical radiotherapy for primary head and neck cancer, and it is established that radiotherapy increases the risk of vascular disease, and therefore likely led to slower transit time as described. Exclusion of these cases only applied to CBF analysis due to the technical challenges described.

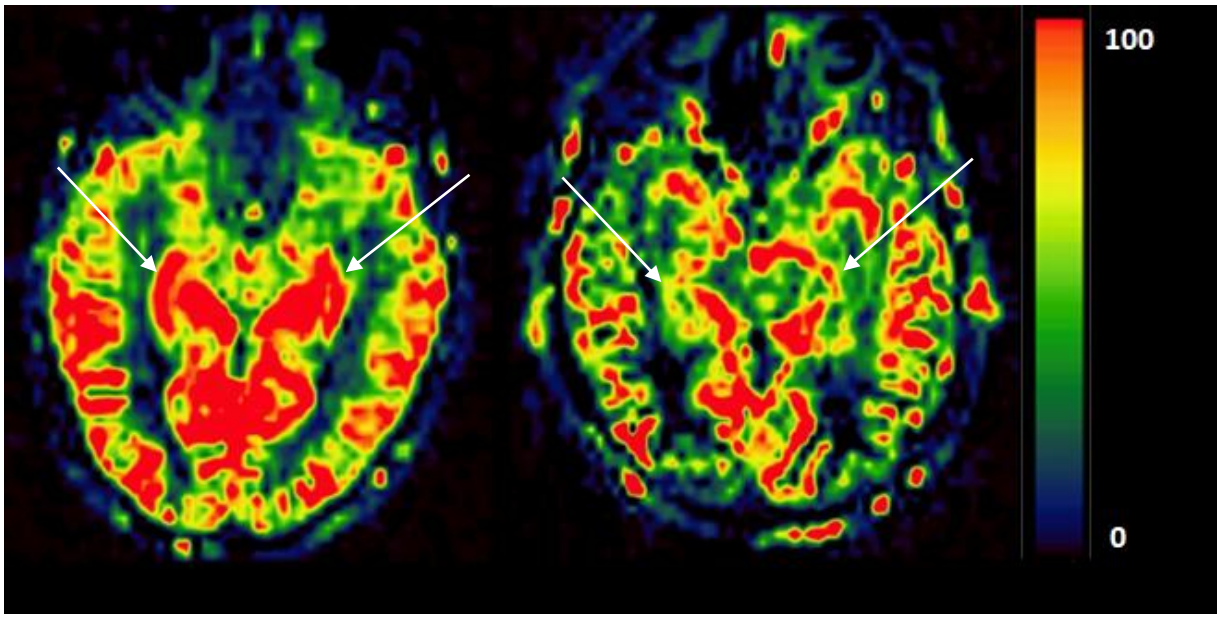

Figure 6.4 Comparison of CBF according to age of the patient at the level of the hippocampus, image on the left of a younger patient (age 48 years) vs. image on the right of an older patient (age 78 years). *Red represents regions of increased perfusion, whilst blue represents regions of lowest perfusion. White arrows indicate the location of hippocampus. CBF values range from 0-100 ml/min/100g.*

Younger participants demonstrated a higher CBF than older participants (Figure 6.4). Increasing age was negatively correlated with cerebral blood flow within the grey matter, which was not statistically significant. Overall correlation coefficient was, r = -0.371, p-value = 0.065. The association between age and combined hippocampi CBF was weaker: r = -0.299, p-value = 0.23 (Figure 6.5).

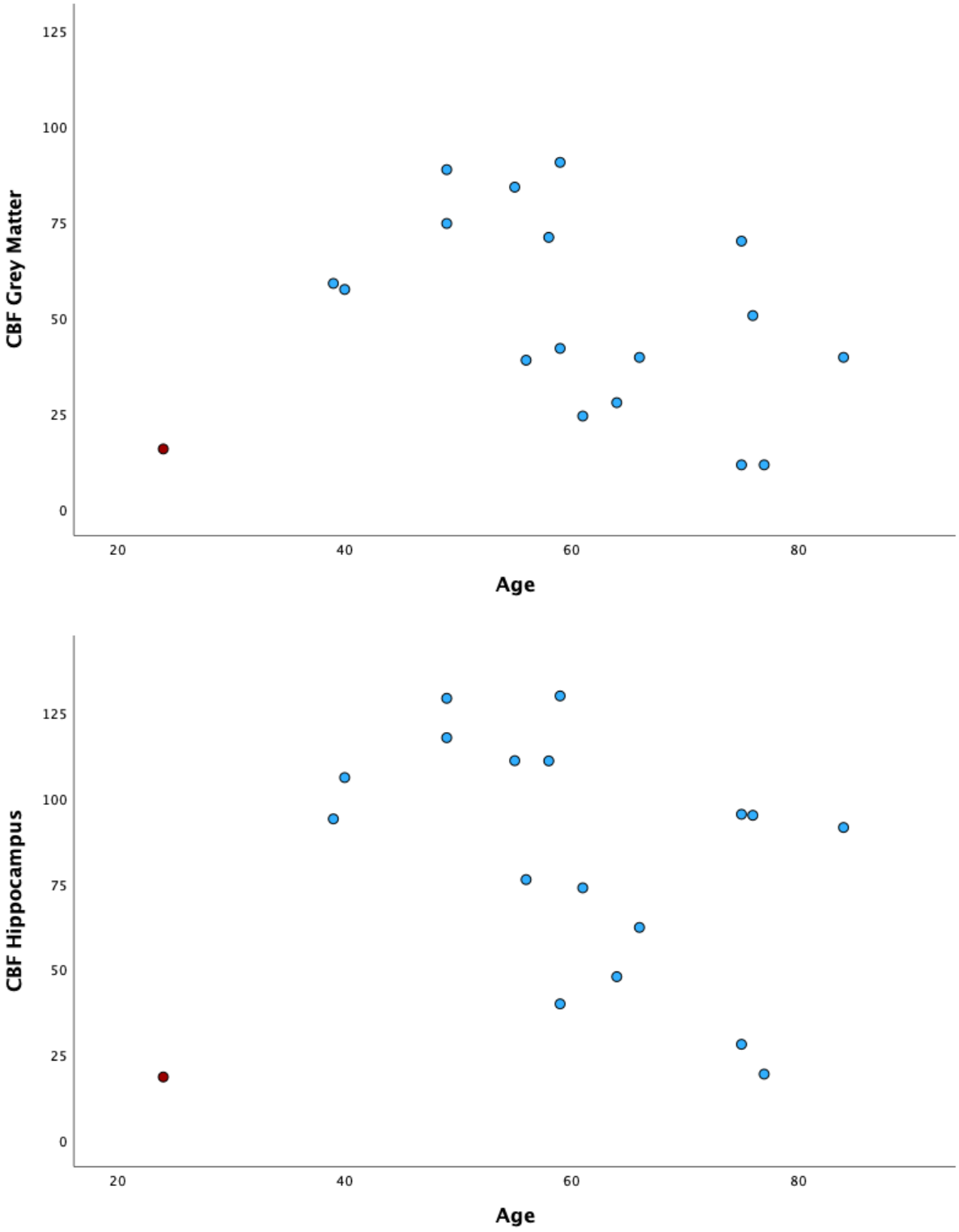

Figure 6.5 Scatter plot demonstrating relationship between of age and mean Cerebral Blood Flow (CBF) CBF in the grey matter (above) and hippocampus (below). *Outlier marked in red. CBF: Cerebral Blood Flow, measured in ml/min/100g*

Left and right hippocampus blood flow were highly correlated, correlation coefficient r = 0.777, p-value = <0.001 (Figure 6.6).

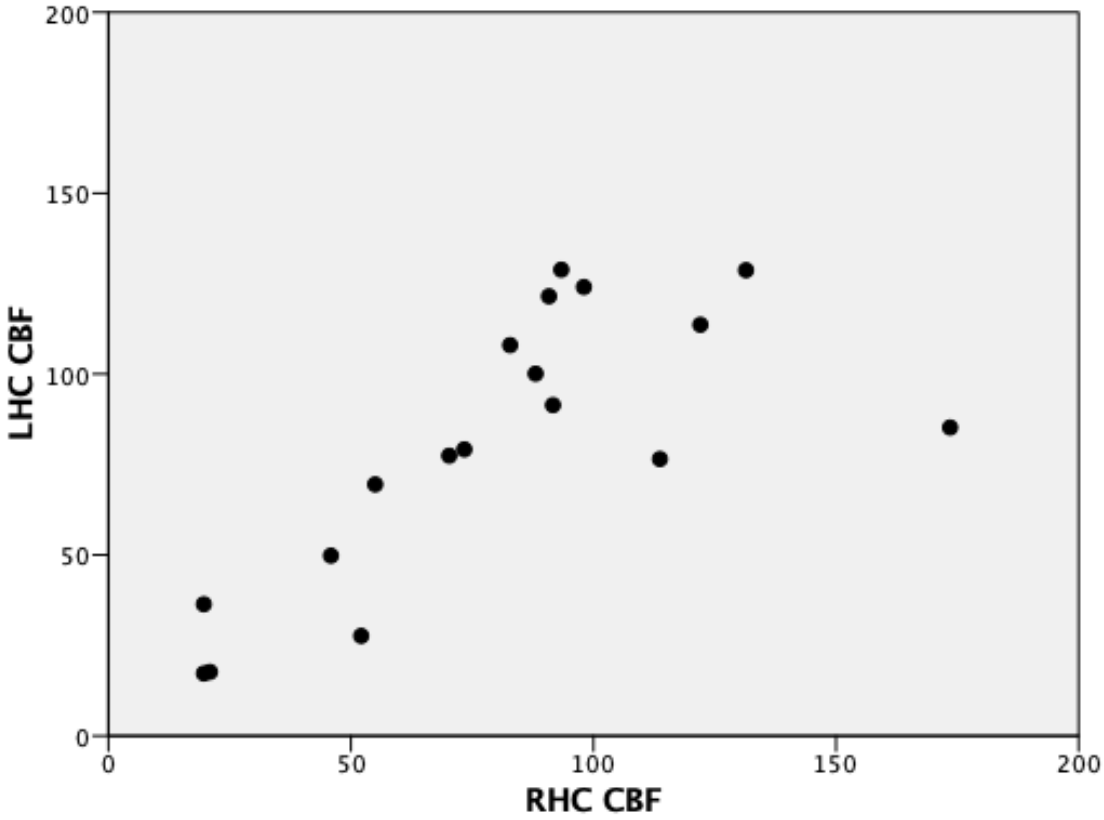

Figure 6.6 Scatter plot demonstrating relationship between right and left hippocampus cerebral blood flow (CBF), measured in ml/min/100g. *RHC: Right Hippocampus, LHC: Left Hippocampus.*

Presence of metastases in the temporal lobe did not have a significant impact on the mean hippocampal CBF (Figure 6.7). Four out of twenty patients had metastases present in the temporal lobe, three on left side and one on the right side. Although, mean left hippocampus CBF was lower in patients who had a metastasis in the left temporal lobe, this was not statistically significant.

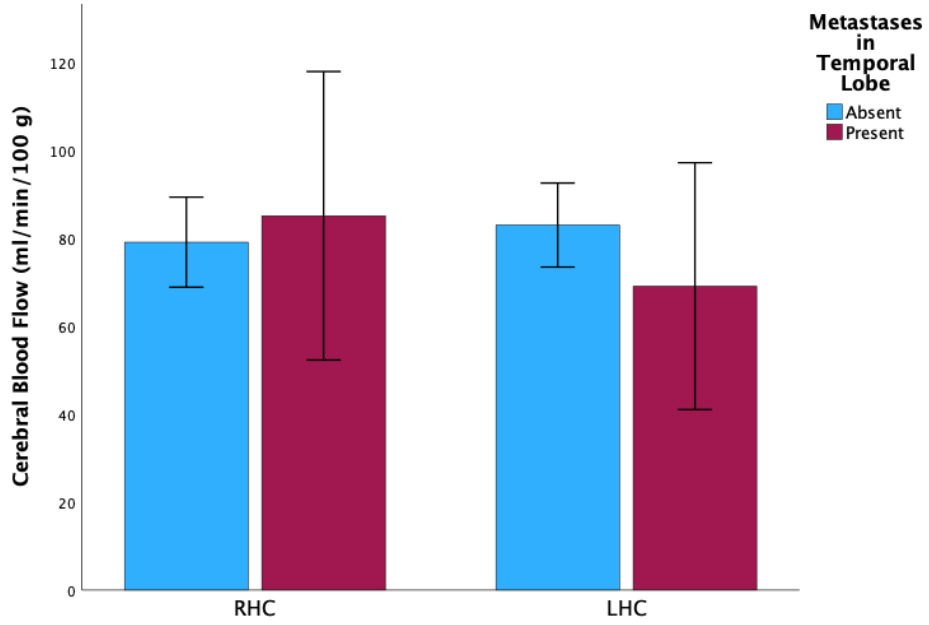

Figure 6.7 Bar chart demonstrating differences in cerebral blood flow of right and left hippocampus according to the presence of metastases in the respective temporal lobes. *Mean CBF in right hippocampus in those without metastasis was 79.13 +/- SD 10.24 compared to those with metastasis present was 85.14 +/- SD 12.52. Mean CBF in left hippocampus in those without metastases was 83.03 +/- 9.57 compared to those with metastases present was 69.12 +/- SD 13.24. None of the differences were statistically significant. RHC: Right hippocampus, LHC: Left hippocampus.*

Patients who received steroids at the time of MRI showed a non-significant lower mean CBF in the hippocampus compared with patients who did not receive steroids (Table 6.3). These group of patients also demonstrated a lower score in NCF testing as demonstrated in Chapter 5. In contrast, patients receiving treatment with SACT demonstrated a higher mean CBF in the hippocampus compared to patients who did not receive SACT (Table 6.3).

CBF (ml/100g/min)	Steroids	No Steroids	p-value
RHC	70.30 (+/- 42.36)	92.75 (+/- 38.06)	0.127
LHC	76.37 (+/- 47.94)	86.13 (+/- 21.69)	0.301
Grey Matter	49.91 (+/- 30.25)	49.60 (+/- 21.82)	0.491

CBF (ml/100g/min)	SACT	No SACT	p-value
RHC	82.69 (+/- 42.64)	59.62 (+/- 19.45)	0.235
LHC	82.73 (+/- 39.48)	64.49 (+/- 20.77)	0.269
Grey Matter	51.82 (+/- 26.95)	33.29 (+/- 7.84)	0.180

Table 6.3 Mean +/- SD Cerebral Blood Flow in Right and Left Hippocampus and grey matter in patients who were receiving steroid (top) at the time of SRS and systemic anti-cancer therapy (bottom) within 6 weeks of SRS.

NCF Test	Hippocampal CBF in patients with normal NCF (ml/100g/min)	Hippocampal CBF in patients with impaired NCF (ml/100g/min)	p-value
HVLT TR*	92.67 (+/- 27.72)	68.17 (+/- 42.01)	0.04
HVLT DR*	94.37 (+/- 26.77)	62.98 (+/- 41.64)	0.035
HVLT Retention	84.85 (+/- 33.38)	64.93 (+/- 49.15)	0.145
HVLT Recognition	79.37 (+/- 35.72)	85.66 (+/- 50.02)	0.447
TMTA	84.09 (+/- 36.63)	62.09 (+/- 38.54)	0.180
TMTB	85.73 (+/- 35.73)	82.91 (+/- 38.28)	0.441
COWAT	82.61 (+/- 39.33)	76.96 (+/- 35.03)	0.545
Digit Span	80.79 (+/- 37.04)	79.11 (+/- 41.30)	0.469
Global Assessment Impaired in Any tests*	92.93(+/-)	75.61 (+/-)	0.001

Table 6.4 Difference in mean hippocampal dose in groups with impaired and retained NCF in each domain and impaired global assessment in any of the NCF domains. *Values represent mean +/- 2SD. HVLT: Hopkin's verbal learning test revised, TR: total recall, DR: delayed recall, TMTA: trail making test A, TMTB: trail making test B, COWAT: Controlled oral word association test.*

Mean CBF in right and left hippocampus was significantly lower in patients with impaired HVLT TR and DR domains (Table 6.4, Figure 6.8), compared with patients with preserved NCF in these domains.

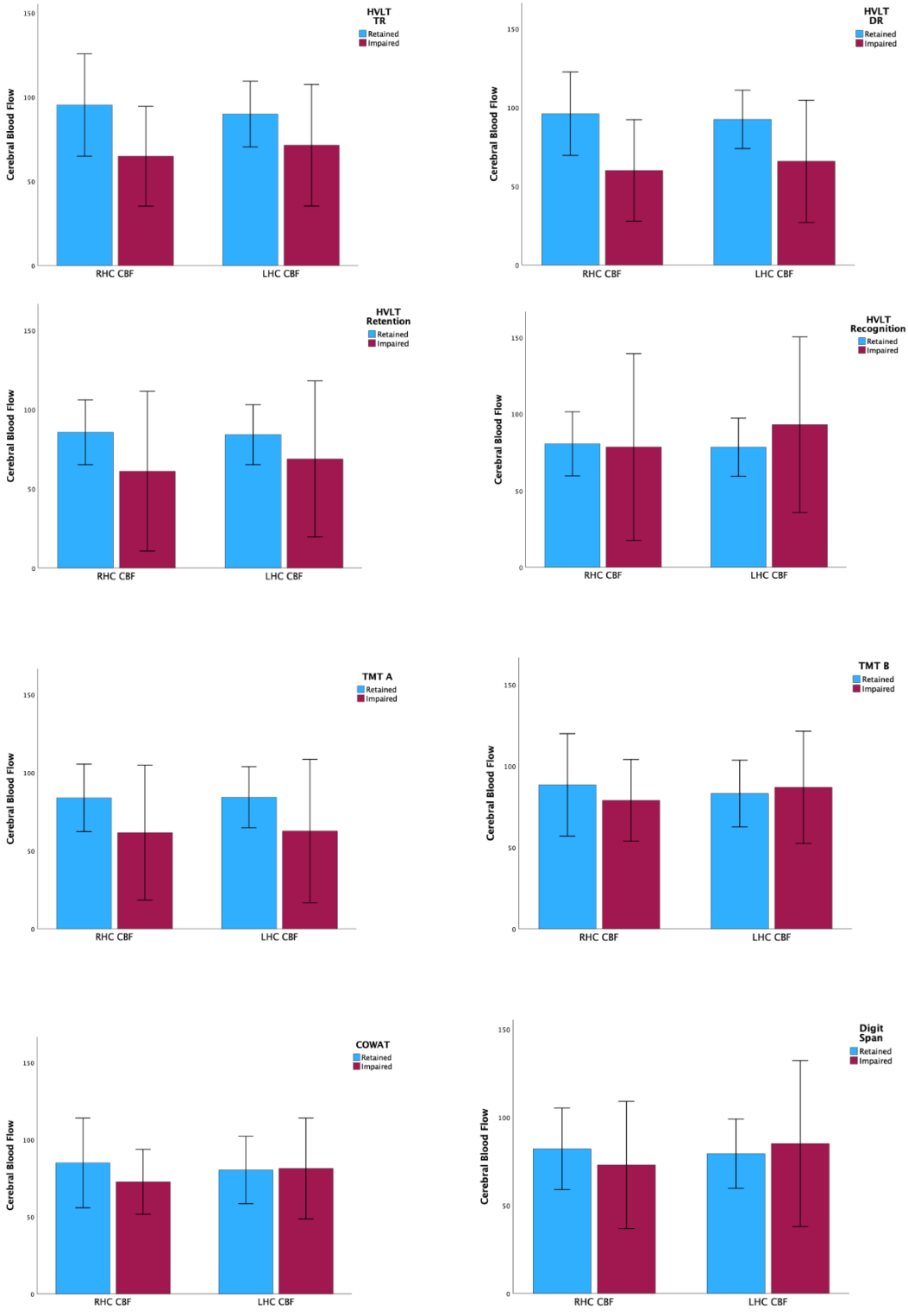

Figure 6.8 Variation in the right and left hippocampal blood flow in each of the NCF test domains. *Error bars represents 95% confidence interval of the mean. HVLT: Hopkin's verbal learning test-revised, TR: Total Recall, DR: Delayed recall, TMTA: trail making test A, TMTB: trial making test B, COWAT: Controlled oral word association test, LHC: Left hippocampus, RHC: right hippocampus, CBF: cerebral blood flow.*

6.4.3 MR Spectroscopy of the hippocampus

The mean and median concentration of the metabolites did not differ significantly between left and right hippocampus (Figure 6.9, Table 6.5). Table 6.5 report the concentration of all metabolites that were measured between 0.5 and 4.2 ppm chemical shift. Metabolites of clinical significance have been described in section 4.4.5, namely NAA, creatine, choline, myo-inositol, and total glutamate molecules (Glx).

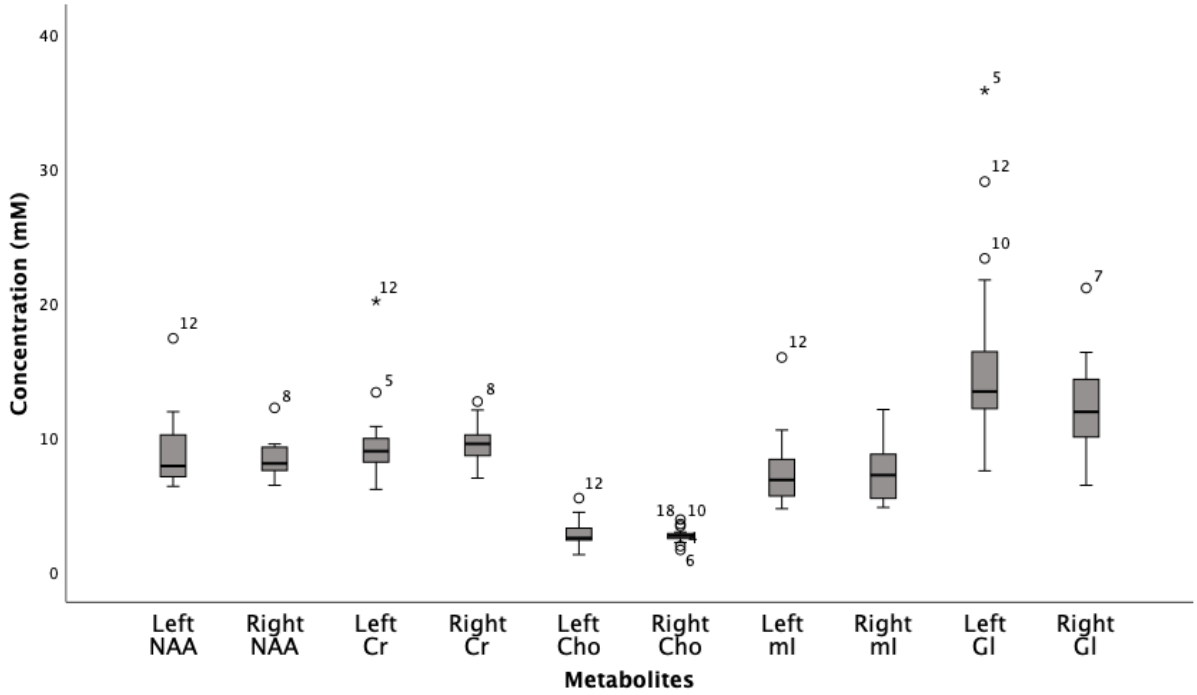

Figure 6.9 Concentration of metabolites with in right and left hippocampus. *The boxes represent median and interquartile range, whiskers represent the range and outliers are identified individually. NAA: N-acetylaspartate, Cr: Creatine, Cho: Choline, mI: Myo-Inositol, Gl: total glutamate molecules.*

Metabolite	Right Hippocampus (mM) Mean (SD)	Left Hippocampus (mM) Mean (SD)
N-Acetyl Aspartate	8.35 (+/-1.37)	8.68 (+/-2.81)
Myo-Inositol	7.75 (+/-2.31)	7.54 (+/-2.88)
Choline	2.67 (+/- 0.54)	2.81 (+/-1.02)
Creatine	9.52 (+/-1.64)	9.76 (+/- 3.29)
Total Glutamate molecules	12.81 (+/-3.65)	16.90 (+/-7.56)
GABA	2.40 (+/-3.44)	2.11 (+/-2.94)
Lactate	0.34 (+/-0.41)	0.36 (+/-0.41)
Total Lipid and Macromolecule at 0.9ppm	5.90 (+/-1.34)	5.68 (+/-2.63)
Total Lipid and Macromolecule at 1.3ppm	5.40 (+/-2.40)	6.70 (+/-3.27)
Total Lipid and Macromolecule at 2.0ppm	11.08 (+/-4.10)	11.05 (+/- 2.40)

Table 6.5 Concentration of metabolites across bilateral hippocampi. The values were comparable between right and left hippocampus and statistical difference was not detected.

There was a weak, non-statistically significant positive correlation between the metabolite concentration and age. An example of the correlation between left and right hippocampus and age is demonstrated with NAA in figure 6.10. A similar pattern was detected for each metabolite concentration and age. There were no statically significant differences in the concentration of metabolites in patients taking steroids or SACT (data not shown).

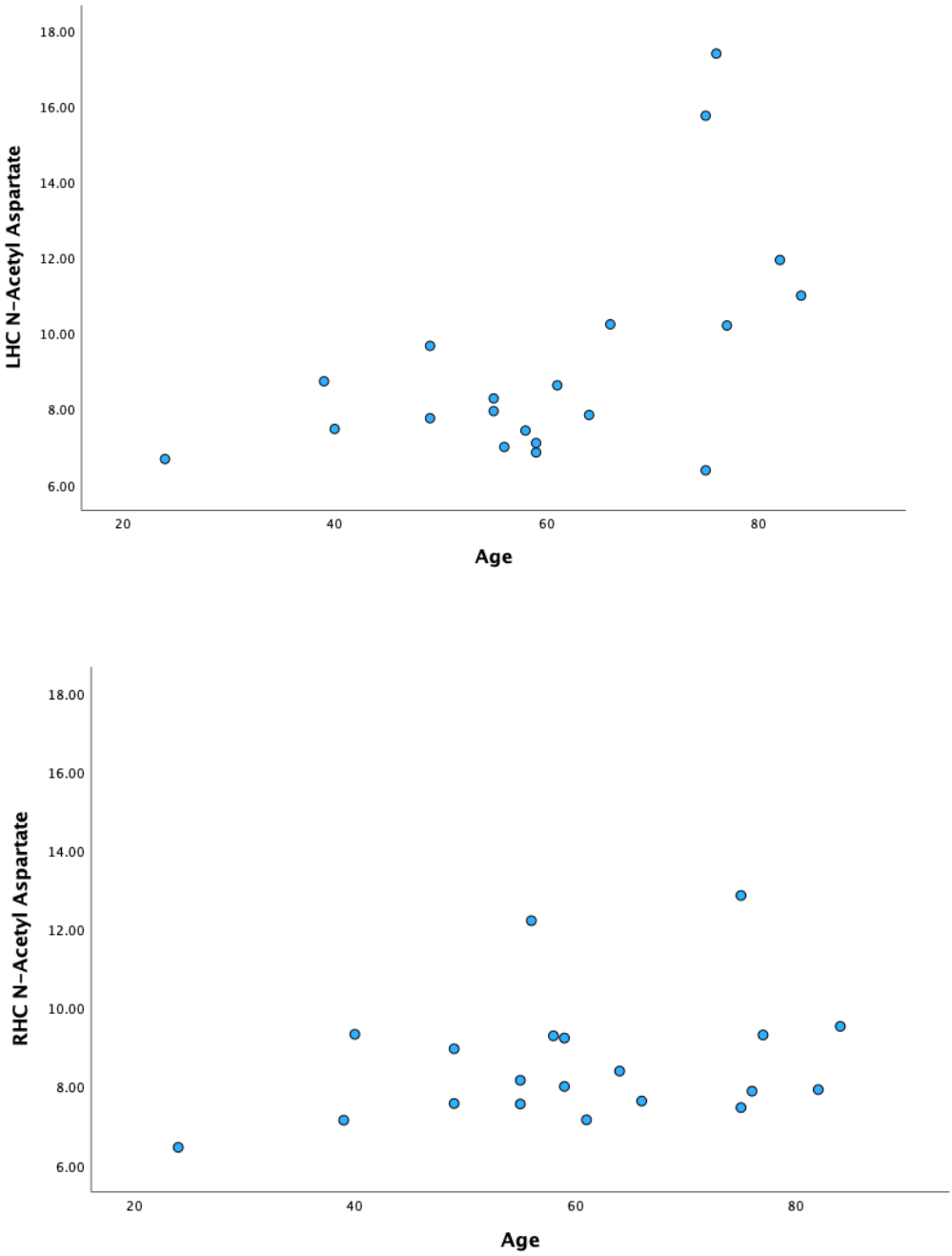

Figure 6.10 Scatter plot showing correlation between age of participants and concentration of N-Acetyl Aspartate detected by MR Spectroscopy.

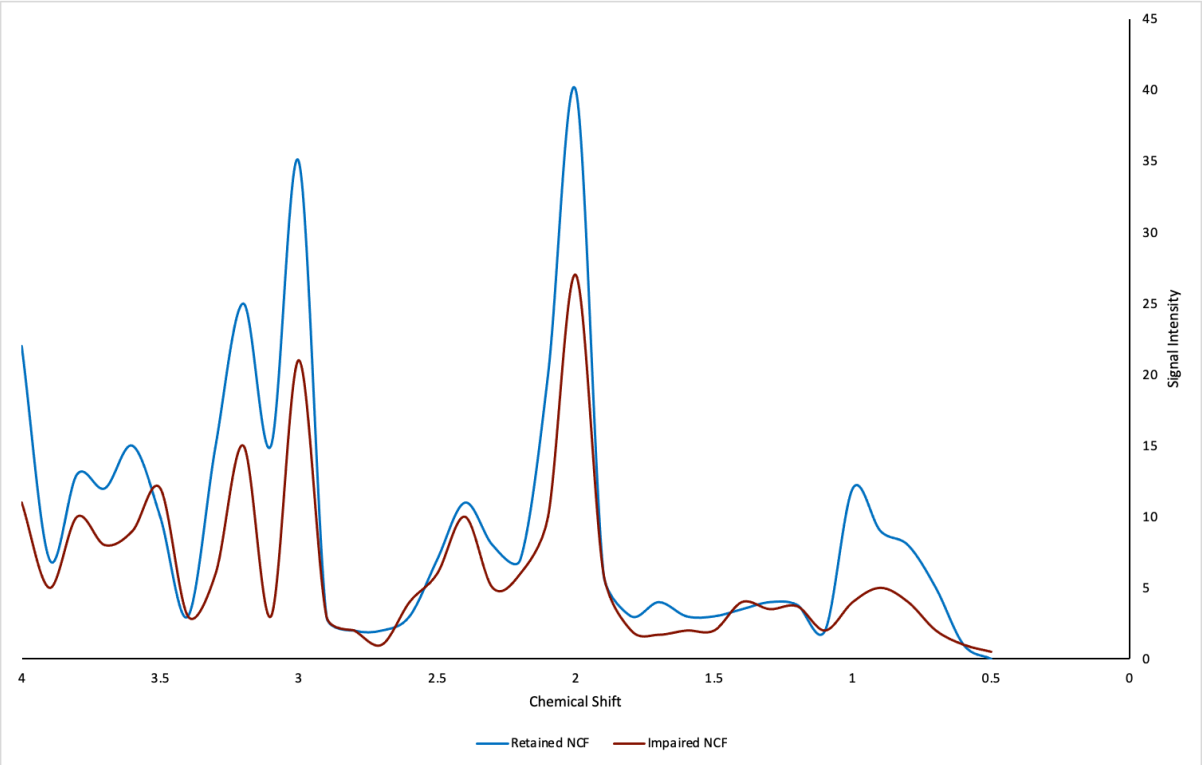

Figure 6.11 Chemical shift of the metabolites detected in a participant with retained NCF in all domains (blue) compared to participant who had NCF impairment across 7 domains (red).

Difference in chemical shift of the metabolites in two participants is demonstrated in Figure 6.11. The chemical shift is of one participant who had NCF impairment across all seven domains had lower concentration of all metabolites compared to the patient who had retained NCF in all domains.

When analysing hippocampal metabolite concentration according to each NCF domain, the mean left hippocampal NAA, creatine, and Glx was significantly lower in the group that displayed impaired verbal memory in the HVLT-TR domain (10.35 vs 8.28, p-value 0.04), (figure 6.12, table 6.6). Similar differences were observed in HVLT-DR, TMT-A and COWAT. These differences were not observed in metabolite concentrations of the right hippocampus.

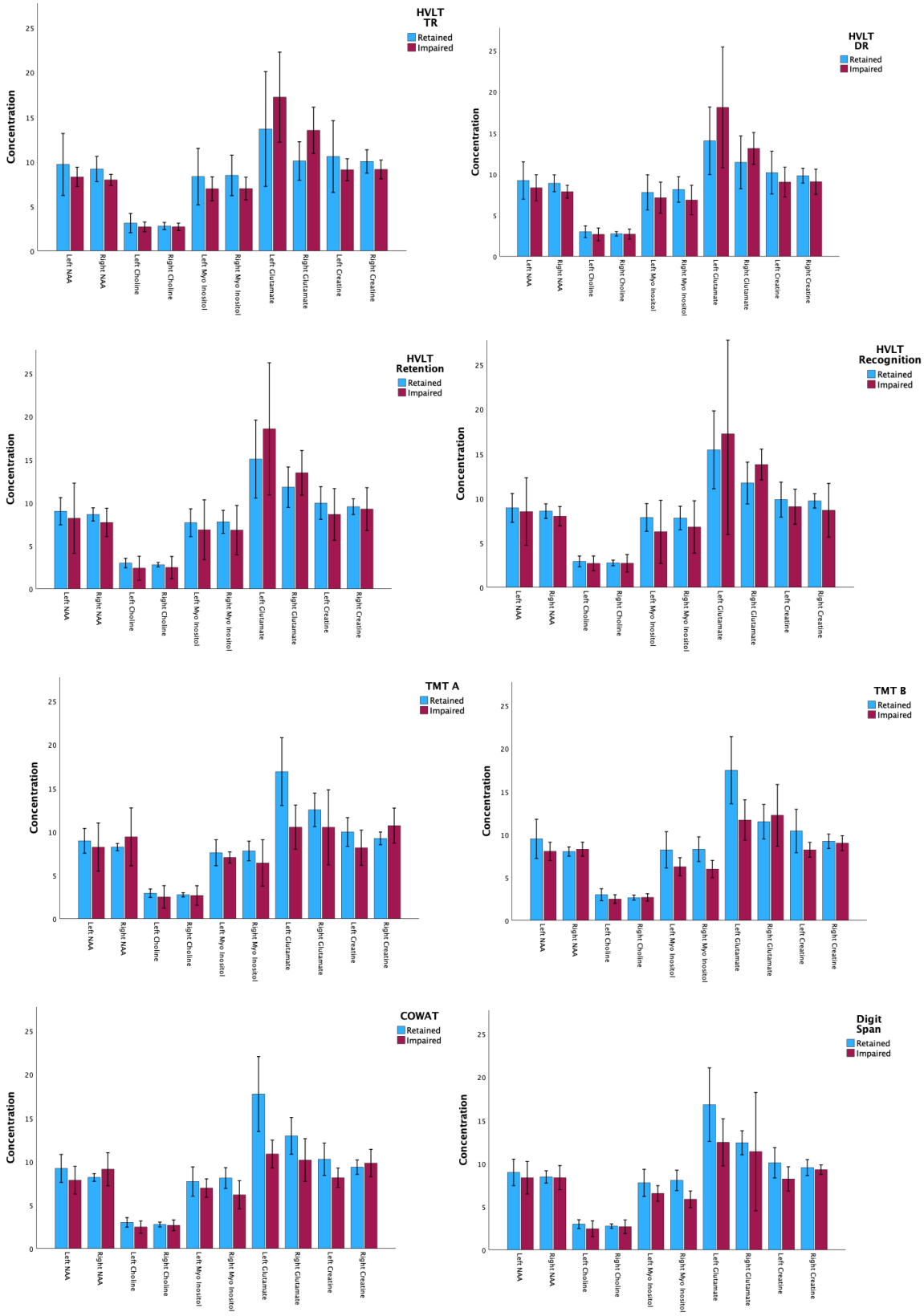

Figure 6.12 Concentration of clinically important metabolites in macromolecules in each of the NCF domains. *Error bars represent 95% confidence interval of the mean. HVLT: Hopkin's verbal learning test-revised, TR: Total Recall, DR: Delayed recall, TMTA: trail making test A, TMTB: trial making test B, COWAT: Controlled oral word association test, NAA: N-acetyl aspartate, Glutamate: Total glutamale molecules.*

NCF Tests	Retained or Impaired	LHC NAA	RHC NAA	LHC Creatine	RHC Creatine	LHC mI	RHC mI	LHC Glx	RHC Glx	LHC Choline	RHC Choline
HVLT TR	Retained	**10.35 (3.8) ***	9.41 (1.9)	**11.3 (4.5) ***	10.32 (1.9)	8.46 (3.7)	8.90 (3.6)	14.15 (6.6)	12.99 (6.2)	3.11 (1.2)	2.78 (0.4)
	Impaired	**8.23 (1.6) ***	7.95 (0.9)	**9.09 (1.8) ***	9.13 (1.6)	6.95 (1.9)	6.99 (1.9)	17.24 (7.5)	13.52 (3.9)	2.68 (0.8)	2.69 (0.6)
HVLT DR	Retained	9.26 (3.0)	8.77 (1.4)	10.14 (3.4)	9.70 (1.2)	7.49 (3.0)	7.49 (3.0)	13.77 (5.5)	12.33 (5.2)	2.99 (1.0)	2.74 (0.4)
	Impaired	9.16 (3.04)	8.41 (1.9)	10.02 (3.6)	9.61 (2.4)	7.80 (2.9)	7.80 (2.9)	18.40 (8.3)	14.44 (4.5)	2.67 (0.9)	2.71 (0.7)
HVLT Ret	Retained	9.06 (2.6)	8.57 (1.3)	9.95 (3.2)	9.48 (1.5)	7.47 (2.8)	7.59 (2.3)	14.80 (7.6)	12.44 (4.6)	2.98 (0.9)	2.80 (0.5)
	Impaired	9.70 (4.0)	8.74 (2.5)	10.51 (4.5)	10.20 (2.5)	8.12 (3.4)	8.63 (4.4)	19.01 (4.3)	15.79 (5.4)	2.39 (0.9)	2.47 (0.8)
HVLT Recog	Retained	9.40 (3.1)	8.77 (1.7)	10.35 (3.8)	9.91 (1.7)	7.98 (3.0)	8.12 (3.1)	15.50 (7.3)	13.15 (5.49)	2.90 (1.1)	2.74 (0.5)
	Impaired	8.51 (2.4)	7.98 (0.7)	9.05 (1.2)	8.66 (1.9)	6.23 (2.2)	6.77 (1.9)	17.25 (7.1)	13.80 (1.1)	2.67 (0.5)	2.69 (0.6)
TMTA	Retained	9.39 (3.1)	8.47 (1.4)	10.43 (3.6)	9.48 (1.8)	7.74 (3.1)	8.10 (3.0)	**16.79 (7.3) ***	13.77 (5.0)	2.92 (0.9)	2.74 (0.5)
	Impaired	8.23 (2.4)	9.41 (2.9)	8.15 (1.8)	10.70 (1.7)	7.03 (0.6)	6.40 (2.3)	**10.52 (2.2) ***	10.51 (3.7)	2.50 (1.1)	2.66 (1.0)
TMTB	Retained	9.51 (3.2)	7.97 (0.8)	10.34 (3.6)	9.16 (1.2)	7.85 (3.2)	7.95 (2.3)	16.85 (5.9)	12.48 (4.2)	2.98 (1.1)	2.64 (0.4)
	Impaired	9.00 (3.0)	8.86 (1.9)	9.44 (3.6)	9.62 (2.1)	7.11 (2.8)	7.22 (3.7)	12.82 (4.3)	13.83 (6.3)	2.47 (0.7)	2.67 (0.6)
COWAT	Retained	9.38 (2.8)	8.03 (0.7)	10.29 (3.3)	9.35 (1.5)	7.60 (3.1)	8.00 (2.7)	**17.49 (8.0) ***	14.08 (4.0)	3.03 (1.0)	2.75 (0.5)
	Impaired	8.92 (3.3)	9.67 (2.2)	9.71 (3.8)	10.25 (2.2)	7.70 (2.6)	7.57 (4.0)	**12.80 (4.0) ***	11.80 (6.4)	2.48 (0.7)	2.67 (0.6)
Digit Span	Retained	9.01 (2.78)	8.39 (1.3)	10.06 (3.2)	9.47 (1.7)	7.55 (2.9)	7.84 (2.3)	16.43 (7.8)	13.00 (3.4)	2.97 (0.9)	2.74 (0.5)
	Impaired	9.83 (3.7)	9.26 (2.3)	10.17 (4.5)	10.23 (2.2)	7.86 (3.1)	7.88 (4.6)	14.10 (4.4)	14.11 (8.5)	2.44 (0.9)	2.67 (0.8)
Any Domain	Retained	10.40 (4.1)	8.15 (0.7)	11.49 (5.0)	9.64 (0.7)	8.22 (4.4)	8.63 (2.9)	15.54 (7.6)	12.22 (5.2)	3.29 (1.5)	2.66 (0.4)
	Impaired	8.82 (2.5)	8.76 (1.8)	9.62 (2.8)	9.67 (2.0)	7.43 (2.4)	7.59 (2.9)	15.95 (7.2)	13.63 (4.9)	2.72 (0.7)	2.74 (0.6)

Table 6.6 Concentration of metabolites in macromolecules in each hippocampus in each of the NCF domains. *The final 2 rows represent changes in concentration in patients with impairment in domain vs patients who had retained NCF in all domains. Statistically significant differences (p-value < 0.05) are highlighted with *. LHC: left hippocampus, RHC: right hippocampus, NAA: N-acetyl aspartate, mI: myo inositol, Glx: total glutamate molecules, HVLT: Hopkins verbal learning test revised, TR: total recall, DR: delayed recall, Ret: retention, Recog: recognition, TMT: trail making test, COWAT: controlled oral work association test.*

6.4.4 Diffusion Tensor Imaging of the Fornix and Cingulum Tracts

FA and MD of the fornix tract were strongly negatively correlated with age (Figure 6.14). In contrast, FA and MD of right and left cingulum tract did not exhibit a similar pattern.

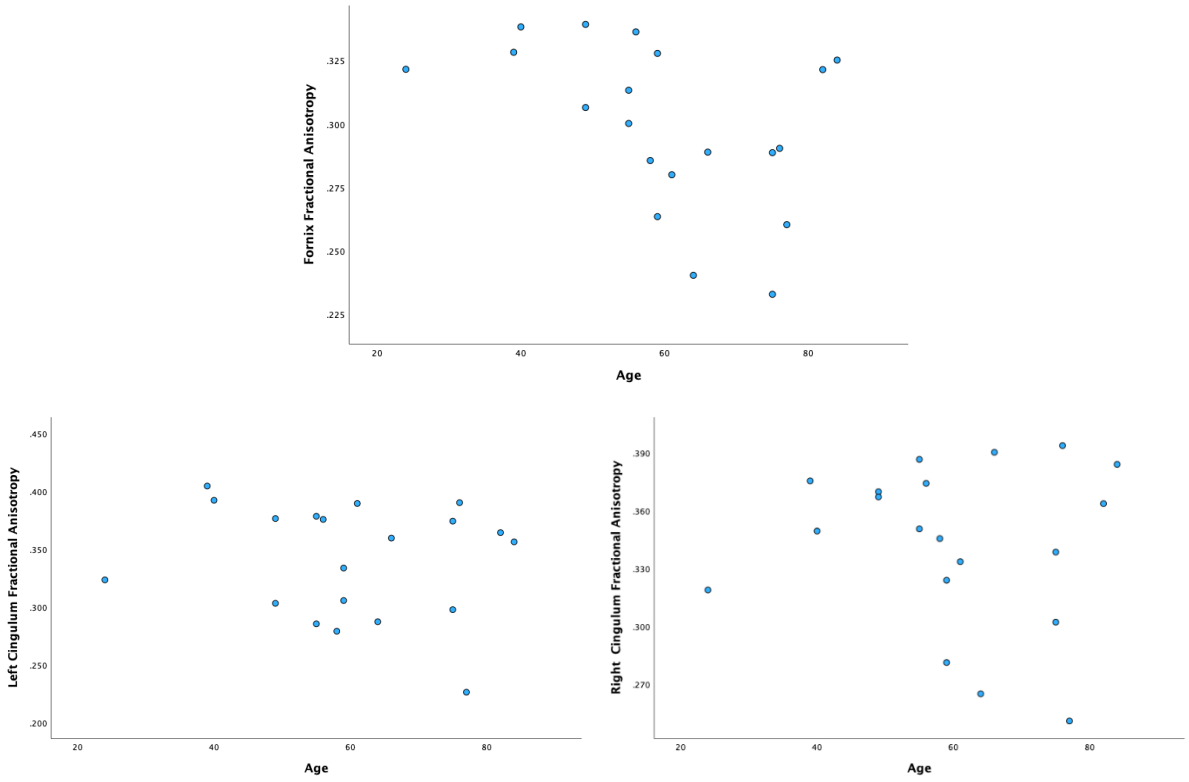

Figure 6.13 Scatter plot demonstrating relationship between age and fractional anisotropy of the fornix tract, (r = -0.502, p-value 0.012), right cingulum (r = -0.067, p-value = 0.39) and left cingulum tract (r = -0.215, p-value = 0.18).

FA of the fornix tract and cingulum was significantly lower in the patients who received steroids compared to those who did not receive steroids. In contrast, these values were higher in patients who received SACT compared to those who did not. MD values did not differ significantly between the groups.

	Tract	Steroids	No Steroids	p-value
FA	Fornix	0.28	0.31	0.027 *
	Left Cingulum	0.322	0.363	0.035 *
	Right Cingulum	0.331	0.357	0.038 *
MD	Fornix	0.00125	0.00127	0.41
	Left Cingulum	0.00145	0.0008	0.19
	Right Cingulum	0.00135	0.0008	0.20

	Tract	SACT	No SACT	p-value
FA	Fornix	0.311	0.286	0.043 *
	Left Cingulum	0.357	0.319	0.038 *
	Right Cingulum	0.357	0.326	0.05 *
MD	Fornix	0.00127	0.00126	0.42
	Left Cingulum	0.0008	0.0015	0.13
	Right Cingulum	0.0008	0.0013	0.18

Table 6.7 Diffusion Tensor Imaging metrics of the fornix and cingulum tracts in patients who received steroid compared to those who did not (top) and in patients who received SACT compared to those who did not. *FA: Fractional Anisotropy, MD: mean diffusivity, SACT: Systemic Anti-cancer Therapy. Statistically significant results are marked with *.*

Example of a fornix tract and cingulum tract is illustrated in Figure 6.14 from a participant. Anatomy of both tracts has been previously described in section 4.4.6. There was no statistically significant difference in the diffusion measures of the tracts in patients who had retained NCF vs those who had impaired NCF in any of the domains (Figure 6.15).

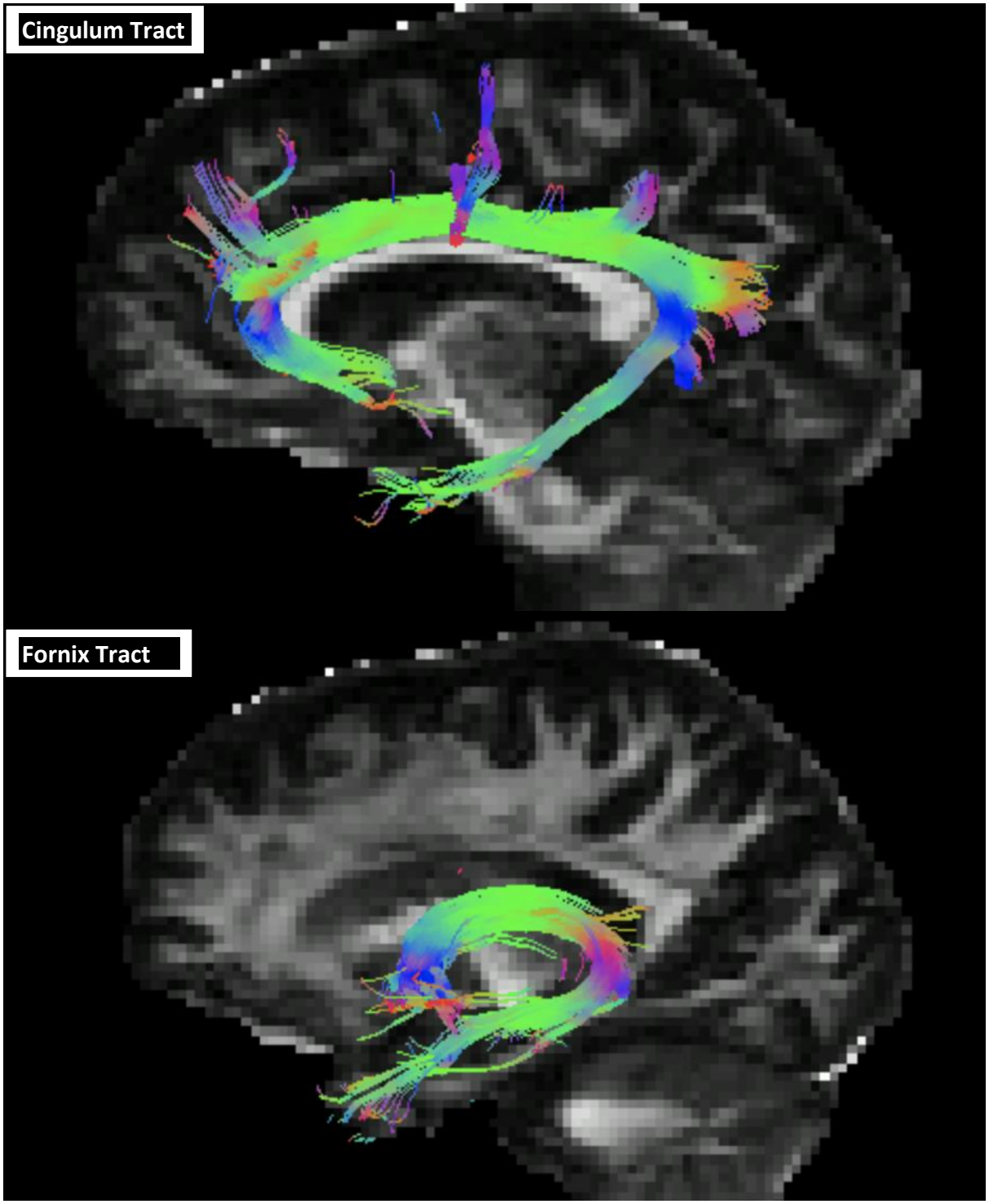

Figure 6.14 Examples of left Cingulum Tract (top), and Fornix Tract (bottom). *Tracts are colour coded in the direction of connectivity: green anterior-posterior, blue – superior-inferior and red left - right.*

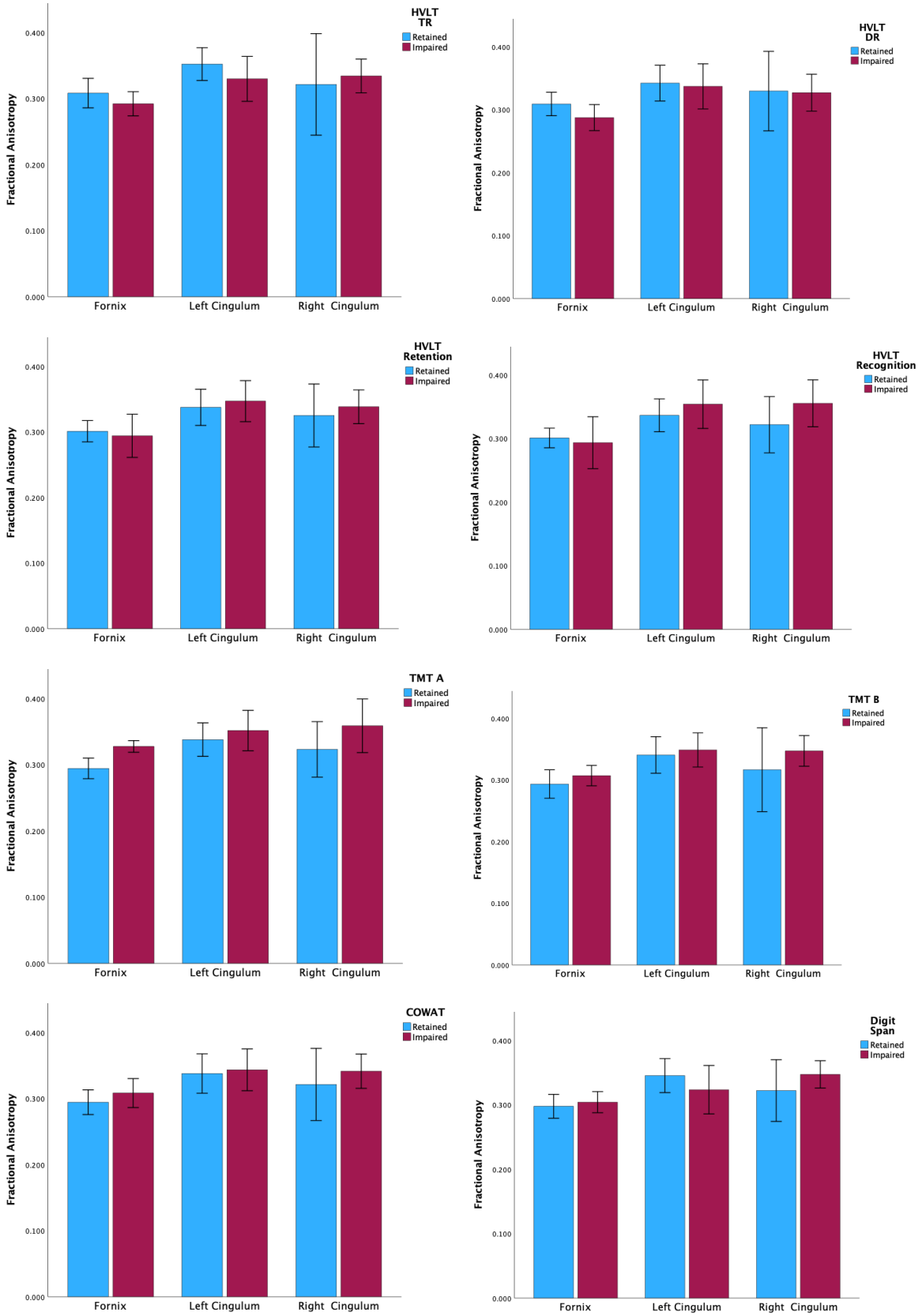

Figure 6.15 Bar Chart demonstrating differences in fractional anisotropy of the three tracts studies in each NCF domain. *HVLT: Hopkin's verbal learning test-revised, TR: Total Recall, DR: Delayed recall, TMTA: trail making test A, TMTB: trial making test B, COWAT: Controlled oral word association test.*

6.4.5 Multivariate Analysis and Identification of Confounding Factors

Multivariate analysis was conducted, and this demonstrated that FA of the fornix was significantly affected by age, whereas other metrics of MRI, namely, CBF, MR Spectroscopy measure and volume did not reach statistical significance. There was no statistical difference between the groups in the eight NCF domains in any of the MRI measures, use of steroid or SACT when Bonferroni correction was conducted. However, when reducing the variables in NCF tests and looking at the group with intact NCF across all domains compared to those with impairment in at least one domain, cerebral blood flow of the hippocampus and MR spectroscopic measurement of NAA, creatine and Glx were statistically significant whilst diffusion measures of the fornix tract and cingulum and volumetric measurements of the hippocampi were not statistically significant.

6.5 Discussion

Patients were able to undergo additional research MRI at CUBRIC satisfactorily. All patients recruited to the MRI arm completed all the baseline MRI scans without any problems. We have demonstrated feasibility of recruiting patients with BM to a study which includes translational imaging component and a significant time commitment from the patients. There is a need for clinical trials relating to primary sites to be more inclusive of patients with BM.

Structural MRI of the hippocampus demonstrated high correlation between left and right hippocampal volumes. The two outliers in the correlation figure both exhibited smaller hippocampus on the left side compared to the right side; both patients had metastases in close proximity of the left hippocampus, and oedema may have resulted in reduced measurements of the volume. Hippocampal volume was strongly negatively correlated with age, however use of concurrent steroids or SACT did not have a significant impact on the volume. Volume loss with age has been previously demonstrated in healthy participants (Nobis *et al*., 2019). There was no statistically significant difference in the mean hippocampal volume when stratified by NCF tests impairment. This could be because hippocampal volume changes are considered to be a late effect (Seibert *et al*., 2017a, Suckert *et al*., 2020), whereas NCF impairment secondary to BM is an acute event and volume loss was not apparent at this time point. Manual delineation was not compared to autodelineation undertaken by FreeSurfer. It is important to note that limitations of FreeSurfer include that it has been designed for brain without the presence of tumour and further validation of this software needs to take place in brain with tumour present.

CBF can be affected by cerebrovascular disease, cardiovascular disease, hypertension, small vessel disease due to conditions such as diabetes mellitus and respiratory disorders affecting oxygenation (Alsop *et al*., 2015). Older participants are more likely to have these conditions, hence affecting the blood flow. We have not demonstrated a statistically significant correlation between grey matter CBF and age. There was one patient who was a young patient aged 23 years with melanoma who was heavily treated with multiple lines of

systemic therapy and exhibited a relatively low CBF in the combined hippocampi. Out of interest, with the outlier excluded, grey matter CBF and age were strongly negatively correlated, r = -0.556 (p-value 0.021). In addition to age being an important factor, hippocampal perfusion can also be affected by the time of day the scan was performed, Apolipoprotein E status, and volume averaging through choroidal vessels and choroid plexus or CSF from dilated temporal horns. Testing for these factors was beyond the work carried out in this thesis as the impact of these factors needs further research.

There was non-significant trend towards higher mean hippocampal CBF in patients having SACT, whereas patients having steroids exhibited lower mean hippocampal CBF. One possibility is that younger patients were likely to receive SACT than older patients in this cohort. In this patient population, mean age of patients having concurrent treatment with SACT at the time of their treatment was 54.5 years compared to 65 years in the group who were not having SACT. Thus, age may be a more important confounding factor compared to use of concomitant steroids or SACT. Mean CBF was significant lower in HVLT-TR and DR domains and if patients had impairment in any domain compared to patients who had retained NCF. Statistical significance was not demonstrated in other NCF tests. HVLT-TR and DR tests are designed to test recall, namely total and delayed recall. Hippocampus is thought to play a crucial role in recall and memory (Dolui *et al*., 2017) and therefore reduced CBF may be a causative factor of impairment in these domains. ASL may produce poor CBF maps in patients with cerebrovascular disease and it will be a key factor to consider in future studies studying ASL.

MRS is often used to study the tumour, however, here this sequence has been performed to study normal tissue and its correlation with NCF in patients with BM. Metabolite measurements in the right and left hippocampi are consistent with previously published studies examining hippocampal spectroscopy. There was no significant difference between the mean and median metabolite values of left and right hippocampi. There was a weak positive correlation with age and metabolite concentration. This contrasts with reported literature where studies have shown reduced metabolite concentration in older adults (Schuff *et al*., 1999, Driscoll *et al*., 2003). This may indicate that SACT is influencing

metabolite level in this cohort of patients as mean age of patients receiving SACT was lower than those who did not receive SACT.

Our data demonstrates that mean concentration of left hippocampal metabolites, i.e., NAA, creatine and Glx was lower in patients who had NCF impairment at baseline pre-treatment. Reduced NAA has been demonstrated in other neurodegenerative diseases such as Alzheimer's disease (Wang *et al*., 2015). This was not observed in the right hippocampus metabolite concentrations. The possible explanation for this could the that four of five patients who had a metastasis in the temporal lobe were on the left side and presence of oedema and metastases may have affected the ipsilateral hippocampus. Another reason for this could be that left and right hippocampus have different function. A school of thought is that right sided hippocampus is associated more with spatial memory and left sided with verbal learning (Hou *et al*., 2013). However, this is not proven and there are differences of opinion and some studies have not shown lateralisation of such tasks (Glikmann-Johnston *et al*., 2008, Cánovas *et al*., 2011). Additionally it has been hypothesised that NCF is supported by structural connectivity to other parts of the cerebrum such as posterior cingulate gyrus and parahippocampal gyrus (Robinson *et al*., 2016). If there is a difference in function of bilateral hippocampi, then this may be important in considering normal tissue complication probability (NTCP) modelling of the hippocampus and it needs to be studied in detail with NCF testing which examine spatial and verbal memory.

DTI of the fornix tract and bilateral cingulum tract demonstrated that FA of the fornix tract was strongly negatively correlated with age, however such correlation was not demonstrated with the cingulum tracts. It's possible that the fornix tract could be more sensitive to age related changes compared to the cingulum tracts (Peiffer *et al*., 2010). The difference between diffusion metrics did not vary between the groups of patients with retained and impaired NCF. This may reflect that changes in diffusion metrics normally indicate white matter changes and these, including volumetric changes, are often considered to be late effects of radiation treatment (Makale *et al*., 2017). DTI metrics of these tracts have been studied widely in patients with Alzheimer's dementia compared to healthy controls (Lo Buono *et al*., 2020, Liu *et al*., 2011). However, acute alterations in the brain function in

patients with BM is likely have a different pathophysiology compared to patients with established diagnoses such as Alzheimer's dementia.

Studies have previously demonstrated how individual measurements from different MRI modalities, i.e., volume, blood flow, spectroscopy and diffusion can be affected in various diseases affecting NCF. In this chapter I have displayed results from each of these MRI modalities and their correlation with clinical and neurocognitive parameters. Whilst this is exploratory work given the small cohort of patients, examining each MRI modality concurrently and linking these data to detailed neurocognitive function data is immensely powerful, and has not been done in such detail in previous studies of patients with BM. When looking at subsequent chapters which examine the post radiotherapy effects and changes in NCF from baseline, it will be important to consider factors such as CBF and spectroscopic measurements of brain metabolites in relation to acute changes, whereas diffusion and volumetric measurements may not differ as much.

There are several limitations of this work. This study recruited a small number of patients with BM who underwent detailed MRI imaging with multiple measures, thus having a high number of variables. There were a small number of patients with BM in the temporal lobe which may be an important confounding factor, although Chapter 5 did not demonstrate significant difference in NCF scores if the metastases was present in the temporal lobe. To study NCF impairment and MRI changes at baseline, a larger prospective study is needed which is challenging to set up. Recent RCTs in patients with BM have demonstrated a high dropout rate due to the complex nature of these patients.

6.6 Conclusions

CBF and changes in metabolites may be more sensitive in detecting early NCF changes secondary to BM compared to diffusion metrics and hippocampal volumes. As discussed in Chapter 1 and 4, earlier changes in the brain occur relating to changes in blood flow and volume before white matter changes and structural changes. The latter two may be key

factors to study in long term radiotherapy effects rather than short term changes, which is the aim of this thesis. The next chapter will describe changes in NCF and correlate this with hippocampal dosimetry followed by correlation of radiotherapy doses to MRI components.

Chapter 7 – Assessment of Neurocognitive Function and Quality of Life following Stereotactic Radiosurgery with translational multiparametric MRI Assessment of the Hippocampi

7.1 Introduction

Studies that have examined changes in neurocognitive function (NCF) following radiotherapy for primary brain tumour and BM has been described in detail in earlier chapters (Chapter 1.2.4 and 4.1). There are several randomised controlled trials that have studied NCF changes at depth following stereotactic radiosurgery (SRS) and whole brain radiotherapy (WBRT) (Sahgal *et al*., 2015, Brown *et al*., 2016a, Aoyama *et al*., 2015, Andrews *et al*., 2004). However, these trials did not include hippocampal dosimetry or MRI assessment to look at structural, physiological, or functional changes in the brain post radiotherapy. Individual studies with smaller number of patients have been conducted looked at various aspects of MRI.

Long term radiotherapy toxicity in patients with primary brain tumour with radiological assessments has been investigated to an extent, however, these have mainly utilised T1 and T2 weighted images and their assessment. Johannesen, *et al*. reported white matter changes with hyperintensity in T2 weighted and FLAIR images in the white matter as well as endocrine abnormalities (Johannesen *et al*., 2003). A study of patients with nasopharyngeal carcinoma demonstrated that development of temporal lobe necrosis post radiotherapy was associated with significant reduction in verbal recall, visual memory, language, and cognitive function. The necrosis was identified as hypointensity on T1 weighted images and T2 hyperintensity on T2 weighted images of the temporal lobes (Cheung *et al*., 2000). Seibert, *et al*., conducted volumetric assessment of the hippocampus at baseline and 1 year after fractionated radiotherapy for primary brain tumour. Mean hippocampal dose was significantly correlated with hippocampal volume loss (r=-0.24, P=.03). Mean hippocampal volume was significantly reduced 1 year after high-dose RT (defined as > 40 Gy), mean -6%, P=.009, but not after low-dose RT (defined as <10 Gy). In multivariate analysis, both radiotherapy dose and patient age were

significant predictors of hippocampal atrophy (P<.01) (Seibert *et al*., 2017a). The same group also looked at variation in cortical atrophy at 1 year in the same group of patients and demonstrated that cortical atrophy was significantly associated with radiation dose in the entorhinal (p-value = 0.01) and inferior parietal cortex (p-value = 0.02). In contrast, radiotherapy dose dependent effect was not found in the pericalcarine cortex and the paracentral lobule, which forms part of the primary parietal cortex responsible for somatosensory function. In the whole-cortex analysis, 9 regions showed significant radiation dose dependent atrophy, including areas responsible for memory, attention, and executive function (p-value = 0.002) (Seibert *et al*., 2017b).

There is limited data on acute radiotherapy toxicities and its pathophysiology. DTI was performed as part of a Phase I trial testing Bortezomib as a radiotherapy sensitiser in patient undergoing WBRT. The group demonstrated statistically significant percentage increase in radial diffusivity of the hippocampus white matter with bortezomib, compared to baseline at 1 month post radiotherapy (16.8%, p-value 0.0007) (Lao *et al*., 2013). Whereas the remaining white matter did not reach significance, suggesting that hippocampus is more sensitive to acute radiotherapy toxicity.

Kovacs *et al*., 2015 compared functional MRI (fMRI) activation in high dose region following treatment with long course chemoradiotherapy for glioblastoma. The group illustrated decreased neural activation during motor and listening tasks at 6 weeks following radiotherapy in regions that received a dose of <40 Gy. This change was observed at 3-month interval fMRI as well (Kovács *et al*., 2015, Wilke *et al*., 2018).

In an animal study, the right hippocampus in mouse brain was irradiated using proton beam radiotherapy with increasing doses between 0 Gy and 85 Gy. Post treatment MRI was performed at regular intervals for up to six months. The group which received the highest dose of radiation, MRI contrast agent leakage occurred in the irradiated brain areas within a week of radiotherapy, whereas in lower doses this occurred later in the follow up period (Suckert *et al*., 2020).

A study conducted by Chan *et al*, irradiated one cerebral hemisphere of rats with single fraction varying between 25-30 Gy and conducted MRI studies including diffusion and MR

spectroscopy (MRS) of the hippocampus 12 months following treatment. The opposite cerebral hemisphere was analysed as the control. They demonstrated that the irradiated side had significantly higher percentage decrease in fractional anisotropy compared to the ipsilateral fimbria of hippocampus (29%) than the external capsule (8%) in DTI, indicating the selective vulnerability of fimbria to radiation treatment. MR spectroscopy showed significantly higher choline, Glx, and lactate peaks by 24%, 25%, and 87%, respectively, were observed relative to creatine in the ipsilateral brain. Post-mortem histology confirmed these white matter degradations as well as glial fibrillary acidic protein and glutamine synthetase immunoreactivity increase in the ipsilateral brain (Chan *et al*., 2009). Another animal study conducted MRS 65 days following hypo fractionated radiotherapy, 40 – 30 Gy in 5 fractions on consecutive days, demonstrated significantly increased levels of neurotransmitter GABA indicating increase in inflammation which was confirmed on histology (Zawaski *et al*., 2017). As smaller study of 11 patients showed reduction in N-Acetyl Aspartate and choline at 4 months post radiotherapy for primary brain tumour with recovery at 8 months (Estève *et al*., 1998).

Hippocampal dosimetry has been studied in fractionated primary brain tumours (Gondi, 2012 and Tsai, 2015). Hippocampal avoidance has been investigated in whole brain radiotherapy (WBRT) (Gondi *et al*., 2014a, Lin *et al*., 2016, Tsai *et al*., 2015). Gondi *et al* and Lin *et al* were both phase II studies and compared their results to historical controls. Gondi *et al*., concluded that age >60 years, presence of minor neurological symptoms at baseline and dose to 100% hippocampus predicted a strong decline in HVLT-TR at 4 months (Gondi *et al*., 2014a). Lin *et al*., hippocampus dose dependent memory decline following WBRT: Dose to 0.1 cc, 10%, 50% and 80% of the composite hippocampus of <12.6 Gy, <8.81 Gy, <7.45 Gy, and <5.83 Gy respectively were significantly associated with NCF preservation (Lin *et al*., 2016). Chang *et al*., have studied hippocampal dosimetry in patients undergoing SRS for 6-12 metastases and beam shaping to reduce the dose to the hippocampus (Chang, 2016). However, to date, there has not been a study evaluating hippocampal dosimetry in patients undergoing SRS and its correlation to NCF testing and multi-parametric MRI imaging.

7.2 Methods

7.2.1 - Neurocognitive function and Quality of Life measurements

Patients receiving SRS underwent NCF tests and additional MRI scans at CUBRIC at baseline before SRS treatment and at 1and 3-month intervals following SRS. Additional NCF was performed at 6-month interval. The study design, NCF and MRI methods have been described in Chapter 4, 5, and 6 in detail. In addition to these tests, quality of life questionnaire (Quality of Life) was completed. Raw NCF test scores were calculated as standardised T scores (Iverson, 2011). Method of calculating the T-scores and definition of retained and impaired NCF has been described in Section 5.2. Those who had a difference in T-score of 10 or more from baseline were considered to have significant NCF impairment following SRS. This is equivalent to a change a one standard deviation. This is a standard metric when comparing NCF changes (Brown *et al*., 2016a). To control for selection bias, only patients who completed all the assessments were included in this analysis.

European Organization for Research and Treatment of Cancer (EORTC) quality of life questionnaire (QLQ) is a validated integrated system for assessing health related QoL of patients with cancer participating in clinical trials (Aaronson *et al*., 1993). It consists of thirty questions encompassing global health status; functional status, namely physical, role, emotional, cognitive, and social functioning; and symptoms. The BN20 supplement encompasses specific symptoms relating to CNS tumours (Taphoorn *et al*., 2010). Table 7.1 summarises the scoring for both questionnaires. Patients were asked to complete the questionnaires and scores relevant to each domain were converted into a raw score and a subsequently scaled score was calculated according to the EORTC manual (Fayers and Bottomley, 2002). The raw score was calculated as the mean of the component items for all scales. Then for functional scales:

$$Score = 1 - \{\frac{(RS - 1)}{range}\} x\ 100$$

And for symptom scale and Global health status and QoL:

$$Score = \{(RS - 1)/range\}\, x\, 100$$

Where RS = raw score and range refers is the difference between possible maximum and the minimum response to individual items in the questionnaire. Global health status QoL questions have a range of six and remaining functional and symptom scales have a range of three. The scaled scores can be a maximum of one hundred. In QoL domains, higher scores represent higher QoL, whereas in symptom domains this represents higher proportion of symptoms (Fayers and Bottomley, 2002).

7.2.2 - Hippocampal contouring and hippocampal radiation dosimetry

The hippocampus was outlined according to the RTOG protocol (Gondi, 2014) retrospectively after the SRS treatment was delivered in order to avoid bias from radiotherapy planners. Patients received standard SRS treatment according to the local and study protocol (See Appendix I).

It was demonstrated in Chapter 2, section 2.4.5, that all dose constraints of the hippocampus (D0.1 cc, D40, D50, D70, and mean dose) were highly correlated with each other. Dose to 40% of the bilateral hippocampi (D40) has been studied in fractionated radiotherapy for primary brain tumours and was associated with significant impairment of NCF (Gondi *et al*., 2012). Given the lack of data on normal tissue complication probability (NTCP) of the hippocampus, I studied three dose constraints:

- Mean dose to the hippocampus
- Dose to 0.1 cc of the hippocampus
- D40% of the hippocampus

To study the significance of hippocampus dose constraint, patients were dichotomized into two groups according to the mean dose received by patients who demonstrated a decline of >10 from baseline NCF T-score.

	Number of Items	Item Numbers Version 3.0
QLQ-C30 Global Health Status/ QoL	2	29, 30
QLQ-C30 Functional Scales		
Physical Functioning	5	1 to 5
Role Functioning	2	6, 7
Emotional Functioning	4	21 to 24
Cognitive Functioning	2	20, 25
Social Functioning	2	26, 27b
QLQ-C30 Symptom Scales		
Fatigue	3	10, 12, 18
Nausea and Vomiting	2	14, 15
Pain	2	9, 19
Dyspnoea	1	8
Insomnia	1	11
Appetite Loss	1	13
Constipation	1	16
Diarrhoea	1	17
Financial Difficulties	1	18
BN20 Symptom Scales		
Future Uncertainty	4	31 to 33, 35
Visual Disorder	3	36 to 38
Motor Dysfunction	3	40, 45, 49
Communication Deficit	3	41 to 43
Headache	1	34
Seizure	1	39
Drowsiness	1	44
Hair Loss	1	46
Itchy Skin	1	47
Leg Weakness	1	48
Bladder Control	1	50

Table 7.1 Scoring the EORTC QLQ-C30 version 3.0 and BN20. *Number of items relate to the total of number of questions which relate to the particular function or symptom. Item numbers relate to the number of question(s) in the questionnaire (Fayers and Bottomley, 2002).*

7.2.3 - MRI imaging measurements

The MRI analysis methods for the following modalities have been described in Chapter 4 in detail. In this chapter four MRI factors were examined in relation to hippocampus dose:

- Volume of the hippocampus
- Blood flow within the hippocampus
- MR Spectroscopy of the hippocampus
- Diffusion Tensor Imaging of the fornix and cingulum tract

The following confounding factors were considered:

- Patient factors – age
- Cancer treatment factors – SACT, Steroids and presence of extracranial disease
- SRS treatment dosimetric factors – The dose received by 10 cc of the brain (D10 cc) and the volume of the brain receiving 12 Gy and 5 Gy (V12 Gy and V5 Gy respectively).

Each patient's follow up NCF score, and MRI data was compared to their baseline and represented as percentage change from baseline in the parameter, therefore this reduced the effect of confounding variables such as age, and cancer treatment factors mentioned above. A negative number denoted a decline a positive number denoted an improvement from baseline.

The primary objective of the study was to correlate hippocampal dosimetry to changes in NCF following SRS. Mean dose delivered to the hippocampus was analysed in patients who demonstrated impaired or preserved NCF following SRS. Dose parameters were identified in the two groups and to study the significance of hippocampus dose parameter identified, the participants were dichotomised according to the dose received: those received ≥ 5 Gy to the hippocampus and those who received <5 Gy to the hippocampus. The dichotomisation was based on the median value of dose received by group that demonstrated NCF impairment. Fisher's exact test was performed to test statistical significance for this categorical data. Multivariate analysis was conducted looking at confounding factors, in particular standard brain dose parameters. Secondary objectives were to correlate NCF changes and hippocampal dosimetry to the four MRI parameters mentioned above. There was no adjustment for multiple comparisons for the secondary

end point analyses, so these results should be interpreted as exploratory. All analysis was done by statistical software, SPSS version 28.0.

The baseline patient factors influencing overall survival have been presented and discussed in Section 5.4.4 including disease burden, presence of extracranial disease and NCF score acting as a surrogate marker for disease burden. Therefore, these have not been discussed again in this chapter. This chapter will focus on the changes in NCF, and MRI measurements following SRS.

7.3 Hypothesis

In this chapter I will explore the following hypotheses:

- Patients receiving a higher dose to the hippocampus will exhibit reduction in NCF scores at 1-, 3- and 6-months following SRS treatment.
- Higher radiotherapy dose to the hippocampus will show reduction in CBF and spectroscopic measurements. However as white matter and structural changes are late radiotherapy toxicities, I hypothesise that these measures may not show changes in the acute time frames measured in this study.

7.4 Results

Out of thirty-one patients who completed baseline assessments, 21, 18, and 14 patients completed 1-month, 3-month, and 6-month NCF testing, respectively. The reasons for not completing are summarised in Figure 7.1. Twenty out of thirty-one patients completed baseline MRI, fifteen completed 1-month MRI and eight patients completed 3-month MRI assessments for the trial. The main reason for withdrawal from the MRI sub-study was progressive extracranial disease and requirement of time commitment.

As described in Table 5.7, 13 (42%) patients had intracranial disease relapse, four were within the SRS field (12.9%). Of those who had progression with the treated field, three underwent surgical resection which confirmed presence of metastatic disease. Median time to progression was 5 months with a range of 2-10 months. Of those who had intracranial recurrence, three patients underwent neurosurgery, five patients had further

SRS, one had WBRT, two had systemic therapy two received best supportive care. Participants' demographics and proportion of patients receiving SACT, and steroids have been summarised in Chapter 5 (Table 5.3 and 5.4 respectively). Median overall survival was 11 months with 95% confidence interval of 8.1-13.4 months. This is consistent with published clinical trials in this cohort of patients (Brown *et al*., 2016a, Aoyama *et al*., 2015, Chang *et al*., 2009).

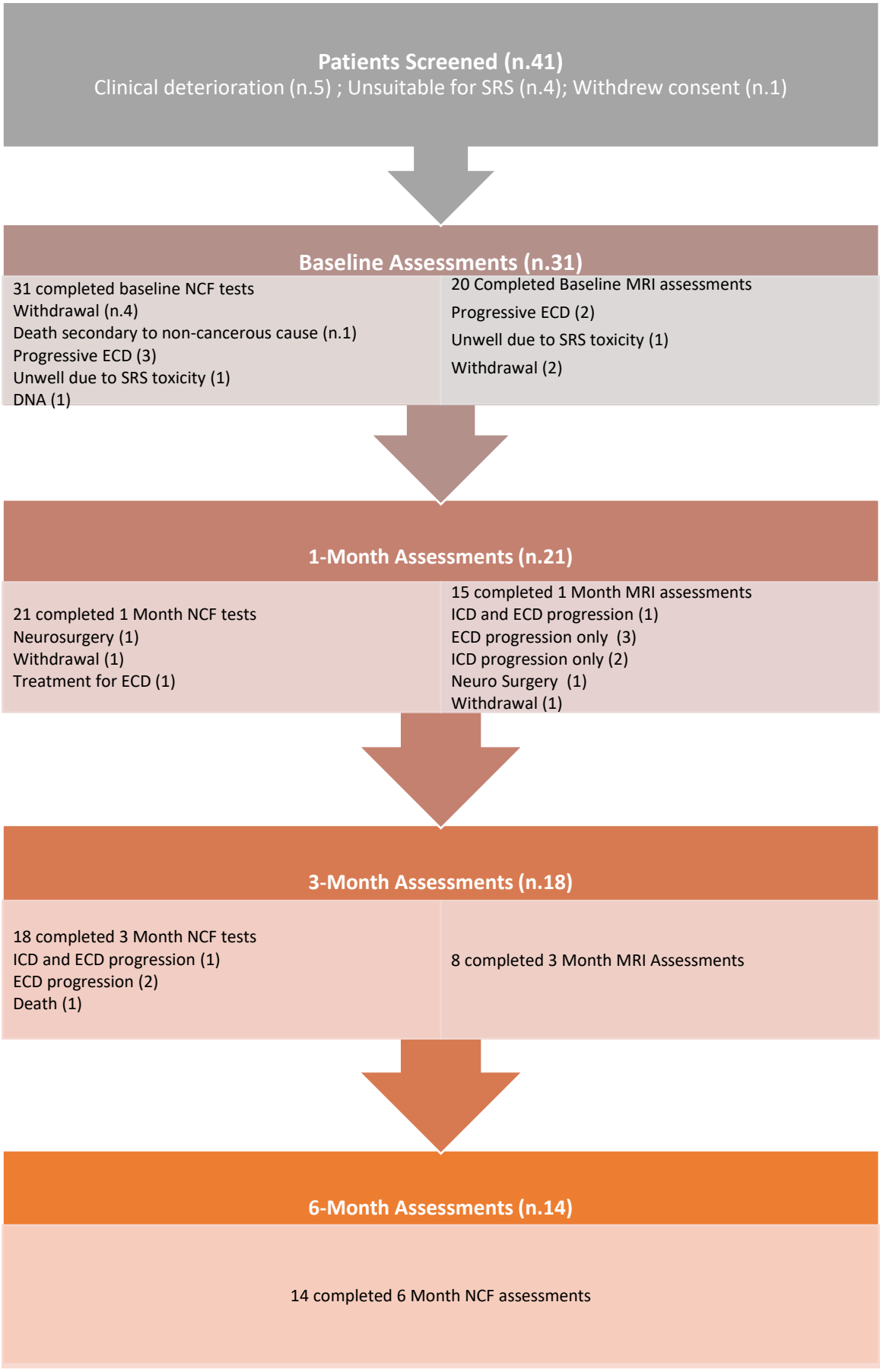

Figure 7.1 Participant flow in the study and summary of reasons for participants not completing the relevant assessments. *ECD: extra cranial disease, ICD: intracranial disease, SRS: stereotactic radiosurgery, DNA: did not attend*

7.4.1 NCF

Nine out of twenty-one patients (42%) patients demonstrated a decline in at least one domain of NCF testing at 1 month, six out of eighteen patients (33%) at 3 months and 1 out of 14 (7%) patients at 6 months. This pattern of reduction was mostly present in verbal memory (HVLT-TR, HVLT-DR, and HVLT-recognition) and executive function domains of NCF tests (TMT-B), although the COWAT test which did not demonstrate this reduction. Conversely, NCF tests focusing on processing speed and attention domains (TMT-A, digit span) did not show a decline following SRS (Figure 7.2). HVLT-TR T-scores strongly correlated with other domains of HVLT test, namely delayed recall, retention, and recognition ($r=0.430$-0.747, p-value<0.05). Thus, for the purposes of comparing NCF scores to hippocampal dosimetry and MRI biomarkers, HVLT TR T-score was used as a surrogate marker for verbal memory. HVLT is one of the widely studied NCF tests and has been validated internationally with 6 versions to be used in patients with NCF impairment (Belkonen, 2011, Benedict *et al*., 1998).

Executive function was measured by trail making test B (TMT-B) and controlled oral word association test (COWAT). There was non-significant trend towards reduction in TMT-B T-scores, however, COWAT did not exhibit any difference between pre and post treatment assessments (Figure 7.2).

Attention was tested by digit span, and processing speed was tested by TMT-A. TMT- A T-score demonstrated an improvement over time which could have been due to simplicity of the test and its repetition (Figure 7.2). Digit span shows an improvement at 1 month and 3 months when compared to baseline followed by non-significant reduction at 6-month interval.

HVLT-Total Recall

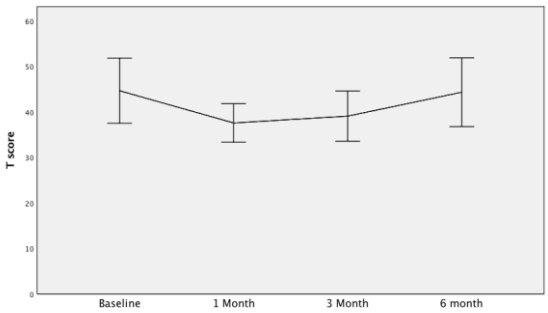

HVLT-Delayed Recall

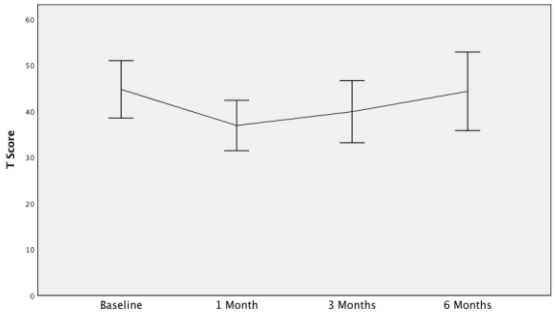

HVLT-Retention

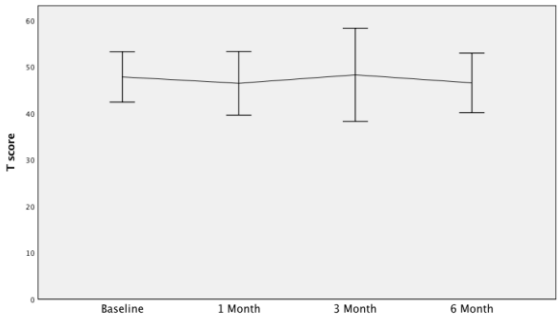

HVLT-Recognition

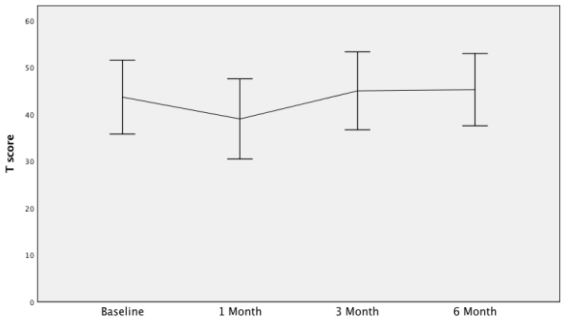

Digit Span

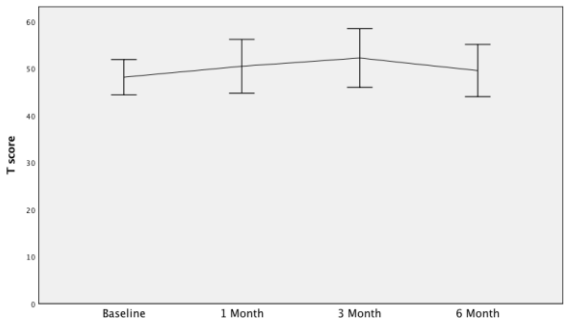

Trail Making Test A

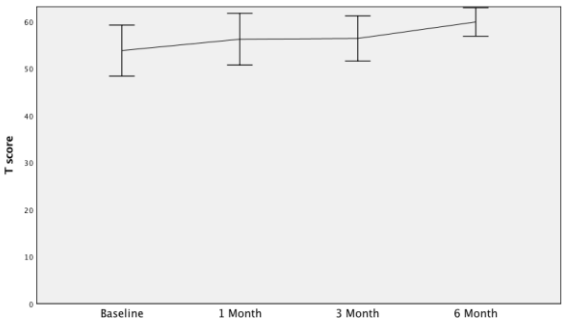

Trail Making Test B

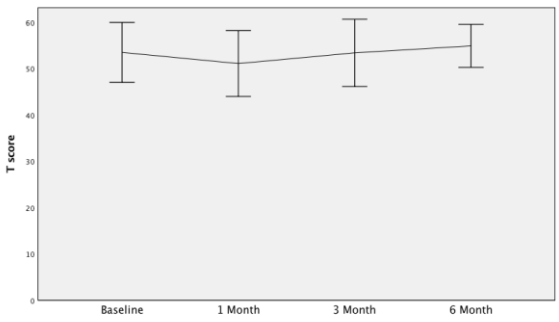

COWAT

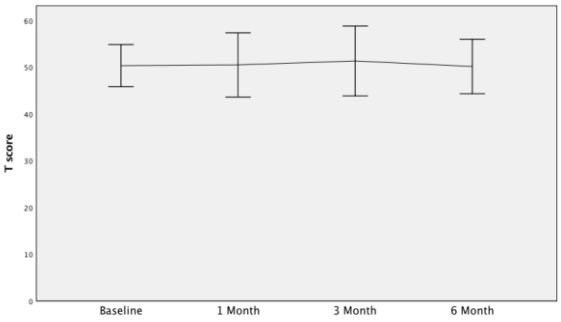

Figure 7.2 Mean and 95% confidence interval of T scores across all 8 NCF tests performed at Baseline, 1 month, 3 Month and 6 Month time points. *HVLT: Hopkin's verbal learning test; COWAT: controlled oral word association test*

Patients with intracranial recurrence demonstrated reduction in HVLT TR T-Scores at 1 and 3 months compared to baseline. NCF decline is more in the recurrence group than the no recurrence group and takes longer to recover in the recurrence group compared with the no recurrence group (Figure 7.3A, Table 7.2A).

In patients who did not receive steroids, there was a trend towards reduced mean HVLT-TR T-score at 1, 3 and 6 months (Figure 7.3 B). Patients who received a course of steroids, which was defined as taking dose of 2 mg or more of dexamethasone for more than 1 week, demonstrated improved NCF at follow up. Looking at percentage differences in the T-score from baseline, there was a significant reduction at 1 month, but no statistical difference was found at 3 and 6 months (Table 7.2 B).

Patients who received SACT exhibited a lower mean HVLT TR T-Score at 1 month, compared to those who did not receive SACT. However, there was no statistically significant difference in the group when stratified by receipt of concurrent SACT (Figure 7.3 C, Table 7.2C).

Percentage Change in HVLT TR T-Score	Disease Recurrence	No Disease Recurrence	p-value
BS and 1-month	-7.17 (-14.41, 0.07)	3.32 (12.78)	0.458
BS and 3-month	-13.02 (-20.59, -5.45)	15.87 (14.35)	0.094
BS and 6-month	1.06 (-4.46, 6.58)	7.27 (9.34)	0.289

Percentage Received Steroid Did not receive p-value

Change in HVLT TR T-Score
BS and 1-month
BS and 3-month
BS and 6-month

Percentage Change in HVLT TR T-Score	Received SACT	Did not receive SACT	p-value
BS and 1-month	-4.19 (-12.28, 3.9)	3.76 (-6.31, 13.73)	0.278
BS and 3-month	3.57 (-5.62, 12.76)	-15.83 (-45.45, 13.79)	0.248
BS and 6-month	6.98 (1.66, 12.3)	-6.16 (-22.23, 9.91)	0.163

C

Table 7.2 Percentage change in HVLT-TR T-Score from baseline to defined follow up time points stratified by intracranial recurrence (A), receipt of steroids (B), and SACT (C). *BS: Baseline; HVLT TR: Hopkins Verbal Learning Test -Revised Total Recall, SACT: Systemic Anti-Cancer Therapy*

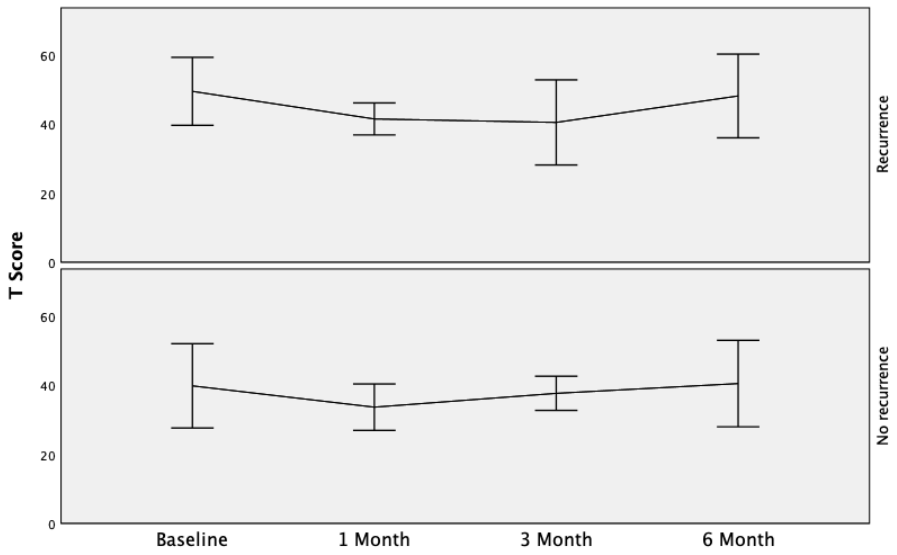

A

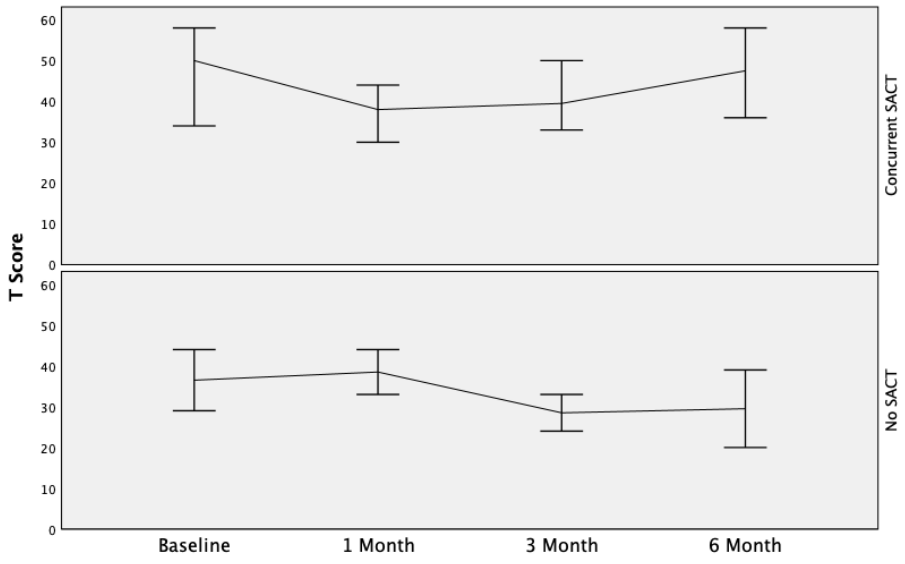

B

C

Figure 7.3 Mean and 95% confidence interval of HVLT-TR T-score at each time point stratified according to recurrence (A), receipt of steroids (B) and concurrent SACT (C)

7.4.2 Hippocampal Dosimetry and NCF

Dose to 0.1 cc of the ipsilateral hippocampus was predictive of reduction in HVLT TR T-scores at 1 month, but less so at 3 months and 6 months interval. Participants who demonstrated a decline in HVLT TR- score at 1 month had a mean dose to 0.1 cc of the hippocampus of 5.39 Gy compared to 2.28 Gy in participants who had maintained HVLT TR T-score, p-value with univariate analysis was 0.026. Hippocampus mean dose and D40 did not demonstrate the same relationship as dose to 0.1 cc (Figure 7.4). Multivariate analysis demonstrated that dose to 0.1 cc of the hippocampus was predictive of decline in HVLT at 1 month (p-value < 0.001) irrespective of whole brain V12 Gy, V5 Gy and D10 cc.

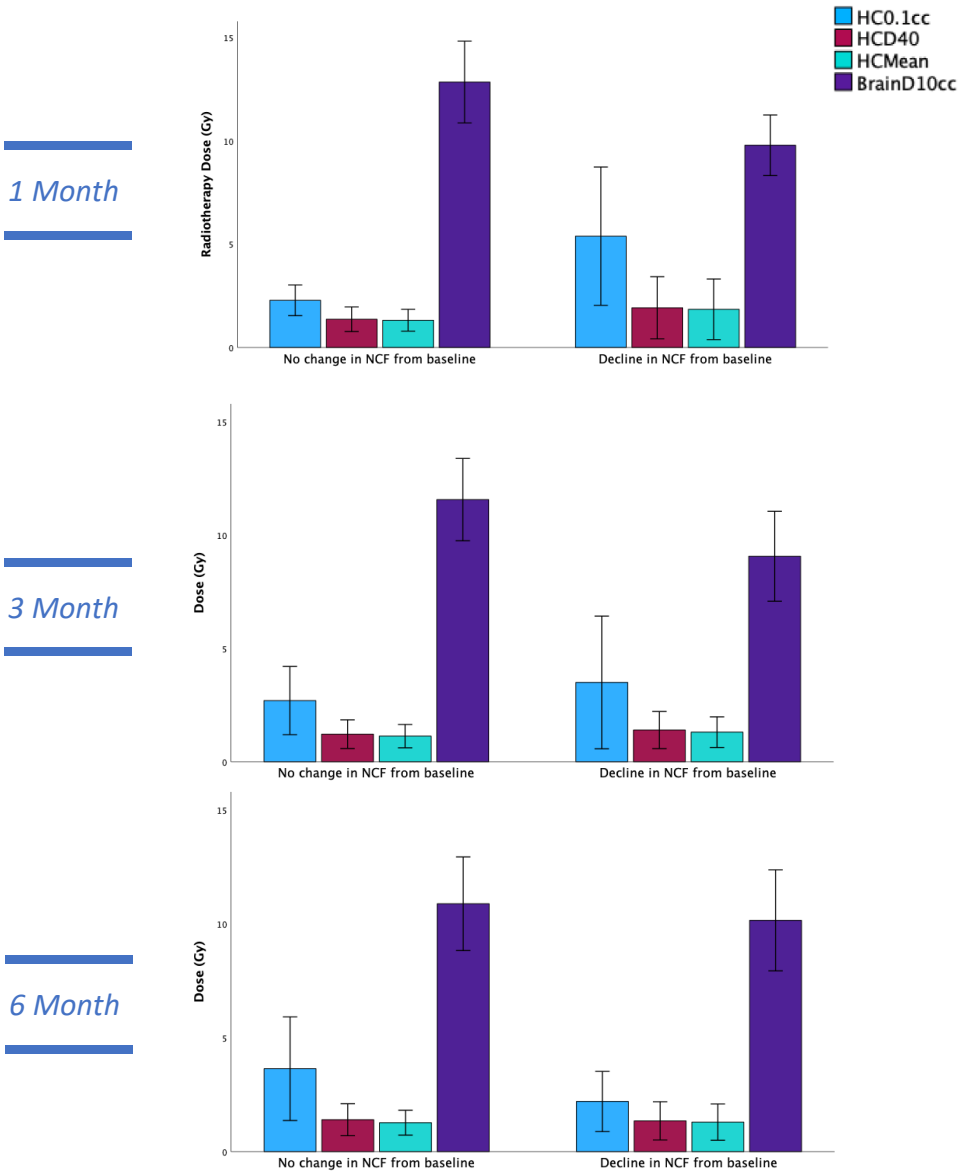

Figure 7.4 Dose to 0.1 cc of the hippocampus (HC 0.1 cc), Dose to 40% of the hippocampal volume (HC D40), mean dose to the hippocampus (HC Mean) and Dose to 10 cc Brain-GTV (Brain D10 cc) in patients who had no change or decline in NCF at each time point. *Bars represent mean with error bars representing 95% confidence interval.*

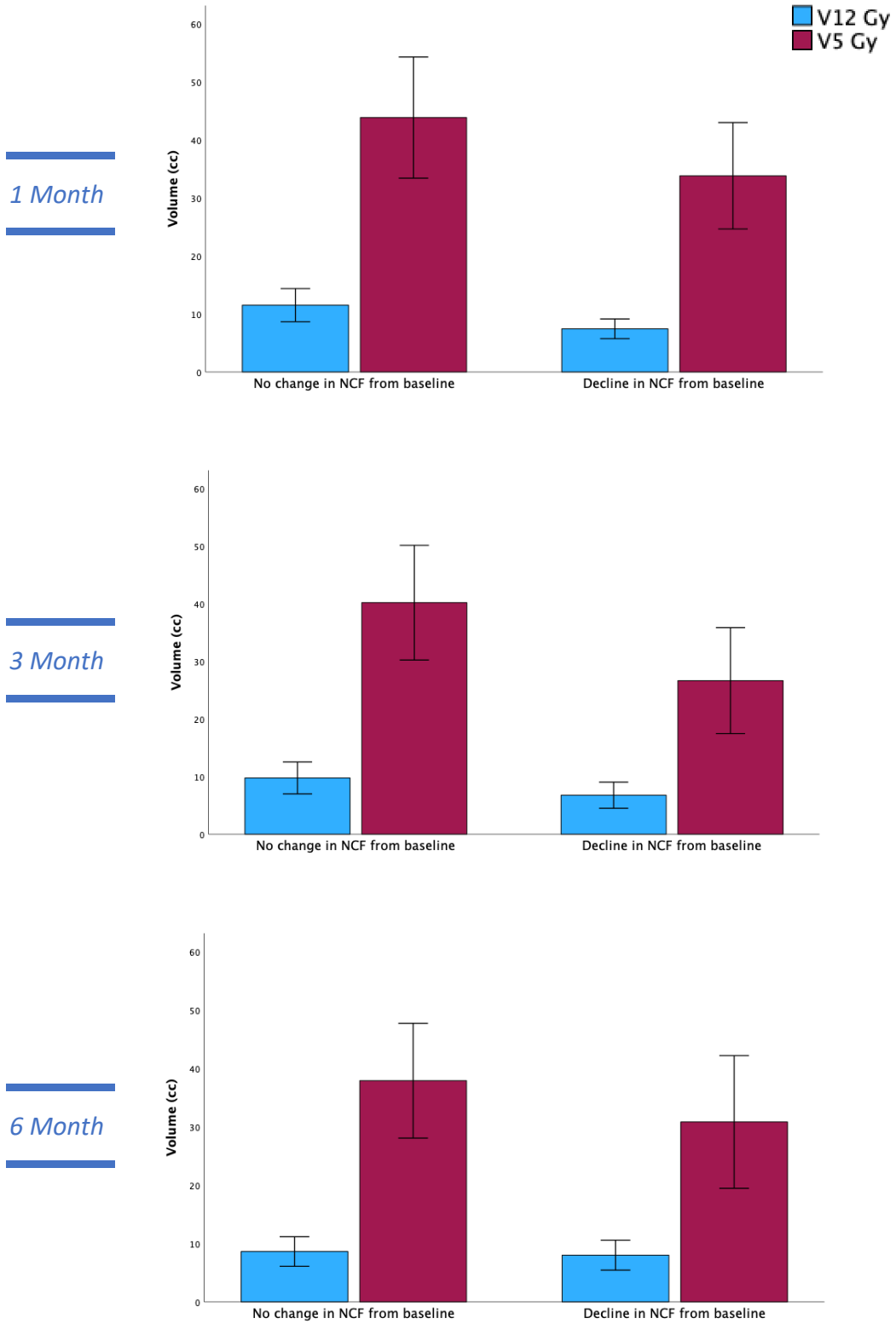

Figure 7.5 Mean and 95% confidence interval brain-GTV volume in cubic centimetres receiving 12 Gy and 5 Gy in patients who had no change or decline in NCF at each time point. *V12 Gy: Volume of Brain-GTV receiving 12 Gy; V5 Gy: Volume of Brain-GTV receiving 5 Gy. Error bars represent 95% confidence interval*

There was no significant difference in the volume of brain receiving 12 Gy and 5 Gy dose between the two groups (Figure 7.5). There was a negative correlation between D 0.1 cc of the hippocampus and difference in NCF testing at 1 month, Spearman's r=0.324 (p-value 0.076) (Figure 7.6).

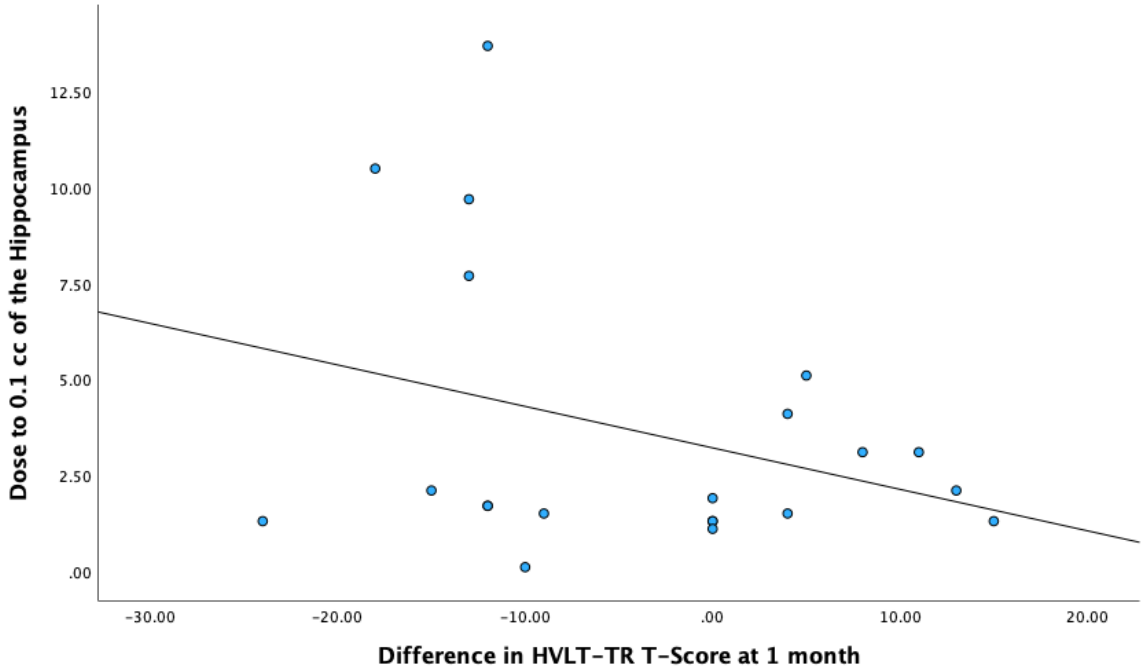

Figure 7.6 Scatter plot demonstrating a negative correlation between dose to 0.1cc of the hippocampus and difference in HVLT-TR score at 1 month. *Each data point refers to individual cases and the line is an interpolation of correlation, r = -0.324.*

Patients who received < 5 Gy to 0.1 cc of the hippocampus demonstrated significantly lower change in mean T-score at 1 month, compared to those who received ≥5 Gy, mean difference in T-score was -1.6, 95%CI -4.3 - 1.1, vs -10.20, 95% CI -14.1-7.7, p-value = 0.04. This difference was not detected at 3 months or 6 months interval (Figure 7.7). Between the two groups, there was no significant difference between the other brain dose parameters of D10 cc, V12 Gy, or V5 Gy.

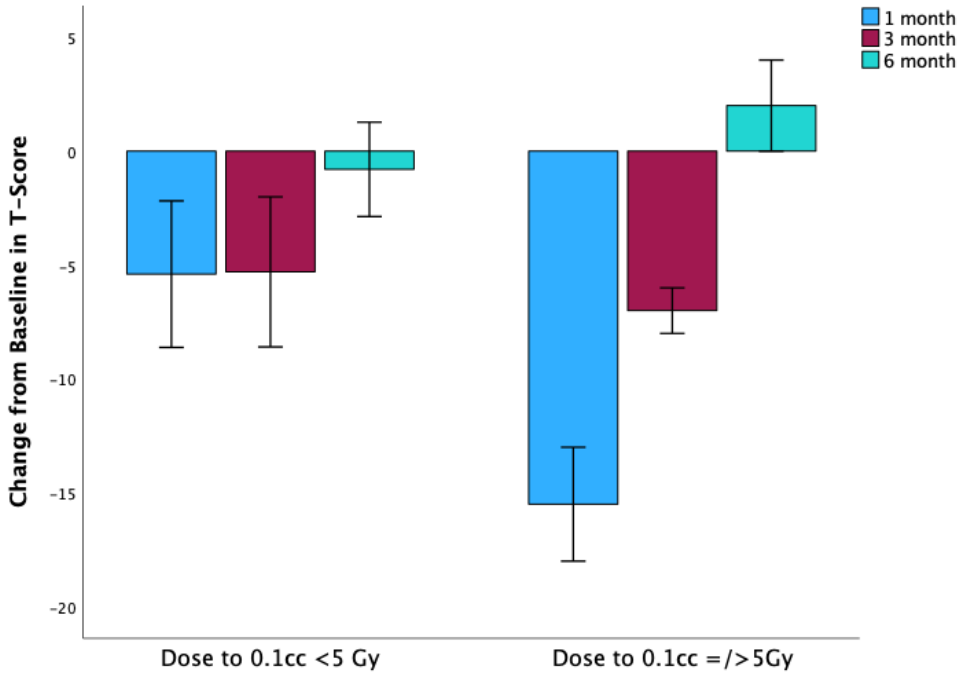

Figure 7.7 Mean difference in T-score from Baseline at 1-,3-, and 6-month interval according to the dose received by the hippocampus. *Error bars represent 95% confidence interval.*

7.4.3 Multiparametric MRI Assessment of the Hippocampus

7.4.3.1 Volume of the hippocampus

There was a reduction in the left hippocampus volume as demonstrated in Figure 7.8 which was apparent at 1 and 3 months in patients who received ≥5 Gy to the left hippocampus, but not in patients <5 Gy, and no significant reduction in the right hippocampus volume was observed. Mean percentage change in the left hippocampus volume at 1-month was -5.9% vs -42.46%, p-value = 0.013, and at 3-month -4.67% vs -53.15%, p-value <0.001, in the group receiving <5 Gy and ≥ 5 Gy respectively (Figure 7.8). An example of participant with reduction in hippocampus volume at 1 and 3 months is demonstrated in Figure 7.9.

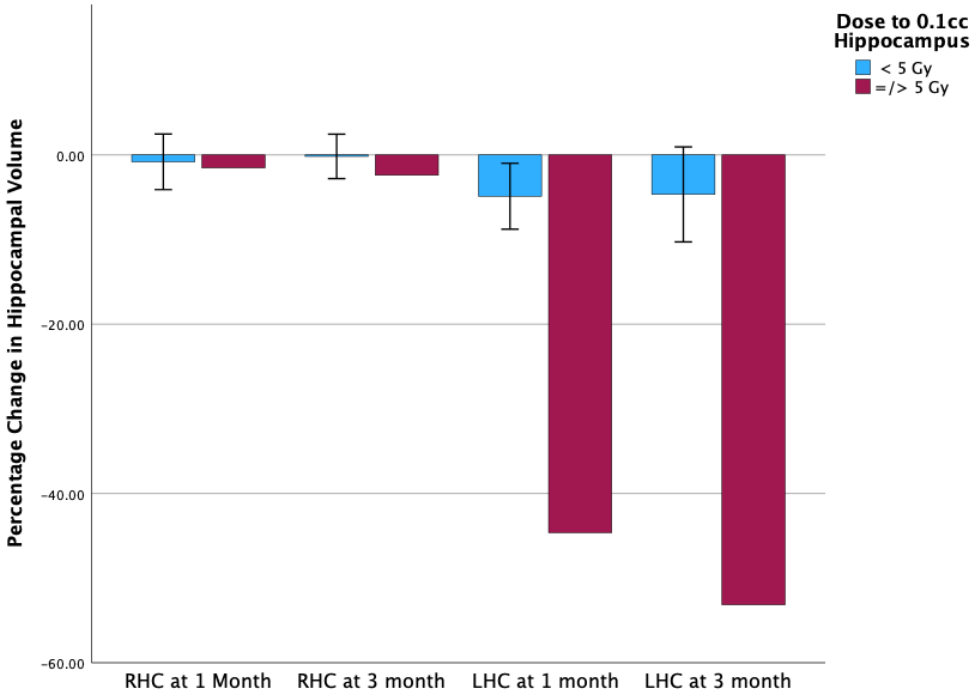

Figure 7.8 Percentage change in right and left hippocampi volume stratified by dose to 0.1 cc of the composite hippocampus. *RHC: right hippocampus, LHC: Left Hippocampus*

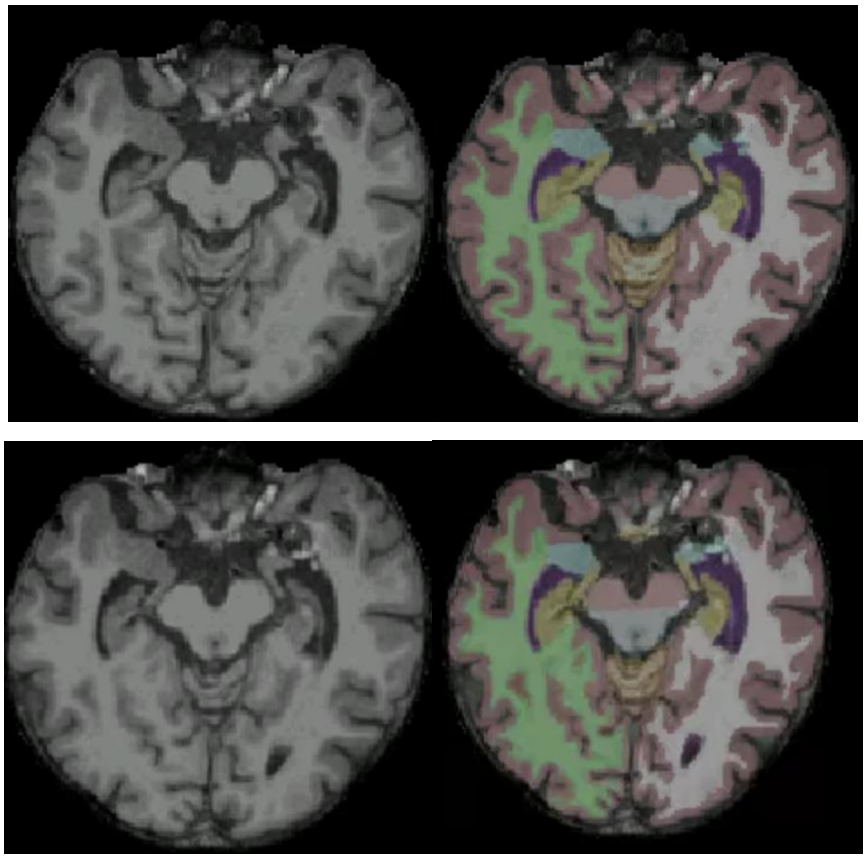

Figure 7.9 Axial slice of T1 weighted image (left) and automated segmentation of cerebral structures (right) created with Freesurfer software (https://surfer.nmr.mgh.harvard.edu/). *Top image was performed at baseline and bottom image was performed at 3 months. Right hippocampus volume was 4292 mm^3 at baseline and 4189 mm^3 at 3 months; left hippocampus volume was 3112 mm^3 at baseline and 2638 mm^3 at 3 months. The dose to D0.1 cc of left hippocampus in this was 7.7 Gy. Green – right cerebral white matter, white – left cerebral white matter, purple – lateral ventricle, maroon – grey matter, light yellow – hippocampus.*

7.4.3.2 Blood flow within the hippocampus

There was relatively more reduction in the mean cerebral blood flow in bilateral hippocampi and cerebral grey matter in the group that received ≥ 5 Gy to 0.1 cc of the hippocampus at 1 month followed by recovery and return to baseline at 3 months (Figure 7.10). None of the groups demonstrated statistical significance.

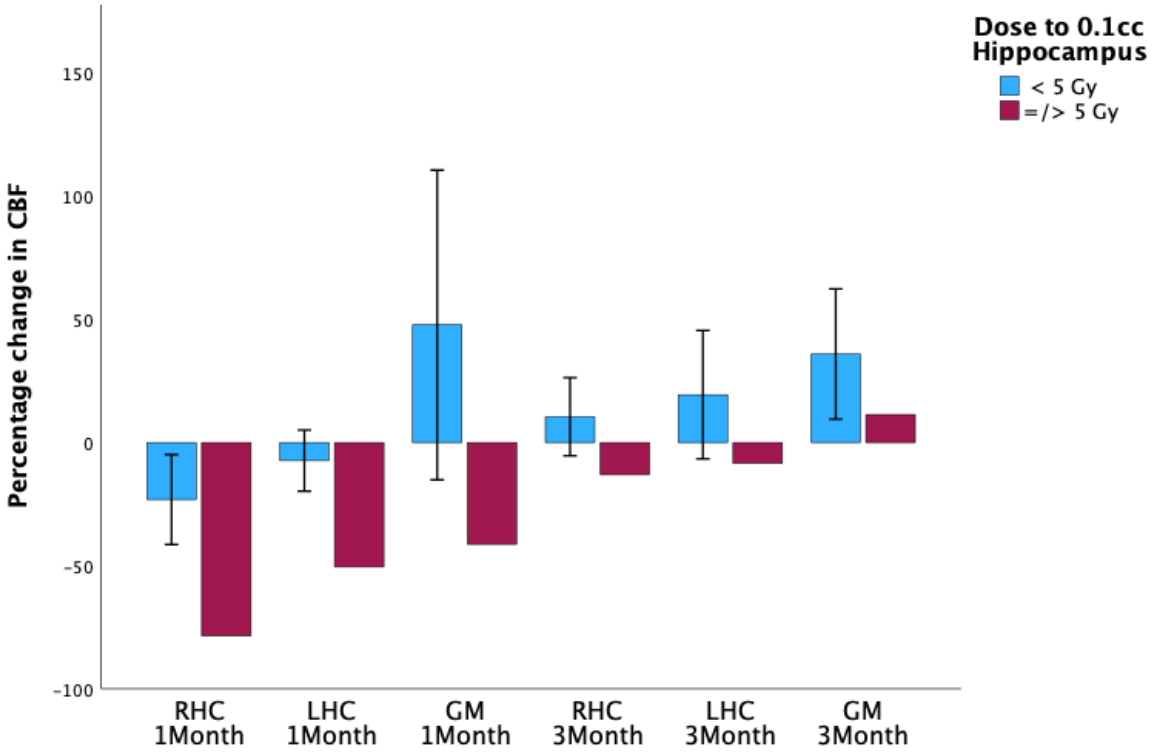

Figure 7.10 Mean percentage change in cerebral blood flow in Right and Left Hippocampi and Grey Matter at 1 and 3 months stratified according to the dose to 0.1cc of the hippocampus. *Error bars represent 95% confidence interval. CBF: cerebral blood flow, RHC: Right Hippocampus, LHC: Left Hippocampus, GM: Grey matter.*

Examples of CBF maps are demonstrated in Figure 7.11 & 7.12. In the two cases presented we demonstrate the reduction in CBF seen one moth after radiotherapy compared with prior to treatment. For the participant presented in Figure 7.11 the D0.1 cc of the hippocampus was 5.10 Gy and D10 cc of the brain was 11.10 Gy. CBF in the right and left hippocampus was reduced by 85% and 65% respectively. The patient presented in Figure 7.12 received 0.1 Gy to 0.1 cc of the hippocampus and D10 cc of the brain was 6.3 Gy. CBF in this case in right and left hippocampus was reduced by 1.2 and 2.9% respectively. CBF in the grey matter was generally lower in the patient presented in 7.11 than in 7.12 figure, their ages were 78 and 39, respectively.

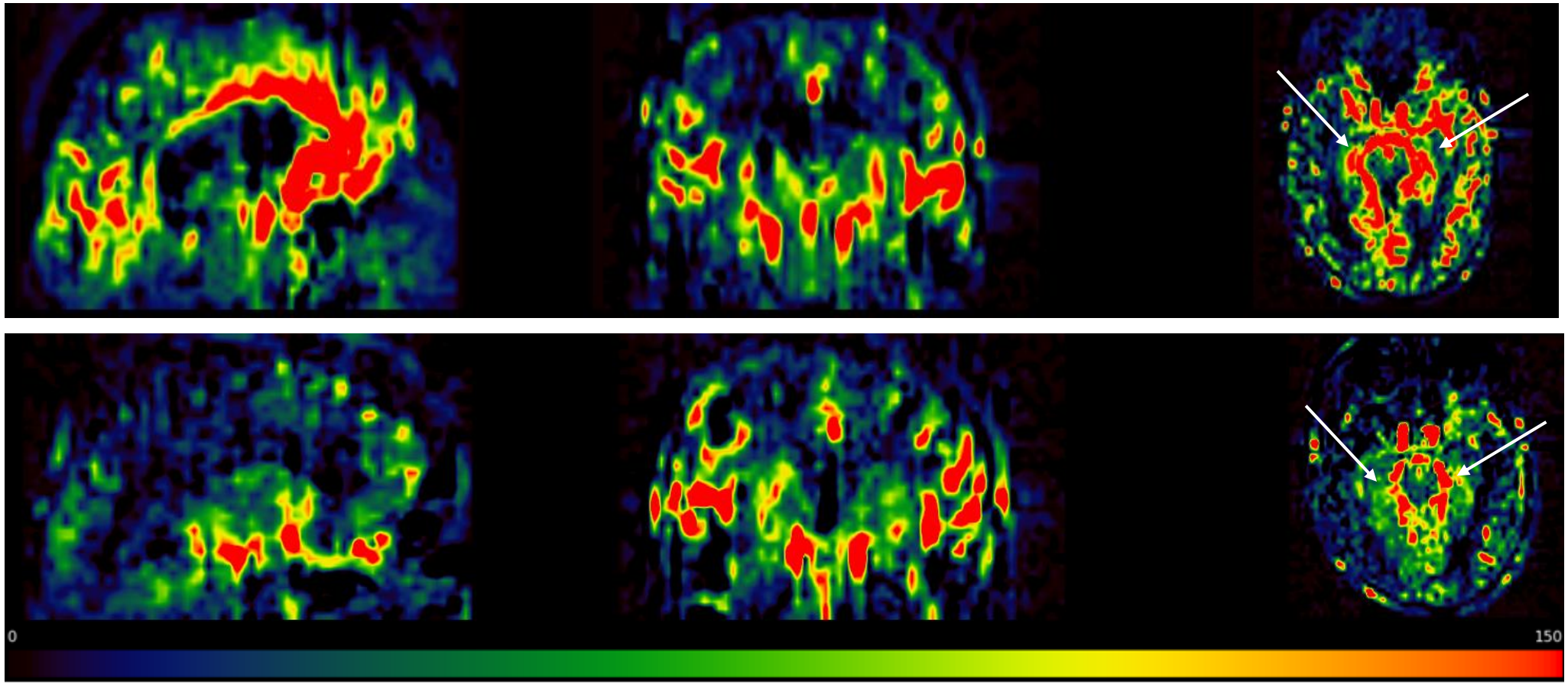

Figure 7.11 Cerebral Flow Map of a patient at Baseline (top) and 1-Month (bottom) time points. *Hippocampus is identified with the pink arrow on the axial slice. Blue-yellow-red map shows the intensity of CBF signal in sagittal (left), coronal (middle) and axial planes. Blue represents CBF close to 0 ml/100g/min and red represents CBF close to 150 ml/100g/min. Mean CBF at baseline was 91.65, 91.42 and 39.58 ml/100g/min in the right hippocampus, left hippocampus and grey matter respectively. At 1-month mean CBF was 14.42, 31.73 and 34.82 ml/100g/min respectively.*

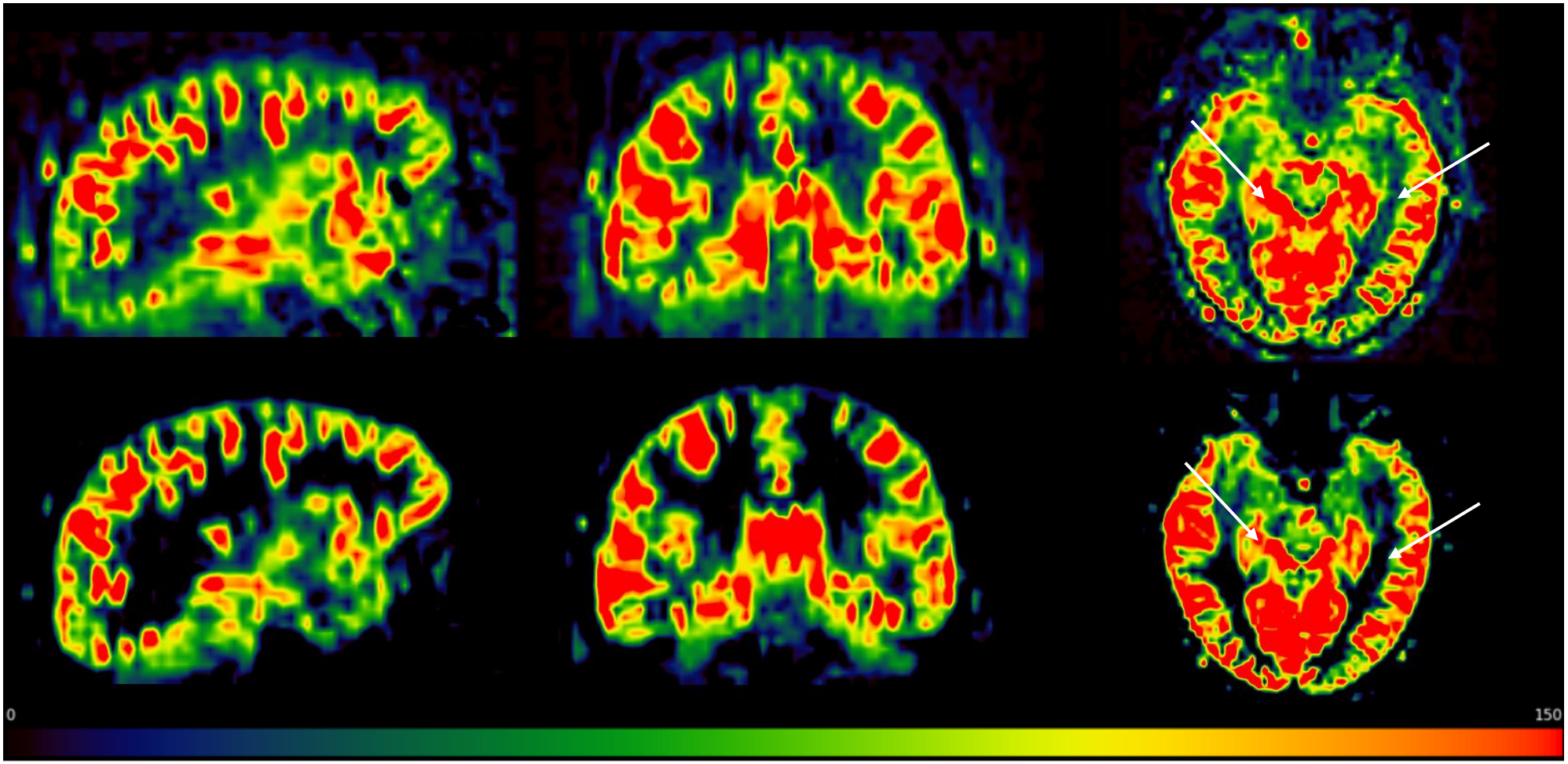

Figure 7.12 Cerebral Flow Map of a patient at Baseline (top) and 1-Month (bottom) time points. *Hippocampus is identified with the pink arrow on the axial slice. Blue-yellow-red map shows the intensity of CBF signal in sagittal (left), coronal (middle) and axial planes. Blue represents CBF close to 0 ml/100g/min and red represents CBF close to 150 ml/100g/min. Mean CBF at baseline was 90.82, 121.50 and 57.32 ml/100g/min in the right hippocampus, left hippocampus and grey matter respectively. At 1-month mean CBF was 89.74, 124.98 and 69.32 ml/100g/min respectively.*

7.4.3.4 MR Spectroscopy of the hippocampus

MR Spectroscopy demonstrated significant change in Glx levels at 1 month, mean percentage difference was 33% increase in the group that received <5 Gy to the D0.1 cc of the hippocampus, compared to 9% reduction in the group which received ≥5 Gy to the D0.1 cc of the hippocampus. At 3 months, there was significant percentage reduction in levels of NAA, choline, Glx, myo-inositol, and creatine in the group that received >5 Gy to 0.1 cc of the hippocampus (Figure 7.13).

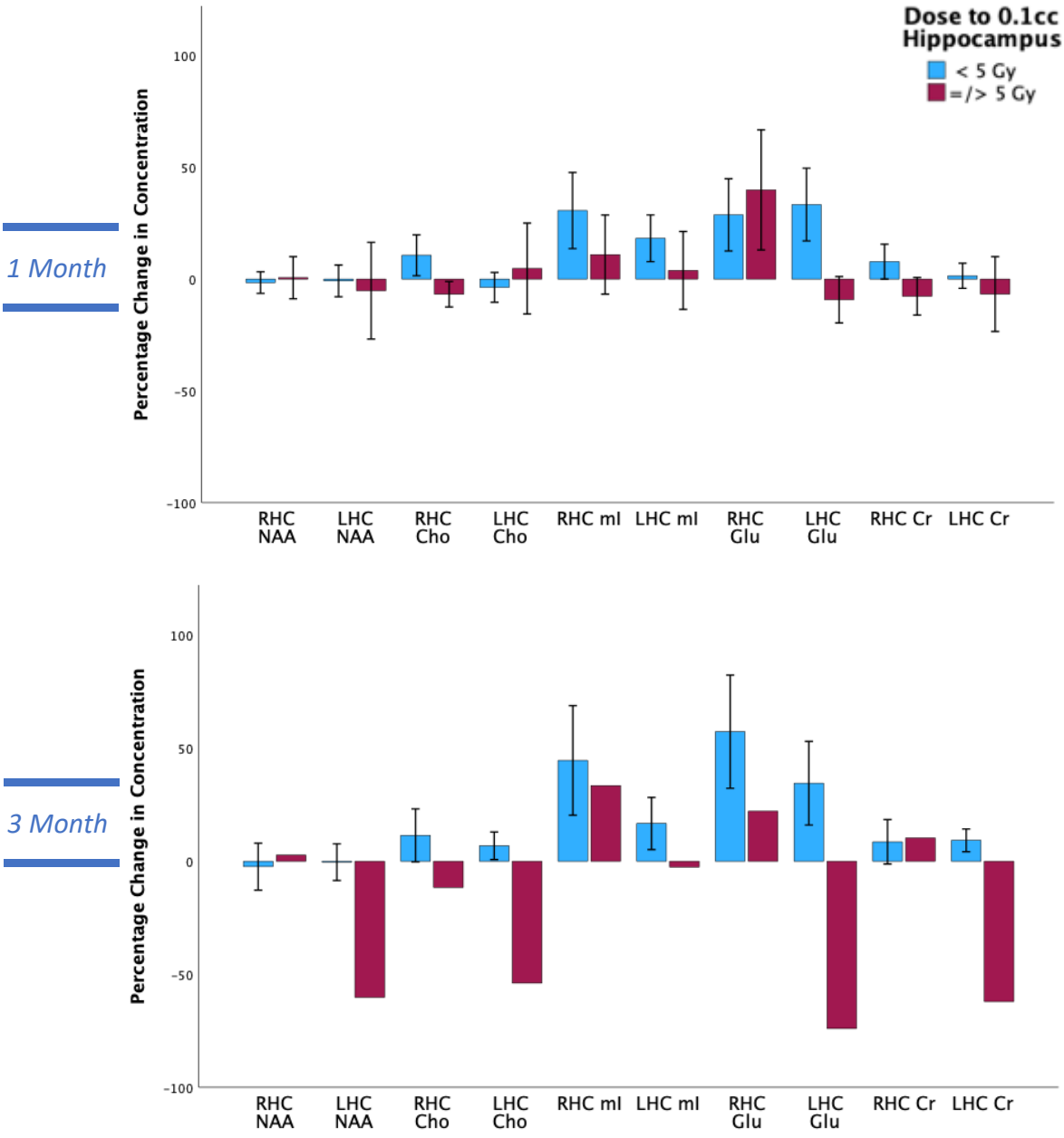

Figure 7.13 Mean percentage changes in the hippocampus metabolites detected at MR Spectroscopy at 1 and 3 months. *Error bars represent 95% confidence interval. RHC: right hippocampus; LHC: left hippocampus, NAA: N-Acetyl Aspartate, Cho: Choline, mI: Myo-Inositol, Glu: Total Glutamate molecules, Cr: Creatine.*

7.4.3.4 Diffusion Tensor Imaging of the fornix and cingulum tracts

Diffusion tensor imaging of the hippocampus showed mean percentage reduction in FA at 1 month with return to baseline at 3 months in those who received more than 5 Gy to the hippocampus. Whereas, in the cingulum tract, FA did not show this pattern (Figure 7.14).

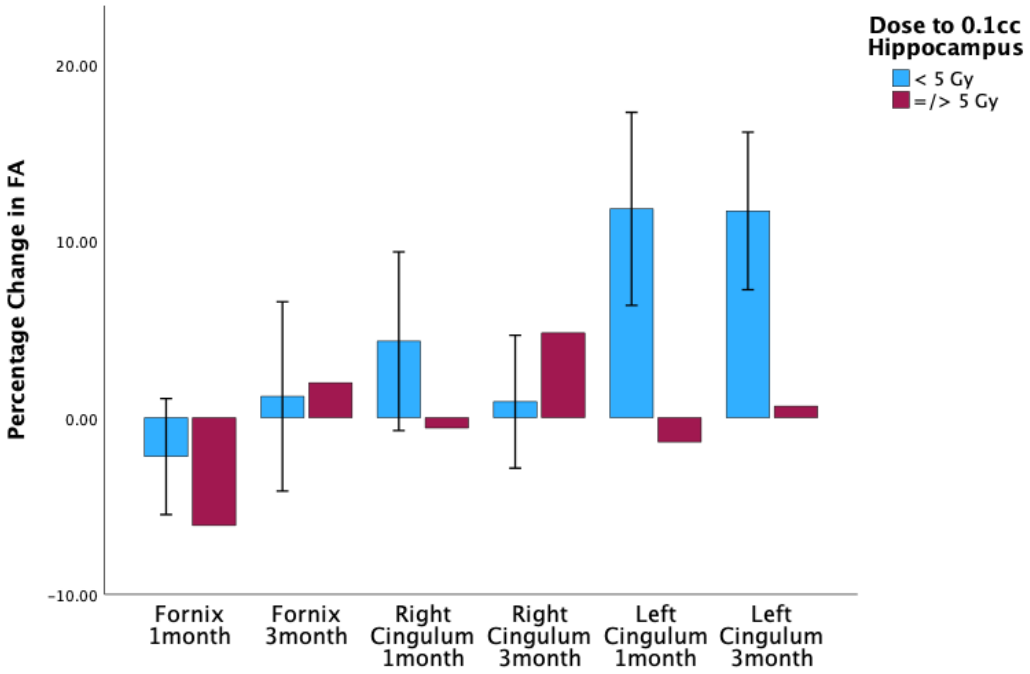

Figure 7.14 Mean percentage change in fractional anisotropy (FA) of the Fornix and bilateral cingulum tract at 1 and 3 months. *Error bar represents 95% confidence interval.*

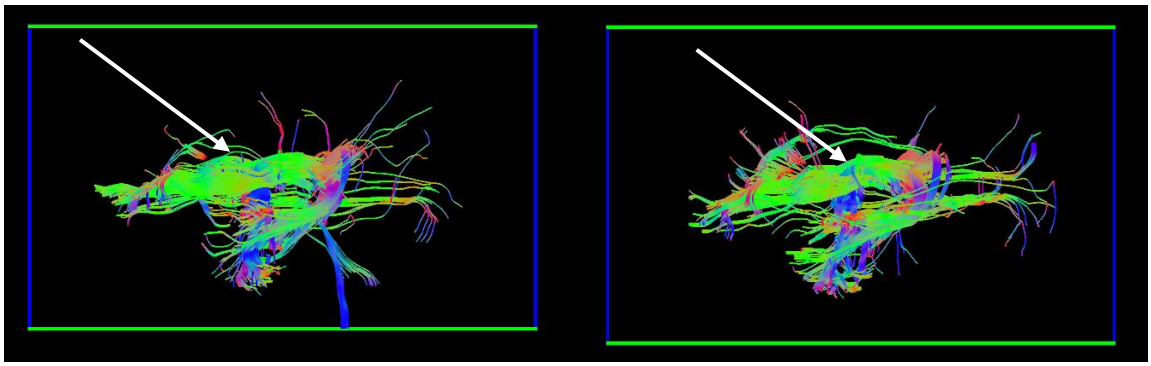

Figure 7.15 Fornix tract of a participant at Baseline (left) and 1-Month (right). The body of the tract is identified with the pink arrow, where it shows a visual reduction in the body of the tract. *FA at baseline and 1Month was 0.337 and 0.299 respectively. Dose to 0.1 cc of the hippocampus in this case was 2.1 Gy. Green fibres direction is anterior to posterior, blue fibres direction is superior to inferior and red fibre direction is right to left.*

7.4.4 Quality of Life

There was a trend toward reduction in global QoL score at 1 month with subsequent improvement at 3 and 6 months with mean scaled score of 66.39, 59.96, 62.75, and 66.67, respectively. Patients with reduced HVLT TR T-score at 1 month exhibited reduced global QoL scores compared to the group with retained T-score: mean scaled score of 67.36 (95% CI 61.99 – 72.73) vs 57.41, (95% CI 54.17 – 60.65) respectively. Detailed assessment of functional domains of the EORTC QLQ-C30 questionnaire demonstrated global reduction in QoL functional domains of physical, role, emotional, cognitive, and social at 1 month followed by recovery at 3 months. There was a reduction at 6 months again (Figure 7.16).

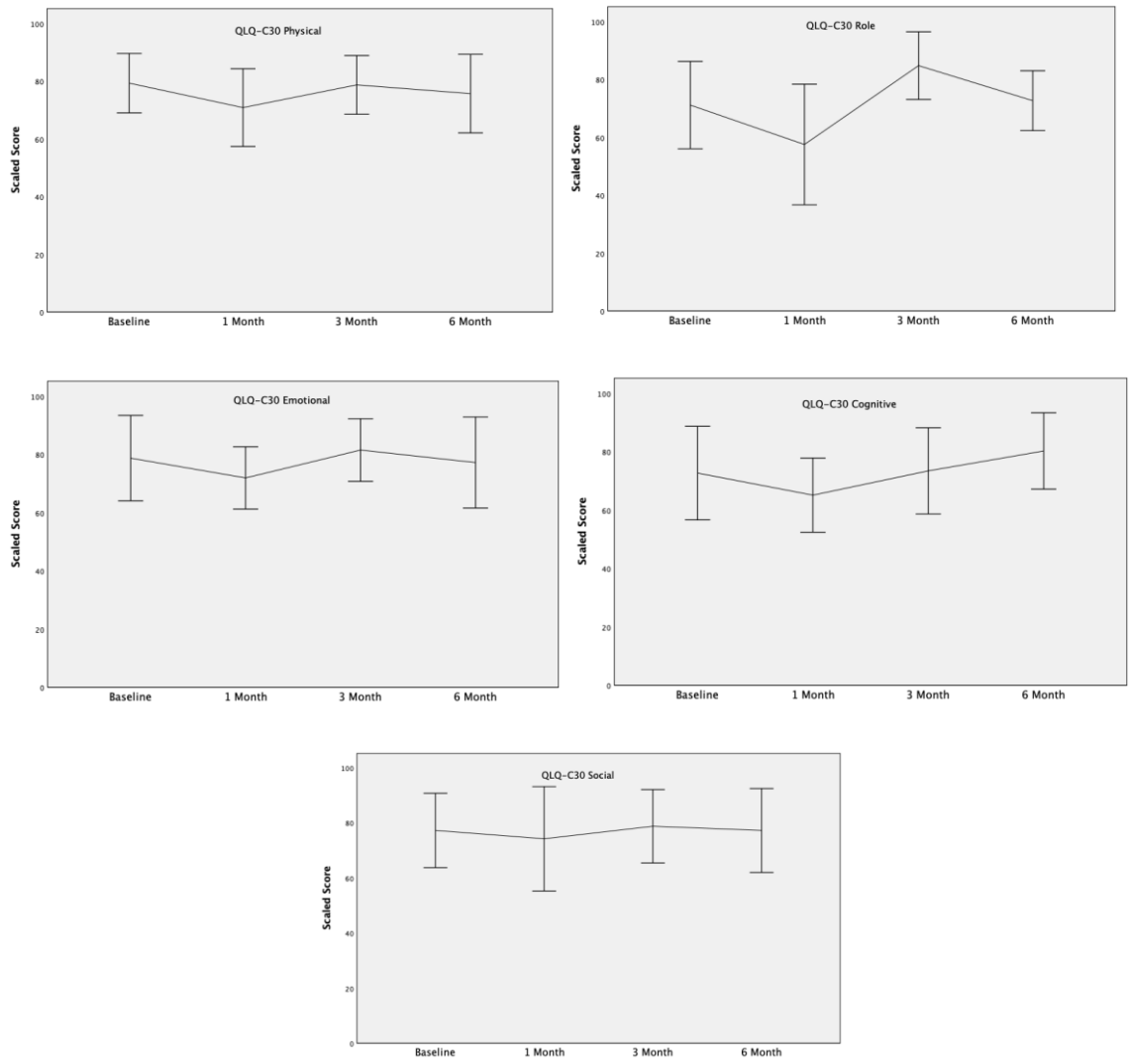

Figure 7.16 Mean and 95% Confidence interval of functional scales in EORT-QLQ C30 Questionnaire at Baseline, 1 month, 3 Month and 6 Month time points. *The 5 domains demonstrated in this figure are Physical, Role, Emotional, Cognitive and Social.*

Patients reported increase in fatigue, motor disturbance, communication difficulties and drowsiness at 1 month which resolved at 3months. There was a trend towards worsening fatigue and motor disturbance at 6-month time point.

7.5 Discussion

The proportion of patients completing 3 month NCF assessment, i.e., 58%, is consistent with the most recent published phase III randomised controlled trial in patients with BM undergoing SRS where 64% of randomised patients completed 3-month NCF tests which was the study's primary end point (Brown *et al*., 2016a). NCF impairment at 3 months was lower in our study, 33% patients demonstrated NCF decline, than that demonstrated in the most recent published literature which demonstrated NCF impairment in 60% of patients 3-months following SRS (Brown *et al*., 2016a). However, Chang *et al*. reported similar levels to our study, with 24% patients demonstrating worsening of NCF at 4 months following SRS (Chang *et al*., 2009). There are several potential confounding factors in this patient cohort such as age, heterogeneous patient population with a variety of primary malignancy diagnoses, patients at various stages of disease receiving a variety of treatment and steroids. Comparing the changes in NCF and MRI parameters as a percentage from baseline was an approach to partly control for these confounding factors.

The challenges of recruiting patients with BM to clinical trials have been described by the response assessment in Neuro-Oncology (RANO) group (Lin *et al*., 2013). Due to burden of extra cranial disease, toxicities of concurrent SACT, symptoms of intracranial disease, challenges of assessing intracranial response with RECIST criteria, and heterogeneity of BM, this cohort of patients remains a group of patients who are often excluded from SACT trials (Lin *et al*., 2013). Clinical trials that focus on patients with BM alone have their own challenges due to the important prognostic and tumour-related variables, that are partly dependent on their primary cancer (Lin *et al*., 2013).

We have demonstrated that patients had a decline in NCF scores of verbal memory and executive function domain at 1 month, followed by a period of recovery and most patients returning to baseline NCF scores at 6-month interval. Whilst we are aware from

published clinical trial data in fractionated brain radiotherapy, including whole brain radiotherapy, that long term NCF impairment is significant (Tsai *et al*., 2015), little research has been performed examining acute toxicity following SRS. This study suggests that transient NCF impairment, associated with reduced quality of life, is an important acute side effect from SRS. We also demonstrated that quality of life was lower in patients who had NCF impairment at 1 month. Functional domain of quality of life mirrored the pattern of change in NCF scores at 1, 3 and 6-month time points.

D0.1 cc of the composite hippocampus was associated with NCF reduction at 1 month in this study. This was not observed at 3- and 6-month time points. Median dose and D40 of the hippocampus did not demonstrate the same relationship. There was a negative correlation between the D0.1 cc of the hippocampus and percentage change in HVLT TR T-score. This suggests that sparing the hippocampus to lowest dose possible may be beneficial in reducing the magnitude of impaired NCF following SRS but may not have any long-term benefit. The radiobiology of single fraction SRS is poorly understood with limited available information on normal tissue complication probability model for the hippocampus; therefore, it is not clear which dose constraint should be utilised in clinical practice. D40 of the hippocampus has been studied in patients with low grade glioma undergoing fractionated radiotherapy. Gondi *et al*., predicted that D40 of >7.3 Gy is associated with NCF impairment post fractionated radiotherapy. however, when the model was tested actual rates of NCF impairment were much lower than the predicted model: 31.8% in the patient cohort vs 99% from predicted model (Jaspers *et al*., 2019). This remains undefined for SRS treatment. Based on this study, one can hypothesise that acute NCF impairments may be related to D0.1 cc dose and relate to acute damage to NCS within the hippocampi, this hippocampus may be a serial organ with an ability to repair. This dose constraint may be different for prediction of long term NCF impairment.

Participants who received >5 Gy to D0.1 cc of the Hippocampus demonstrated lower blood flow in the hippocampus, lower left hippocampal volume, lower Fornix FA, and lower concentration of Glx at 1 month. At 3-month interval, CBF and Fornix FA had returned to baseline, however there was reduction in metabolite concentration (NAA, choline, Glx, and creatine). There was only one patient at 3 months in the cohort that received >5 Gy.

Change in hippocampal volume is considered a late toxicity of radiotherapy in patients receiving fractionated radiotherapy (Seibert *et al*., 2017a). This has not been studied in patients undergoing SRS and it is possible that higher dose per fraction in SRS may have an earlier impact on hippocampal volume. The T1 weighted image demonstrated in this chapter of a participant who had a lower hippocampal volume at 1 and 3 months received 7.7 Gy to 0.1 cc of the left hippocampus. Multivariate analysis did not demonstrate a discriminatory imaging biomarker for NCF impairment or the hippocampus dose, probably because of the small number of participants.

There was a greater reduction in CBF of bilateral hippocampus and grey matter at 1 month with return to baseline at 3 months. This is consistent with the hypothesis that vascular endothelial damage may occur hours following radiotherapy, is considered to be an acute effect of radiotherapy (Makale *et al*., 2017, Greene-Schloesser *et al*., 2012). Although age is an important confounding factor in looking at CBF, percentage reduction in CBF in the hippocampus and grey matter was independent of age of the participant.

Changes in some MR spectroscopy markers signify inflammation, e.g., Glx and myo-inositol, whilst changes in NAA, choline and creatine are considered markers of neuronal health (Allaili *et al*., 2015, Caserta *et al*., 2008). Therefore, these can be decreased in various pathophysiology including demyelination, gliosis, white matter necrosis and vascular abnormalities (Greene-Schloesser *et al*., 2012). MRS may detect early changes before diffusion metrics are affected. Usually, metabolites are presented as a ratio to choline and/ or creatine. In this patient cohort, there was a reduction in both of these metabolites, as there was in the other metabolites, therefore, these results may represent changes of a greater magnitude (Gussew *et al*., 2012). Lactate is regarded clinically as a marker of necrosis and inflammation. In this patient cohort, there was a general increase in lactate levels following SRS, but there was no correlation found with the changed in HVLT TR T-scores. Potential neuroinflammatory component form the MRS could potentially be assessed with translocator protein PET in a future study.

Transient demyelination may happen within weeks of radiotherapy, which may account for the transient reduction in FA values of the Fornix in this patient cohort (Greene-Schloesser *et al*., 2012). Long term white matter damage can occur, months and years

following radiotherapy, and this has been studied in patients undergoing fractionated radiotherapy. There was a recovery of FA values at 3 months, suggesting that changes seen at 1 month were more consistent with acute transient demyelination.

In patients with a limited prognosis, it is critically important to minimise acute toxicities of SRS in order to preserve quality of life in this patient cohort. Minimising D0.1 cc of the hippocampus, may be important and an important OAR to consider in SRS planning. We have demonstrated in Chapter 3, that this is possible to do so that beam shaping can allow sparing of the hippocampus to achieve the minimum dose possible without compromising the PTV which may help reduce acute toxicity of SRS and preserve QoL in a patient population with limited prognosis.

This study has several important limitations. There were a small number of patients at baseline and 58% patients completed 3 months assessment. It was not possible to control for primary cancer site as suggested by the RANO group. Numbers of patients in the translational MRI study are also small and therefore statistical significance of these data and observations are limited. As other published trials are affected by confounding factors, so was this study, however we minimised this in the study. As it is challenging to conduct studies with large number of patients in this cohort, it may be possible to combine the data from other trials who have utilised standardised NCF scores as recommended by RANO group (Lin *et al*., 2013), to conduct NTCP modelling of the hippocampus in patients undergoing SRS.

7.6 Conclusion

Dose to 0.1 cc of the hippocampus was associated with reduced NCF score at 1 month, and this correlated with reduced quality of life in the patients in our study. Proportion of patients demonstrating reduction in NCF at 3 months was lower than expected, which is encouraging. These results suggest that NCF impairment may be considered an acute toxicity of SRS. Patients with low NCF scores demonstrated poorer global quality of life and as this cohort of patients have a relatively low overall median survival of 10-12 months this is clearly an important observation. Supportive measures such as clinical

psychology support and memory may play a key role in enhancing QoL of this patient group.

Chapter 8 – Multi-Parametric Assessment of Brain Metastases, response following SRS and Effect of Radiation on the surrounding normal brain tissue

8.1 Introduction

The majority of BM are diagnosed radiologically. NICE recommends performing standard structural MRI which is defined as T2- weighted, FLAIR, DWI series and T1-weighted pre and post contrast volume unless MRI is contraindicated (NICE, 2018). There are radiological features that are considered to differentiate between primary brain tumour, other conditions such as meningioma and benign brain conditions and BM. Usually histological confirmation after MRI diagnosis of metastases is not deemed necessary in the context of known malignancy, unless there has been a long disease-free interval with absent systemic metastatic disease or if BM are the only site of disease in cases of malignancy of unknown origin (Gerrard and Franks, 2004, Takei *et al*., 2016). Histological confirmation poses many challenges as patients may not be fit enough to undergo neurosurgery or have metastases in an accessible site (Nayak *et al*., 2012, Ali *et al*., 2021). Main differential diagnoses of BM include primary brain tumour, lymphoma, and abscess.

Therefore, understanding of the microstructure of metastases, to better enable radiological diagnosis and characterisation of metastases, and its implications for choosing the most appropriate treatment modality is of significant clinical and research interest. Key radiological features which have been studied in patients with BM include:

- **Presence of oedema** – Vasogenic oedema surrounding the metastases can be substantial and is unrelated to the size of the lesion when compared to high grade glioma (Chen *et al*., 2012, Hakyemez *et al*., 2010). Although, some metastases may exhibit little or no oedema (Potts *et al*., 1980). This is important as screening for BM may detect early small metastases without presence of oedema. Screening for BM is part of standard staging in patients undergoing radical treatment for stage II and III non-small cell lung carcinoma and patients with at least stage IIB melanoma (NICE, 2019, NICE, 2015).

- **Border of the tumour** – BM largely have a well-defined border which displaces the surrounding brain tissue, which is in contrast to the diffuse infiltration of primary brain tumours (Fabian and Walker, 2019).
- **MR Spectroscopy** of the tumour – Whilst MR spectroscopy can reliably differentiate between benign and malignant processes this technique hasn't been able to differentiate between primary and secondary malignant processes in the brain reliably (Bulakbasi *et al*., 2003, Hollingworth *et al*., 2006). One study compared spectroscopic measurement of metabolites of the peritumoural T2 regions and reported significantly higher proportion of Cho/Cr and Cho/NAA ratios in patients with primary brain tumour compared to BM (Server *et al*., 2010).
- **Diffusion weighted imaging and diffusion tensor imaging** – BM and high grade glioma demonstrate restricted diffusion which is demonstrated as lower values of apparent diffusion coefficient (ADC) (Al-Okaili *et al*., 2006). Diffusion imaging of the peritumoural region may be able to differentiate between high grade glioma and BM (Lee *et al*., 2011). However, some studies have reported no difference between the two groups (Bulakasi, 2009).
- **Cerebral Blood Flow (CBF)** – CBF measurement via arterial spin labelling (ASL) has been utilised in differentiating between primary glioma and BM. High grade glioma tends to exhibit higher CBF in the tumour and peritumoural oedema compared to BM (Solozhentseva *et al*., 2022). Low grade glioma tend to show lower CBF values compared to HGG and BM (Jain, 2011). Whilst it may be challenging to differentiate BM from HGG based on perfusion alone, and other characteristics mentioned above will have to be taken into account; perfusion imaging can differentiate BM from other diagnostic entities such as cerebral abscess, as BM tend to have higher blood flow compared to benign lesions (Hakyemez *et al*., 2006, Hakyemez *et al*., 2010).

A study demonstrated that combination of diffusion (FA and ADC) and blood flow metrics (CBF and cerebral blood volume) increased the sensitivity and specificity of diagnosing high grade glioma, low grade glioma and BM (Durmo *et al*., 2018). Another group investigated combining DWI and perfusion imaging, which did not find a statistically significant difference between ADC and CBF measure of HGG or metastases (Calli *et al*., 2006).

Imaging following the treatment also poses a challenge of differentiating between true and pseudoprogression as increasing size of metastases may not indicate tumour progression (Pope, 2018, Galldiks *et al*., 2020). A small study of 6 patients following SRS for BM demonstrated that low ADC <1000 x 10^{-6} mm^2/s, high relative cerebral blood volume ratio >2.1 and high choline: creatine ratio >1.8 was suggested of recurrence (Sawlani *et al*., 2019). In this study MRI was performed at varying intervals of 7-29 weeks post treatment, therefore it is difficult to compare changes that may occur during the first few weeks following SRS. All the patients included had demonstrated enlargement of the treated metastases i.e., patients whose metastases reduced in size following SRS were not included for comparison. Another study reported reduction in median relative ADC at 1 week and 1 month following SRS and WBRT in responders compared to non-responders (Jakubovic *et al*., 2016).

CBF has been shown to vary during treatment for BM. CBF in the BM was reduced more than that of grey matter during radiotherapy. Reduction of 24.61-33.75% was reported in the CBF during radiotherapy in this study, however, correlation with radiotherapy dose was not identified and response to treatment was not examined. (Hou *et al*., 2022). Another study demonstrated relative reduction in cerebral blood volume at 1 month post radiotherapy and this was predictive of progression (Jakubovic *et al*., 2014). In contrast, a study of 26 patients demonstrated an early increase in perfusion at 4-8 weeks following radiotherapy was associated with an increased risk of tumour progression (Almeida-Freitas *et al*., 2014).

BOLD imaging, more commonly referred as fMRI, has been utilised in studying brain connectivity (Damoiseaux *et al*., 2006). Deoxyhaemoglobin is paramagnetic, therefore induces a signal loss in T2* weighted images and BOLD contrast (Posner and Raichle, 1994). BOLD signal in the tumour cannot reliably detect oxygenation or hypoxia as it is dependent on presence of haemorrhage, blood flow, blood volume, and vasculature of the lesion (O'Connor *et al*., 2019). Task based BOLD imaging has been recognised in surgical planning in mapping the functional motor and language areas (Bogomolny *et al*., 2004, Kamran *et al*., 2014). In contrast, resting state fMRI (rs fMRI) identifies default mode network which identifies areas of brain activity at rest and may play a role in memory retrieval (Allan *et al*., 2015). Variation in rs fMRI has been described in

Alzheimer's disease and epilepsy (Zhang *et al*., 2020b, Hu *et al*., 2017). However, such changes in of rs fMRI has not been studied following radiotherapy.

Vascular, Extracellular and Restricted Diffusion Cytometry in Tumours (VERDICT) is a non-invasive MRI method that estimates and maps microstructural features of cancerous tissue using diffusion MRI. This imaging technique was initially developed by the imaging group in University College London to study prostate cancer and correlate VERDICT parameters with histology (Panagiotaki *et al*., 2014). The group showed that this method was reliable and reproducible in correlating cell radii and intracellular water fraction with Gleason score (Bonet-Carne *et al*., 2019). VERDICT has been used in imaging animal models and human with brain tumour. In animal models, this imaging sequence has shown to predict response early with reduction in cell radii in high grade glioma. However, this was not reliable in low grade glioma models (Roberts *et al*., 2020). This has not been used in assessing response following radiotherapy in human.

Changes after fractionated radiotherapy for high grade glioma has been shown with doses as low as 10 Gy resulting in reduced FA and increased MD in the white matter at 4-6 months and 9-11 months following treatment (Connor *et al*., 2016). Animal models have also demonstrated significantly reduced FA at 4 and 40 weeks in the external capsule following radiation, which correlated with demyelination, axonal degeneration, and coagulative necrosis in the white matter (Wang *et al*., 2013).

The aim of this chapter is to study changes in blood flow of the metastases and its impact on treatment response. We also utilised this opportunity for patients to undergo MRI scans in the novel Connectome scanner specifically to study detailed DTI analysis of the peritumoural tracts and feasibility of VERDICT sequence in patients with BM.

8.2 Hypothesis

Main hypothesis for this chapter is that with additional information from MRI regarding perfusion and microstructure diffusion imaging, it may be possible to identify non-responders early.

8.3 Methods

Four modalities of MRI were used to assess the response of metastases to treatment and changes in the tissue microstructure: Standard T1 FSPGR, T2 FLAIR, ASL, and VERDICT. Resting state BOLD and multi-shell DTI (CHARMED) was performed to test changes in the surrounding brain regions. All MRI scans were performed at baseline prior to receiving SRS and 1-month and 3-month following treatment. MRI parameters for these sequences have been defined in Table 4.10. MRI analysis, process of registration and pre-processing has been described in Chapter 4. ROI masks were created to delineate the region of metastases and oedema using the T1 FSPGR & T2 TSE and T2 FLAIR image and co-registered to ASL, VERDICT, BOLD and DTI images to obtain the mathematical value using FSL software (https://fsl.fmrib.ox.ac.uk/fsl/fslwiki/). Figure 8.1 illustrates and example of delineation of metastases and oedema.

The RANO group has described a method of assessing response of BM using bidimensional method (RANO-BM). Description of the response is summarised in Table 8.1 (Lin *et al*., 2015). The non-enhanced images from the CUBRIC scanner were reviewed in conjunction with enhanced imaging to allow for tumour segmentation and RANO scoring.

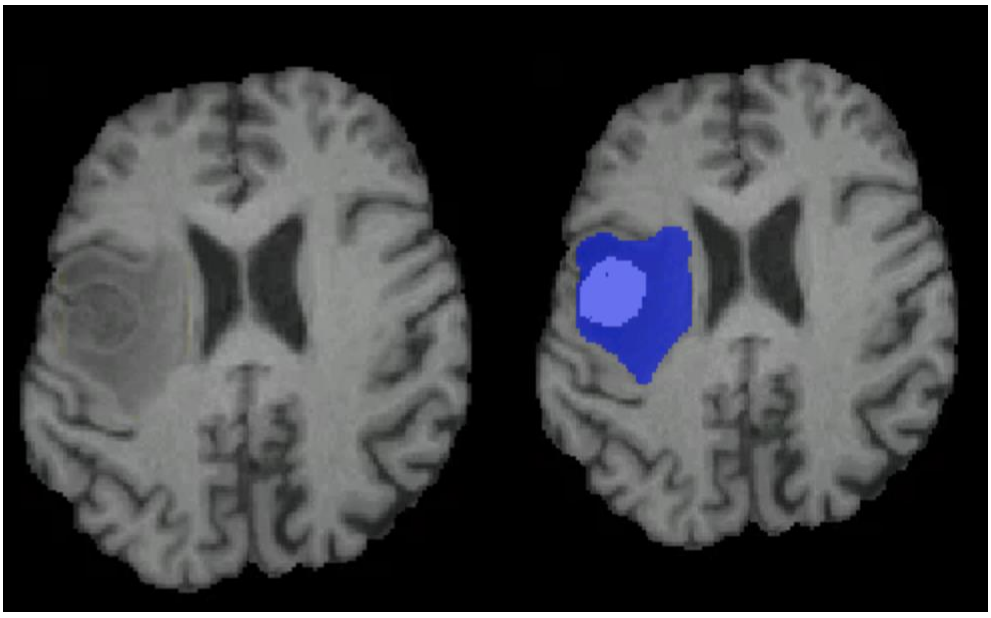

Figure 8.1 T1 FSPGR sequence in axial slice demonstrating delineation of metastases mask (light blue) and oedema mask (dark blue). Image on the right is for reference of the masks created.

Complete response	**Disappearance of all CNS target lesions sustained for at least 4 weeks; with no new lesions, no use of corticosteroids, and patient is stable or improved clinically.**
Partial response	At least a 30% decrease in the sum longest diameter of CNS target lesions, taking as reference the baseline sum longest diameter sustained for at least 4 weeks; no new lesions; stable to decreased corticosteroid dose; stable or improved clinically.
Progressive disease	At least a 20% increase in the sum longest diameter of CNS target lesions, taking as reference the smallest sum on study (this includes the baseline sum if that is the smallest on study). In addition to the relative increase of 20%, at least one lesion must increase by an absolute value of 5 mm or more to be considered progression.
Stable disease	Neither sufficient shrinkage to qualify for partial response nor sufficient increase to qualify for progressive disease, taking as reference the smallest sum longest diameter while on study.

Table 8.1 Summary of RANO-BM criteria for response assessment in patients with brain metastases.

8.3.1 Cerebral Blood Flow

Method and MRI sequence of calculating CBF has been described in section 4.4.3. It has been illustrated in chapter 6 that age can have a major impact on CBF measurements, therefore, to control for age, CBF was calculated as ratio to that of grey matter.

8.3.2 Blood Oxygenation Level Dependent

BOLD signal was measured using rs fMRI sequence. The raw images were pre-processed using the FMRIB Software Library (FSL) and Analysis of Functional NeuroImages Software (AFNI) (Jenkinson *et al*., 2012a). Multivariate exploratory linear optimised decomposition into independent components (MELODIC) is a tool within FSL that was used to create the BOLD maps. MELODIC independent component analysis is a model free method of analysing rs fMRI (Beckmann *et al*., 2005). The advantage of using this method is that it

creates model free spatial maps and therefore is able to identify true BOLD signal at rest. The disadvantage is that it also identifies noise and is sensitive to motion and cardiac signals, therefore it requires visual analysis of the images to exclude spatial maps that do not represent true signal. The signal in a particular region is given as an arbitrary unit which is relative to the background brain tissue (Beckmann *et al*., 2005). The main interest in BOLD signal is change following SRS, therefore baseline BOLD data is not presented.

8.3.3 Multi-Shell Diffusion Tensor Imaging

CHARMED MRI sequence was performed on the Connectome MRI scanner at CUBRIC in Cardiff University (Assaf and Basser, 2005). Raw DWI data was pre-processed using the methods described in section 4.4.6. Peritumoural tracts were identified using whole brain tractography and fused structural images with metastases delineated as a ROI. Explore DTI version 4.8.6 software was used to perform tractography and extract the diffusion metrics. Four diffusion scalar measures were measured – FA, apparent fibre density (AFD), RD and MD (Leemans *et al*., 2009). CHARMED sequence allows estimation of nerve fibre density

8.3.4 VERDICT

VERDICT sequence was performed on the Connectome MRI scanner at CUBRIC. The raw images were pre-processed as described in section 4.4.6. The eddy corrected images were analysed using the accelerated microstructure imaging via convex optimisation (AMICO) method (Daducci *et al*., 2015, Bonet-Carne *et al*., 2019). This method has been developed by Prof Alexander's group in University College London for use in prostate cancer MRI and has been developed to fit the VERDICT parameters of intracellular fraction, vascular faction, extra-cellular extra-vascular fraction, and cell radii in the brain. This method has shown high levels of repeatability with reduced processing time and more accurate in estimating parameters than other version of VERDICT data processing and has also been used in analysing primary brain tumours (Bonet-Carne *et al*., 2019). This gives estimation of the following parameters:

- Intracellular Space (*f*IC)

- Vascular Space (*f*VASC)
- Extracellular, Extravascular Space (*f*EES)
- Cell Radius

8.3.5 Statistical Analysis

Statistical Analysis was performed using mathematical analytical software programme Matlab Statistics and Machine Learning Toolbox Matlab 2015a and SPSS version 28.0. Mann-Whitney U Test was performed to test the statistical significance. A statistical significance of a p-value <0.05 was used. As the group of patients was divided into two groups, it was not possible to conduct Bonferroni's correction for repeated measures. Correlation analysis was conducted using Spearman's correlation.

8.4 Results

MRI data of twenty-six metastases in twenty patients who had MRI scans at CUBRIC were included in this chapter. Demographics for these patients has been described in Table 5.3. Of the twenty-six metastases, six metastases were thought to have shown evidence of at least 30% growth radiologically and clinically with increasing dose of steroids as per RANO-BM criteria (Table 8.2). Three of these were surgically resected and histological diagnosis of malignancy was confirmed. The remaining three patients died at 3-, 4-, and 5-months following SRS, all of which were neurological deaths, therefore it is likely that increase in size identified at the initial post treatment MRI was true progression.

Response	n. (%)
Progressive Disease	6 (23)
Stable Disease	8 (31)
Partial Response	9 (35)
Complete Response	3 (11)

Table 8.2 Summary of response to SRS treatment according to RANO-BM of all 26 metastases.

8.4.1 Baseline MRI Characteristics and Correlation with Clinical Symptoms

Volume of metastases and oedema were highly correlated (r = 0.717, p-value <0.001). Patients who had neurological symptoms demonstrated significantly higher mean oedema volume, compared to the mean metastases volume. Whereas the mean oedema and metastases volume were both significantly higher in patient who had seizures compared to those who did not have seizures (Table 8.3 & Figure 8.2).

Volume (mm^3)	Neurological Symptoms		p-value
	Present	**Absent**	
Metastases	3902 (1,756-6,048)	3,343 (1,156 -5,530)	0.563
Oedema	26,605 (13,308 -39,892)	4,398 (0-9,903)	<0.001*

Volume (mm^3)	Seizure Activity		p-value
	Present	**Absent**	
Metastases	5,708 (4,874-6,542)	2,715 (862-4,568)	<0.001*
Oedema	35,349 (24,910-45,788)	12,832 (15,77-24,087)	<0.001*

Table 8.3 Mean and 95% confidence interval of the metastases and oedema volume in patients who had neurological symptoms and seizures. **Group which demonstrated statistical significance*

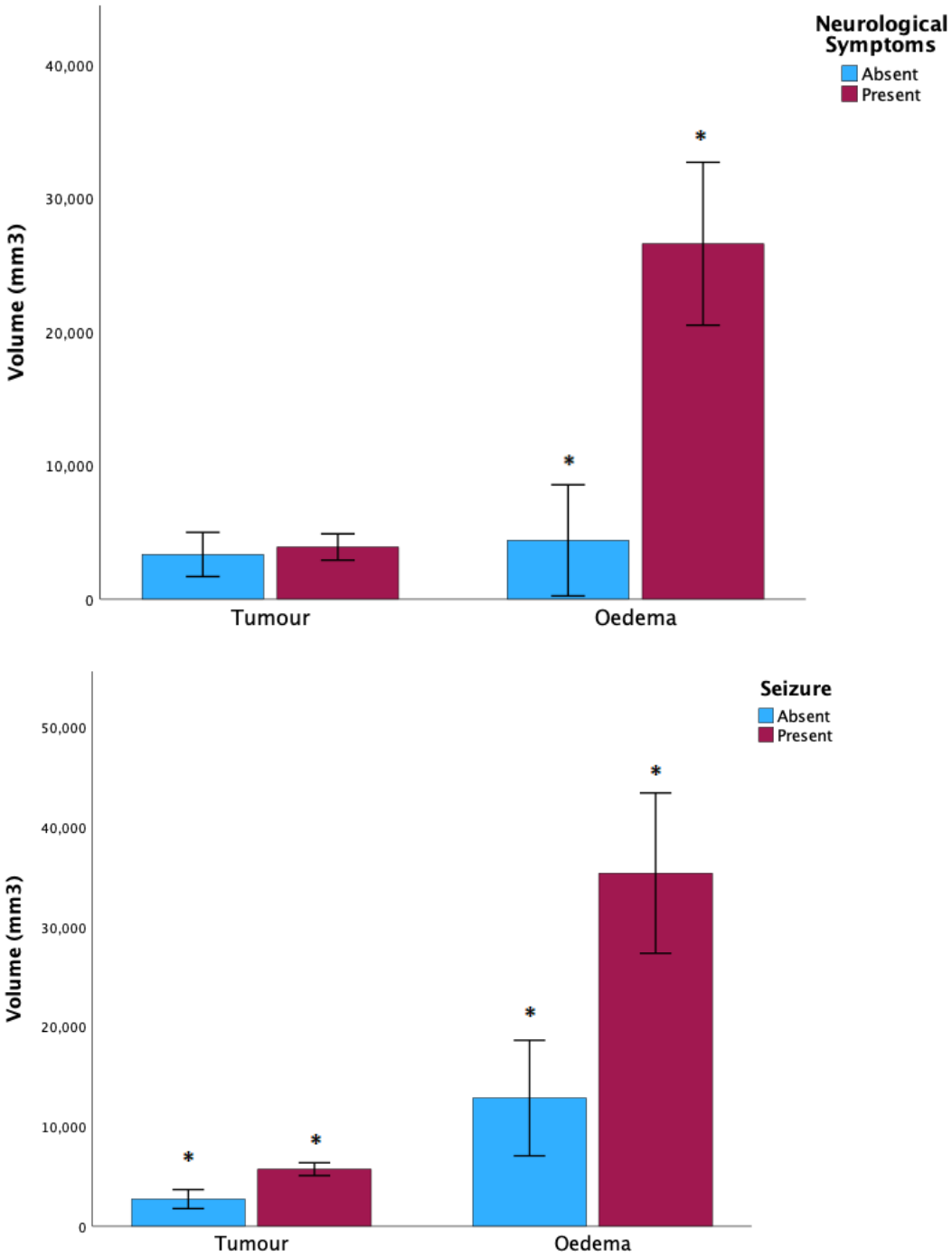

Figure 8.2 Bar Charts illustrating metastases and oedema volume in patients who demonstrated neurological symptoms and seizures. *Error bars represent 95% confidence interval. * represents statistically signigicant results.*

8.4.2 Effect of SRS on peritumoural regions

8.4.2.1 Peri-tumoural Tracts

Analysis of multi-shell diffusion tensor imaging using the CHARMED MRI sequence, performed on the Connectome MRI scanner, was used to demonstrate peritumoural

tracts. The relevant peritumoural tracts identified using whole brain tractography related to each of the metastases are summarised in Table 8.4.

Tract	Laterality	n.
Cingulum	Right	2
Cingulum	Left	3
Corticospinal	Right	4
Corticospinal	Left	3
Superior Longitudinal Fasciculus	Right	3
Superior Longitudinal Fasciculus	Left	2
Inferior Fronto-Occipital Fasciculus	Left	3
Arcuate Fasciculus	Right	2
Uncinate Fasciculus	Left	2
Inferior Longitudinal Fasciculus	Left	1
Anterior Thalamic Radiation	Left	1

Table 8.4 Names and laterality of the peritumoural tracts identified by whole brain tracking for each brain metastases.

There was a statistically significant difference in the diffusion scalar measurements of the ipsilateral tracts compared to the same tract in the contralateral cerebral hemisphere at baseline. The ipsilateral tracts demonstrated statistically significant lower mean FA, AFD and higher values of RD and MD compared with the contralateral tracts (Figure 8.3, Table 8.5). The mean difference in the four DTI scalar measurements did not differ significantly according to the present of neurological symptoms or presence seizures. There was no correlation between changes in diffusion metrics and tumour and oedema volume (r=0.147, r=-0.143 respectively, p-value >0.05).

	Ipsilateral Tracts	Contralateral Tracts	p-value
Fractional Anisotropy	0.39 (0.36-0.42)	0.43 (0.41-0.45)	<0.001
Apparent Fibre Density	0.21 (0.20-0.23)	0.23 (0.22-0.25)	<0.001
Radial Diffusivity	6.8×10^{-4} ($6.27\text{-}7.22 \times 10^{-4}$)	5.9×10^{-4} ($5.69\text{-}6.20 \times 10^{-4}$)	<0.001
Mean Diffusivity	8.65×10^{-4} ($8.26\text{-}9.03 \times 10^{-4}$)	7.71×10^{-4} ($7.10\text{-}8.34 \times 10^{-4}$)	<0.001

Table 8.5 Mean and Confidence Interval of the four diffusion scalar metrics comparing the ipsilateral and contralateral side.

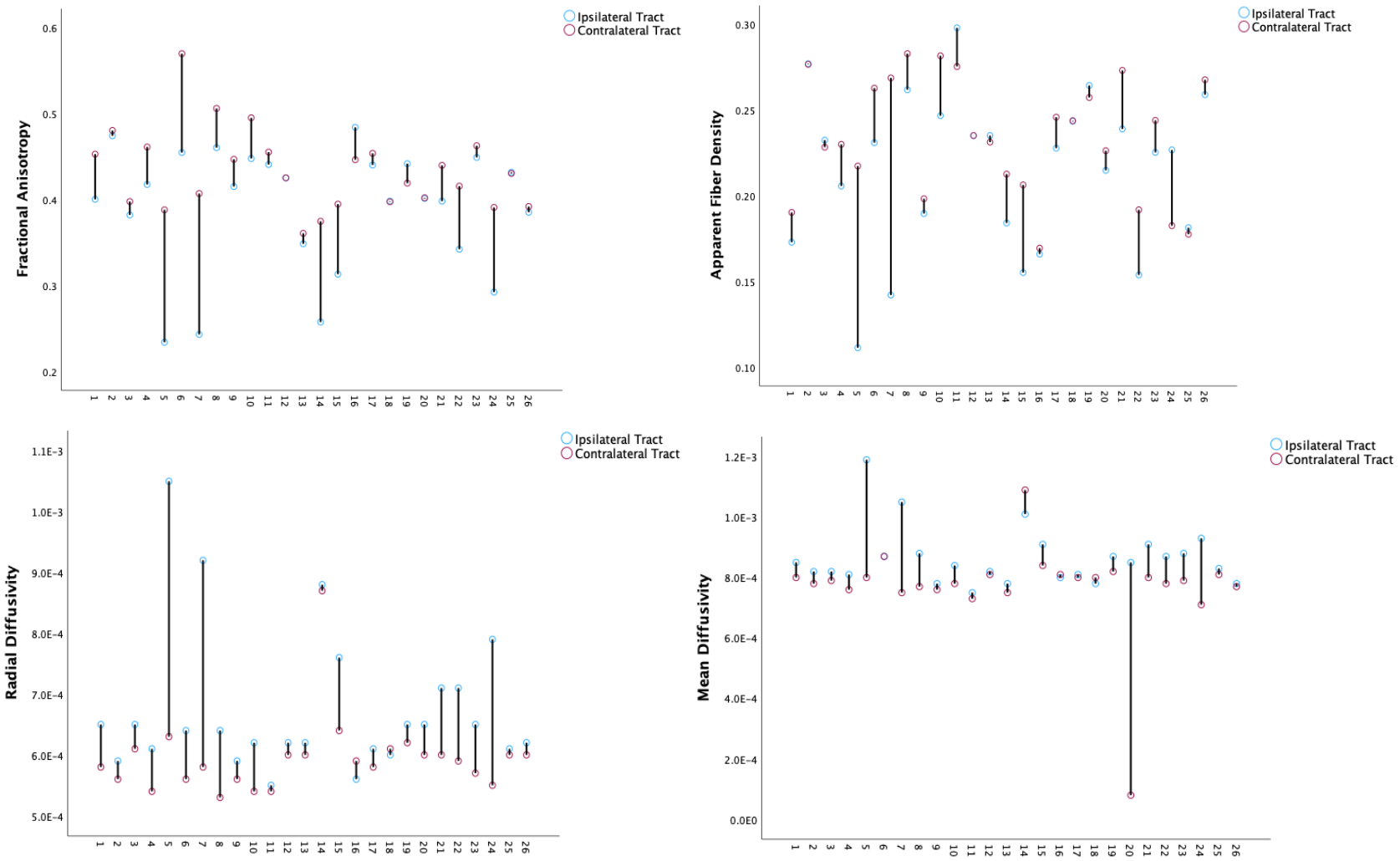

Figure 8.3 Scalar diffusion metric of each metastasis: Fractional Anisotropy, Apparent Fibre Density, Radial Diffusivity and Mean Diffusivity of ipsilateral and contralateral tract with respect to the metastases. *Each data point refers to a metastasis in the brain.*

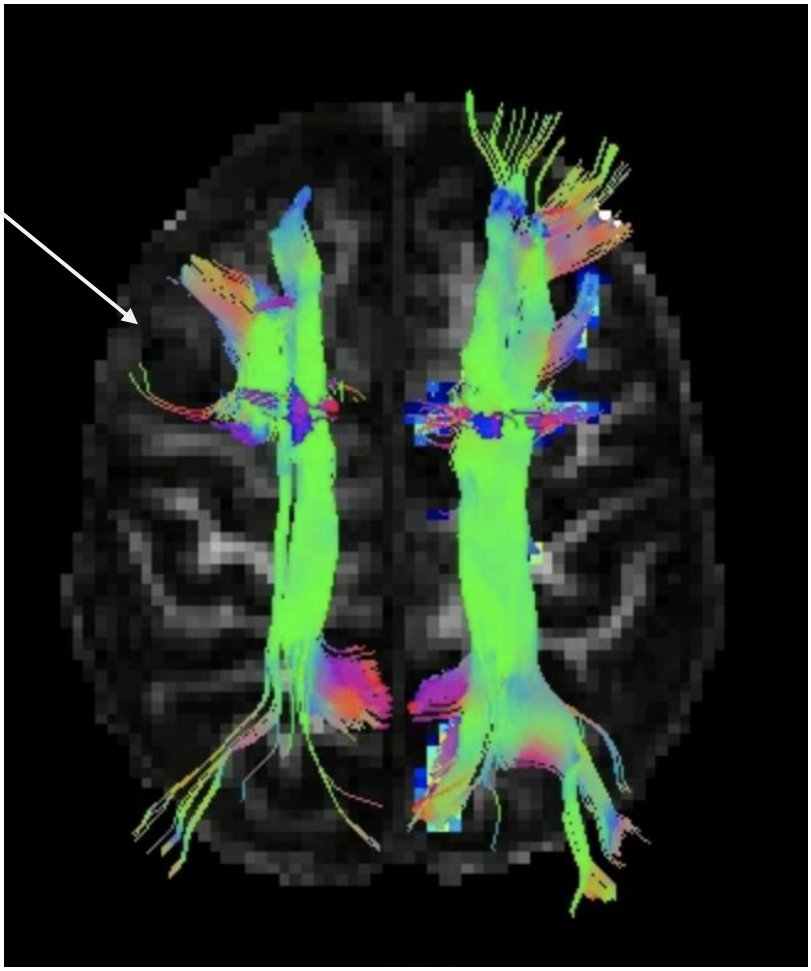

Figure 8.4 Superior Longitudinal Fasciculus Tract demonstrated on axial slice. Location of metastases is identified via a white arrow. *This imaging is of a 67 year male with renal cell carcinoma who was on concurrent immunotherapy. The tracts are colour coded in the direction of orientation: Green – anterior-posterior; Blue – Superior-Inferior; Red – Right-left.*

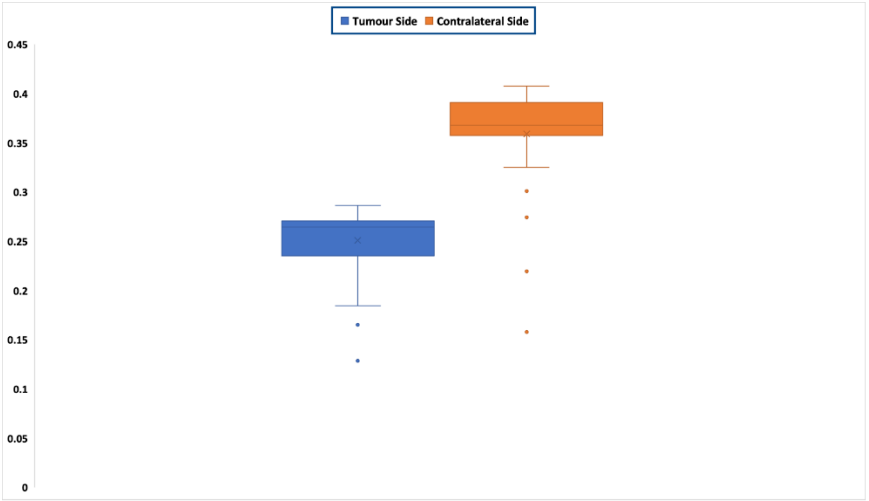

Figure 8.5 Box Plot demonstrating difference in fractional anisotropy along the tracts demonstrated in Figure 8.4.

FA positively correlated with apparent fibre density (AFD) and negatively correlated with MD and RD (data not shown) therefore results for FA has been demonstrated for the tract analysis going forward.

Figure 8.4 demonstrates the superior longitudinal fasciculus tract bilaterally for an example patient. On the right side, which was the side of metastases, the tract appears to be pushed medially whereas on the contralateral side the tract appears to be penetrating to the surrounding brain tissue. Figure 8.5 demonstrates the difference in measurement of FA along the length of the tract in anterior-posterior direction for the same patient. FA levels are reduced at each point along the length of the tract.

There was no statistically significant difference in the mean FA, AFD, RD and MD of the ipsilateral tract pre and post SRS (data not shown). Therefore, to study post SRS changes, I explored changes in FA along the nerve fibre tracts (Figures 8.6-8.9). First example is demonstrated in Figure 8.6 & 8.7 of a patient who had a complete response to SRS at their 3-month scan. This patient has a right sided metastasis in the right parietal lobe and the peritumoural tract was the superior longitudinal fasciculus. Figure 8.6 demonstrates that on the ipsilateral side of the metastasis, the nerve fires are displaced by the metastasis, however on the contralateral side the tract has penetrating fibres as expected. At one month, there is evidence of recovery with increasing measurement of FA (Figure 8.7A), followed by reduction at 3 months again in vicinity of the tumour relating to the anterior segment of the tract.

The second example (Figure 8.8 and 8.9) demonstrated is of a patient whose metastases showed conventional radiological evidence of increase in size following treatment and increased oedema and underwent surgical resection of the metastasis which confirmed presence of metastatic cancer. The arcuate fasciculus on the ipsilateral side demonstrated reduced penetration and distortion and tract density which is reflected in lower FA values in Figure 8.9 in vicinity of the BM, relating to the anterior segment of the tract. On the ipsilateral side, FA showed a generalised reduction at 1- and 3- months and a more marked reduction at the 1- and 3-month time point in vicinity of the tumour (Figure 8.9A). Whereas

there was no difference in the tract visualisation or FA values at 1 and 3 months on the contralateral side.

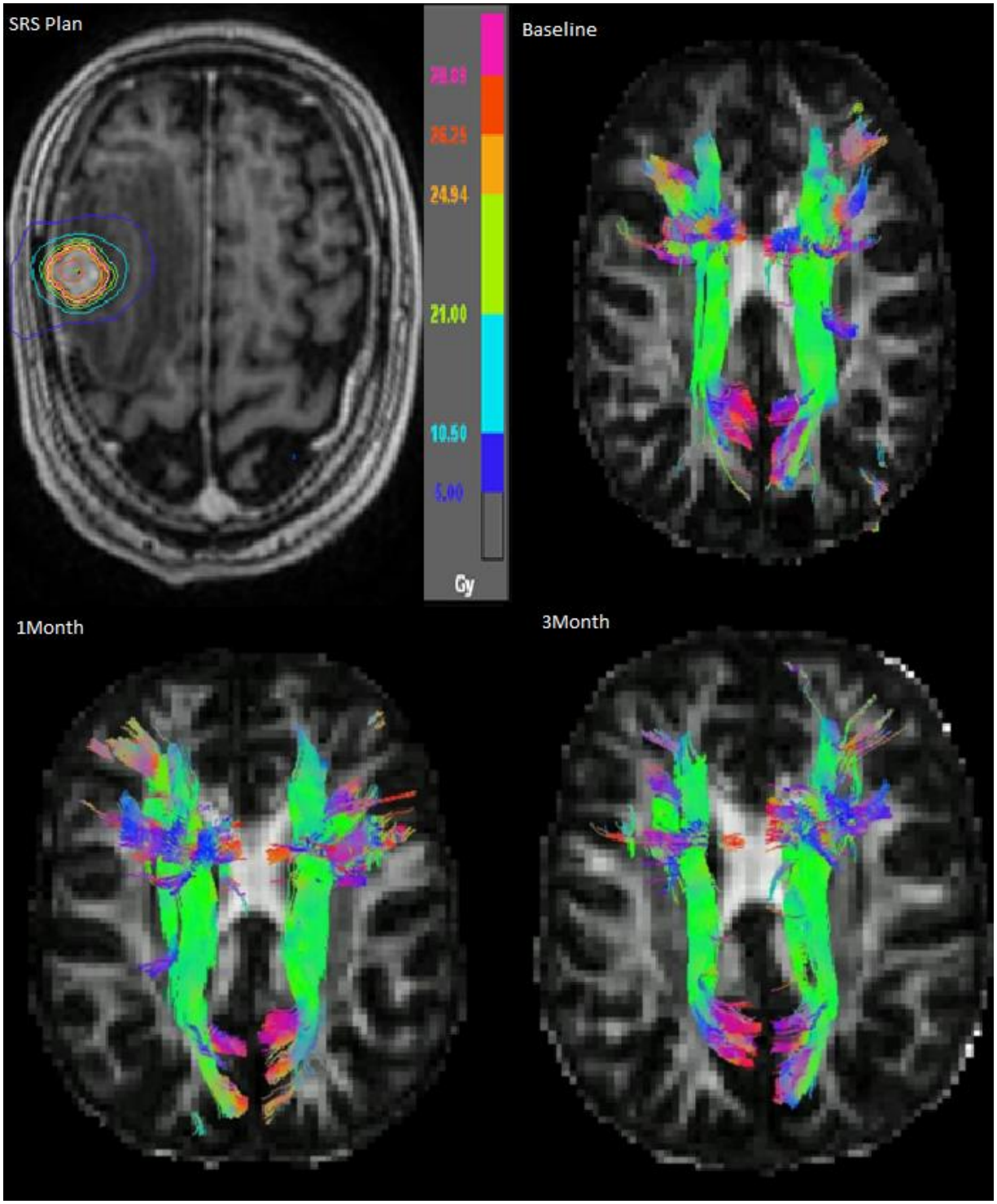

Figure 8.6 SRS Plan and Changes in the Superior Longitudinal Fasciculus fibre tract as baseline (before SRS) and at 1-Month and 3-Month following SRS. *The images are of a 67 year old male with renal cell carcinoma receiving immunotherapy. The tracts are colour coded in the direction of orientation: Green – anterior-posterior; Blue – Superior-Inferior; Red – Right-left.*

A

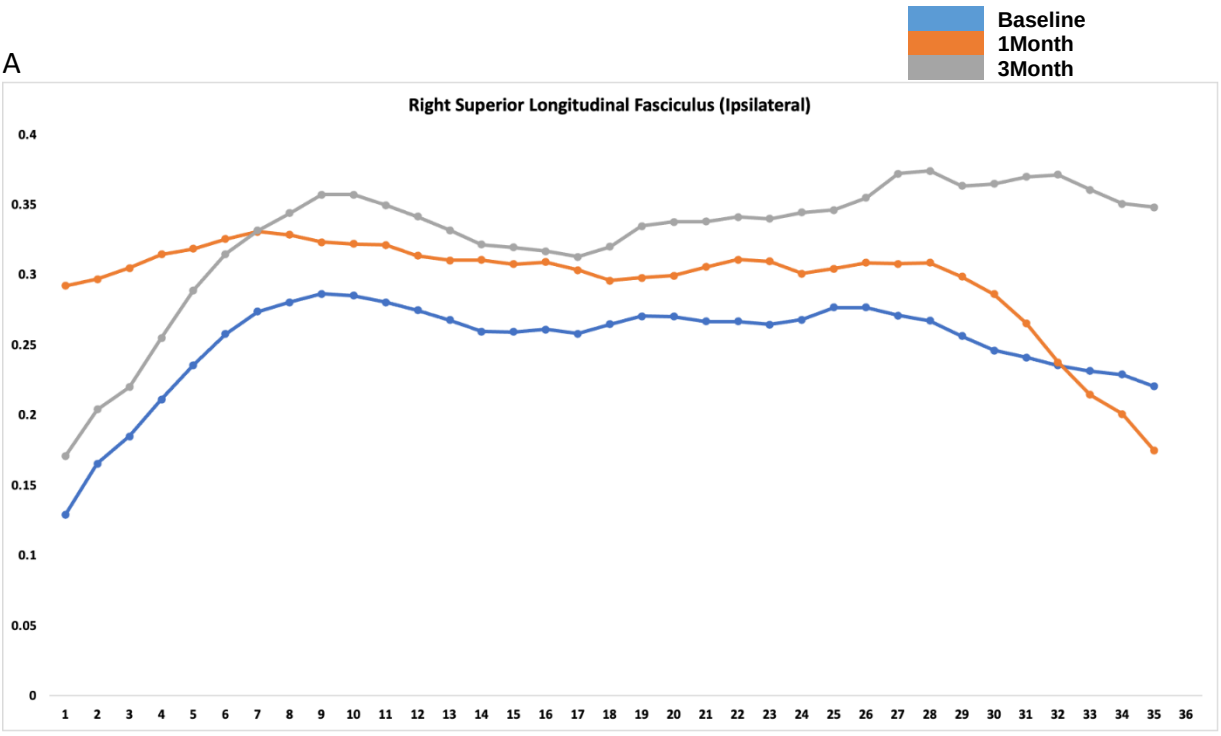

B

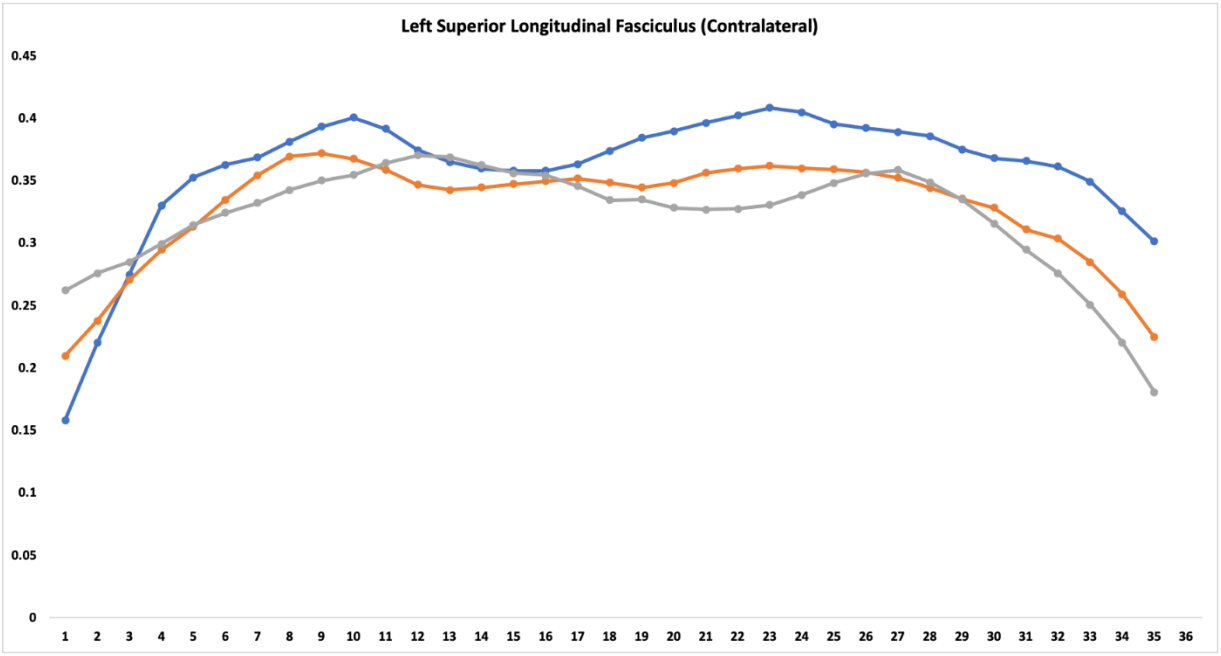

Figure 8.7 Line graph demonstrating FA values at baseline, 1 month and 3 month of bilateral superior longitudinal fasciculus tracts demonstrated in Figure 8.6. *A – Ipsilateral tract to the metastases shows increased FA at 1- and 3- months along the tract. B – Contralateral tract to the metastases shows increased FA at 1- and 3- months along the tract.*

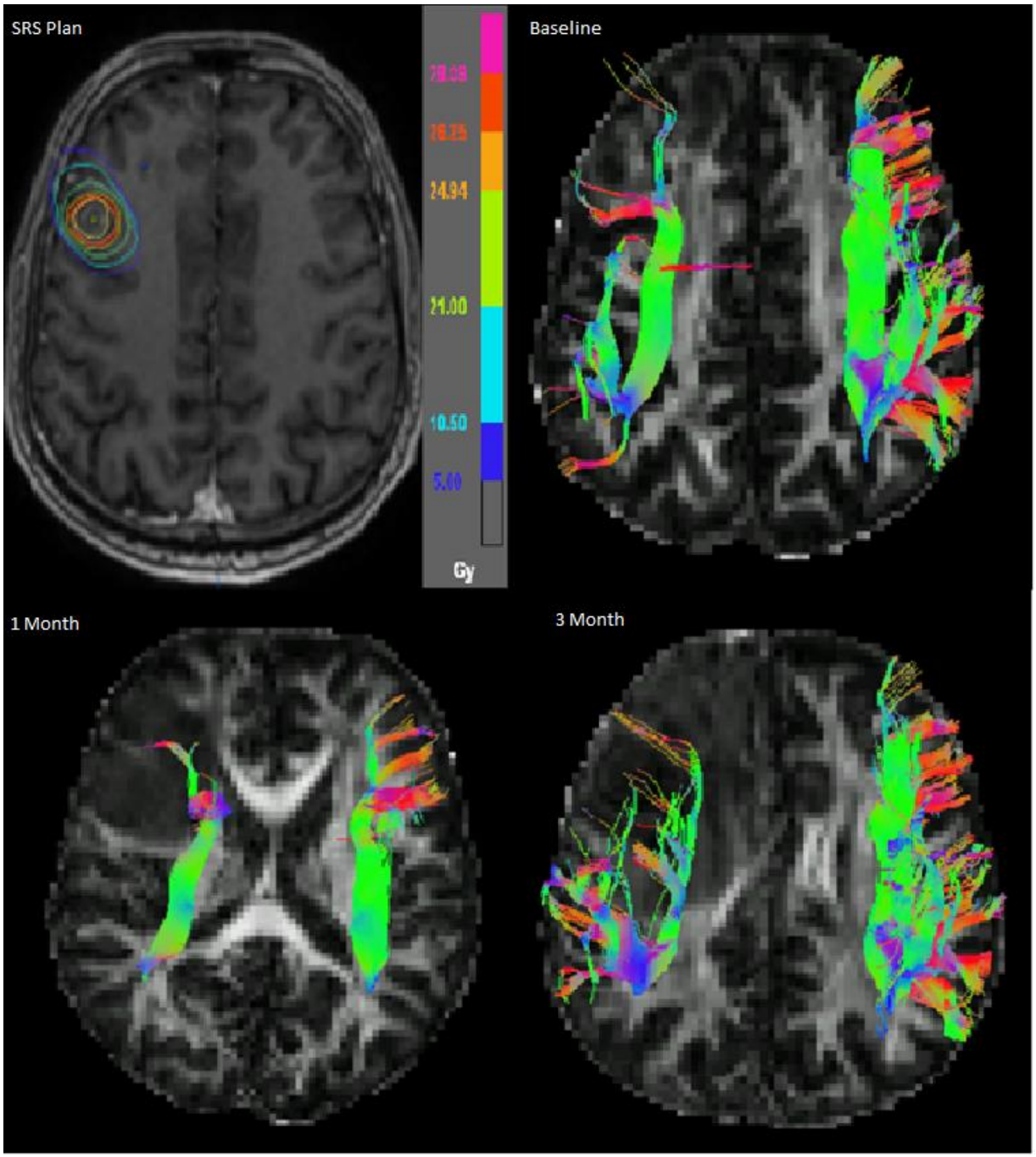

Figure 8.8 SRS Plan and Changes in the Arcuate Fasciculus fibre tract as baseline (before SRS) and at 1-Month and 3-Month following SRS. *This is a case of 58 year old male patient with melanoma who was not on any systemic therapy. The tracts are colour coded in the direction of orientation: Green – anterior-posterior; Blue – Superior-Inferior; Red – Right-left. The ipsilateral side demonstrating distortion and displacement of the tract.*

A

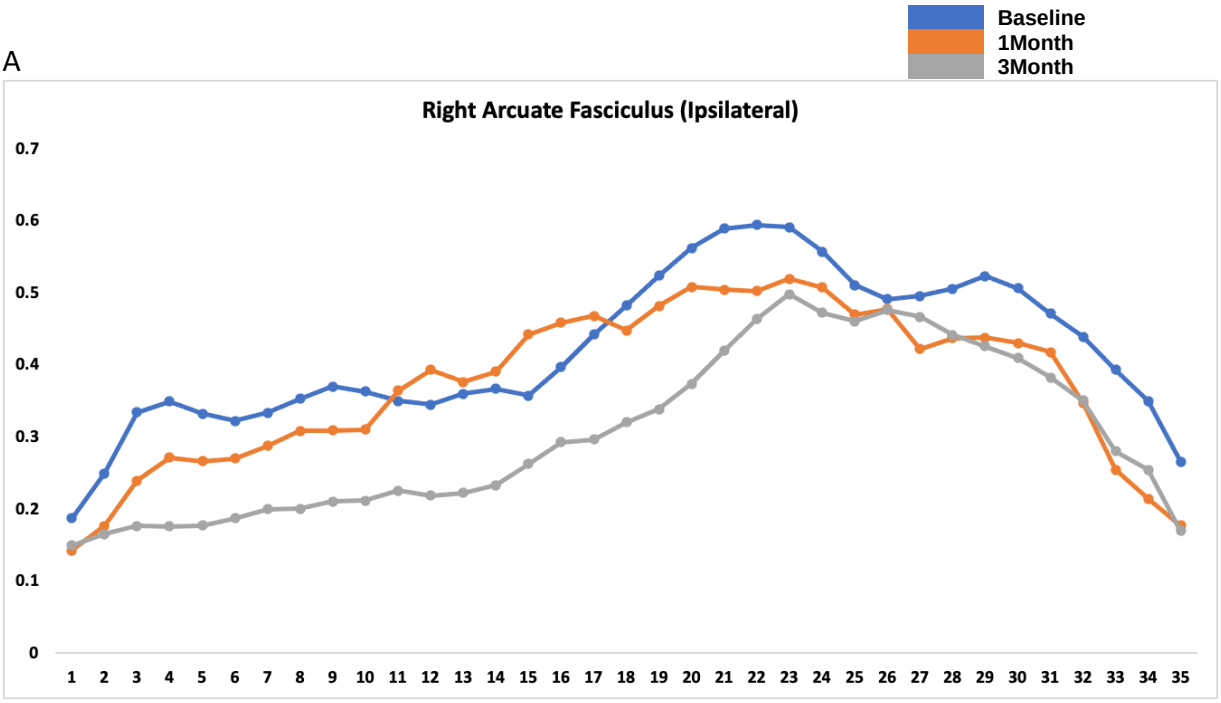

B

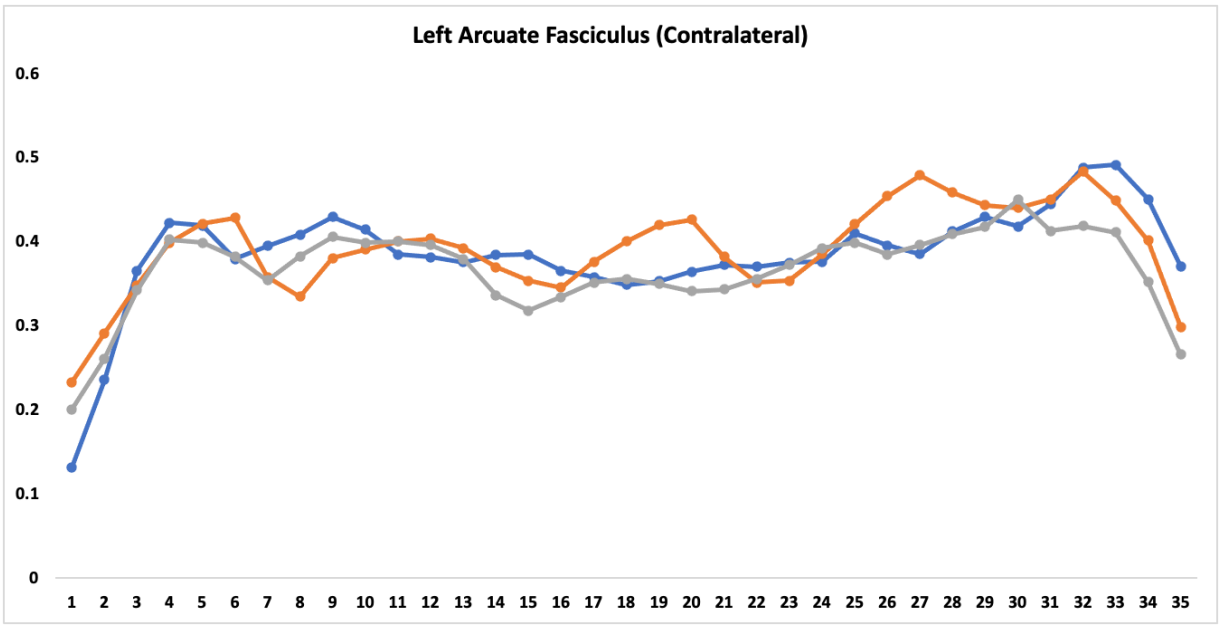

Figure 8.9 Line graph demonstrating FA values at baseline, 1 month and 3 month of bilateral arcuate fasciculus tracts demonstrated in Figure 8.8. *A – Ipsilateral tract to the metastases shows increased FA at 1- and 3- months along the tract. B – Contralateral tract to the metastases shows increased FA at 1- and 3- months along the tract.*

8.4.2.2 *Changes in resting state network following SRS using BOLD maps*

There was no significant difference between the mean BOLD signal of default mode network in ipsilateral and contralateral hemisphere at baseline (mean signal intensity 1.11, 0.46 respectively, p-value 0.31). There was a reduction in the mean BOLD signal of default mode network in the ipsilateral hemisphere at 1 month and improvement at 3 months. There was no statistically significant difference in contralateral hemisphere BOLD signal at 1 month or 3 months when compared to baseline (Figure 8.10, Table 8.6).

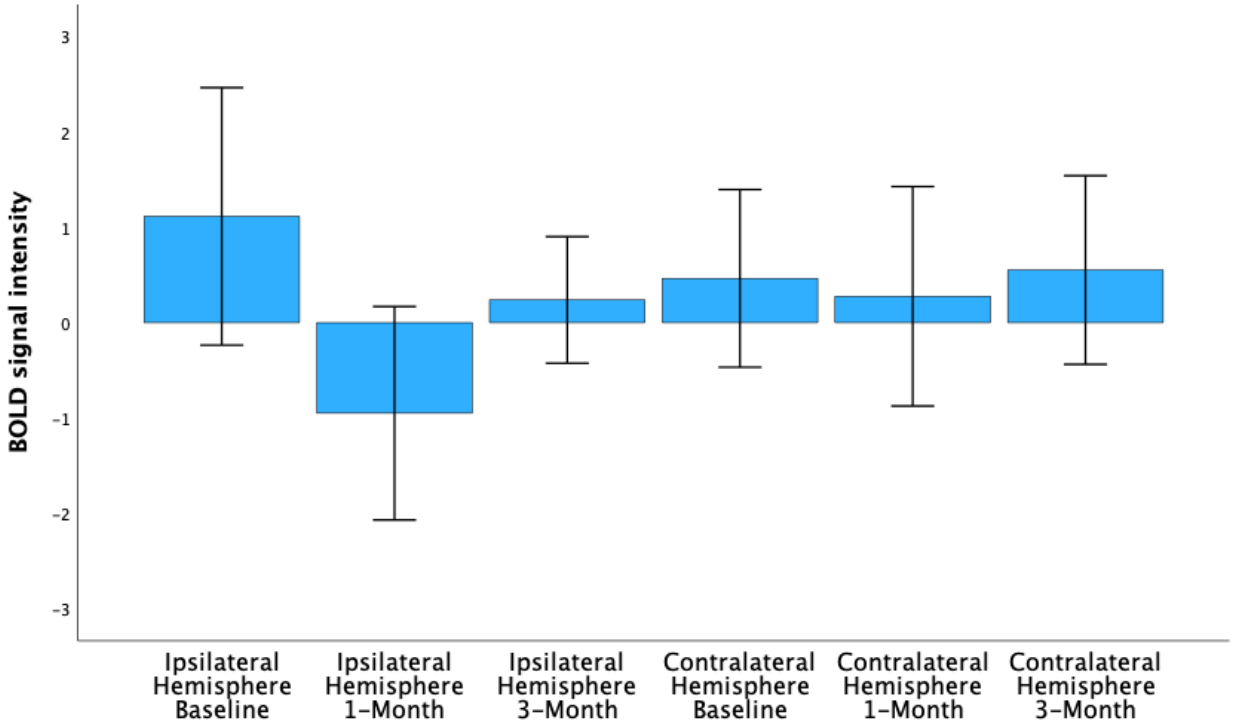

Figure 8.10 Mean BOLD signal in Ipsilateral and Contralateral hemisphere at Baseline, 1-month and 3-month time points. Error bars represent 95% confidence interval.

	Ipsilateral	Contralateral
Baseline	1.11	0.46
1-Month	-0.95	0.28
3-Month	0.24	0.55
p-value (Baseline and 1-Month)	**0.03***	0.49
p-value (Baseline and 3-Month)	0.10	0.66

Table 8.6 Mean BOLD signal intensity in peritumoural region receiving more than 2 Gy in the ipsilateral and contralateral hemisphere. *Statistically significant result is marker *.*

Figure 8.11 shows visual changes in the BOLD signal in the region of SRS dose deposition. At baseline, BOLD signal is reduced in the vicinity of metastases and oedema at baseline. At 1-month, BOLD signal was reduced further in regions receiving 2 Gy. BOLD signal shows signs of recovering to baseline at 3 months with increasing signal in the grey matter.

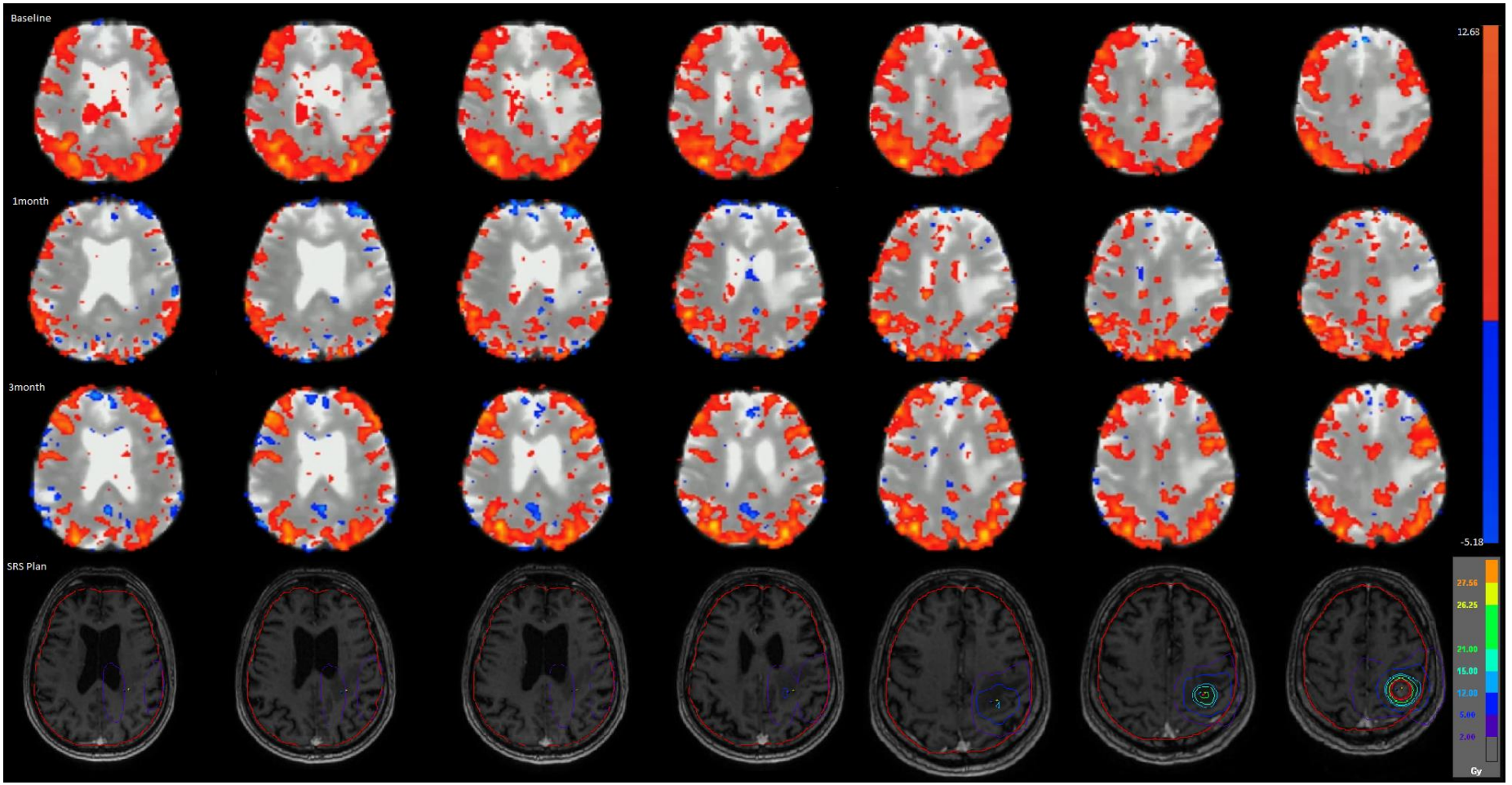

Figure 8.11 SRS dose distribution and BOLD map of Default Mode Network at Baseline (before SRS), 1-Month and 3-Month following SRS. The red and blue are indicators of temporal correlation and anti-correlation in the signal intensity-time plots. *This is a case of 67 year old male patient with colo-rectal cancer who was not on any systemic therapy.*

8.4.3 Tumour Blood Flow, Oxygenation and Microstructure

8.4.3.1 Cerebral Blood Flow and BOLD Signal of the Metastases

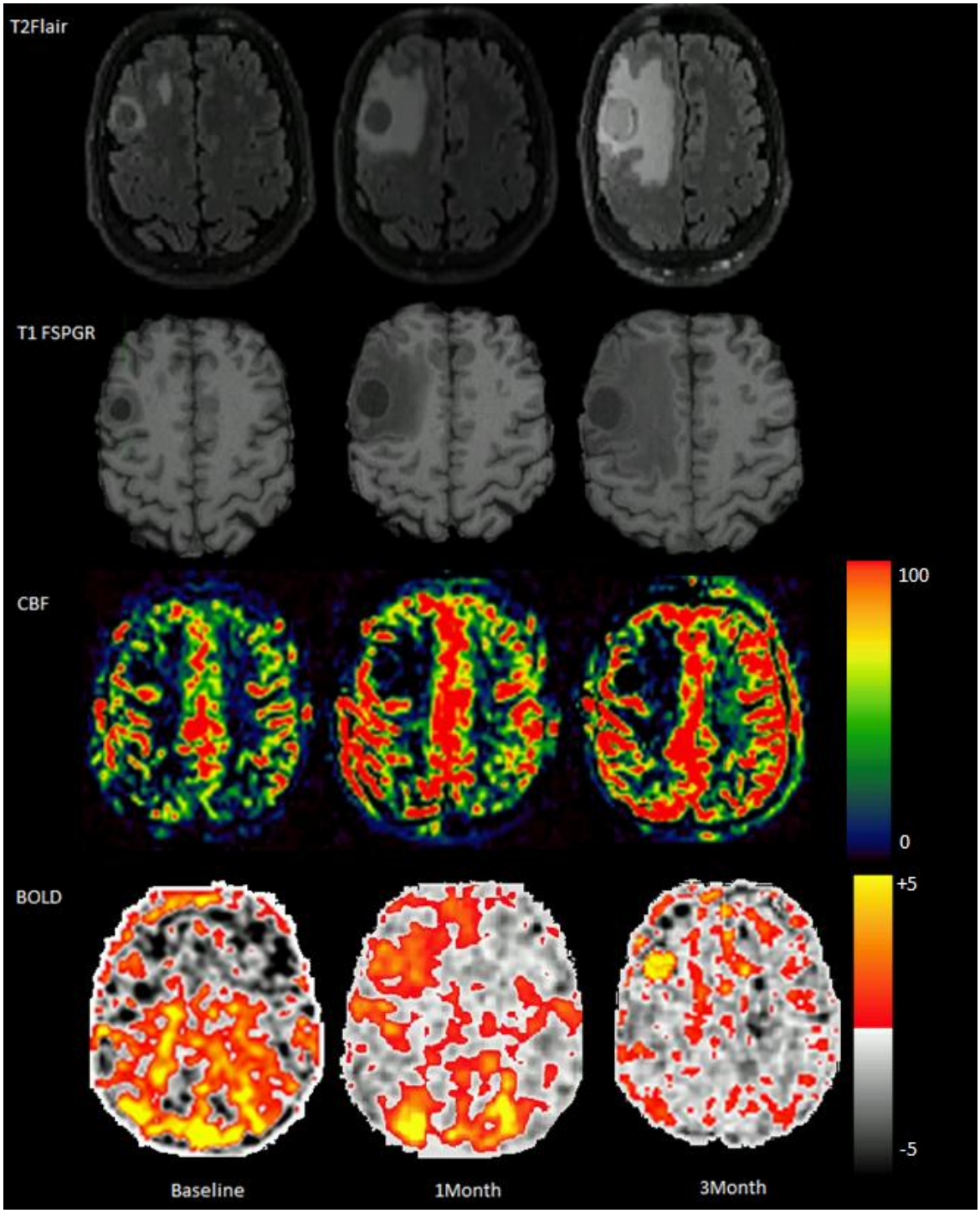

Figure 8.12 Structural, Cerebral Blood Flow Map and Blood Oxygen Level Dependent Map of the right frontal lobe metastases in a participant who illustrated evidence of progression. *This is a case of 58 year old male patient with melanoma who was not on any systemic therapy. T2 FLAIR: T2 weighted fluid-attenuated inversion recovery; T1 FSPGR: T1-weighted Fast Spoiled Gradient Echo, CBF: Cerebral Blood Flow, BOLD: Blood Oxygen Level Dependent. In this example, CBF is low in the growing metastases, whereas BOLD map shows increased BOLD signal within the metastases.*

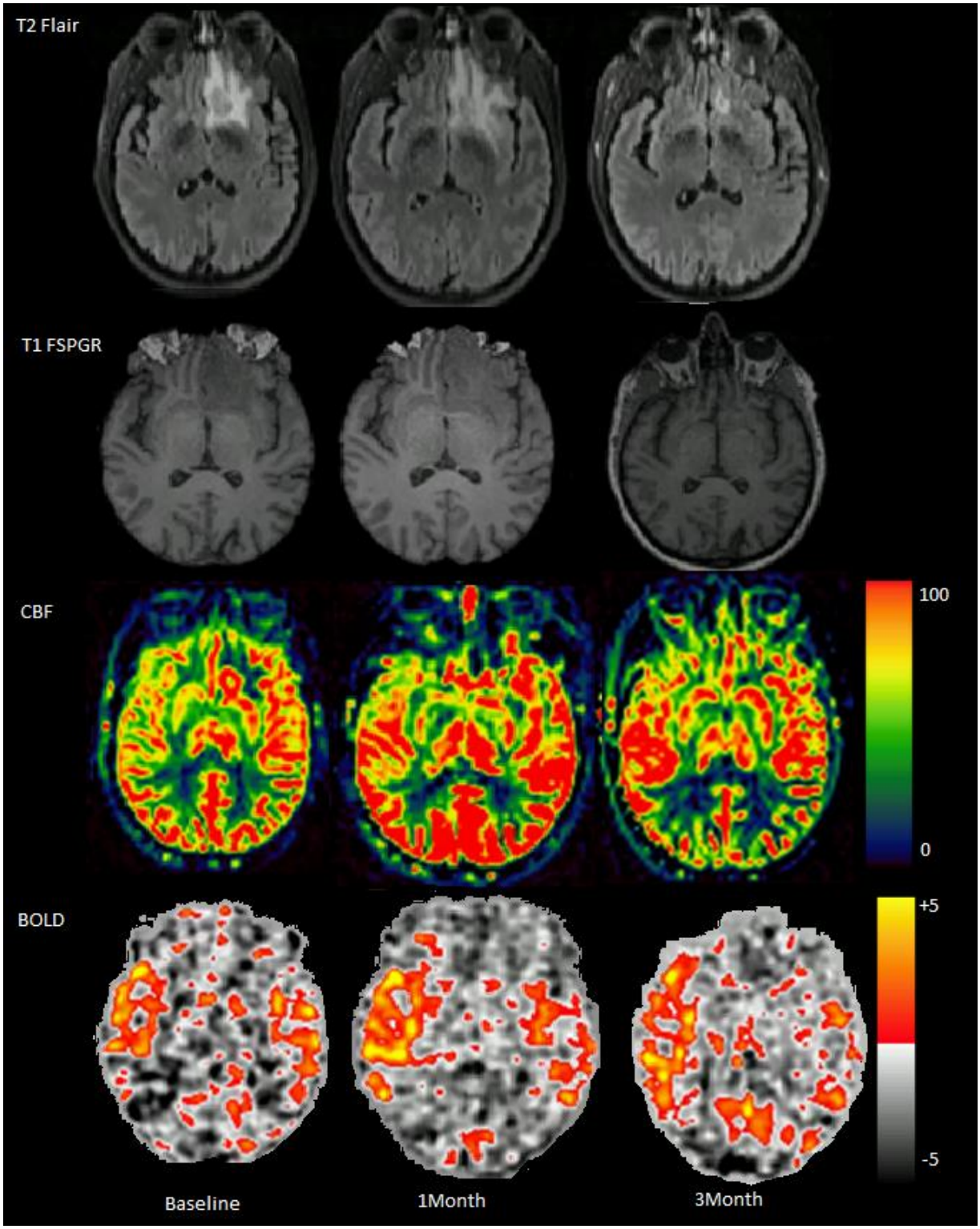

Figure 8.13 Structural, Cerebral Blood Flow Map and Blood Oxygen Level Dependent Map of the left inferior frontal lobe metastases in a participant who illustrated evidence of complete response. *This is a case of 48 year old female patient with NSCLC. T2 FLAIR: T2 weighted fluid-attenuated inversion recovery; T1 FSPGR: T1-weighted Fast Spoiled Gradient Echo, CBF: Cerebral Blood Flow, BOLD: Blood Oxygen Level Dependent. In this example, CBF is high at baseline and 1 month in the metastases, whereas BOLD map shows decreased BOLD signal within the metastases.*

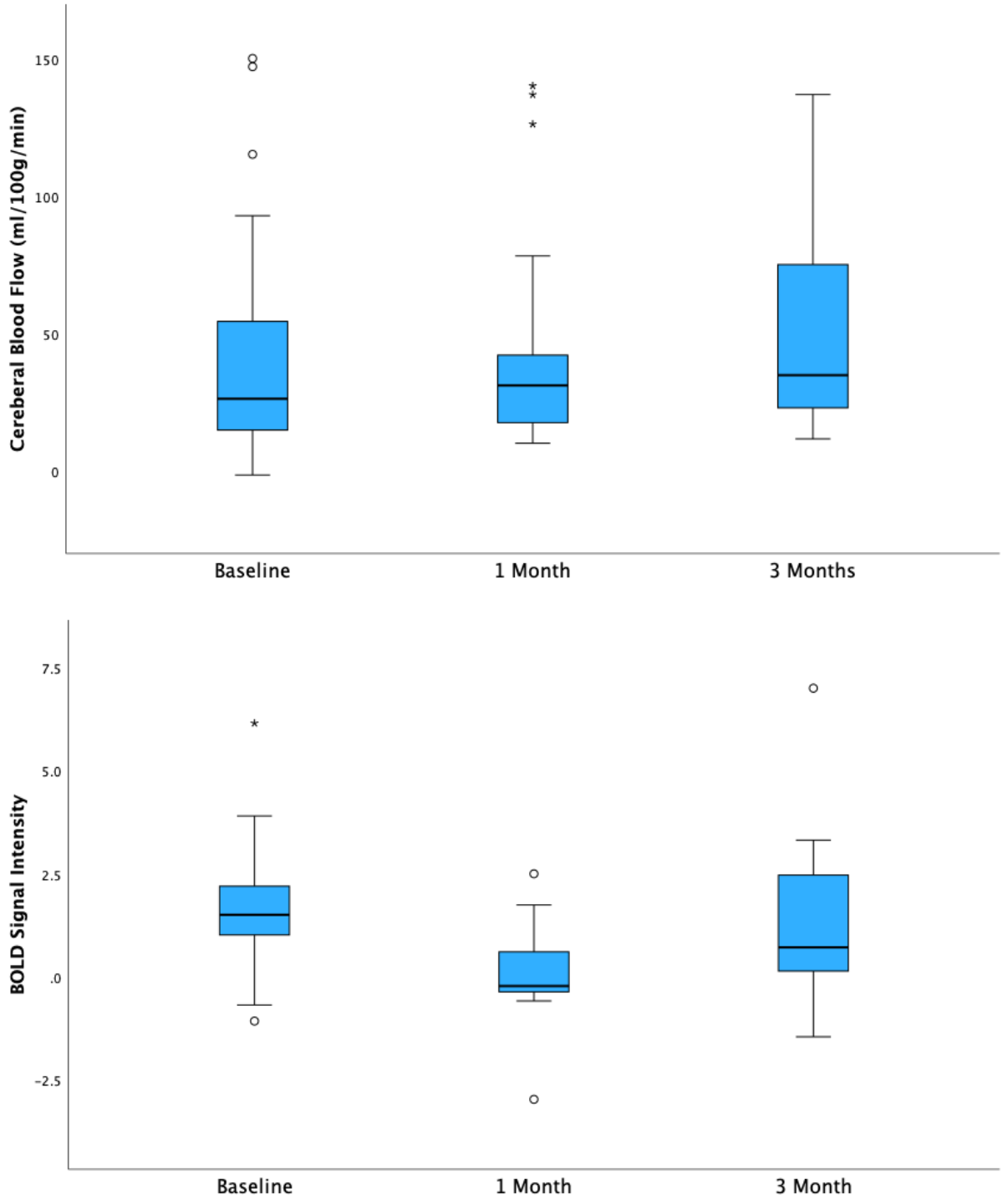

Figure 8.14 Baseline CBF and BOLD Signal at each time point for all metastases. *Box represents interquartile range. 'o' represents mild outliers, '*' represents extreme outliers.*

Figure 8.12 and 8.13 demonstrates the corresponding T1 FSPGR, T2 FLAIR, CBF and BOLD maps at each time point of example patients who had progressive disease and complete response at baseline, 1-month, and 3-month time point, respectively. Figure 8.12

demonstrates low CBF values within in the metastases at baseline, 1 month and 3 months with an increased signal in BOLD map. In contrast, Figure 8.13 demonstrates high CBF within the metastasis at baseline with normalisation of CBF map by 3 months, and reduced BOLD signal at baseline, 1 and 3 months.

Median CBF of the metastases was 26.35, 31.18, 34.93 ml/100g/min at baseline, 1 month and 3 months, respectively. Median BOLD signal intensity of the metastases was 2.15, -0.23, 0.41 at baseline, 1 month and 3 months respectively (Figure 8.14).

Baseline CBF in the metastases was significantly lower in patients who demonstrated evidence of stable disease or partial response at their first standard post treatment MRI at 3 months compared to patients who had progressive disease, 20 vs 104 ml/100g/min, p-value = 0.03). This also reflected in the BM:GM ratio as demonstrated in Figure 8.15. There was no statistically significant difference in CBF at 1 month and 3 months between the two groups. However, BM:GM ratio of the BM 1 month following SRS was significantly higher in patients who demonstrated evidence of stable disease or partial response compared to the group who had progressive disease. There was no significant different in the group at 3 months (Figure 8.15, Table 8.7).

BOLD signal in the metastases between the groups did not vary significantly (Figure 8.16, Table 8.7).

	Baseline			1 Month			3 Month		
	SD/PR (median, range)	PD (median, range)	p-value	SD/ PR (median, range)	PD (median, range)	p-value	SD/ PR (median, range)	PD (median, range)	p-value
CBF (ml/100g/min)	20, 5-52	104, 55-150	0.03*	32, 10-140	28, 19-35	0.286	35, 12-137	74, 32-116	0.485
BOLD Signal (arbitrary value)	1.2, -1.25-3.9	0.3, -1.5-6.2	0.590	0, -3.1, -3.9	0.7, 0.6, 1.6	0.211	0.7, -1.5-3.3	7	0.455
VERDICT cell radii (µm)	8, 5-10	6.2, 6-8	0.089	7.9, 6.2-10.7	7.8, 6.1-9.8	0.345	8.1, 5.1-9.2	8	1.00
VERDICT fIC	0.76, 0.64-0.97	0.8, 0.78-0.81	0.663	0.72, 0.64-0.91	0.61, 0.71-0.5	0.415	0.7, 0.68-0.72	0.9	0.429
VERDICT fEES	0.19, 0.11-0.39	0.26, 0.17-0.3	0.512	0.25, 0.2-0.27	0.27, 0.25-0.29	1.00	0.18, 0.13-0.23	0.23	0.429
VERDICT fVASC	0.03, 0.002-0.08	0.008, 0.002-0.01	0.342	0.007, 0.002-0.2	0.005, 0.004-0.008	0.455	0.02, 0.01-0.08	0.03	1.00

Table 8.7 Measurements of blood flow, BOLD signal, and VERDICT measurements of metastases at each time point in patients with stable disease or partial response compared to those with progression disease. *Statistically significant p-value is marked *. CBF: cerebral blood flow, BOLD: Blood – Oxygen Level Dependent, VERDICT: Vascular and Endothelial Restricted Diffusion Cytometry in Tumours, fIC: Intracellular fraction, fEES: Extracellular extravascular fraction, fVASC: Vascular fraction, SD: Stable disease, PR: Partial response, PD: Progressive disease*

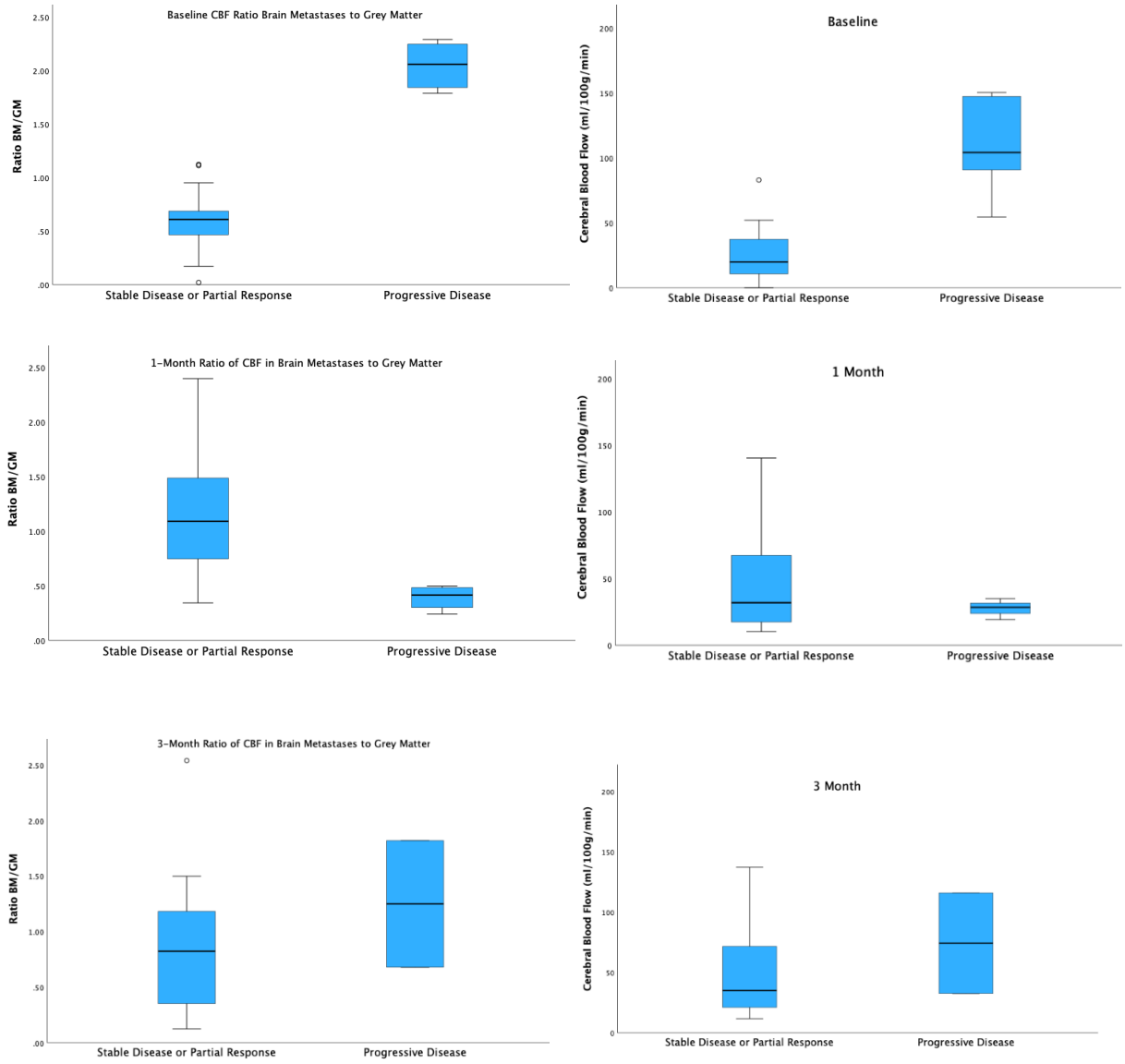

Figure 8.15 Box plots demonstrating variation in raw CBF values and Ratio of Cerebral Blood Flow of Metastases to that of Grey Matter at Baseline, 1Month and 3 Month in patient who had stable disease/partial response or progressive disease. *BM: brain metastases, GM: Grey Matter.*

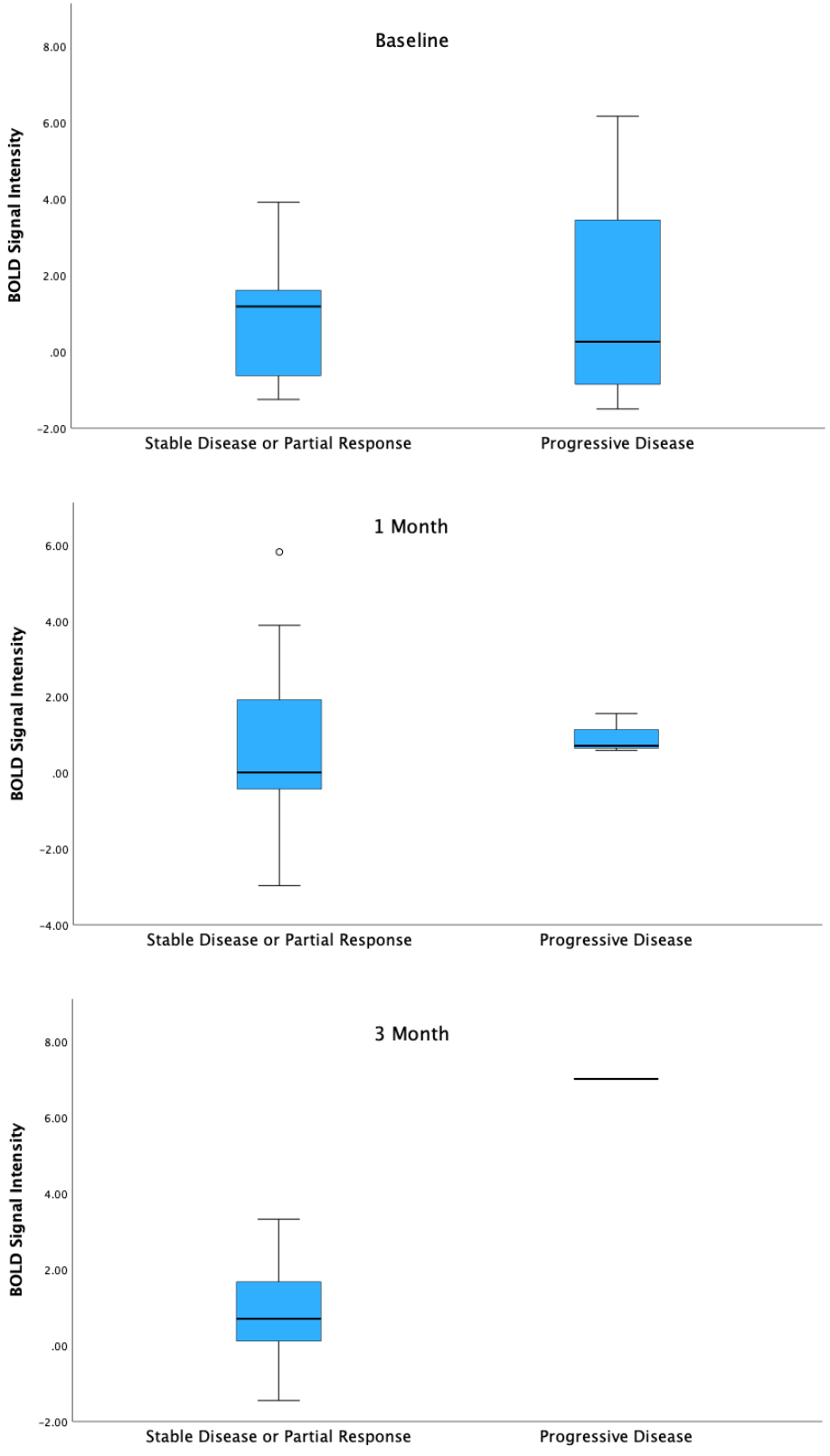

Figure 8.16 – BOLD signal in patients with stable disease/partial response vs progressive disease at each time point

8.4.3.2 Vascular, Extracellular and Restricted Diffusion Cytometry in Tumours (VERDICT) in Brain Metastases

The VERDICT sequence demonstrated changes before and after treatment. Using this sequence, we were able to identify difference in the cell radius, intracellular and extracellular extravascular space compared to the normal brain tissue at baseline and following SRS (Figure 8.17 and 8.18).

The Median fIC was 0.781, 0.733, and 0.727, median fEES was 0.189, 0.251, and 0.199, and median fVASC was 0.262, 0.007, and 0.319 for all patients at baseline, 1 month, and 3 months, respectively. Median cell radius was 8.0 at all the time points. There was no statistically significant difference found between baseline and 1 month and baseline and 3 months in any of these four measures (Figure 8.19). There was no statistical difference in the median cell radius of the metastases according to the varying histology (data not shown).

Figure 8.17 and 8.18 illustrates examples of a patient who had disease progression and a patient who had complete response to treatment, respectively. In Figure 8.17 illustrates reducing fIC with increasing *f*EES and cell radius measurements at 1 month and 3 months compared to baseline. Whereas in Figure 8.18 it demonstrates increasing *f*IC and decreasing *f*EES and cell radius measurements at 1 month, and levels similar to remaining normal brain at 3 months.

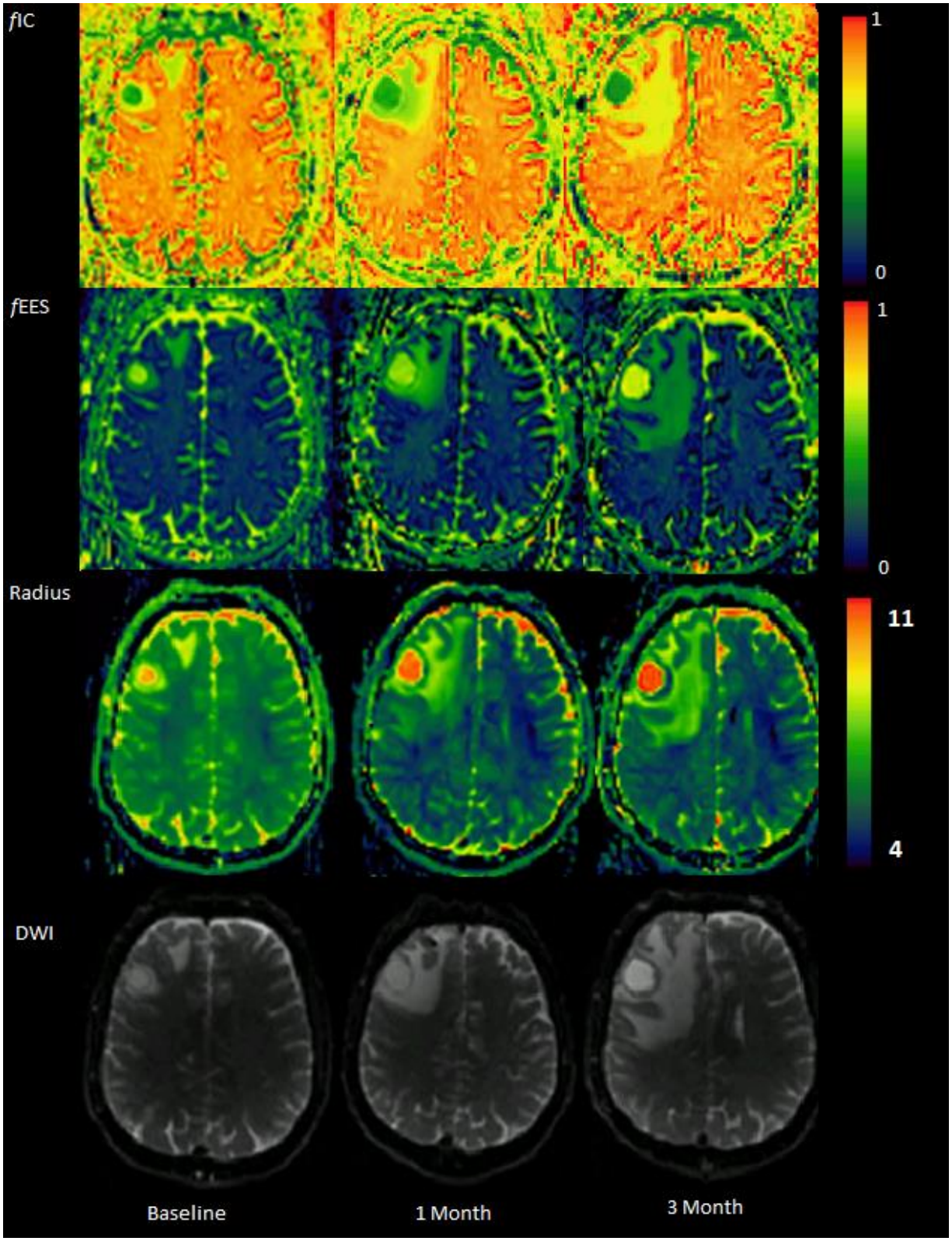

Figure 8.17 Changes in VERDICT measures of brain metastasis showing reduced intracellular space (fIC), increased extracellular extravascular space (fEES) and increasing cell radius at 3 months compared to baseline in a patient who had progression of metastases proven histologically. *This is a case of 58 year old male patient with melanoma who was not on any systemic therapy. fIC: Intracellular Space, fEES: Extracellular, Extravascular Space, Radius: Estimates of Cell Radius in micrometres, DWI: Raw Diffusion weighted B0 image.*

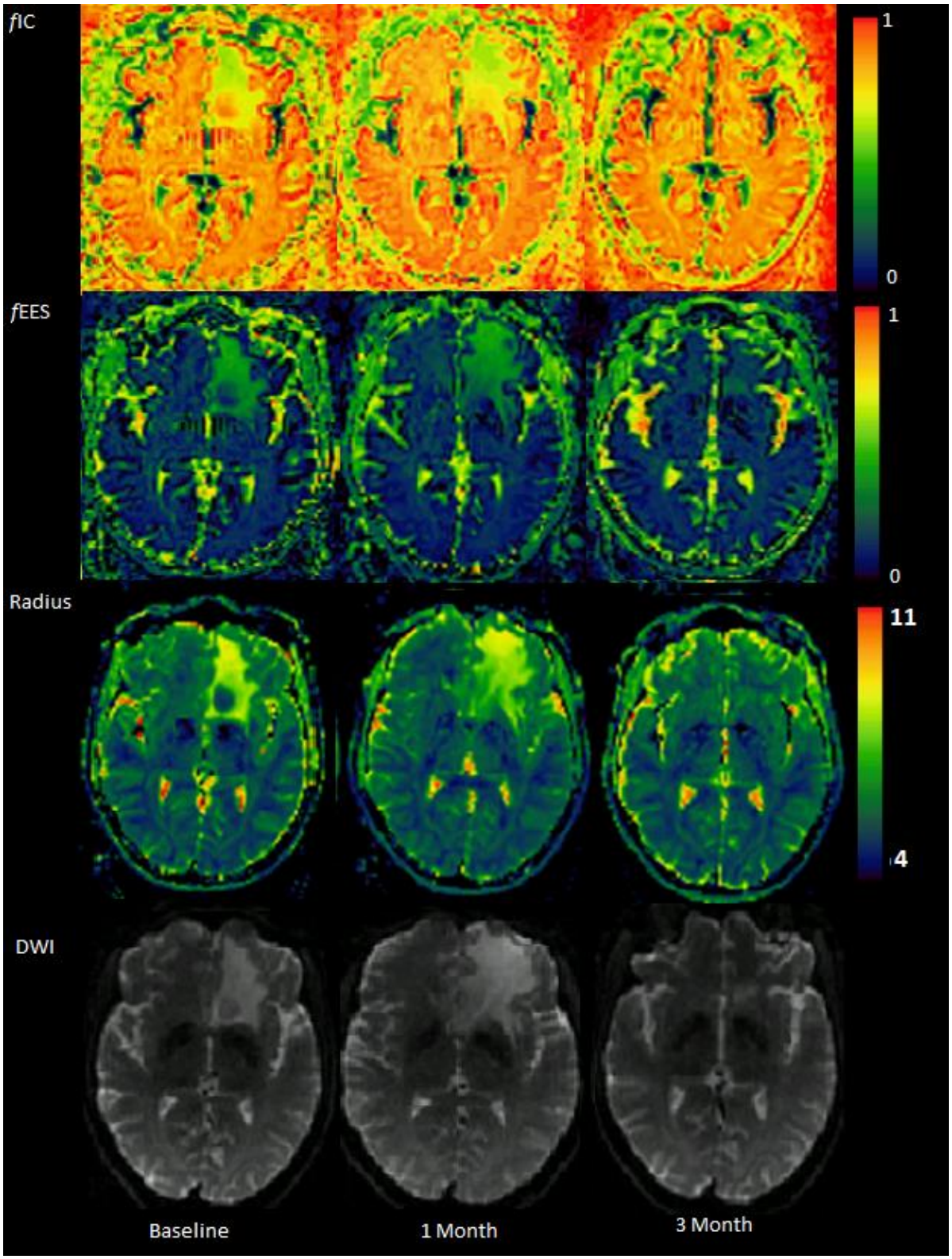

Figure 8.18 Changes in VERDICT measures of brain metastasis showing increased intracellular space (fIC), reduced extracellular extravascular space (fEES) and reduced cell radius at 3 months compared to baseline in a patient who had complete response to treatment. *This is a case of 48 year old female patient with NSLC. fIC: Intracellular Space, fEES: Extracellular, Extravascular Space, Radius: Estimates of Cell Radius in micrometres, DWI: Raw Diffusion weighted B0 image.*

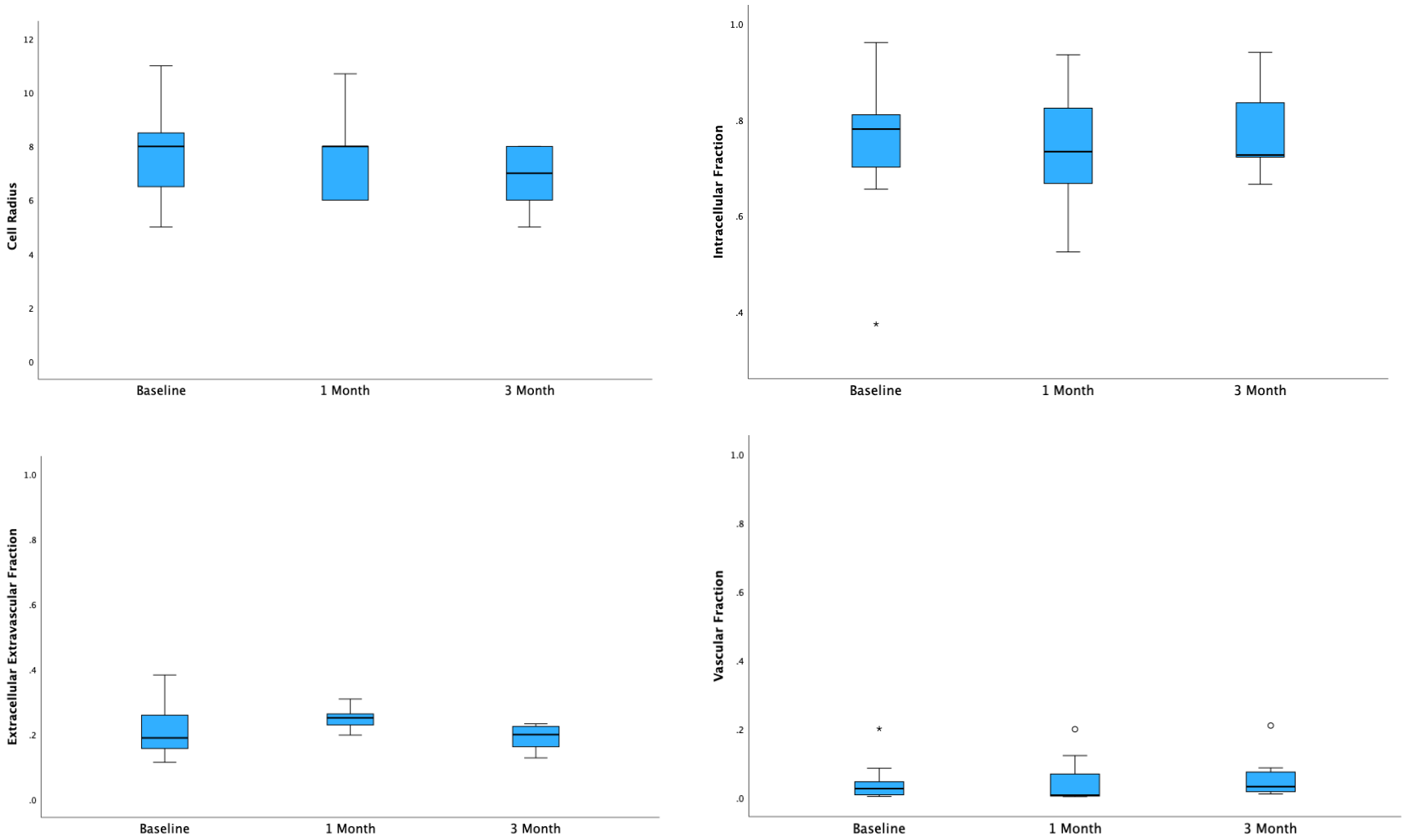

Figure 8.19 VERDICT measurements in all participants at each time point. *Cell radius is measured in micrometeres.*

Reduced median *f*IC at 1 month was evident in patients who had progression at their first MRI compared to those with stable disease, 0.61 and 0.71 respectively, however statistical significance was not reached (Figure 8.20, Table 8.7). There was no significant difference between *f*EES, *f*VASC and cell radius Comparison at 3 months was difficult as there was one patient in the progression group (Figure 8.20, Table 8.7).

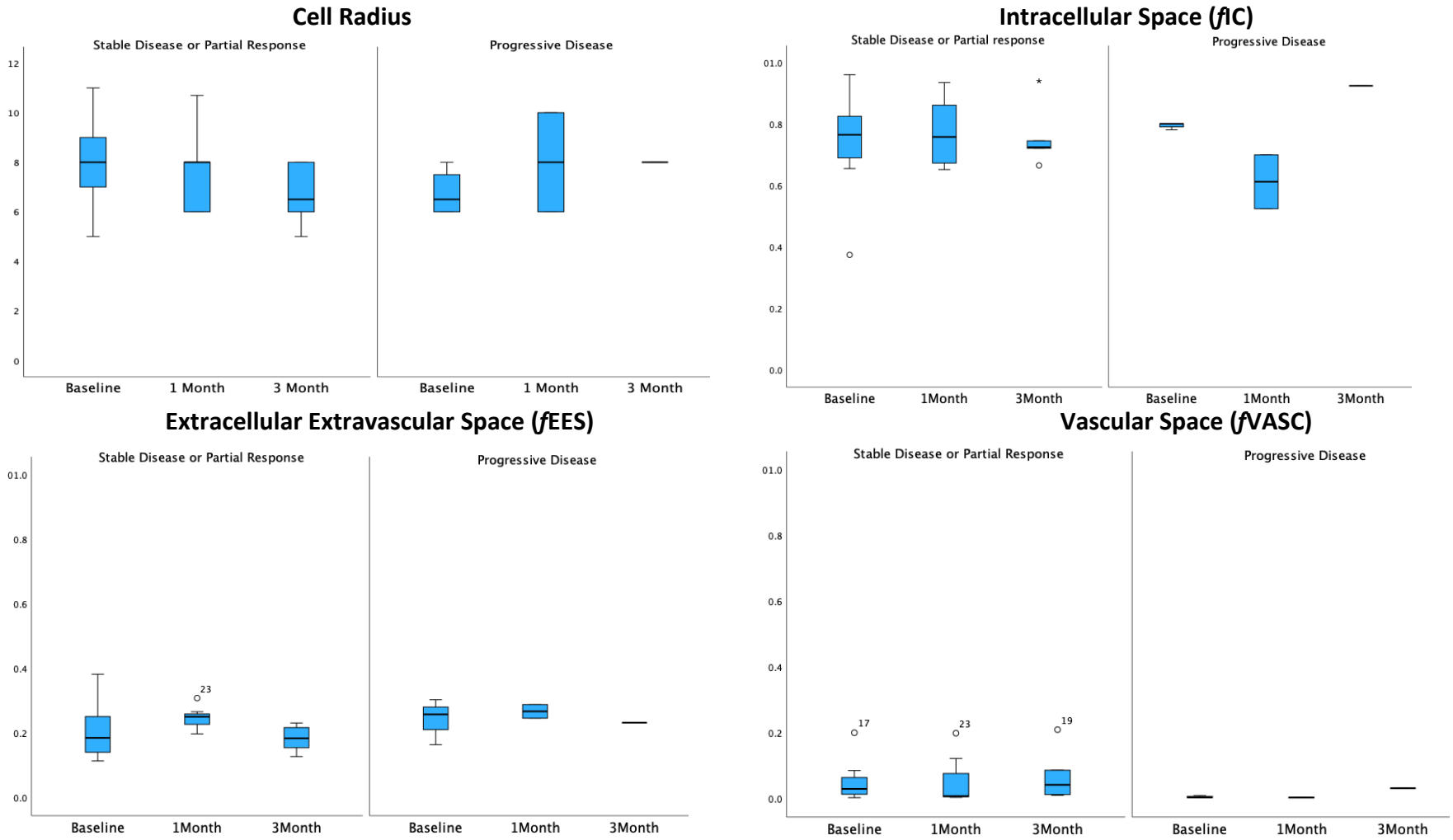

Figure 8.20 Box plots demonstrating change in intracellular, extracellular extravascular, and vascular fractions and estimation of cell radius as detected by VERDICT at baseline, 1 month and 3 months in patients who had stable disease or progression. *Cell radius was measured in μm; at 3 months, there was 1 patient in the progression group.*

8.5 Discussion

This chapter has described the use of novel MRI sequence to assess changes in the peritumoural regions post SRS and physiological and microstructural changes in the metastases. This is the first-time patients with brain tumours, primary or secondary, have undergone MRI scans using the Connectome microstructure MRI scanner. We have demonstrated that scans were well tolerated as patients were able to complete all the assessments, and that novel MRI sequences show changes with SRS.

BM and oedema volume were both significantly higher in patients who presented with seizure, compared to those who did not exhibit seizure activity. In contrast, metastases volume varied significantly according to the presence of neurological symptoms and oedema was more important for this cohort. There was a strong correlation between volume of metastases and oedema which is in contrast with published studies (Chen *et al*., 2012, Hakyemez *et al*., 2010).

Multi-shell DTI imaging has allowed to obtain detailed tractography with measurements of scalar diffusion metrics along the length of the tract which showed reduction in the region of SRS dose deposition of the tract. This has allowed far greater imaging detail to be obtained of these tracts than is possible with standard diffusion imaging. There was no statistical difference in the mean diffusion measures of the tract between baseline, 1-month, and 3-month. Therefore, measuring mean FA, MD, RD and AFD of the whole tract may not be immensely helpful when assessing changes following radiotherapy. Sequences such as CHARMED performed on the connectome scanner allow microstructural measurement of diffusion scalar metrics which may be more crucial to understand radiotherapy related white matter damage. BM do no tend to invade the surrounding brain structure; however, this form of imaging may play an important role in primary brain tumour where tumours may invade or grow along the white matter tracts and therefore will lead to a greater understanding of tumour microstructure (Yen *et al*., 2009, Sternberg *et al*., 2014).

Radiotherapy reduces BOLD signals from default mode network at 1 month with evidence of recovery at 3 months. Alteration in default mode network has been demonstrated in patients with cognitive impairment (Zhang *et al*., 2020b), epilepsy (Hu *et al*., 2017), however, this has not been demonstrated following radiotherapy. Acute reduction in BOLD signal at 1 month could be related to reduced oxygenation and blood flow following radiotherapy. Reduced blood flow has been demonstrated in regions receiving more than 10 Gy following radiotherapy (Hou *et al*., 2022). Alteration in default mode network may play a crucial role in cognition and memory retrieval, therefore it is possible that reduction in BOLD signal could be related to changes in cognition in this patient cohort. In order to study changes in the physiology and connectivity of the brain following radiotherapy, we can hypothesise that radiation can alter default mode network and microstructure tractography can detect changes in peritumoural white matter tracts, therefore it will be important to study the correlation of these two imaging modalities in depth.

This work highlights the importance of using multiparametric MRI assessment following SRS treatment in order to assess signs of true progression. ASL sequences are currently being utilised in clinical practice to differentiate between pseudoprogression and true progression (Deibler *et al*., 2008). However, in this cohort, one patient who had evidence of progression demonstrated reduced CBF at each time point. Therefore, CBF alone may not be a sensitive marker of true progression. Increased CBF may also signify the presence of hypoxia. Studies have shown that CBF can increase up to two-fold in presence of hypoxia (Xu and Lamanna, 2006). Hypoxia is an important factor in radioresistant disease and hypoxia modifiers have been tested in clinical trials in non-neurological tumours (Bouleftour *et al*., 2021). Patients who had stable disease or partial response demonstrated a significantly higher CBF at 1 month, compared to those who showed lower CBF at 1 month. In a study of pontine glioma in children, higher CBF was associated with pseudoprogression (Calmon *et al*., 2018). Another study showed a global reduction in CBF of the metastases during radiotherapy, but this group did not look at response to treatment (Hou *et al*., 2022). In this cohort of participants, three patients underwent neurosurgical resection for progressive disease, all demonstrated reduced CBF at 1 month. Histology from all three confirmed presence of metastatic disease. Therefore, these participants had histologically proven progressive disease. Tumour signal in

BOLD imaging is in the exploratory phase and is challenging as it can be affected by haemorrhage, (Bogomolny *et al*., 2004). Combining CBF and BOLD signal may give more information about oxygenation, cerebral blood volume and blood flow within the metastases (Yetkin and Mendelsohn, 2002).

Although VERDICT has been performed in patients with prostate cancer and in animals for primary brain tumour (Roberts *et al*., 2020, Bonet-Carne *et al*., 2019), it has never been performed in patients with either primary or secondary brain tumours. In this cohort of patients, VERDICT demonstrated that the BM demonstrated higher *f*IC and lower *f*EES compared to oedema. The only patient who had progression showed lower *f*IC, and higher values of *f*EES and cell radius at 1 and 3 months compared to patients who responded, but this has to be considered exploratory analysis due to low patient numbers. *f*VASC did not show correlation with CBF. VERDICT model assumptions in brain tumours must be studied further and its clinical value needs to be investigated further.

We have demonstrated potential changes detected in ASL, BOLD, and VERDICT measures that were different in participants who demonstrated evidence of progression compared to those who either had stable disease or partial response. The changes in physiology of BM may represent progression which can be detected at 1 month imaging. For example, those who are deemed fit for surgery and SRS so that salvage surgical option can be offered early in the right cohort of patients, i.e., metastases in an accessible site, fit for surgery, controlled or little ECD, good prognosis. However, this will need careful discussions with the primary cancer site and Neuro-oncology multi-disciplinary teams. Alternatively, it may be possible to consider altering systemic therapy early in these patients rather than waiting for the first MRI which is routinely performed at 3 months following treatment (NICE, 2018). As there are increasing use of immunotherapy and targeted agents which may penetrate the blood brain barrier more than traditional cytotoxic chemotherapy. We can hypothesise based on these data that patients who have progression demonstrate lower CBF/GM ratio, lower *f*VASC, lower *f*IC and higher *f*EES at 1 month. These potential biomarkers will need robust validation in a larger study. Other studies have combined MR Spectroscopy with DWI of the metastases (Jakubovic *et al*., 2016, Sawlani *et al*., 2019). Therefore, we would propose that future studies

to assess response to SRS should include ASL, DTI, VERDICT in addition to MR Spectroscopy and routine structural T1 & T2 weighted imaging.

Despite some imaging biomarkers being used extensively in research and showing exciting potential, limited number of biomarkers are used to guide clinical decisions. Two translational gaps have been identified: gap between a biomarker being evaluated in vitro and in vivo to forming a reliable measure to test hypothesis in clinical cancer research; second gap from clinical cancer research to a biomarker being used in routine clinical practice in the management of patients with cancer within the healthcare system (O'Connor *et al*., 2017). This work has attempted to form hypotheses for future clinical cancer research which will be discussed in the next chapter.

There was no significant difference according to the diagnosis of primary malignancy. This is likely because of small number of patients for each primary cancer and smaller number of follow up imaging in patients.

This study has several limitations. There are a small number of patients at each time point, therefore it is challenging to draw any conclusive statistical meaning from the data presented. VERDICT is a sequence that has been compared to histological findings, and patients in this study did not have histology. However, as brain metastasis is, largely, considered a radiological diagnosis, it is important to have a robust way of assessing the BM at diagnosis and following treatment. Due to reduction in participant numbers by 3 months, it introduces a bias as most of the complete data points relates to patient who showed a durable response to treatment. Imaging studies are challenging to organise for two main reasons: patient's commitment to research scans and financial constraints. The challenges of recruiting patient with BM to clinical trials has been discussed in section 7.4. This is a heterogenous group of patients who have the complexity of extracranial disease presence, systemic therapy, and symptoms of intracranial disease burden and due to this, there is a high dropout rate in previously reported trials (Chang *et al*., 2009, Brown *et al*., 2016a). RANO group advises designing BM trial for a particular histology, e.g., melanoma or NSCLC in order to control for bias that primary malignancy can bring into such a study. However such a

study is difficult to design that is focussed on BM only and will be challenging to set up (Lin *et al*., 2013).

8.6 Conclusion

This work highlights the importance of performing multiparametric MRI early following SRS to assess disease response. T1FSPGR with contrast and T2FLAIR may not provide enough information to assess response early and size alone, may not be reliable. However, with the addition of blood flow and microstructure diffusion imaging, it may be possible to identify non-responders early so that they can be considered for alternative treatment strategy which could be systemic therapy or neurosurgical resection depending on the accessibility of the metastases and patient's fitness. Rigorous trials are needed in this area to develop a deeper understanding of non-invasive imaging biomarkers to predict response to SRS.

Chapter 9 – Thesis Conclusions and Future Work

9.1 Discussion of overall results

Patients with BM have limited survival. Controlling the BM plays a pivotal role in prolonging their overall survival. Due to the challenges of SACT penetrating the blood brain barrier, local treatments such as SRS and surgical resection are considered fundamental in controlling BM. These treatments have been shown to provide local control and prolonged survival compared to WBRT and supportive care in patients with limited intracranial disease. Despite the precision of SRS, clinical trials have demonstrated that 24-60% of patients may develop NCF impairment following treatment with SRS alone. The primary hypothesis for this thesis was NCF Impairment following SRS treatment is dependent on the hippocampus dose.

The hippocampus has been studied in WBRT for BM and fractionated radiotherapy for primary brain tumour, however this has not been examined in the same detail in patients with BM undergoing SRS. Hippocampal avoidance WBRT techniques have been developed and results of the phase II HIPPO trial are awaited which is looking at hippocampal sparing (HS) WBRT vs conventional WBRT after surgical resection or radiosurgery in patients with favourable prognosis with 1-4 BM. The hippocampus is not currently delineated routinely during SRS treatment planning.

In order to study the significance of hippocampal dose in patients with limited BM undergoing SRS, I conducted a retrospective analysis of consecutive patients who underwent SRS in 1 year at Velindre Cancer Centre. This was followed by a dosimetric radiotherapy planning study to examine the feasibility of reducing radiotherapy dose to the hippocampus expecting a major factor to be the proximity of the BM to the hippocampus. I then designed a prospective observational study of patients undergoing SRS looking at baseline clinical, NCF and multiparametric MRI imaging of the hippocampus. NCF tests were conducted according to recommendations by the RANO group. During my research time, I developed MRI sequences particularly focusing on ASL to study perfusion and MR Spectroscopy. All patients

underwent NCF and MRI at baseline, 1- and 3-month time point. Additional NCF tests were performed at the 6-month time point. Research MRI scans were performed at the Cardiff University Brain Research Imaging Centre (CUBRIC). This study was approved by Research Ethics Committee and supported by Velindre Cancer Centre Research and Development department, and the Wales Cancer Research Centre. I utilised this opportunity for patients to undergo novel imaging using the Connectome microstructure MRI scanner at CUBRIC to examine tumour and its microenvironment and microstructural diffusion measurements. This was the first time, as far as we are aware, for patients with BM to undergo MR scans using this novel MRI scanner.

9.1.1 Importance of the Hippocampus in SRS treatment

I first studied a retrospective case series of patients over one calendar year who underwent SRS at our centre. The hippocampus was delineated according to the RTOG protocol retrospectively on the plan that was used to treat patients and the dose was re-calculated. In Chapter 2, I demonstrated that out of 30 patients, 7 patients received >5 Gy to 0.1 cc of the hippocampus and 8 patients received 2-4.9 Gy. Key factors that led to dose of > 5 Gy to 0.1 cc of the hippocampus were presence of metastases in the temporal lobe and cerebellum, distance from PTV to the hippocampus less than 1 cm, and proximity of metastases to the brain stem and optic chiasm. As the hippocampus is in close proximity to the brainstem and optic chiasm, the hippocampus may receive a higher dose as a consequence of avoiding these key structures during SRS planning.

Therefore, I hypothesized that by delineating the hippocampus, I may be able to reduce the dose delivered to the hippocampus. In Chapter 3, I illustrated that it is possible to reduce the dose to the hippocampus using dynamic conformal arc therapy without compromising plan conformity, homogeneity, dose to the PTV and other OARs. Therefore, accounting for the hippocampus as an organ at risk during SRS treatment planning results in a reduced dose to the hippocampus in all patients.

Following analysis of the retrospective data, I designed a prospective observational study of patients undergoing SRS. Patients underwent standard SRS treatment, and the hippocampus was delineated retrospectively to avoid bias during treatment planning. This was ethically justifiable as delineating the hippocampus is not routine clinical practice and dose constraint has not yet been defined. Patients underwent NCF testing at baseline, 1, 3 and 6 months along with translational MRI scans to study structural, physiological, metabolic and diffusion changes in the hippocampus at baseline, 1 and 3-month time points. As hippocampus is located close to the ventricles, it can be challenging to perform ASL sequences and methods of MR spectroscopy analysis were performed and validated on healthy volunteers.

I took this opportunity to study NCF and prognostic factors at baseline. In Chapter 5, I illustrated the importance of identifying patients with impaired NCF at presentation as I demonstrated that impaired baseline NCF is associated with poorer survival. NCF tests can be time consuming and challenging for patients and require the expertise of clinical psychologist. Other prognostic factors include WHO performance status, burden of intracranial disease and presence of extracranial disease. The GPA prognosis scoring system for patients with BM, which was developed following combining prognostic factors from five studies, does not account for NCF impairment at baseline. My study suggests that NCF may also be an important prognostic marker to be considered. Therefore, in order to conduct larger studies in patients with BM, there is a need to develop robust prognostic markers in this cohort including NCF. This finding should be validated in future BM trial. To develop robust prognostic markers, larger multi-centre studies including NCF assessment at baseline, to help refine the current GPA scoring system, in patients with BM.

Chapter 6 explored baseline MRI findings of the hippocampus in relation to changes in NCF and confounding variables, such as, age, concurrent use of SACT and steroids. To reduce the impact of the confounding variables and study changes in MRI measurements I studied percentage change from baseline rather than the raw data in the following chapter. Although there was a trend towards lower CBF and levels of NAA and creatine in patients with impaired verbal memory and lower levels of Glx in patients with impaired executive function, these values did not reach statistical significance at baseline.

Follow up NCF testing showed a decline at 1 month, followed by recovery at 3 and 6 months compared to baseline testing in Chapter 7. Therefore, on this basis and from the data in our study, we can reject the primary hypothesis of the prospective study which was SRS treatment can cause NCF decline at 3 months. This is a reassuring finding for this cohort of patients given the limited overall survival. We have illustrated that patients who receive >5 Gy to D0.1 cc of the ipsilateral hippocampus have decline in HVLT-TR score at the 1-month time interval following SRS which may be considered an acute toxicity of SRS. From this study we can extrapolate that D0.1 cc to the ipsilateral hippocampus may play a key role in NCF decline at 1 month, which may be considered to be a measure of acute toxicity. Previous reported trials measuring NCF impairment following SRS have measured NCF impairment at 3-4 months following treatment (Brown *et al*., 2016a, Chang *et al*., 2009).

The dose parameter for the hippocampus for the development of acute NCF decline that I have identified was. D0.1 cc >5 Gy which contrasts to D40 >7.3 Gy of the hippocampus which has been described as an important dose constraint in patients undergoing fractionated radiotherapy for primary brain tumours (Gondi *et al*., 2012). There could be two underlying reasons for this finding. Firstly, we have observed acute toxicity following SRS and I have demonstrated that NCF decline recovers to baseline by 6 months. This contrasts with the study conducted by Gondi *et al*., where long term NCF decline was measured at 18 months following radiotherapy (Gondi *et al*., 2012). Thus, the underlying pathophysiology of acute and late NCF impairment may differ as seen in other structures. The acute NCF impairment may be related to D0.1 cc with an ability to repair. Hippocampus has NCS which may be a serial organ in relation to acute NCF impairment followed by a degree of repair. Secondly, this could be due to radiobiological differences in single fraction SRS compared to fractionated radiotherapy which is delivered over several weeks. Larger doses of >10 Gy per fraction can cause secondary cell kill in normal tissue by inducing cell death by vascular damage (Park *et al*., 2012) and endothelial cell damage. However, there are contradictory reports as some studies suggests that the LQ model, which describes cell kill at lower doses in a fractionated radiotherapy course, may still apply in SRS (Brown *et al*., 2014).

Dose to point maximum also gives rise to the hypothesis that the hippocampus may be a serial organ in relation to acute toxicity of NCF decline. NTCP modelling for the hippocampus, particularly for SRS treatments, has not been examined in depth. Most toxicities from CNS SRS include radiation necrosis, brainstem necrosis and optic neuropathy, all of which are late toxicities. Whilst it is not possible to conduct histopathological studies examining normal tissue complication in the hippocampus in humans, there are some animal studies that have examined cell kill in the hippocampus. Acharya *et al*., demonstrated reduction in hippocampal neural stem cell by 66% with dose as low as 1 Gy at 5 days post radiation (Acharya *et al*., 2010). It is not known if an acute reduction in neural stem cells is recoverable or leads to chronic reduction, which could potentially lead to long-term loss of hippocampal volume and function. Thus, there is a need to understand changes of neural stem cells following SRS at longer time intervals than they have been studied so far. The impossibility of performing histological studies increases the importance of novel imaging modalities.

It has been demonstrated that decline in the NCF correlated with reduction in the QoL measure at 1 month on the EORTC QLQ-C30 score. World Health Organisation and Cancer Research UK, state that the aim of palliative treatments in patients with metastatic disease is to control symptoms of cancer, lengthen life and improve QoL. Treatment for BM is considered to be of palliative intent. We have demonstrated that patients undergoing SRS have median overall survival of 10 - 12 months. Thus, maintaining or trying to improve QoL is vital in this patient cohort. By limiting the dose to the ipsilateral hippocampus to <5 Gy as an optimal dose constraint, we may be able to achieve this.

Long term NCF impairment following SRS was not measured due to the constraints of this study. Long term NCF impairment is of research interest, which has been studied in primary tumours, however, in order to study this in the SRS population, patients predicted to have a survival of >12 months should be examined. This may be challenging to design given the heterogeneity at presentation in patients with BM, however, we would advocate incorporation of robust prognostic tools which, based on finding of this thesis, include baseline NCF testing.

Multiparametric MR imaging of the hippocampus demonstrated a trend towards reduction in volume, blood flow, MRS levels of Glx and FA of the fornix tract following SRS at 1 month. At 3 months, there was an improvement in blood flow and FA, however volume and MRS measurements of NAA, creatine, and choline demonstrated reduction. Whilst it is difficult to draw statistical significance due to the small patient numbers and multiple measurements, we can hypothesise that initial vascular damage secondary to radiotherapy leads to changes in the neuronal cells later which may be identified as loss of volume and reduction in metabolites. White matter damage has been demonstrated when studying late effects of radiotherapy and the 3-month time point may be too early to detect this. I only demonstrated reduction in left hippocampal volume, possibly because it was the dose to the left hippocampus that was high in this cohort as the patients at follow up only had left sided metastases. Lack of changes in the right hippocampus volume and metabolites at 3 months supports the evidence further that these changes are related to radiotherapy.

9.1.2 Multiparametric MRI Imaging of the Brain Metastases

In clinical practice standard MRI sequences for patients with BM include T1 and T2 weighted MRI, T1 with contrast, T2 FLAIR. If clinically indicated, patients may also undergo DWI, ASL and MR Spectroscopy scans. However, these are not performed routinely. As BM are largely a radiological diagnosis, there is a clinical need to understand its physiology and microstructure to enhance local control and use appropriate treatments. In chapter 8, we have illustrated that BM vary in their perfusion and BOLD signal at baseline.

This is the first study that we are aware of where patients with BM have undergone MRI scans using the microstructure Connectome scanner. This scanner carries an advantage of high gradient strength which can give insight into microstructure details of the brain and some clues as to the tumour microenvironment. The two main sequences we used were VERDICT and CHARMED. Both sequences are built on the basis of DTI sequences. VERDICT utilises low *b*-values and uses a mathematical model to estimate water content in three spaces intracellular, intravascular, and extracellular extravascular volumes and cell radius.

CHARMED utilises high *b*-values and provides estimation of directionality of nerve fibre which may be multidirectional.

At baseline, CHARMED sequence has demonstrated reduction in FA, AFD and increase in RD and MD in the ipsilateral peritumoural tracts compared to the same tract in the contralateral cerebral hemisphere. Diffusion metrics may only alter in the vicinity of high dose of radiotherapy, therefore studying mean FA, MD, RD and AFD of the whole tract may not show a significant difference. Microstructure MRI scan can provide in depth information along the nerve fibre tract which opens possibility for future studies to gain further understanding of nerve fibre damage and whether tracts effectively have functional reserve. CHARMED has demonstrated the need to study DTI in detail.

The VERDICT scans demonstrated that metastases component of *f*IC, *f*EES and *f*VASC may change following SRS. The VERDICT scans done after SRS showed a difference between the progressing patient and the non-progressing patients; the former showed decreasing intracellular volume, whereas the extravascular extracellular volume was similar across patients who had evidence of partial response or progressive disease. At 3 months, the patient who had progressed showed increasing intracellular volume, possibly due to increasing number of cancer cells.

Brain tumour imaging and assessment of response is challenging when differentiating true progression from pseudoprogression. There have been studies that have looked at several MRI parameters to differentiate between the two phenomena. I have demonstrated that increased CBF in the metastases at baseline and reduced CBF:GM ratio at 1 month following SRS was more likely to lead to true progression. A study looking at pontine glioma in children reported that increased CBF following radiotherapy was associated with pseudoprogression (Calmon *et al*., 2018). However, pontine glioma is likely to have a different physiological response to treatment. In addition, patients would have received fractionated radiotherapy for this tumour. CBF is not a true representation of tumour oxygenation. Increased CBF can be a response to tissue hypoxia, therefore may be a surrogate marker for hypoxia.

Tumour BOLD signal did not vary significantly between the progressors and non-progressors. BOLD imaging can be employed to study oxygenation in the tumour; however, BOLD signal can be affected by necrosis, haemorrhage, and neovascularisation of the tumour. Although BOLD signal is widely used to map out the relevant functional areas of the brain as part of neurosurgical planning, Significance of BOLD signal detected in BM has not been studied before. Hypoxia is a well know marker for radioresistance, therefore it is of clinical importance to understand the tumour oxygenation. This is important in BM and primary brain tumour.

Reporting recommendations for tumour marker prognostic studies (REMARK) checklist consists of twenty items to report for published tumour marker prognostic studies. The group recommends including a transparent and full description of research goals and hypotheses, subject selection, specimen and assay considerations, marker measurement methods, statistical design and analysis, and study results (Altman *et al*., 2012). Future study design to study the hypothesis generated from this work need to take these guidelines into account.

9.1.3 Potential application for Primary Brain tumour

Multi-parametric imaging is equally valuable in patients with primary brain tumour to understand the microstructure at baseline and assess response to treatment. It is thought that primary brain tumours may invade the tumour tracts compared to BM which tend to push the tracts. CHARMED imaging of primary brain tumour may be able to identify this. There is a need to adapt planning volumes for primary brain tumour as increased margins may be needed in the direction of fibre tract invasion and reduced across the fibre tracts rather than circumferential margin that is applied currently.

Understanding the difference between pseudoprogression and progression is of research and clinical interest; it aids decision making regarding further lines of therapy or re-irradiation. Thus, it is clinically important to differentiate between the two processes. MRS and microstructure MRI may be utilised as a research tool to evaluate drug absorption in the

brain and understanding of factors influencing the blood brain barrier so that intracranial drug availability can be enhanced. The VERDICT sequence may be able to differentiate between different types of gliomas by providing an insight into tumour microstructure and it may be able to differentiate between true and pseudoprogression following radiotherapy. Therefore, utilising microstructure MRI as a research tool to understand these mechanisms may allow us to overcome the barriers in treating primary brain tumours.

Studying tumour hypoxia in primary brain tumour can lead identifying patients who may respond less well to standard therapeutic interventions and then in turn research studies to examine the role of hypoxia modifiers. Tumour hypoxia in primary brain tumour can be studied by combining BOLD and ASL sequences which may predict response to radiotherapy.

9.2 Limitations of the study

There are several limitations of this research. There are a small number of patients at each time point and there is a 52% drop out rate by 3 months in the NCF arm and 66% in the MRI arm. This dropout rate is similar to other reported trials in patients undergoing SRS for BM. However, this inherently introduces a bias as patients remaining at 6 months' time point in the study may be the ones with favourable prognosis. One way of reducing the bias is examining patients remaining at the primary end point, i.e., 3 months. In order to reduce this bias, patients included in the analysis were the patients who completed all the assessments in Chapter 7. This reduced the number of patients in the overall analysis. We could overcome this by conducting a much larger study, but this would require multi-centre co-operation and the specialist nature of the CUBRIC scanner means this would be challenging.

Overall survival in this patient cohort is affected by the primary malignancy and the heterogeneity of the patient cohort undergoing treatment with BM. Patients may present with synchronous or metachronous brain disease and often, symptomatic BM are treated before commencing SACT such as chemotherapy or immunotherapy. This is because SACT such as chemotherapy has reduced rates of intracranial response rate compared to

extracranial disease and immunotherapy can cause a disease flare and one of prerequisites for commencing immunotherapy is controlled BM. Patients with a targetable mutation, may be treated with an appropriate TKI with or without SRS. Therefore, at the time of SRS, extracranial disease can either be potentially controllable or controlled. For the former group, disease biology and its potential response to systemic therapy is unknown. There is a need to improve understanding of the cancer biology and predictive biomarkers to therapy to identify poor and good responders to treatment so that patients' treatment can be tailored appropriately. The variability of primary cancer and its treatment can be reduced by looking at specific patient cohorts, for e.g., patients with non-small cell lung cancer undergoing immunotherapy. Studies such as this, may take a long time to recruit and will require multi-centre co-operation. This will be crucial to study long-term NCF changes following SRS.

As far as we are aware, this study is unique in assessing and coupling hippocampal dosimetry in patients undergoing SRS with NCF testing and translational multiparametric MRI analysing structural, functional, physiological and diffusion analysis of the hippocampus, metastases, and surrounding brain parenchyma. As this was planned to be an observational and hypothesis generating study, we measured multiple parameters of NCF test data and MRI measurements, therefore it is difficult to draw meaningful statistical significance in this cohort. The translational MRI changes described in Chapter 7 and 8 need robust validation in larger studies. At the time the study was done, CUBIC has relatively new scanners and phantom calibrations were not carried out. It is now standard that calibration is carried out with a phantom.

In assessing tumour physiology and microenvironment, this study has the drawback of lacking histological confirmation of the BM and matching the physiological measurements with histopathological findings. Performing these MRI sequences in patients with primary brain tumours would allow validation of these findings by histopathological correlation.

Whilst conducting the SRS replanning study, we attempted to reduce the dose as much as possible, however, planning software's function more effectively with a defined dose

constraint. This research has demonstrated a potential dose constraint that future planning studies can validate and aim to achieve.

9.2.1 Contribution from others

This research has had contributions from individuals all of whom have been mentioned in the acknowledgment section. The candidate conducted all of the literature review, MRI analysis of the raw data, NCF data analysis, statistical analysis. Patient recruitment was conducted by the candidate in conjunction with consultant neuro-oncologists treating patients with SRS. For each experimental chapter, the contributions have been specified below:

- Chapter 3 – The radiotherapy replans were carried out by the candidate and reviewed by a physicist and a consultant neuro-oncologist for data integrity.
- Chapter 4, – Physicists and radiographers from CUBRIC advised and assisted the candidate in MRI protocol and analysis method for spectroscopy, ASL, BOLD, DTI and FreeSurfer.
- Chapter 5 – NCF tests were conducted by the same clinical psychologist at each time point, raw scores were calculated by the psychologist and checked by an experienced neuropsychologist. These were further analysed by the candidate.
- Chapter 6, 7, 8 – NCF and MRI work was conducted as described above. Quality of life raw scores were calculated by the candidate.

9.3 Future work

There is a need to understand NTCP of the hippocampus in patients undergoing SRS and fractionated brain radiotherapy further. Trials in this cohort of patients are difficult to recruit and there is a significant dropout rate as discussed in this thesis. Therefore, developing a multi-centre/ multi-national consortium of trial groups that have conducted studies in this cohort of patients and have performed standardised NCF testing as described by the RANO group at the same time point may be the most effective way forward for future studies in patients with BM. The largest of these trials is the most recent trial conducted by Brown *et al*.

Therefore, we would propose retrospectively measuring hippocampal dosimetry in the patients included in that trial followed by combining this dataset to perform NTCP modelling of the hippocampus. A prospective cohort study including hippocampal sparing SRS with baseline and 6- and 12-month NCF for surviving patients with a sub study of advanced MRI would be needed to overcome the multiple confounding factors y*et al*low detailed analysis of a small cohort of patients.

This work has shown the impact of BM and SRS on NCF, and the potential benefit of hippocampal sparing to preserve NCF without affecting tumour control. We have also shown the acceptability of serial NCF and multiparametric MRI studies to patients with brain tumours with a short life expectancy. We have shown the ability to produce high quality, reproducible and reliable MRI images in patient with BMs, and feel that further MRI-based research would be productive in patients with primary brain tumours.

Physiological imaging which provides information about perfusion and oxygenation can identify hypoxic regions. In our study, CBF and BOLD are unable to provide enough information independently about the tumour environment and levels of hypoxia, and thus its impact on progression or response. It is understood that hypoxia in tumours leads to radioresistance and worse prognosis. Hypoxia modifiers have demonstrated a survival advantage in other tumours, for example the BCON trial showed a significantly improved overall survival at 3 years in patients who were treated with carbogen and nicotinamide concurrently with radical radiotherapy compared to the group treated with radiotherapy alone (Song *et al*., 2019). Studying hypoxia and its role in treatment resistance and tumour invasion in BM and primary brain tumours is of research interest. In order to study oxygenation and hypoxia in the tumour, we have designed a study to calculate the oxygen extraction factor in patients with glioma. In this study patients with a diagnosis of glioma will undergo structural and functional MRI to study vascular and metabolic function. This combines BOLD, ASL and quantitative susceptibility mapping. Information from these three sequences will be used in combination to map blood flow, vascular reactivity, and brain oxygen consumption. Data from changes in CBF and BOLD signal from this study in BM

described in this thesis has been used to design the MRI protocol for the follow up study. The aim of this study is to identify areas of hypoxia and correlate this to tumour response.

Understanding microenvironment of primary brain tumour is also of clinical significance. VERDICT, for example, may be able to better direct stereotactic biopsies by identifying cellular areas within the tumour and it could provide an insight into cell radius, intracellular volume, vascular volume, and extracellular and extravascular volume, which can vary according to the tumour and grade particularly in primary brain tumours. This could be utilised in assessing response to therapy and to differentiate between true progression and pseudoprogression. Microstructural imaging may also allow differentiating between grades in inaccessible tumours and support development and design of novel drugs by identifying new therapeutic targets, as our imaging modalities offer the potential to study on-target effects.

9.3.1 Hypothesis for Future Studies

Based on this study, I propose the following hypothesis for future research which needs to be validated with a larger data set in patients with BM:

1. Dose to 0.1 cc of the hippocampus of >5 Gy is a clinically relevant dose constraint associated with decline in NCF at 1 month in patients undergoing SRS.
2. Baseline changes in perfusion of the metastases can predict response to SRS, metastases with low CBF are more likely to respond to SRS.

9.4 Conclusions

The long-term outcome of patients with both primary and secondary brain tumours remains poor and are rightly identified by Cancer Research UK as a cancer of unmet need. I hope this will allow further support of imaging studies which offer a unique, non-invasive window into the tumour, its microenvironment, and the effects of treatment on normal tissue.

Bibliography

AARONSON, N. K., AHMEDZAI, S., BERGMAN, B., BULLINGER, M., CULL, A., DUEZ, N. J., FILIBERTI, A., FLECHTNER, H., FLEISHMAN, S. B., DE HAES, J. C. & *ET AL*. 1993. The European Organization for Research and Treatment of Cancer QLQ-C30: a quality-of-life instrument for use in international clinical trials in oncology. *J Natl Cancer Inst,* 85**,** 365-76.

ACHARYA, M. M., CHRISTIE, L. A., LAN, M. L., GIEDZINSKI, E., FIKE, J. R., ROSI, S. & LIMOLI, C. L. 2011. Human neural stem cell transplantation ameliorates radiation-induced cognitive dysfunction. *Cancer Res,* 71**,** 4834-45.

ACHARYA, M. M., LAN, M. L., KAN, V. H., PATEL, N. H., GIEDZINSKI, E., TSENG, B. P. & LIMOLI, C. L. 2010. Consequences of ionizing radiation-induced damage in human neural stem cells. *Free Radic Biol Med,* 49**,** 1846-55.

ACOSTA-CABRONERO, J. & NESTOR, P. J. 2014. Diffusion tensor imaging in Alzheimer's disease: insights into the limbic-diencephalic network and methodological considerations. *Front Aging Neurosci,* 6**,** 266.

AJITHKUMAR, T., PRICE, S., HORAN, G., BURKE, A. & JEFFERIES, S. 2017. Prevention of radiotherapy-induced neurocognitive dysfunction in survivors of paediatric brain tumours: the potential role of modern imaging and radiotherapy techniques. *The Lancet Oncology,* 18**,** e91-e100.

AL-OKAILI, R. N., KREJZA, J., WANG, S., WOO, J. H. & MELHEM, E. R. 2006. Advanced MR imaging techniques in the diagnosis of intraaxial brain tumors in adults. *Radiographics,* 26 Suppl 1**,** S173-89.

ALEXANDER, E. & LOEFFLER, J. S. 1993. *Stereotactic Radiosurgery* New York, Health Professions Division.

ALI, S., GÓRSKA, Z., DUCHNOWSKA, R. & JASSEM, J. 2021. Molecular Profiles of Brain Metastases: A Focus on Heterogeneity. *Cancers,* 13**,** 2645.

ALLAILI, N., VALABREGUE, R., AUERBACH, E. J., GUILLEMOT, V., YAHIA-CHERIF, L., BARDINET, E., JABOURIAN, M., FOSSATI, P., LEHERICY, S. & MARJANSKA, M. 2015. Single-voxel (1)H spectroscopy in the human hippocampus at 3 T using the LASER sequence: characterization of neurochemical profile and reproducibility. *NMR Biomed,* 28**,** 1209-17.

ALLAN, T. W., FRANCIS, S. T., CABALLERO-GAUDES, C., MORRIS, P. G., LIDDLE, E. B., LIDDLE, P. F., BROOKES, M. J. & GOWLAND, P. A. 2015. Functional Connectivity in MRI Is Driven by Spontaneous BOLD Events. *PLoS One,* 10**,** e0124577.

ALMEIDA-FREITAS, D. B., PINHO, M. C., OTADUY, M. C. G., BRAGA, H. F., MEIRA-FREITAS, D. & DA COSTA LEITE, C. 2014. Assessment of irradiated brain metastases using dynamic contrast-enhanced magnetic resonance imaging. *Neuroradiology,* 56**,** 437-443.

ALSOP, D. C., DETRE, J. A., GOLAY, X., GÜNTHER, M., HENDRIKSE, J., HERNANDEZ-GARCIA, L., LU, H., MACINTOSH, B. J., PARKES, L. M., SMITS, M., OSCH, M. J. P. V., WANG, D. J., WONG, E. C. & ZAHARCHUK, G. 2015. Recommended Implementation of Arterial Spin Labeled Perfusion MRI for Clinical Applications: A consensus of the ISMRM Perfusion Study Group and the European Consortium for ASL in Dementia. *Magnetic Resonance in Medicine,* 73**,** 102-16.

ALTMAN, D. G., MCSHANE, L. M., SAUERBREI, W. & TAUBE, S. E. 2012. Reporting recommendations for tumor marker prognostic studies (REMARK): explanation and elaboration. *BMC Medicine,* 10**,** 51.

ANDERSSON, J. L., SKARE, S. & ASHBURNER, J. 2003. How to correct susceptibility distortions in spin-echo echo-planar images: application to diffusion tensor imaging. *Neuroimage,* 20**,** 870-88.

ANDERSSON, J. L. R. & SOTIROPOULOS, S. N. 2016. An integrated approach to correction for off-resonance effects and subject movement in diffusion MR imaging. *Neuroimage,* 125**,** 1063-1078.

ANDREWS, D. W., SCOTT, C. B., SPERDUTO, P. W., FLANDERS, A. E., GASPAR, L. E., SCHELL, M. C., WERNER-WASIK, M., DEMAS, W., RYU, J., BAHARY, J.-P., SOUHAMI, L., ROTMAN, M., MEHTA, M. P. & CURRAN, W. J. 2004. Whole brain radiation therapy with or without stereotactic radiosurgery boost for patients with one to three brain metastases: phase III results of the RTOG 9508 randomised trial. *The Lancet,* 363**,** 1665-1672.

ANDREWS, R. N., METHENY-BARLOW, L. J., PEIFFER, A. M., HANBURY, D. B., TOOZE, J. A., BOURLAND, J. D., HAMPSON, R. E., DEADWYLER, S. A. & CLINE, J. M. 2017. Cerebrovascular Remodeling and Neuroinflammation is a Late Effect of Radiation-Induced Brain Injury in Non-Human Primates. *Radiat Res,* 187**,** 599-611.

ANTONIA, S. J., VILLEGAS, A., DANIEL, D., VICENTE, D., MURAKAMI, S., HUI, R., KURATA, T., CHIAPPORI, A., LEE, K. H., DE WIT, M., CHO, B. C., BOURHABA, M., QUANTIN, X., TOKITO, T., MEKHAIL, T., PLANCHARD, D., KIM, Y.-C., KARAPETIS, C. S., HIRET, S., OSTOROS, G., KUBOTA, K., GRAY, J. E., PAZ-ARES, L., DE CASTRO CARPEÑO, J., FAIVRE-FINN, C., RECK, M., VANSTEENKISTE, J., SPIGEL, D. R., WADSWORTH, C., MELILLO, G., TABOADA, M., DENNIS, P. A. & ÖZGÜROĞLU, M. 2018. Overall Survival with Durvalumab after Chemoradiotherapy in Stage III NSCLC. *New England Journal of Medicine,* 379**,** 2342-2350.

AOYAMA, H., TAGO, M., SHIRATO, H. & JAPANESE RADIATION ONCOLOGY STUDY GROUP, I. 2015. Stereotactic Radiosurgery With or Without Whole-Brain Radiotherapy for Brain Metastases: Secondary Analysis of the JROSG 99-1 Randomized Clinical Trial. *JAMA Oncol,* 1**,** 457-64.

ARBIT, E., WROŃSKI, M., BURT, M. & GALICICH, J. H. 1995. The treatment of patients with recurrent brain metastases. A retrospective analysis of 109 patients with nonsmall cell lung cancer. *Cancer,* 76**,** 765-773.

ARMSTRONG, C. L., HUNTER, J. V., HACKNEY, D., SHABBOUT, M., LUSTIG, R. W., GOLDSTEIN, B., WERNER-WASIK, M. & CURRAN, W. J., JR. 2005. MRI changes due to early-delayed conformal radiotherapy and postsurgical effects in patients with brain tumors. *Int J Radiat Oncol Biol Phys,* 63**,** 56-63.

ASHPOLE, N. M., WARRINGTON, J. P., MITSCHELEN, M. C., YAN, H., SOSNOWSKA, D., GAUTAM, T., FARLEY, J. A., CSISZAR, A., UNGVARI, Z. & SONNTAG, W. E. 2014. Systemic influences contribute to prolonged microvascular rarefaction after brain irradiation: a role for endothelial progenitor cells. *Am J Physiol Heart Circ Physiol,* 307**,** H858-68.

ASSAF, Y. & BASSER, P. J. 2005. Composite hindered and restricted model of diffusion (CHARMED) MR imaging of the human brain. *NeuroImage,* 27**,** 48-58.

ASSAF, Y. & PASTERNAK, O. 2008. Diffusion tensor imaging (DTI)-based white matter mapping in brain research: a review. *J Mol Neurosci,* 34**,** 51-61.

AUSTIN, B. P., NAIR, V. A., MEIER, T. B., XU, G., ROWLEY, H. A., CARLSSON, C. M., JOHNSON, S. C. & PRABHAKARAN, V. 2011. Effects of hypoperfusion in Alzheimer's disease. *J Alzheimers Dis,* 26 Suppl 3**,** 123-33.

AWAD, R., FOGARTY, G., HONG, A., KELLY, P., NG, D., SANTOS, D. & HAYDU, L. 2013. Hippocampal avoidance with volumetric modulated arc therapy in melanoma brain metastases - the first Australian experience. *Radiation oncology (London, England),* 8**,** 62.

BACHELOT, T., ROMIEU, G., CAMPONE, M., DIÉRAS, V., CROPET, C., DALENC, F., JIMENEZ, M., LE RHUN, E., PIERGA, J. Y., GONÇALVES, A., LEHEURTEUR, M., DOMONT, J., GUTIERREZ, M., CURÉ, H., FERRERO, J. M. & LABBE-DEVILLIERS, C. 2013. Lapatinib plus capecitabine in patients with previously untreated brain metastases from HER2-positive metastatic breast cancer (LANDSCAPE): a single-group phase 2 study. *Lancet Oncol,* 14**,** 64-71.

BAISDEN, J. M., BENEDICT, S.H., SHENG, K., READ, P.W.., AND LARNER, J.M, 2007. Helical TomoTherapy in the treatment of central nervous system metastasis. *Neurosurg Focus,* 22.

BAMMER, R. 2003. Basic principles of diffusion-weighted imaging. *Eur J Radiol,* 45**,** 169-84.

BARNHOLTZ-SLOAN, J. S., SLOAN, A. E., DAVIS, F. G., VIGNEAU, F. D., LAI, P. & SAWAYA, R. E. 2004. Incidence proportions of brain metastases in patients diagnosed (1973 to 2001) in the Metropolitan Detroit Cancer Surveillance System. *J Clin Oncol,* 22**,** 2865-72.

BECKMANN, C. F., DELUCA, M., DEVLIN, J. T. & SMITH, S. M. 2005. Investigations into resting-state connectivity using independent component analysis. *Philos Trans R Soc Lond B Biol Sci,* 360**,** 1001-13.

BELKONEN, S. 2011. Hopkins Verbal Learning Test. *In:* KREUTZER, J. S., DELUCA, J. & CAPLAN, B. (eds.) *Encyclopedia of Clinical Neuropsychology.* New York, NY: Springer New York.

BENEDICT, R. H., SCHRETLEN, D., GRONINGER, L. & BRANDT, J. 1998. Hopkins Verbal Learning Test–Revised: Normative data and analysis of inter-form and test-retest reliability. *The Clinical Neuropsychologist,* 12**,** 43-55.

BINDAL, R. K., SAWAYA, R., LEAVENS, M. E., HESS, K. R. & TAYLOR, S. H. 1995. Reoperation for recurrent metastatic brain tumors. *Journal of Neurosurgery,* 83**,** 600-604.

BISWAL, B., YETKIN, F. Z., HAUGHTON, V. M. & HYDE, J. S. 1995. Functional connectivity in the motor cortex of resting human brain using echo-planar MRI. *Magn Reson Med,* 34**,** 537-41.

BLOCK, W., TRABER, F., VON WIDDERN, O., METTEN, M., SCHILD, H., MAIER, W., ZOBEL, A. & JESSEN, F. 2009. Proton MR spectroscopy of the hippocampus at 3 T in patients with unipolar major depressive disorder: correlates and predictors of treatment response. *Int J Neuropsychopharmacol,* 12**,** 415-22.

BLÜML, S. 2013. Magnetic Resonance Spectroscopy: Basics. *MR Spectroscopy of Pediatric Brain Disorders.*

BOBINSKI, M., DE LEON, M. J., WEGIEL, J., DESANTI, S., CONVIT, A., SAINT LOUIS, L. A., RUSINEK, H. & WISNIEWSKI✠, H. M. 1999. The histological validation of post mortem magnetic resonance imaging-determined hippocampal volume in Alzheimer's disease. *Neuroscience,* 95**,** 721-725.

BOGOMOLNY, D. L., PETROVICH, N. M., HOU, B. L., PECK, K. K., KIM, M. J. J. & HOLODNY, A. I. 2004. Functional MRI in the Brain Tumor Patient. *Topics in Magnetic Resonance Imaging,* 15**,** 325-335.

BONET-CARNE, E., JOHNSTON, E., DADUCCI, A., JACOBS, J. G., FREEMAN, A., ATKINSON, D., HAWKES, D. J., PUNWANI, S., ALEXANDER, D. C. & PANAGIOTAKI, E. 2019. VERDICT-AMICO: Ultrafast fitting algorithm for non-invasive prostate microstructure characterization. *NMR Biomed,* 32**,** e4019.

BOULEFTOUR, W., ROWINSKI, E., LOUATI, S., SOTTON, S., WOZNY, A. S., MORENO-ACOSTA, P., MERY, B., RODRIGUEZ-LAFRASSE, C. & MAGNE, N. 2021. A Review of the Role of Hypoxia in Radioresistance in Cancer Therapy. *Med Sci Monit,* 27**,** e934116.

BRACHT, T., JONES, D. K., BELLS, S., WALTHER, S., DRAKESMITH, M. & LINDEN, D. 2016. Myelination of the right parahippocampal cingulum is associated with physical activity in young healthy adults. *Brain Struct Funct,* 221**,** 4537-4548.

BROWN, J. M., CARLSON, D. J. & BRENNER, D. J. 2014. The tumor radiobiology of SRS and SBRT: are more than the 5 Rs involved? *Int J Radiat Oncol Biol Phys,* 88**,** 254-62.

BROWN, P. D., BALLMAN, K. V., CERHAN, J. H., ANDERSON, S. K., CARRERO, X. W., WHITTON, A. C., GREENSPOON, J., PARNEY, I. F., LAACK, N. N. I., ASHMAN, J. B., BAHARY, J. P., HADJIPANAYIS, C. G., URBANIC, J. J., BARKER, F. G., 2ND, FARACE, E., KHUNTIA, D., GIANNINI, C., BUCKNER, J. C., GALANIS, E. & ROBERGE, D. 2017. Postoperative stereotactic radiosurgery compared with whole brain radiotherapy for resected metastatic brain disease (NCCTG N107C/CEC·3): a multicentre, randomised, controlled, phase 3 trial. *Lancet Oncol,* 18**,** 1049-1060.

BROWN, P. D., BROWN, C. A., POLLOCK, B. E., GORMAN, D. A. & FOOTE, R. L. 2002. Stereotactic Radiosurgery for Patients with “Radioresistant” Brain Metastases. *Neurosurgery,* 51**,** 656-667.

BROWN, P. D., JAECKLE, K., BALLMAN, K. V., FARACE, E., CERHAN, J. H., ANDERSON, S. K., CARRERO, X. W., BARKER, F. G., 2ND, DEMING, R., BURRI, S. H., MENARD, C., CHUNG, C., STIEBER, V. W., POLLOCK, B. E., GALANIS, E., BUCKNER, J. C. & ASHER, A. L. 2016a. Effect of Radiosurgery Alone vs Radiosurgery With Whole Brain Radiation Therapy on Cognitive Function in Patients With 1 to 3 Brain Metastases: A Randomized Clinical Trial. *JAMA,* 316**,** 401-409.

BROWN, P. D., JAECKLE, K., BALLMAN, K. V., FARACE, E., CERHAN, J. H., ANDERSON, S. K., CARRERO, X. W., BARKER, F. G., 2ND, DEMING, R., BURRI, S. H., MENARD, C., CHUNG, C., STIEBER, V. W., POLLOCK, B. E., GALANIS, E., BUCKNER, J. C. & ASHER, A. L. 2016b. Effect of Radiosurgery Alone vs Radiosurgery With Whole Brain Radiation Therapy on Cognitive Function in Patients With 1 to 3 Brain Metastases: A Randomized Clinical Trial. *JAMA,* 316**,** 401-9.

BROWN, P. D., PUGH, S., LAACK, N. N., WEFEL, J. S., KHUNTIA, D., MEYERS, C., CHOUCAIR, A., FOX, S., SUH, J. H., ROBERGE, D., KAVADI, V., BENTZEN, S. M., MEHTA, M. P. & WATKINS-BRUNER, D. 2013. Memantine for the prevention of cognitive dysfunction in patients receiving whole-brain radiotherapy: a randomized, double-blind, placebo-controlled trial. *Neuro Oncol,* 15**,** 1429-37.

BRUMMELMAN, P., SATTLER, M. G. A., MEINERS, L. C., ELDERSON, M. F., DULLAART, R. P. F., VAN DEN BERG, G., KOERTS, J., TUCHA, O., WOLFFENBUTTEL, B. H. R., VAN DEN BERGH, A. C. M. & VAN BEEK, A. P. 2012. Cognitive performance after postoperative

pituitary radiotherapy: a dosimetric study of the hippocampus and the prefrontal cortex. *European journal of endocrinology,* 166 2**,** 171-9.
BUBB, E. J., METZLER-BADDELEY, C. & AGGLETON, J. P. 2018. The cingulum bundle: Anatomy, function, and dysfunction. *Neuroscience & Biobehavioral Reviews,* 92**,** 104-127.
BULAKASI, N. 2009. Diffusion-tensor imaging in brain tumors. *Imaging Med,* 1**,** 155-171.
BULAKBASI, N., KOCAOGLU, M., ORS, F., TAYFUN, C. & UÇÖZ, T. 2003. Combination of single-voxel proton MR spectroscopy and apparent diffusion coefficient calculation in the evaluation of common brain tumors. *AJNR Am J Neuroradiol,* 24**,** 225-33.
BURHAN, A. M., BARTHA, R., BOCTI, C., BORRIE, M., LAFORCE, R. J. & SOUCY, J. 2013. Role of emerging neuroimaging modalities in patients with cognitive impairment: a review from the Canadian Consensus Conference on the Diagnosis and Treatment of Dementia 2012. *Alzheimer's Research & Therapy,* 5.
BURMAN, C., KUTCHER, G. J., EMAMI, B. & GOITEIN, M. 1991. Fitting of normal tissue tolerance data to an analytic function. *Int J Radiat Oncol Biol Phys,* 21**,** 123-35.
BYRNE, F. R. M. 2000. The Hopkins Verbal Learning Test had high sensitivity and good specificity for detecting mild dementia in older people. *International Joural of Geriatric Psychiatry,* 15**,** 17-24.
CALLI, C., KITIS, O., YUNTEN, N., YURTSEVEN, T., ISLEKEL, S. & AKALIN, T. 2006. Perfusion and diffusion MR imaging in enhancing malignant cerebral tumors. *Eur J Radiol,* 58**,** 394-403.
CALMON, R., PUGET, S., VARLET, P., DANGOULOFF-ROS, V., BLAUWBLOMME, T., BECCARIA, K., GREVENT, D., SAINTE-ROSE, C., CASTEL, D., DEBILY, M. A., DUFOUR, C., BOLLE, S., DHERMAIN, F., SAITOVITCH, A., ZILBOVICIUS, M., BRUNELLE, F., GRILL, J. & BODDAERT, N. 2018. Cerebral blood flow changes after radiation therapy identifies pseudoprogression in diffuse intrinsic pontine gliomas. *Neuro Oncol,* 20**,** 994-1002.
CÁNOVAS, R., LEÓN, I., SERRANO, P., ROLDÁN, M. D. & CIMADEVILLA, J. M. 2011. Spatial navigation impairment in patients with refractory temporal lobe epilepsy: evidence from a new virtual reality-based task. *Epilepsy Behav,* 22**,** 364-9.
CASERTA, M. T., RAGIN, A., HERMIDA, A. P., AHRENS, R. J. & WISE, L. 2008. Single voxel magnetic resonance spectroscopy at 3 Tesla in a memory disorders clinic: early right hippocampal NAA/Cr loss in mildly impaired subjects. *Psychiatry Res,* 164**,** 154-9.
CERESOLI, G. L., CAPPUZZO, F., GREGORC, V., BARTOLINI, S., CRINÒ, L. & VILLA, E. 2004. Gefitinib in patients with brain metastases from non-small-cell lung cancer: a prospective trial. *Ann Oncol,* 15**,** 1042-7.
CHAN, K. C., KHONG, P. L., CHEUNG, M. M., WANG, S., CAI, K. X. & WU, E. X. 2009. MRI of late microstructural and metabolic alterations in radiation-induced brain injuries. *J Magn Reson Imaging,* 29**,** 1013-20.
CHANG, E. L., WEFEL, J. S., HESS, K. R., ALLEN, P. K., LANG, F. F., KORNGUTH, D. G., ARBUCKLE, R. B., SWINT, J. M., SHIU, A. S., MAOR, M. H. & MEYERS, C. A. 2009. Neurocognition in patients with brain metastases treated with radiosurgery or radiosurgery plus whole-brain irradiation: a randomised controlled trial. *The Lancet Oncology,* 10**,** 1037-1044.
CHANG, J. S., MA, L., BARANI, I. J., MCDERMOTT, M. W., SNEED, P. K. & LARSON, D. A. 2016. Hippocampal Dose With Radiosurgery for Multiple Intracranial Targets: The Rationale for Proactive Beam Shaping. *Technology in cancer research & treatment,* 15**,** 555-559.
CHAPPELL, M., MACINTOSH, B. & OKELL, T. 2017. *Introduction to Perfusion Quantification using Arterial Spin Labelling,* Oxford, Oxford University Press.

CHEN, G., HUYNH, M., CHEN, A., FEHRENBACHER, L., GANDARA, D. & LAU, D. 2008. Chemotherapy for brain metastases in small-cell lung cancer. *Clin Lung Cancer,* 9**,** 35-8.

CHEN, X., YIN, X., AI, L., CHEN, Q., LI, S. & DAI, J. 2012. Differentiation between brain glioblastoma multiforme and solitary metastasis: qualitative and quantitative analysis based on routine MR imaging. *American journal of neuroradiology,* 33**,** 1907-1912.

CHEUNG, M., CHAN, A. S., LAW, S. C., CHAN, J. H. & TSE, V. K. 2000. Cognitive function of patients with nasopharyngeal carcinoma with and without temporal lobe radionecrosis. *Arch Neurol,* 57**,** 1347-52.

CHINCARINI, A., SENSI, F., REI, L., GEMME, G., SQUARCIA, S., LONGO, R., BRUN, F., TANGARO, S., BELLOTTI, R., AMOROSO, N., BOCCHETTA, M., REDOLFI, A., BOSCO, P., BOCCARDI, M., FRISONI, G. B. & NOBILI, F. 2016. Integrating longitudinal information in hippocampal volume measurements for the early detection of Alzheimer's disease. *NeuroImage,* 125**,** 834-847.

CHOO, I. H., LEE, D. Y., OH, J. S., LEE, J. S., LEE, D. S., SONG, I. C., YOUN, J. C., KIM, S. G., KIM, K. W., JHOO, J. H. & WOO, J. I. 2010. Posterior cingulate cortex atrophy and regional cingulum disruption in mild cognitive impairment and Alzheimer's disease. *Neurobiol Aging,* 31**,** 772-9.

COLACO, R.J., MARTIN, P., KLUGER, H.M., YU, J.B., AND CHIANG, V.L. 2016. Does immunotherapy increase the rate of radiation necrosis after radiosurgical treatment of brain metastases?. *J Neurosurg,* 125 (1), 17-23

CONNOR, M., KARUNAMUNI, R., MCDONALD, C., WHITE, N., PETTERSSON, N., MOISEENKO, V., SEIBERT, T., MARSHALL, D., CERVINO, L., BARTSCH, H., KUPERMAN, J., MURZIN, V., KRISHNAN, A., FARID, N., DALE, A. & HATTANGADI-GLUTH, J. 2016. Dose-dependent white matter damage after brain radiotherapy. *Radiother Oncol,* 121**,** 209-216.

CONSORTIUM, S. 2019 Stereotactic Ablative Body Radiation Therapy (SABR): A Resource. UK

CONSORTIUM, S. U. 2019. Stereotactic Ablative Body Radiation Therapy (SABR): A Resource.

CRINÒ, L., BRONTE, G., BIDOLI, P., CRAVERO, P., MINENZA, E., CORTESI, E., GARASSINO, M. C., PROTO, C., CAPPUZZO, F., GROSSI, F., TONINI, G., SAROBBA, M. G., PINOTTI, G., NUMICO, G., SAMARITANI, R., CIUFFREDA, L., FRASSOLDATI, A., BREGNI, M., SANTO, A., PIANTEDOSI, F., ILLIANO, A., DE MARINIS, F., TAMBERI, S., GIANNARELLI, D. & DELMONTE, A. 2019. Nivolumab and brain metastases in patients with advanced non-squamous non-small cell lung cancer. *Lung Cancer,* 129**,** 35-40.

CRUK. 2015. *Cancer Statistics for the UK* [Online]. United Kingdom: Cancer Research UK Available: https://www.cancerresearchuk.org/health-professional/cancer-statistics-for-the-uk#heading-Zero [Accessed 30/09/2021 2021].

DADUCCI, A., CANALES-RODRIGUEZ, E. J., ZHANG, H., DYRBY, T. B., ALEXANDER, D. C. & THIRAN, J. P. 2015. Accelerated Microstructure Imaging via Convex Optimization (AMICO) from diffusion MRI data. *Neuroimage,* 105**,** 32-44.

DALE, A. M., FISCHL, B. & SERENO, M. I. 1999. Cortical surface-based analysis. I. Segmentation and surface reconstruction. *Neuroimage,* 9**,** 179-94.

DAMOISEAUX, J. S., ROMBOUTS, S. A., BARKHOF, F., SCHELTENS, P., STAM, C. J., SMITH, S. M. & BECKMANN, C. F. 2006. Consistent resting-state networks across healthy subjects. *Proc Natl Acad Sci U S A,* 103**,** 13848-53.

DANIELA FALCO, M., GIANCATERINO, S., D'ANDREA, M., GIMENEZ DE LORENZO, R., TRIGNANI, M., CARAVATTA, L., DI CARLO, C., DI BIASE, S., ALLAJBEJ, A. & GENOVESI, D.

2018. Hippocampal sparing approach in fractionated stereotactic brain VMAT radio therapy: A retrospective feasibility analysis. *J Appl Clin Med Phys,* 19**,** 86-93.

DAVIES, M. A., SAIAG, P., ROBERT, C., GROB, J. J., FLAHERTY, K. T., ARANCE, A., CHIARION-SILENI, V., THOMAS, L., LESIMPLE, T., MORTIER, L., MOSCHOS, S. J., HOGG, D., MÁRQUEZ-RODAS, I., DEL VECCHIO, M., LEBBÉ, C., MEYER, N., ZHANG, Y., HUANG, Y., MOOKERJEE, B. & LONG, G. V. 2017. Dabrafenib plus trametinib in patients with BRAF(V600)-mutant melanoma brain metastases (COMBI-MB): a multicentre, multicohort, open-label, phase 2 trial. *Lancet Oncol,* 18**,** 863-873.

DE LUCA, M., BECKMANN, C. F., DE STEFANO, N., MATTHEWS, P. M. & SMITH, S. M. 2006. fMRI resting state networks define distinct modes of long-distance interactions in the human brain. *Neuroimage,* 29**,** 1359-67.

DEANGELIS LM, D. J., POSNER JB 1989. Radiation-induced dementia in patients cured of brain metastases. *Neurology,* 39**,** 789-796.

DEASY, J. O., BLANCO, A. I. & CLARK, V. H. 2003. CERR: A computational environment for radiotherapy research. *Medical Physics,* 30**,** 979-985.

DEBOWSKI M. 2018. *Brain lobes - annotated MRI. Case study, Radiopaedia.org* [Online]. [Accessed 26 November 2023 2023].

DEIBLER, A. R., POLLOCK, J. M., KRAFT, R. A., TAN, H., BURDETTE, J. H. & MALDJIAN, J. A. 2008. Arterial Spin-Labeling in Routine Clinical Practice, Part 2: Hypoperfusion Patterns. *American Journal of Neuroradiology,* 29**,** 1235-1241.

DELL'ACQUA, F., SCIFO, P., RIZZO, G., CATANI, M., SIMMONS, A., SCOTTI, G. & FAZIO, F. 2010. A modified damped Richardson–Lucy algorithm to reduce isotropic background effects in spherical deconvolution. *NeuroImage,* 49**,** 1446-1458.

DI CARLO, C., TRIGNANI, M., CARAVATTA, L., VINCIGUERRA, A., AUGURIO, A., PERROTTI, F., DI TOMMASO, M., NUZZO, M., GIANCATERINO, S., FALCO, M. D. & GENOVESI, D. 2018. Hippocampal sparing in stereotactic radiotherapy for brain metastases: To contour or not contour the hippocampus? *Cancer radiotherapie : journal de la Societe francaise de radiotherapie oncologique,* 22**,** 120-125.

DOLUI, S., VIDORRETA, M., WANG, Z., NASRALLAH, I. M., ALAVI, A., WOLK, D. A. & DETRE, J. A. 2017. Comparison of PASL, PCASL, and background-suppressed 3D PCASL in mild cognitive impairment. *Hum Brain Mapp,* 38**,** 5260-5273.

DRISCOLL, I., HAMILTON, D. A., PETROPOULOS, H., YEO, R. A., BROOKS, W. M., BAUMGARTNER, R. N. & SUTHERLAND, R. J. 2003. The Aging Hippocampus: Cognitive, Biochemical and Structural Findings. *Cerebral Cortex,* 13**,** 1344-1351.

DURMO, F., LATT, J., RYDELIUS, A., ENGELHOLM, S., KINHULT, S., ASKANER, K., ENGLUND, E., BENGZON, J., NILSSON, M., BJORKMAN-BURTSCHER, I. M., CHENEVERT, T., KNUTSSON, L. & SUNDGREN, P. C. 2018. Brain Tumor Characterization Using Multibiometric Evaluation of MRI. *Tomography,* 4**,** 14-25.

DWAN, T. M., OWNSWORTH, T., CHAMBERS, S., WALKER, D. G. & SHUM, D. H. 2015. Neuropsychological assessment of individuals with brain tumor: comparison of approaches used in the classification of impairment. *Front Oncol,* 5**,** 56.

ELAHI, F. M., MARX, G., COBIGO, Y., STAFFARONI, A. M., KORNAK, J., TOSUN, D., BOXER, A. L., KRAMER, J. H., MILLER, B. L. & ROSEN, H. J. 2017. Longitudinal white matter change in frontotemporal dementia subtypes and sporadic late ons*et al*zheimer's disease. *Neuroimage Clin,* 16**,** 595-603.

EMAMI, B. 2013. Tolerance of Normal Tissue to Therapeutic Radiation. *Reports of Radiotherapy and Oncology,* 1**,** 35-48.

ESTÈVE, F., RUBIN, C., GRAND, S., KOLODIÉ, H. & LE BAS, J. F. 1998. Transient metabolic changes observed with proton MR spectroscopy in normal human brain after radiation therapy. *Int J Radiat Oncol Biol Phys,* 40**,** 279-86.

FABIAN, M. & WALKER, M. 2019. The neuropathology of brain metastases. *Diagnostic Histopathology,* 25**,** 1-7.

FAYERS, P. & BOTTOMLEY, A. 2002. Quality of life research within the EORTC-the EORTC QLQ-C30. European Organisation for Research and Treatment of Cancer. *Eur J Cancer,* 38 Suppl 4**,** S125-33.

FEUVRET, L., NOEL, G., MAZERON, J. J. & BEY, P. 2006. Conformity index: a review. *Int J Radiat Oncol Biol Phys,* 64**,** 333-42.

FIELDS, R. D. 2008. White matter in learning, cognition and psychiatric disorders. *Trends Neurosci,* 31**,** 361-70.

FISCHL, B., SALAT, D. H., BUSA, E., ALBERT, M., DIETERICH, M., HASELGROVE, C., VAN DER KOUWE, A., KILLIANY, R., KENNEDY, D., KLAVENESS, S., MONTILLO, A., MAKRIS, N., ROSEN, B. & DALE, A. M. 2002. Whole brain segmentation: automated labeling of neuroanatomical structures in the human brain. *Neuron,* 33**,** 341-55.

FOX, M. D., SNYDER, A. Z., VINCENT, J. L., CORBETTA, M., VAN ESSEN, D. C. & RAICHLE, M. E. 2005. The human brain is intrinsically organized into dynamic, anticorrelated functional networks. *Proc Natl Acad Sci U S A,* 102**,** 9673-8.

FREDERIK VERNIMMEN, M. S. M. S. 2014. Stereotactic Radiotherapy in the Management of Epilepsy. *International Journal of Neurorehabilitation,* 01.

GALLDIKS, N., KOCHER, M., CECCON, G., WERNER, J. M., BRUNN, A., DECKERT, M., POPE, W. B., SOFFIETTI, R., LE RHUN, E., WELLER, M., TONN, J. C., FINK, G. R. & LANGEN, K. J. 2020. Imaging challenges of immunotherapy and targeted therapy in patients with brain metastases: response, progression, and pseudoprogression. *Neuro Oncol,* 22**,** 17-30.

GARCIA-BARROS, M., PARIS, F., CORDON-CARDO, C., LYDEN, D., RAFII, S., HAIMOVITZ-FRIEDMAN, A., FUKS, Z. & KOLESNICK, R. 2003. Tumor response to radiotherapy regulated by endothelial cell apoptosis. *Science,* 300**,** 1155-9.

GASPAR, L., SCOTT, C., ROTMAN, M., ASBELL, S., PHILLIPS, T., WASSERMAN, T., MCKENNA, W. G. & BYHARDT, R. 1997. Recursive partitioning analysis (RPA) of prognostic factors in three Radiation Therapy Oncology Group (RTOG) brain metastases trials. *Int J Radiat Oncol Biol Phys,* 37**,** 745-51.

GAVRILOVIC, I. T. & POSNER, J. B. 2005. Brain metastases: epidemiology and pathophysiology. *J Neurooncol,* 75**,** 5-14.

GERRARD, G. E. & FRANKS, K. N. 2004. Overview of the diagnosis and management of brain, spine, and meningeal metastases. *Journal of Neurology, Neurosurgery & Psychiatry,* 75**,** ii37-ii42.

GERSTENECKER, A., NABORS, L. B., MENESES, K., FIVEASH, J. B., MARSON, D. C., CUTTER, G., MARTIN, R. C., MEYERS, C. A. & TRIEBEL, K. L. 2014. Cognition in patients with newly diagnosed brain metastasis: profiles and implications. *J Neurooncol,* 120**,** 179-85.

GLASSER, M. F., SOTIROPOULOS, S. N., WILSON, J. A., COALSON, T. S., FISCHL, B., ANDERSSON, J. L., XU, J., JBABDI, S., WEBSTER, M., POLIMENI, J. R., VAN ESSEN, D. C.

& JENKINSON, M. 2013. The minimal preprocessing pipelines for the Human Connectome Project. *Neuroimage,* 80**,** 105-24.

GLIKMANN-JOHNSTON, Y., SALING, M. M., CHEN, J., COOPER, K. A., BEARE, R. J. & REUTENS, D. C. 2008. Structural and functional correlates of unilateral mesial temporal lobe spatial memory impairment. *Brain,* 131**,** 3006-18.

GOLDBERG, S. B., GETTINGER, S. N., MAHAJAN, A., CHIANG, A. C., HERBST, R. S., SZNOL, M., TSIOURIS, A. J., COHEN, J., VORTMEYER, A., JILAVEANU, L., YU, J., HEGDE, U., SPEAKER, S., MADURA, M., RALABATE, A., RIVERA, A., ROWEN, E., GERRISH, H., YAO, X., CHIANG, V. & KLUGER, H. M. 2016. Pembrolizumab for patients with melanoma or non-small-cell lung cancer and untreated brain metastases: early analysis of a non-randomised, open-label, phase 2 trial. *Lancet Oncol,* 17**,** 976-983.

GONDI, V., HERMANN, B. P., MEHTA, M. P. & TOME, W. A. 2012. Hippocampal dosimetry predicts neurocognitive function impairment after fractionated stereotactic radiotherapy for benign or low-grade adult brain tumors. *Int J Radiat Oncol Biol Phys,* 83**,** e487-93.

GONDI, V., PUGH, S. L., TOME, W. A., CAINE, C., CORN, B., KANNER, A., ROWLEY, H., KUNDAPUR, V., DENITTIS, A., GREENSPOON, J. N., KONSKI, A. A., BAUMAN, G. S., SHAH, S., SHI, W., WENDLAND, M., KACHNIC, L. & MEHTA, M. P. 2014a. Preservation of memory with conformal avoidance of the hippocampal neural stem-cell compartment during whole-brain radiotherapy for brain metastases (RTOG 0933): a phase II multi-institutional trial. *J Clin Oncol,* 32**,** 3810-6.

GONDI, V., TOME, W. A., ROWLEY, H. A. & MEHTA, M. P. 2014b. Hippocampal Contouring: A Contouring Atlas for RTOG 0933.

GOSS, G., TSAI, C. M., SHEPHERD, F. A., AHN, M. J., BAZHENOVA, L., CRINO, L., DE MARINIS, F., FELIP, E., MORABITO, A., HODGE, R., CANTARINI, M., JOHNSON, M., MITSUDOMI, T., JANNE, P. A. & YANG, J. C. 2018. CNS response to osimertinib in patients with T790M-positive advanced NSCLC: pooled data from two phase II trials. *Ann Oncol,* 29**,** 687-693.

GREENE-SCHLOESSER, D., ROBBINS, M. E., PEIFFER, A. M., SHAW, E. G., WHEELER, K. T. & CHAN, M. D. 2012. Radiation-induced brain injury: A review. *Front Oncol,* 2**,** 73.

GREICIUS, M. D., KRASNOW, B., REISS, A. L. & MENON, V. 2003. Functional connectivity in the resting brain: a network analysis of the default mode hypothesis. *Proc Natl Acad Sci U S A,* 100**,** 253-8.

GRESS, D. R. 2001. Aging and Dementia: More Gray Hair and Less Gray Matter. *American Journal of Neuroradiology,* 22**,** 1641-1642.

GRISWOLD, M. A., JAKOB, P. M., HEIDEMANN, R. M., NITTKA, M., JELLUS, V., WANG, J., KIEFER, B. & HAASE, A. 2002. Generalized autocalibrating partially parallel acquisitions (GRAPPA). *Magnetic Resonance in Medicine,* 47**,** 1202-1210.

GUSSEW, A., ERDTEL, M., HIEPE, P., RZANNY, R. & REICHENBACH, J. R. 2012. Absolute quantitation of brain metabolites with respect to heterogeneous tissue compositions in 1H-MR spectroscopic volumes. *Magnetic Resonance Materials in Physics, Biology and Medicine,* 25**,** 321-333.

HAKYEMEZ, B., ERDOGAN, C., BOLCA, N., YILDIRIM, N., GOKALP, G. & PARLAK, M. 2006. Evaluation of different cerebral mass lesions by perfusion-weighted MR imaging. *Journal of magnetic resonance imaging : JMRI,* 24**,** 817-824.

HAKYEMEZ, B., ERDOGAN, C., GOKALP, G., DUSAK, A. & PARLAK, M. 2010. Solitary metastases and high-grade gliomas: radiological differentiation by morphometric analysis and perfusion-weighted MRI. *Clin Radiol,* 65**,** 15-20.

HART, M. G., GRANT, R., WALKER, M. & DICKINSON, H. 2005. Surgical resection and whole brain radiation therapy versus whole brain radiation therapy alone for single brain metastases. *Cochrane Database Syst Rev***,** CD003292.

HASHEMI, R. H., BRADLEY, W. G. & LISANTI, C. J. 2010. *MRI: The Basics* United States of America Lippincott Williams and Wilkins

HASTINGS, R. S., PARSEY, R. V., OQUENDO, M. A., ARANGO, V. & MANN, J. J. 2004. Volumetric Analysis of the Prefrontal Cortex, Amygdala, and Hippocampus in Major Depression. *Neuropsychopharmacology,* 29**,** 952-959.

HELD, K. D. 2006. *Radiobiology for the Radiologist, by Eric J. Hall and Amato J. Giaccia,* USA, Lippincott Williams & Wilkins.

HENSCHEL, L., CONJETI, S., ESTRADA, S., DIERS, K., FISCHL, B. & REUTER, M. 2020. FastSurfer - A fast and accurate deep learning based neuroimaging pipeline. *NeuroImage,* 219**,** 117012.

HERMAN, M. A., TREMONT-LUKATS, I., MEYERS, C. A., TRASK, D. D., FROSETH, C., RENSCHLER, M. F. & MEHTA, M. P. 2003. Neurocognitive and functional assessment of patients with brain metastases: a pilot study. *Am J Clin Oncol,* 26**,** 273-9.

HIDA, T., NOKIHARA, H., KONDO, M., KIM, Y. H., AZUMA, K., SETO, T., TAKIGUCHI, Y., NISHIO, M., YOSHIOKA, H., IMAMURA, F., HOTTA, K., WATANABE, S., GOTO, K., SATOUCHI, M., KOZUKI, T., SHUKUYA, T., NAKAGAWA, K., MITSUDOMI, T., YAMAMOTO, N., ASAKAWA, T., ASABE, R., TANAKA, T. & TAMURA, T. 2017. Alectinib versus crizotinib in patients with ALK-positive non-small-cell lung cancer (J-ALEX): an open-label, randomised phase 3 trial. *Lancet,* 390**,** 29-39.

HOCHSTENBAG, M. M., TWIJNSTRA, A., WILMINK, J. T., WOUTERS, E. F. & TEN VELDE, G. P. 2000. Asymptomatic brain metastases (BM) in small cell lung cancer (SCLC): MR-imaging is useful at initial diagnosis. *J Neurooncol,* 48**,** 243-8.

HOGERVORST, E., COMBRINCK, M., LAPUERTA, P., RUE, J., SWALES, K. & BUDGE, M. 2002. The Hopkins Verbal Learning Test and screening for dementia. *Dement Geriatr Cogn Disord,* 13**,** 13-20.

HOLLINGWORTH, W., MEDINA, L. S., LENKINSKI, R. E., SHIBATA, D. K., BERNAL, B., ZURAKOWSKI, D., COMSTOCK, B. & JARVIK, J. G. 2006. A systematic literature review of magnetic resonance spectroscopy for the characterization of brain tumors. *AJNR Am J Neuroradiol,* 27**,** 1404-11.

HORN, L., MANSFIELD, A. S., SZCZĘSNA, A., HAVEL, L., KRZAKOWSKI, M., HOCHMAIR, M. J., HUEMER, F., LOSONCZY, G., JOHNSON, M. L., NISHIO, M., RECK, M., MOK, T., LAM, S., SHAMES, D. S., LIU, J., DING, B., LOPEZ-CHAVEZ, A., KABBINAVAR, F., LIN, W., SANDLER, A. & LIU, S. V. 2018. First-Line Atezolizumab plus Chemotherapy in Extensive-Stage Small-Cell Lung Cancer. *N Engl J Med,* 379**,** 2220-2229.

HOU, C., GONG, G., WANG, L., SU, Y., LU, J. & YIN, Y. 2022. The Study of Cerebral Blood Flow Variations during Brain Metastases Radiotherapy. *Oncol Res Treat,* 45**,** 130-137.

HOU, G., YANG, X. & YUAN, T.-F. 2013. Hippocampal Asymmetry: Differences in Structures and Functions. *Neurochemical Research,* 38**,** 453-460.

HU, C. Y., GAO, X., LONG, L., LONG, X., LIU, C., CHEN, Y., XIE, Y., LIU, C., XIAO, B. & HU, Z. Y. 2017. Altered DMN functional connectivity and regional homogeneity in partial epilepsy patients: a seventy cases study. *Oncotarget,* 8**,** 81475-81484.

HUANG, H., FAN, X., WEINER, M., MARTIN-COOK, K., XIAO, G., DAVIS, J., DEVOUS, M., ROSENBERG, R. & DIAZ-ARRASTIA, R. 2012. Distinctive disruption patterns of white matter tracts in Alzheimer's disease with full diffusion tensor characterization. *Neurobiol Aging,* 33**,** 2029-45.

IUCHI, T., SHINGYOJI, M., SAKAIDA, T., HATANO, K., NAGANO, O., ITAKURA, M., KAGEYAMA, H., YOKOI, S., HASEGAWA, Y., KAWASAKI, K. & IIZASA, T. 2013. Phase II trial of gefitinib alone without radiation therapy for Japanese patients with brain metastases from EGFR-mutant lung adenocarcinoma. *Lung Cancer,* 82**,** 282-7.

IVERSON, G. L. 2011. T Scores. *In:* KREUTZER, J. S., DELUCA, J. & CAPLAN, B. (eds.) *Encyclopedia of Clinical Neuropsychology.* New York, NY: Springer New York.

JAIN, R. 2011. Perfusion CT imaging of brain tumors: an overview. *AJNR Am J Neuroradiol,* 32**,** 1570-7.

JAKUBOVIC, R., SAHGAL, A., SOLIMAN, H., MILWID, R., ZHANG, L., EILAGHI, A. & AVIV, R. I. 2014. Magnetic resonance imaging-based tumour perfusion parameters are biomarkers predicting response after radiation to brain metastases. *Clin Oncol (R Coll Radiol),* 26**,** 704-12.

JAKUBOVIC, R., ZHOU, S., HEYN, C., SOLIMAN, H., ZHANG, L., AVIV, R. & SAHGAL, A. 2016. The predictive capacity of apparent diffusion coefficient (ADC) in response assessment of brain metastases following radiation. *Clin Exp Metastasis,* 33**,** 277-84.

JASPERS, J., MÈNDEZ ROMERO, A., HOOGEMAN, M. S., VAN DEN BENT, M., WIGGENRAAD, R. G. J., TAPHOORN, M. J. B., EEKERS, D. B. P., LAGERWAARD, F. J., LUCAS CALDUCH, A. M., BAUMERT, B. G. & KLEIN, M. 2019. Evaluation of the Hippocampal Normal Tissue Complication Model in a Prospective Cohort of Low Grade Glioma Patients—An Analysis Within the EORTC 22033 Clinical Trial. *Frontiers in Oncology,* 9.

JENA, R., PRICE, S. J., BAKER, C., JEFFERIES, S. J., PICKARD, J. D., GILLARD, J. H. & BURNET, N. G. 2005. Diffusion tensor imaging: possible implications for radiotherapy treatment planning of patients with high-grade glioma. *Clin Oncol (R Coll Radiol),* 17**,** 581-90.

JENKINSON, M., BECKMANN, C. F., BEHRENS, T. E., WOOLRICH, M. W. & SMITH, S. M. 2012a. FSL. *Neuroimage,* 62**,** 782-90.

JENKINSON, M., BECKMANN, C. F., BEHRENS, T. E. J., WOOLRICH, M. W. & SMITH, S. M. 2012b. FSL. *NeuroImage,* 62**,** 782-790.

JOHANNESEN, T. B., LIEN, H. H., HOLE, K. H. & LOTE, K. 2003. Radiological and clinical assessment of long-term brain tumour survivors after radiotherapy. *Radiother Oncol,* 69**,** 169-76.

JONES, D. K., ALEXANDER, D. C., BOWTELL, R., CERCIGNANI, M., DELL'ACQUA, F., MCHUGH, D. J., MILLER, K. L., PALOMBO, M., PARKER, G. J. M., RUDRAPATNA, U. S. & TAX, C. M. W. 2018. Microstructural imaging of the human brain with a 'super-scanner': 10 key advantages of ultra-strong gradients for diffusion MRI. *Neuroimage,* 182**,** 8-38.

KAMRAN, M., HACKER, C. D., ALLEN, M. G., MITCHELL, T. J., LEUTHARDT, E. C., SNYDER, A. Z. & SHIMONY, J. S. 2014. Resting-state blood oxygen level-dependent functional magnetic resonance imaging for presurgical planning. *Neuroimaging Clin N Am,* 24**,** 655-69.

KELLNER, E., DHITAL, B., KISELEV, V. G. & REISERT, M. 2016. Gibbs-ringing artifact removal based on local subvoxel-shifts. *Magnetic Resonance in Medicine,* 76**,** 1574-1581.

KLOS, K. J. & O'NEILL, B. P. 2004. Brain metastases. *Neurologist,* 10**,** 31-46.

KOIZUMI, T., SASAKI, S., SAKAMOTO, A. & KOBAYASHI, T. 2013. Efficacy of erlotinib plus concurrent whole-brain radiation therapy for patients with brain metastases from non-small cell lung cancer. *Ann Palliat Med,* 2**,** 111-3.

KONOPKA-FILIPPOW, M., SIERKO,E., AND WOJTUKIEWICZ, M.Z. 2019. Benefits and difficulties during brain radiotherapy planning with hippocampus sparing. *Oncology in Clinical Practice* 15**,** 104-110.

KOVÁCS, Á., EMRI, M., OPPOSITS, G., PISÁK, T., VANDULEK, C., GLAVÁK, C., SZALAI, Z., BIRÓ, G., BAJZIK, G. & REPA, I. 2015. Changes in functional MRI signals after 3D based radiotherapy of glioblastoma multiforme. *J Neurooncol,* 125**,** 157-66.

KROLL, H., ZAHARCHUK, G., CHRISTEN, T., HEIT, J. J. & IV, M. 2017. Resting-State BOLD MRI for Perfusion and Ischemia. *Top Magn Reson Imaging,* 26**,** 91-96.

LALONDRELLE, S. & KHOO, V. 2009. Brain metastases. *BMJ Clin Evid,* 2009.

LAO, C. D., FRIEDMAN, J., TSIEN, C. I., NORMOLLE, D. P., CHAPMAN, C., CAO, Y., LEE, O., SCHIPPER, M., VAN POZNAK, C., HAMSTRA, D., LAWRENCE, T., HAYMAN, J. & REDMAN, B. G. 2013. Concurrent whole brain radiotherapy and bortezomib for brain metastasis. *Radiat Oncol,* 8**,** 204.

LEE, E. J., TERBRUGGE, K., MIKULIS, D., CHOI, D. S., BAE, J. M., LEE, S. K. & MOON, S. Y. 2011. Diagnostic value of peritumoral minimum apparent diffusion coefficient for differentiation of glioblastoma multiforme from solitary metastatic lesions. *AJR Am J Roentgenol,* 196**,** 71-6.

LEE, M. H., HACKER, C. D., SNYDER, A. Z., CORBETTA, M., ZHANG, D., LEUTHARDT, E. C. & SHIMONY, J. S. 2012. Clustering of resting state networks. *PLoS One,* 7**,** e40370.

LEEMANS, A., JEURISSEN, B., SIJBERS, J. & JONES, D. K. ExploreDTI: a graphical toolbox for processing, analyzing, and visualizing diffusion MR data. 2009.

LEKSELL, L. 1951. The stereotactic method and radiosurgery of the brain. *Acta chir scand,* 102**,** 316-319.

LENGYEL, Z., REKO, G., MAJTENYI, K., PISCH, J., CSORNAI, M., LESZNYAK, J., TRON, L. & ESIK, O. 2003. Autopsy verifies demyelination and lack of vascular damage in partially reversible radiation myelopathy. *Spinal Cord,* 41**,** 577-85.

LEYDEN, K. M., KUCUKBOYACI, N. E., PUCKETT, O. K., LEE, D., LOI, R. Q., PAUL, B. & MCDONALD, C. R. 2015. What does diffusion tensor imaging (DTI) tell us about cognitive networks in temporal lobe epilepsy? *Quant Imaging Med Surg,* 5**,** 247-63.

LI, J., BENTZEN, S. M., LI, J., RENSCHLER, M. & MEHTA, M. P. 2008. Relationship between neurocognitive function and quality of life after whole-brain radiotherapy in patients with brain metastasis. *Int J Radiat Oncol Biol Phys,* 71**,** 64-70.

LIN, C., WENDT, R. E., 3RD, EVANS, H. J., ROWE, R. M., HEDRICK, T. D. & LEBLANC, A. D. 1994. Eddy current correction in volume-localized MR spectroscopy. *J Magn Reson Imaging,* 4**,** 823-7.

LIN, N. U., LEE, E. Q., AOYAMA, H., BARANI, I. J., BARBORIAK, D. P., BAUMERT, B. G., BENDSZUS, M., BROWN, P. D., CAMIDGE, D. R., CHANG, S. M., DANCEY, J., DE VRIES, E. G. E., GASPAR, L. E., HARRIS, G. J., HODI, F. S., KALKANIS, S. N., LINSKEY, M. E., MACDONALD, D. R., MARGOLIN, K., MEHTA, M. P., SCHIFF, D., SOFFIETTI, R., SUH, J. H., VAN DEN BENT, M. J., VOGELBAUM, M. A. & WEN, P. Y. 2015. Response

assessment criteria for brain metastases: proposal from the RANO group. *The Lancet Oncology,* 16**,** e270-e278.

LIN, N. U., WEFEL, J. S., LEE, E. Q., SCHIFF, D., VAN DEN BENT, M. J., SOFFIETTI, R., SUH, J. H., VOGELBAUM, M. A., MEHTA, M. P., DANCEY, J., LINSKEY, M. E., CAMIDGE, D. R., AOYAMA, H., BROWN, P. D., CHANG, S. M., KALKANIS, S. N., BARANI, I. J., BAUMERT, B. G., GASPAR, L. E., HODI, F. S., MACDONALD, D. R. & WEN, P. Y. 2013. Challenges relating to solid tumour brain metastases in clinical trials, part 2: neurocognitive, neurological, and quality-of-life outcomes. A report from the RANO group. *The Lancet Oncology,* 14**,** e407-e416.

LIN, S. Y., YANG, C. C., CHUANG, C. C., PAI, P. C., TSAI, P. F., TSAN, D. L. & TSENG, C. K. 2016. OC-0349: Hippocampal dosimetry predicts the change in neurocognitive functions after whole brain radiotherapy. *Radiotherapy and Oncology,* 119.

LIU, Y., SPULBER, G., LEHTIMÄKI, K. K., KÖNÖNEN, M., HALLIKAINEN, I., GRÖHN, H., KIVIPELTO, M., HALLIKAINEN, M., VANNINEN, R. & SOININEN, H. 2011. Diffusion tensor imaging and tract-based spatial statistics in Alzheimer's disease and mild cognitive impairment. *Neurobiol Aging,* 32**,** 1558-71.

LO BUONO, V., PALMERI, R., CORALLO, F., ALLONE, C., PRIA, D., BRAMANTI, P. & MARINO, S. 2020. Diffusion tensor imaging of white matter degeneration in early stage of Alzheimer's disease: a review. *Int J Neurosci,* 130**,** 243-250.

LONG, G. V., ATKINSON, V., LO, S., SANDHU, S., GUMINSKI, A. D., BROWN, M. P., WILMOTT, J. S., EDWARDS, J., GONZALEZ, M., SCOLYER, R. A., MENZIES, A. M. & MCARTHUR, G. A. 2018. Combination nivolumab and ipilimumab or nivolumab alone in melanoma brain metastases: a multicentre randomised phase 2 study. *Lancet Oncol,* 19**,** 672-681.

LU, V. M., JUE, T. R., PHAN, K. & MCDONALD, K. L. 2018. Quantifying the prognostic significance in glioblastoma of seizure history at initial presentation: A systematic review and meta-analysis. *Clinical Neurology and Neurosurgery,* 164**,** 75-80.

MACINTOSH, B. J. & GRAHAM, S. J. 2013. Magnetic resonance imaging to visualize stroke and characterize stroke recovery: a review. *Frontiers in neurology,* 4**,** 60-60.

MAGNUSON, W. J., LESTER-COLL, N. H., WU, A. J., YANG, T. J., LOCKNEY, N. A., GERBER, N. K., BEAL, K., AMINI, A., PATIL, T., KAVANAGH, B. D., CAMIDGE, D. R., BRAUNSTEIN, S. E., BORETA, L. C., BALASUBRAMANIAN, S. K., AHLUWALIA, M. S., RANA, N. G., ATTIA, A., GETTINGER, S. N., CONTESSA, J. N., YU, J. B. & CHIANG, V. L. 2017. Management of Brain Metastases in Tyrosine Kinase Inhibitor-Naïve Epidermal Growth Factor Receptor-Mutant Non-Small-Cell Lung Cancer: A Retrospective Multi-Institutional Analysis. *J Clin Oncol,* 35**,** 1070-1077.

MAHAJAN, A., AHMED, S., MCALEER, M. F., WEINBERG, J. S., LI, J., BROWN, P., SETTLE, S., PRABHU, S. S., LANG, F. F., LEVINE, N., MCGOVERN, S., SULMAN, E., MCCUTCHEON, I. E., AZEEM, S., CAHILL, D., TATSUI, C., HEIMBERGER, A. B., FERGUSON, S., GHIA, A., DEMONTE, F., RAZA, S., GUHA-THAKURTA, N., YANG, J., SAWAYA, R., HESS, K. R. & RAO, G. 2017. Post-operative stereotactic radiosurgery versus observation for completely resected brain metastases: a single-centre, randomised, controlled, phase 3 trial. *Lancet Oncol,* 18**,** 1040-1048.

MAKALE, M. T., MCDONALD, C. R., HATTANGADI-GLUTH, J. A. & KESARI, S. 2017. Mechanisms of radiotherapy-associated cognitive disability in patients with brain tumours. *Nat Rev Neurol,* 13**,** 52-64.

MARGOLIN, K., ERNSTOFF, M. S., HAMID, O., LAWRENCE, D., MCDERMOTT, D., PUZANOV, I., WOLCHOK, J. D., CLARK, J. I., SZNOL, M., LOGAN, T. F., RICHARDS, J., MICHENER, T., BALOGH, A., HELLER, K. N. & HODI, F. S. 2012. Ipilimumab in patients with melanoma and brain metastases: an open-label, phase 2 trial. *Lancet Oncol,* 13**,** 459-65.

MARSH, J. C., GODBOLE, R., DIAZ, A. Z., GIELDA, B. T. & TURIAN, J. V. 2011. Sparing of the hippocampus, limbic circuit and neural stem cell compartment during partial brain radiotherapy for glioma: A dosimetric feasibility study. *Journal of Medical Imaging and Radiation Oncology,* 55**,** 442-449.

MCDUFF, S. G., TAICH, Z. J., LAWSON, J. D., SANGHVI, P., WONG, E. T., BARKER, F. G., 2ND, HOCHBERG, F. H., LOEFFLER, J. S., WARNKE, P. C., MURPHY, K. T., MUNDT, A. J., CARTER, B. S., MCDONALD, C. R. & CHEN, C. C. 2013. Neurocognitive assessment following whole brain radiation therapy and radiosurgery for patients with cerebral metastases. *J Neurol Neurosurg Psychiatry,* 84**,** 1384-91.

MCROBBIE, D. W., MOORE, E. A., GRAVES, M. J. & PRINCE, M. R. 2007. *MRI: From Picture to Proton* United Kingdom Cambridge University Press

MEGIAS, D., PHILLIPS, M., CLIFTON-HADLEY, L., HARRON, E., EATON, D. J., SANGHERA, P. & WHITFIELD, G. 2017. Dose specification for hippocampal sparing whole brain radiotherapy (HS WBRT): considerations from the UK HIPPO trial QA programme. *The British Journal of Radiology,* 90**,** 20160829.

MEHTA, M. P., RODRIGUS, P., TERHAARD, C. H., RAO, A., SUH, J., ROA, W., SOUHAMI, L., BEZJAK, A., LEIBENHAUT, M., KOMAKI, R., SCHULTZ, C., TIMMERMAN, R., CURRAN, W., SMITH, J., PHAN, S. C., MILLER, R. A. & RENSCHLER, M. F. 2003. Survival and neurologic outcomes in a randomized trial of motexafin gadolinium and whole-brain radiation therapy in brain metastases. *J Clin Oncol,* 21**,** 2529-36.

METZLER-BADDELEY, C., MOLE, J. P., SIMS, R., FASANO, F., EVANS, J., JONES, D. K., AGGLETON, J. P. & BADDELEY, R. J. 2019. Fornix white matter glia damage causes hippocampal gray matter damage during age-dependent limbic decline. *Scientific Reports,* 9**,** 1060.

MEYERS, C. A., HESS, K. R., YUNG, W. K. & LEVIN, V. A. 2000. Cognitive function as a predictor of survival in patients with recurrent malignant glioma. *J Clin Oncol,* 18**,** 646-50.

MIELKE, M. M., OKONKWO, O. C., OISHI, K., MORI, S., TIGHE, S., MILLER, M. I., CERITOGLU, C., BROWN, T., ALBERT, M. & LYKETSOS, C. G. 2012. Fornix integrity and hippocampal volume predict memory decline and progression to Alzheimer's disease. *Alzheimer's & Dementia,* 8**,** 105-113.

MIKKELSEN, T. & HEARSHEN, D. 2008. CHAPTER 28 - Magnetic Resonance Spectroscopy. *In:* NEWTON, H. B. & JOLESZ, F. A. (eds.) *Handbook of Neuro-Oncology NeuroImaging.* San Diego: Academic Press.

MINNITI, G., CLARKE, E., LANZETTA, G., OSTI, M. F., TRASIMENI, G., BOZZAO, A., ROMANO, A. & ENRICI, R. M. 2011. Stereotactic radiosurgery for brain metastases: analysis of outcome and risk of brain radionecrosis. *Radiat Oncol,* 6**,** 48.

MINTZ, A. H., KESTLE, J., RATHBONE, M. P., GASPAR, L., HUGENHOLTZ, H., FISHER, B., DUNCAN, G., SKINGLEY, P., FOSTER, G. & LEVINE, M. 1996. A randomized trial to assess the efficacy of surgery in addition to radiotherapy in patients with a single cerebral metastasis. *Cancer,* 78**,** 1470-1476.

MONJE, M. L., VOGEL, H., MASEK, M., LIGON, K. L., FISHER, P. G. & PALMER, T. D. 2007. Impaired human hippocampal neurogenesis after treatment for central nervous system malignancies. *Ann Neurol,* 62**,** 515-20.

MOORE, A. R. & O'KEEFFE, S. T. 1999. Drug-induced cognitive impairment in the elderly. *Drugs Aging,* 15**,** 15-28.

MORATAL, D., VALLÉS-LUCH, A., MARTÍ-BONMATÍ, L. & BRUMMER, M. 2008. k-Space tutorial: an MRI educational tool for a better understanding of k-space. *Biomedical imaging and intervention journal,* 4**,** e15-e15.

MORO-SIBILOT D, S. E., DE CASTRO CARPEÑO J, LESNIEWSKI-KMAK K, AERTS JG, VILLATORO R, KRAAIJ K, NACERDDINE K, DYACHKOVA Y, SMITH KT, GIRVAN A, VISSEREN-GRUL C, SCHNABEL PA 2015. Non-small cell lung cancer patients with brain metastases treated with first-line platinum-doublet chemotherapy: Analysis from the European FRAME study. *Lung Cancer,* 90**,** 427-432.

MULVENNA, P., NANKIVELL, M., BARTON, R., FAIVRE-FINN, C., WILSON, P., MCCOLL, E., MOORE, B., BRISBANE, I., ARDRON, D., HOLT, T., MORGAN, S., LEE, C., WAITE, K., BAYMAN, N., PUGH, C., SYDES, B., STEPHENS, R., PARMAR, M. K. & LANGLEY, R. E. 2016. Dexamethasone and supportive care with or without whole brain radiotherapy in treating patients with non-small cell lung cancer with brain metastases unsuitable for resection or stereotactic radiotherapy (QUARTZ): results from a phase 3, non-inferiority, randomised trial. *The Lancet,* 388**,** 2004-2014.

NAYAK, L., LEE, E. Q. & WEN, P. Y. 2012. Epidemiology of brain metastases. *Curr Oncol Rep,* 14**,** 48-54.

NAZEM-ZADEH, M. R., CHAPMAN, C. H., LAWRENCE, T. L., TSIEN, C. I. & CAO, Y. 2012. Radiation therapy effects on white matter fiber tracts of the limbic circuit. *Med Phys,* 39**,** 5603-13.

NCCN 2016. Melanoma USA

NICE 2015. Melanoma: Assessment and Management [NG14]. UK

NICE 2018. Brain tumours (primary) and brain metastases in adults. UK.

NICE 2019. Lung cancer: diagnosis and management. UK: NICE.

NIEDER, C., BERBERICH, W. & SCHNABEL, K. 1997. Tumor-related prognostic factors for remission of brain metastases after radiotherapy. *International Journal of Radiation Oncology* Biology* Physics,* 39**,** 25-30.

NIEDER, C., NESTLE, U., MOTAREF, B., WALTER, K., NIEWALD, M. & SCHNABEL, K. 2000. Prognostic factors in brain metastases: should patients be selected for aggressive treatment according to recursive partitioning analysis (RPA) classes? *International Journal of Radiation Oncology* Biology* Physics,* 46**,** 297-302.

NIEDER, C., NORUM, J., DALHAUG, A., AANDAHL, G. & PAWINSKI, A. 2013. Radiotherapy versus best supportive care in patients with brain metastases and adverse prognostic factors. *Clinical & Experimental Metastasis,* 30**,** 723-729.

NIEDER, C., SPANNE, O., MEHTA, M. P., GROSU, A. L. & GEINITZ, H. 2011. Presentation, patterns of care, and survival in patients with brain metastases: what has changed in the last 20 years? *Cancer,* 117**,** 2505-12.

NOBIS, L., MANOHAR, S. G., SMITH, S. M., ALFARO-ALMAGRO, F., JENKINSON, M., MACKAY, C. E. & HUSAIN, M. 2019. Hippocampal volume across age: Nomograms derived from over 19,700 people in UK Biobank. *Neuroimage Clin,* 23**,** 101904.

O'CONNOR, J. P. B., ABOAGYE, E. O., ADAMS, J. E., AERTS, H. J. W. L., BARRINGTON, S. F., BEER, A. J., BOELLAARD, R., BOHNDIEK, S. E., BRADY, M., BROWN, G., BUCKLEY, D. L., CHENEVERT, T. L., CLARKE, L. P., COLLETTE, S., COOK, G. J., DESOUZA, N. M., DICKSON, J. C., DIVE, C., EVELHOCH, J. L., FAIVRE-FINN, C., GALLAGHER, F. A., GILBERT, F. J., GILLIES, R. J., GOH, V., GRIFFITHS, J. R., GROVES, A. M., HALLIGAN, S., HARRIS, A. L., HAWKES, D. J., HOEKSTRA, O. S., HUANG, E. P., HUTTON, B. F., JACKSON, E. F., JAYSON, G. C., JONES, A., KOH, D.-M., LACOMBE, D., LAMBIN, P., LASSAU, N., LEACH, M. O., LEE, T.-Y., LEEN, E. L., LEWIS, J. S., LIU, Y., LYTHGOE, M. F., MANOHARAN, P., MAXWELL, R. J., MILES, K. A., MORGAN, B., MORRIS, S., NG, T., PADHANI, A. R., PARKER, G. J. M., PARTRIDGE, M., PATHAK, A. P., PEET, A. C., PUNWANI, S., REYNOLDS, A. R., ROBINSON, S. P., SHANKAR, L. K., SHARMA, R. A., SOLOVIEV, D., STROOBANTS, S., SULLIVAN, D. C., TAYLOR, S. A., TOFTS, P. S., TOZER, G. M., VAN HERK, M., WALKER-SAMUEL, S., WASON, J., WILLIAMS, K. J., WORKMAN, P., YANKEELOV, T. E., BRINDLE, K. M., MCSHANE, L. M., JACKSON, A. & WATERTON, J. C. 2017. Imaging biomarker roadmap for cancer studies. *Nature Reviews Clinical Oncology,* 14**,** 169-186.

O'CONNOR, J. P. B., ROBINSON, S. P. & WATERTON, J. C. 2019. Imaging tumour hypoxia with oxygen-enhanced MRI and BOLD MRI. *Br J Radiol,* 92**,** 20180642.

O'DONNELL, L. J. & WESTIN, C. F. 2011. An introduction to diffusion tensor image analysis. *Neurosurg Clin N Am,* 22**,** 185-96, viii.

OHNISHI, T., HOSHI, H., NAGAMACHI, S., JINNOUCHI, S., FLORES, L. G., 2ND, FUTAMI, S. & WATANABE, K. 1995. High-resolution SPECT to assess hippocampal perfusion in neuropsychiatric diseases. *J Nucl Med,* 36**,** 1163-9.

OISHI, K., MIELKE, M. M., ALBERT, M., LYKETSOS, C. G. & MORI, S. 2011. DTI analyses and clinical applications in Alzheimer's disease. *J Alzheimers Dis,* 26 Suppl 3**,** 287-96.

OKOUKONI, C., MCTYRE, E. R., AYALA PEACOCK, D. N., PEIFFER, A. M., STROWD, R., CRAMER, C., HINSON, W. H., RAPP, S., METHENY-BARLOW, L., SHAW, E. G. & CHAN, M. D. 2017. Hippocampal dose volume histogram predicts Hopkins Verbal Learning Test scores after brain irradiation. *Adv Radiat Oncol,* 2**,** 624-629.

PADDICK, I. 2000. A simple scoring ratio to index the conformity of radiosurgical treatment plans. *Journal of neurosurgery,* 93.

PADDICK, I. A. L., B. 2006. A simple dose gradient measurement tool to complement the conformity index. *Journal of neurosurgery,* 105**,** 194-201.

PAGET, S. 1889. The distribution of secondary growths in cancer of the breast. *The Lancet,* 133**,** 571-573.

PANAGIOTAKI, E., WALKER-SAMUEL, S., SIOW, B., JOHNSON, S. P., RAJKUMAR, V., PEDLEY, R. B., LYTHGOE, M. F. & ALEXANDER, D. C. 2014. Noninvasive quantification of solid tumor microstructure using VERDICT MRI. *Cancer Res,* 74**,** 1902-12.

PAPALAZAROU, C., KLOP, G. J., MILDER, M. T. W., MARIJNISSEN, J. P. A., GUPTA, V., HEIJMEN, B. J. M., NUYTTENS, J. & HOOGEMAN, M. S. 2017. CyberKnife with integrated CT-on-rails: System description and first clinical application for pancreas SBRT. *Med Phys,* 44**,** 4816-4827.

PARK, H. J., GRIFFIN, R. J., HUI, S., LEVITT, S. H. & SONG, C. W. 2012. Radiation-induced vascular damage in tumors: implications of vascular damage in ablative hypofractionated radiotherapy (SBRT and SRS). *Radiat Res,* 177**,** 311-27.

PASCHAL, C. B. & MORRIS, H. D. 2004. K-space in the clinic. *Journal of Magnetic Resonance Imaging,* 19**,** 145-159.

PATCHELL, R. A., TIBBS, P. A., WALSH, J. W., DEMPSEY, R. J., MARUYAMA, Y., KRYSCIO, R. J., MARKESBERY, W. R., MACDONALD, J. S. & BYRON YOUNG, B. 1990. A Randomized Trial of Surgery in the Treatment of Single Metastases to the Brain. *N Engl J Med,* 322**,** 494-500.

PATEL, A. J., SUKI, D., HATIBOGLU, M. A., ABOUASSI, H., SHI, W., WILDRICK, D. M., LANG, F. F. & SAWAYA, R. 2010. Factors influencing the risk of local recurrence after resection of a single brain metastasis. *J Neurosurg,* 113**,** 181-9.

PEIFFER, A. M., SHI, L., OLSON, J. & BRUNSO-BECHTOLD, J. K. 2010. Differential effects of radiation and age on diffusion tensor imaging in rats. *Brain Res,* 1351**,** 23-31.

PINKHAM, M. B., SANGHERA, P., WALL, G. K., DAWSON, B. D. & WHITFIELD, G. A. 2015. Neurocognitive Effects Following Cranial Irradiation for Brain Metastases. *Clin Oncol (R Coll Radiol),* 27**,** 630-9.

PLATTA, C. S., KHUNTIA, D., MEHTA, M. P. & SUH, J. H. 2010. Current treatment strategies for brain metastasis and complications from therapeutic techniques: a review of current literature. *Am J Clin Oncol,* 33**,** 398-407.

POPE, W. B. 2018. Brain metastases: neuroimaging. *Handbook of clinical neurology,* 149**,** 89-112.

POPP, I., RAU, S., HINTZ, M., SCHNEIDER, J., BILGER, A., FENNELL, J. T., HEILAND, D. H., ROTHE, T., EGGER, K., NIEDER, C., URBACH, H. & GROSU, A. L. 2020. Hippocampus-avoidance whole-brain radiation therapy with a simultaneous integrated boost for multiple brain metastases. *Cancer,* 126**,** 2694-2703.

POSNER, M. I. & RAICHLE, M. E. 1994. *Images of mind*, Scientific American Library/Scientific American Books.

POSPISIL, P., KAZDA, T., BULIK, M., DOBIASKOVA, M., BURKON, P., HYNKOVA, L., SLAMPA, P. & JANCALEK, R. 2015. Hippocampal proton MR spectroscopy as a novel approach in the assessment of radiation injury and the correlation to neurocognitive function impairment: initial experiences. *Radiat Oncol,* 10**,** 211.

POTTS, D. G., ABBOTT, G. F. & VON SNEIDERN, J. V. 1980. National Cancer Institute study: evaluation of computed tomography in the diagnosis of intracranial neoplasms. III. Metastatic tumors. *Radiology,* 136**,** 657-64.

POWER, J. D., COHEN, A. L., NELSON, S. M., WIG, G. S., BARNES, K. A., CHURCH, J. A., VOGEL, A. C., LAUMANN, T. O., MIEZIN, F. M., SCHLAGGAR, B. L. & PETERSEN, S. E. 2011. Functional network organization of the human brain. *Neuron,* 72**,** 665-78.

PROVENCHER, S. 2013. LCModel & LCMgui User's Manual; 2016. Version.

PRUITT, A. A. 2017. Epidemiology, Treatment, and Complications of Central Nervous System Metastases. *Continuum (Minneap Minn),* 23**,** 1580-1600.

RAICHLE, M. E. 1998. Behind the Scenes of Functional Brain Imaging: A Historical and Physiological Perspective. *Proceedings of the National Academy of Sciences of the United States of America,* 95**,** 765-772.

RANE, S., ALLY, B. A., HUSSEY, E., WILSON, T., THORNTON-WELLS, T., GORE, J. C. & DONAHUE, M. J. 2013. Inverse correspondence between hippocampal perfusion and verbal memory performance in older adults. *Hippocampus,* 23**,** 213-20.

REUNGWETWATTANA, T., NAKAGAWA, K., CHO, B. C., COBO, M., CHO, E. K., BERTOLINI, A., BOHNET, S., ZHOU, C., LEE, K. H. & NOGAMI, N. 2018. CNS response to osimertinib

versus standard epidermal growth factor receptor tyrosine kinase inhibitors in patients with untreated EGFR-mutated advanced non-small-cell lung cancer. *Journal of Clinical Oncology,* 36**,** 3290-+.

RIINA, M. D., STAMBAUGH, C. K. & HUBER, K. E. 2020. Hippocampal Dosimetry and the Necessity of Hippocampal-Sparing in Gamma Knife Stereotactic Radiosurgery for Extensive Brain Metastases. *Adv Radiat Oncol,* 5**,** 180-188.

ROBERTS, T. A., HYARE, H., AGLIARDI, G., HIPWELL, B., D'ESPOSITO, A., IANUS, A., BREEN-NORRIS, J. O., RAMASAWMY, R., TAYLOR, V., ATKINSON, D., PUNWANI, S., LYTHGOE, M. F., SIOW, B., BRANDNER, S., REES, J., PANAGIOTAKI, E., ALEXANDER, D. C. & WALKER-SAMUEL, S. 2020. Noninvasive diffusion magnetic resonance imaging of brain tumour cell size for the early detection of therapeutic response. *Scientific Reports,* 10**,** 9223.

ROBINSON, J. L., SALIBI, N. & DESHPANDE, G. 2016. Functional connectivity of the left and right hippocampi: Evidence for functional lateralization along the long-axis using meta-analytic approaches and ultra-high field functional neuroimaging. *Neuroimage,* 135**,** 64-78.

RODRIGUEZA, G., VITALIA,P., CALVINIB, P., BORDONI, C., GIRTLER, N., TADDEIC, G., MARIANI, G., AND NOBILI F. 2000. Hippocampal perfusion in mild Alzheimer's disease. *Psychiatry Research: Neuroimaging,* 100**,** 65-74.

SAHGAL, A., AOYAMA, H., KOCHER, M., NEUPANE, B., COLLETTE, S., TAGO, M., SHAW, P., BEYENE, J. & CHANG, E. L. 2015. Phase 3 trials of stereotactic radiosurgery with or without whole-brain radiation therapy for 1 to 4 brain metastases: individual patient data meta-analysis. *Int J Radiat Oncol Biol Phys,* 91**,** 710-7.

SALKELD, A. L., UNICOMB, K., HAYDEN, A. J., VAN TILBURG, K., YAU, S. & TIVER, K. 2014. Dosimetric comparison of volumetric modulated arc therapy and linear accelerator-based radiosurgery for the treatment of one to four brain metastases. *J Med Imaging Radiat Oncol,* 58**,** 722-8.

SAWLANI, V., DAVIES, N., PATEL, M., FLINTHAM, R., FONG, C., HEYES, G., CRUICKSHANK, G., STEVEN, N., PEET, A., HARTLEY, A., BENGHIAT, H., MEADE, S. & SANGHERA, P. 2019. Evaluation of Response to Stereotactic Radiosurgery in Brain Metastases Using Multiparametric Magnetic Resonance Imaging and a Review of the Literature. *Clin Oncol (R Coll Radiol),* 31**,** 41-49.

SCHIMMEL, W. C. M., GEHRING, K., EEKERS, D. B. P., HANSSENS, P. E. J. & SITSKOORN, M. M. 2018. Cognitive effects of stereotactic radiosurgery in adult patients with brain metastases: A systematic review. *Adv Radiat Oncol,* 3**,** 568-581.

SCHOUTEN, L. J., RUTTEN, J., HUVENEERS, H. A. & TWIJNSTRA, A. 2002. Incidence of brain metastases in a cohort of patients with carcinoma of the breast, colon, kidney, and lung and melanoma. *Cancer,* 94**,** 2698-705.

SCHUFF, N., AMENDA, D. L., KNOWLTONF, R., WEINERA, M. W., NORMANC, D. & FEINB, G. 1999. Age-related metabolite changes and volume loss in the hippocampus by magnetic resonance spectroscopy and imaging. *Neurobiology of Aging,* 20**,** 279-285.

SCHULER, M., WU, Y. L., HIRSH, V., O'BYRNE, K., YAMAMOTO, N., MOK, T., POPAT, S., SEQUIST, L. V., MASSEY, D., ZAZULINA, V. & YANG, J. C. 2016. First-Line Afatinib versus Chemotherapy in Patients with Non-Small Cell Lung Cancer and Common Epidermal Growth Factor Receptor Gene Mutations and Brain Metastases. *J Thorac Oncol,* 11**,** 380-90.

SEIBERT, T. M., KARUNAMUNI, R., BARTSCH, H., KAIFI, S., KRISHNAN, A. P., DALIA, Y., BURKEEN, J., MURZIN, V., MOISEENKO, V., KUPERMAN, J., WHITE, N. S., BREWER, J. B., FARID, N., MCDONALD, C. R. & HATTANGADI-GLUTH, J. A. 2017a. Radiation Dose-Dependent Hippocampal Atrophy Detected With Longitudinal Volumetric Magnetic Resonance Imaging. *Int J Radiat Oncol Biol Phys,* 97**,** 263-269.

SEIBERT, T. M., KARUNAMUNI, R., KAIFI, S., BURKEEN, J., CONNOR, M., KRISHNAN, A. P., WHITE, N. S., FARID, N., BARTSCH, H., MURZIN, V., NGUYEN, T. T., MOISEENKO, V., BREWER, J. B., MCDONALD, C. R., DALE, A. M. & HATTANGADI-GLUTH, J. A. 2017b. Cerebral Cortex Regions Selectively Vulnerable to Radiation Dose-Dependent Atrophy. *Int J Radiat Oncol Biol Phys,* 97**,** 910-918.

SERVER, A., JOSEFSEN, R., KULLE, B., MAEHLEN, J., SCHELLHORN, T., GADMAR, Ø., KUMAR, T., HAAKONSEN, M., LANGBERG, C. W. & NAKSTAD, P. H. 2010. Proton magnetic resonance spectroscopy in the distinction of high-grade cerebral gliomas from single metastatic brain tumors. *Acta Radiol,* 51**,** 316-25.

SHAW, E., SCOTT, C., SUH, J., KADISH, S., STEA, B., HACKMAN, J., PEARLMAN, A., MURRAY, K., GASPAR, L., MEHTA, M., CURRAN, W. & GERBER, M. 2003. RSR13 plus cranial radiation therapy in patients with brain metastases: comparison with the Radiation Therapy Oncology Group Recursive Partitioning Analysis Brain Metastases Database. *J Clin Oncol,* 21**,** 2364-71.

SHAW, E., SCOTT, C., SOUHAMI, L., DINAPOLI, R., BAHARY, J., KLINE, R., WHARAM, M., SCHULTZ, C., DAVEY, P., LOEFFLER, J., ROWE, J.D., MARKS, L., FISHER, B., AND SHIN, K. 1996. Radiosrugery for the Treatment of Previously Irradiated Recurrent Primary Brain Tumour and Brain Metastases: Initial Report of Radiation Therapy Oncology Group Protocol 90-05. *International Joural of Radiation Oncology, Biology and Physics* 34**,** 647-654.

SHINOHARA, C., GOBBEL, G. T., LAMBORN, K. R., TADA, E. & FIKE, J. R. 1997. Apoptosis in the Subependyma of Young Adult Rats after Single and Fractionated Doses of X-Rays. *CANCER RESEARCH,* 57**,** 2694-2702.

SLOSAREK, K., BEKMAN, B., WENDYKIER, J., GRZADZIEL, A., FOGLIATA, A. & COZZI, L. 2018. In silico assessment of the dosimetric quality of a novel, automated radiation treatment planning strategy for linac-based radiosurgery of multiple brain metastases and a comparison with robotic methods. *Radiat Oncol,* 13**,** 41.

SMEDBY, K. E., BRANDT, L., BACKLUND, M. L. & BLOMQVIST, P. 2009. Brain metastases admissions in Sweden between 1987 and 2006. *Br J Cancer,* 101**,** 1919-24.

SMITH, S. M. 2002. Fast robust automated brain extraction. *Hum Brain Mapp,* 17**,** 143-55.

SMITH, S. M., FOX, P. T., MILLER, K. L., GLAHN, D. C., FOX, P. M., MACKAY, C. E., FILIPPINI, N., WATKINS, K. E., TORO, R., LAIRD, A. R. & BECKMANN, C. F. 2009. Correspondence of the brain's functional architecture during activation and rest. *Proc Natl Acad Sci U S A,* 106**,** 13040-5.

SOLOMON, B. J., MOK, T., KIM, D. W., WU, Y. L., NAKAGAWA, K., MEKHAIL, T., FELIP, E., CAPPUZZO, F., PAOLINI, J., USARI, T., IYER, S., REISMAN, A., WILNER, K. D., TURSI, J. & BLACKHALL, F. 2014. First-line crizotinib versus chemotherapy in ALK-positive lung cancer. *N Engl J Med,* 371**,** 2167-77.

SOLOZHENTSEVA, K., BATALOV, A., ZAKHAROVA, N., GORYAYNOV, S., POGOSBEKYAN, E. & PRONIN, I. 2022. The Role of 3D-pCASL MRI in the Differential Diagnosis of Glioblastoma and Brain Metastases. *Front Oncol,* 12**,** 874924.

SONG, Y. P., MISTRY, H., CHOUDHURY, A. & HOSKIN, P. 2019. Long-term outcomes of hypoxia modification in bladder preservation: Update from BCON trial. *Journal of Clinical Oncology,* 37**,** 356-356.

SPERDUTO, P. W., CHAO, S. T., SNEED, P. K., LUO, X., SUH, J., ROBERGE, D., BHATT, A., JENSEN, A. W., BROWN, P. D., SHIH, H., KIRKPATRICK, J., SCHWER, A., GASPAR, L. E., FIVEASH, J. B., CHIANG, V., KNISELY, J., SPERDUTO, C. M. & MEHTA, M. 2010. Diagnosis-specific prognostic factors, indexes, and treatment outcomes for patients with newly diagnosed brain metastases: a multi-institutional analysis of 4,259 patients. *Int J Radiat Oncol Biol Phys,* 77**,** 655-61.

SPITZER, M., KWONG, K. K., KENNEDY, W., ROSEN, B. R. & BELLIVEAU, J. W. 1995. Category-specific brain activation in fMRI during picture naming. *Neuroreport,* 6**,** 2109-12.

STAAT, K. & SEGATORE, M. 2005. The phenomenon of chemo brain. *Clin J Oncol Nurs,* 9**,** 713-21.

STANISZ, G. J., ODROBINA, E. E., PUN, J., ESCARAVAGE, M., GRAHAM, S. J., BRONSKILL, M. J. & HENKELMAN, R. M. 2005. T1, T2 relaxation and magnetization transfer in tissue at 3T. *Magnetic Resonance in Medicine,* 54**,** 507-512.

STERNBERG, E. J., LIPTON, M. L. & BURNS, J. 2014. Utility of diffusion tensor imaging in evaluation of the peritumoral region in patients with primary and metastatic brain tumors. *AJNR Am J Neuroradiol,* 35**,** 439-44.

SUCKERT, T., BEYREUTHER, E., MÜLLER, J., AZADEGAN, B., MEINHARDT, M., RASCHKE, F., BODENSTEIN, E., VON NEUBECK, C., LÜHR, A., KRAUSE, M. & DIETRICH, A. 2020. Late Side Effects in Normal Mouse Brain Tissue After Proton Irradiation. *Front Oncol,* 10**,** 598360.

SUNDGREN, P. C. 2009. MR spectroscopy in radiation injury. *AJNR Am J Neuroradiol,* 30**,** 1469-76.

SUSKO, M. S., GARCIA, M. A., MA, L., NAKAMURA, J. L., RALEIGH, D. R., FOGH, S., THEODOSOPOULOS, P., MCDERMOTT, M., SNEED, P. K. & BRAUNSTEIN, S. E. 2020. Stereotactic Radiosurgery to More Than 10 Brain Metastases: Evidence to Support the Role of Radiosurgery for Ideal Hippocampal Sparing in the Treatment of Multiple Brain Metastases. *World neurosurgery,* 135**,** e174-e180.

TABOURET, E., CHINOR, O., METELLUS, P., TALLET, A., VIENSE, P., AND GONCALVES, A. 2012. Recent Trends in Epidemiology of Brain Metastases: An Overview. *ANTICANCER RESEARCH 32: 4655-4662 (2012),* 32**,** 4655-4662

TAKEI, H., ROUAH, E. & ISHIDA, Y. 2016. Brain metastasis: clinical characteristics, pathological findings and molecular subtyping for therapeutic implications. *Brain Tumor Pathology,* 33**,** 1-12.

TAPHOORN, M. J., CLAASSENS, L., AARONSON, N. K., COENS, C., MAUER, M., OSOBA, D., STUPP, R., MIRIMANOFF, R. O., VAN DEN BENT, M. J., BOTTOMLEY, A., GROUP, E. Q. O. L., BRAIN CANCER, N. & RADIOTHERAPY, G. 2010. An international validation study of the EORTC brain cancer module (EORTC QLQ-BN20) for assessing health-related quality of life and symptoms in brain cancer patients. *Eur J Cancer,* 46**,** 1033-40.

TAWBI, H. A., FORSYTH, P. A., ALGAZI, A., HAMID, O., HODI, F. S., MOSCHOS, S. J., KHUSHALANI, N. I., LEWIS, K., LAO, C. D., POSTOW, M. A., ATKINS, M. B., ERNSTOFF, M. S., REARDON, D. A., PUZANOV, I., KUDCHADKAR, R. R., THOMAS, R. P., TARHINI, A., PAVLICK, A. C., JIANG, J., AVILA, A., DEMELO, S. & MARGOLIN, K. 2018. Combined

Nivolumab and Ipilimumab in Melanoma Metastatic to the Brain. *New England Journal of Medicine,* 379**,** 722-730.

THOMAS, A. G., KOUMELLIS, P. & DINEEN, R. A. 2011. The fornix in health and disease: an imaging review. *Radiographics,* 31**,** 1107-21.

TOMASI, D. & VOLKOW, N. D. 2012. Resting functional connectivity of language networks: characterization and reproducibility. *Mol Psychiatry,* 17**,** 841-54.

TRINGALE, K. R., NGUYEN, T., BAHRAMI, N., MARSHALL, D. C., LEYDEN, K. M., KARUNAMUNI, R., SEIBERT, T. M., KAY GORMAN, M., CONNOR, M., BURKEEN, J., PICCIONI, D. E., FARID, N., HATTANGADI-GLUTH, J. A. & MCDONALD, C. R. 2019. Identifying early diffusion imaging biomarkers of regional white matter injury as indicators of executive function decline following brain radiotherapy: A prospective clinical trial in primary brain tumor patients. *Radiother Oncol,* 132**,** 27-33.

TSAI, P. F., YANG, C. C., CHUANG, C. C., HUANG, T. Y., WU, Y. M., PAI, P. C., TSENG, C. K., WU, T. H., SHEN, Y. L. & LIN, S. Y. 2015. Hippocampal dosimetry correlates with the change in neurocognitive function after hippocampal sparing during whole brain radiotherapy: a prospective study. *Radiat Oncol,* 10**,** 253.

TSAO, M., XU, W. & SAHGAL, A. 2012. A meta-analysis evaluating stereotactic radiosurgery, whole-brain radiotherapy, or both for patients presenting with a limited number of brain metastases. *Cancer,* 118**,** 2486-93.

TURGEON, G. A., WEICKHARDT, A., AZAD, A. A., SOLOMON, B. & SIVA, S. 2019. Radiotherapy and immunotherapy: a synergistic effect in cancer care. *Med J Aust,* 210**,** 47-53.

VAN DEN HEUVEL, M., MANDL, R. & HULSHOFF POL, H. 2008. Normalized cut group clustering of resting-state FMRI data. *PLoS One,* 3**,** e2001.

VAN GESTEL, D., VERELLEN, D., VAN DE VOORDE, L., DE OST, B., DE KERF, G., VANDERVEKEN, O., VAN LAER, C., VAN DEN WEYNGAERT, D., VERMORKEN, J. B. & GREGOIRE, V. 2013. The potential of helical tomotherapy in the treatment of head and neck cancer. *Oncologist,* 18**,** 697-706.

VANCE KEELING, O. A., SALAHUDDIN AHMAD AND SABBIR HOSSAIN 2016. Dosimetric comparison of intracranial metastasis treatment using two radiosurgery systems: TrueBeam STx with VMAT and Gamma Knife Model 4C. *Journal of Radiosurgery and SBRT,* 4**,** 235-243.

VASILOPOULOU, K., PAPATHANASIOU, P., MICHOPOULOS, J., BOUFIDOU, F., OULIS, P., NIKOLAOU, C., PANTELIS, C., VELAKOULIS, D. & LYKOURAS, L. 2011. [A volumetric study of brain structures in subtypes of depression]. *Psychiatriki,* 22**,** 120-31.

VECHT, C. J., HAAXMA-REICHE, H., NOORDIJK, E. M., PADBERG, G. W., VOORMOLEN, J. H., HOEKSTRA, F. H., TANS, J. T., LAMBOOIJ, N., METSAARS, J. A., WATTENDORFF, A. R. & *ET AL*. 1993. Treatment of single brain metastasis: radiotherapy alone or combined with neurosurgery? *Ann Neurol,* 33**,** 583-90.

VERMA, S., MILES, D., GIANNI, L., KROP, I. E., WELSLAU, M., BASELGA, J., PEGRAM, M., OH, D.-Y., DIÉRAS, V., GUARDINO, E., FANG, L., LU, M. W., OLSEN, S. & BLACKWELL, K. 2012. Trastuzumab Emtansine for HER2-Positive Advanced Breast Cancer. *New England Journal of Medicine,* 367**,** 1783-1791.

VIGLIANI, M. C., DUYCKAERTS, C., HAUW, J. J., POISSON, M., MAGDELENAT, H. & DELATTRE, J. Y. 1999. Dementia following treatment of brain tumors with radiotherapy administered alone or in combination with nitrosourea-based chemotherapy: A clinical and pathological study. *Journal ofNeuro-Oncology,* 41**,** 137-149.

WALKER, A. J., RUZEVICK, J., MALAYERI, A. A., RIGAMONTI, D., LIM, M., REDMOND, K. J. & KLEINBERG, L. 2014. Postradiation imaging changes in the CNS: how can we differentiate between treatment effect and disease progression? *Future Oncol,* 10**,** 1277-97.

WANG, H., TAN, L., WANG, H. F., LIU, Y., YIN, R. H., WANG, W. Y., CHANG, X. L., JIANG, T. & YU, J. T. 2015. Magnetic Resonance Spectroscopy in Alzheimer's Disease: Systematic Review and Meta-Analysis. *J Alzheimers Dis,* 46**,** 1049-70.

WANG, S., QIU, D., SO, K. F., WU, E. X., LEUNG, L. H., GU, J. & KHONG, P. L. 2013. Radiation induced brain injury: assessment of white matter tracts in a pre-clinical animal model using diffusion tensor MR imaging. *J Neurooncol,* 112**,** 9-15.

WARRINGTON, J. P., CSISZAR, A., JOHNSON, D. A., HERMAN, T. S., AHMAD, S., LEE, Y. W. & SONNTAG, W. E. 2011. Cerebral microvascular rarefaction induced by whole brain radiation is reversible by systemic hypoxia in mice. *Am J Physiol Heart Circ Physiol,* 300**,** H736-44.

WESTBROOK, C., ROTH, C. K. & TALBOT, J. 2008. *MRI in Practice* United Kingdom Blackwell Publishing

WHITFIELD, G. A., KENNEDY, S. R., DJOUKHADAR, I. K. & JACKSON, A. 2014. Imaging and target volume delineation in glioma. *Clin Oncol (R Coll Radiol),* 26**,** 364-76.

WILKE, C., GROSSHANS, D., DUMAN, J., BROWN, P. & LI, J. 2018. Radiation-induced cognitive toxicity: pathophysiology and interventions to reduce toxicity in adults. *Neuro Oncol,* 20**,** 597-607.

WONG, E. C., BUXTON, R. B. & FRANK, L. R. 1998. Quantitative imaging of perfusion using a single subtraction (QUIPSS and QUIPSS II). *Magn Reson Med,* 39**,** 702-8.

WONG, J., HIRD, A., KIROU–MAURO, A., NAPOLSKIKH, J. & CHOW, E. 2008. Quality of life in brain metastases radiation trials: a literature review. *Current Oncology* 15**,** 25-45.

XU, K. & LAMANNA, J. C. 2006. Chronic hypoxia and the cerebral circulation. *J Appl Physiol (1985),* 100**,** 725-30.

YEN, P. S., TEO, B. T., CHIU, C. H., CHEN, S. C., CHIU, T. L. & SU, C. F. 2009. White Matter tract involvement in brain tumors: a diffusion tensor imaging analysis. *Surg Neurol,* 72**,** 464-9; discussion 469.

YEO, B. T., KRIENEN, F. M., SEPULCRE, J., SABUNCU, M. R., LASHKARI, D., HOLLINSHEAD, M., ROFFMAN, J. L., SMOLLER, J. W., ZÖLLEI, L., POLIMENI, J. R., FISCHL, B., LIU, H. & BUCKNER, R. L. 2011. The organization of the human cerebral cortex estimated by intrinsic functional connectivity. *J Neurophysiol,* 106**,** 1125-65.

YETKIN, F. Z. & MENDELSOHN, D. 2002. Hypoxia imaging in brain tumors. *Neuroimaging Clin N Am,* 12**,** 537-52.

YIDONG MA, M. L., YONG YIN, LI KONG, XINDONG SUN, XIUTONG LIN, AND JINMING YU, 2010. Hypofractionated Stereotactic Radiotherapy for Brain Metastases: A Dosimetric and Treatment Efficiency Comparison Between Volumetric Modulated Arc Therapy and Intensity Modulated Radiotherapy. *Technology in Cancer Research and Treatment,* 9**,** 499-507.

YORKE, E. D. 2001. Modeling the effects of inhomogeneous dose distributions in normal tissues. *Semin Radiat Oncol,* 11**,** 197-209.

ZAWASKI, J. A., SABEK, O. M., VOICU, H., EASTWOOD LEUNG, H. C. & GABER, M. W. 2017. Effect of Brain Tumor Presence During Radiation on Tissue Toxicity: Transcriptomic and Metabolic Changes. *Int J Radiat Oncol Biol Phys,* 99**,** 983-993.

ZHANG, I., ANTONE, J., LI, J., SAHA, S., RIEGEL, A. C., VIJEH, L., LAURITANO, J., MARRERO, M., SALAS, S., SCHULDER, M., ZINKIN, H., GOENKA, A. & KNISELY, J. 2017. Hippocampal-sparing and target volume coverage in treating 3 to 10 brain metastases: A comparison of Gamma Knife, single-isocenter VMAT, CyberKnife, and TomoTherapy stereotactic radiosurgery. *Pract Radiat Oncol,* 7**,** 183-189.

ZHANG, L., ZUO, X.-N., NG, K. K., CHONG, J. S. X., SHIM, H. Y., ONG, M. Q. W., LOKE, Y. M., CHOO, B. L., CHONG, E. J. Y., WONG, Z. X., HILAL, S., VENKETASUBRAMANIAN, N., TAN, B. Y., CHEN, C. L.-H. & ZHOU, J. H. 2020a. Distinct BOLD variability changes in the default mode and salience networks in Alzheimer's disease spectrum and associations with cognitive decline. *Scientific Reports,* 10**,** 6457.

ZHANG, L., ZUO, X. N., NG, K. K., CHONG, J. S. X., SHIM, H. Y., ONG, M. Q. W., LOKE, Y. M., CHOO, B. L., CHONG, E. J. Y., WONG, Z. X., HILAL, S., VENKETASUBRAMANIAN, N., TAN, B. Y., CHEN, C. L. & ZHOU, J. H. 2020b. Distinct BOLD variability changes in the default mode and salience networks in Alzheimer's disease spectrum and associations with cognitive decline. *Sci Rep,* 10**,** 6457.

Appendix I – Study Protocol

An observational study of neurocognitive function in patients undergoing Stereotactic Radiosurgery at Velindre Cancer Centre

Version 1.0 (14/10/2016)

Version 2.0 (03/11/2016)

Version 3.0 (10/02/2017)

Version 3.1 (04/03/2019)

1. Investigators (in Alphabetical Order)

Dr Helen Bulbeck
Founder and Director of Brain Trust Charity
Brain Trust Charity
4 Yvery Court
Castle Road
Cowes
PO31 7QG
Tel: 0778 8722156
Email: Helen@braintrust.org.uk

Prof William Gray
Professor of Functional Neurosurgery, Neurosciences & Mental Health Research Institute
Cardiff University Brain Research Imaging Centre (CUBRIC)
School of Psychology
Maindy Road,
Cardiff
CF24 4HQ
Tel: 029 2068 8491
Email: GrayWP@cardiff.ac.uk

Mr Chris Hurt
Senior Research Fellow (Statistics)
Centre for Trials Research,
College of Biomedical & Life Sciences
7th Floor, Neuadd Meirionnydd,
Heath Park, Cardiff
CF14 4YS
Tel: 029 2068 7471

Email: hurtcn@cardiff.ac.uk

Dr Anne Johnson
Consultant Clinical Psychologist
Velindre Cancer Centre
Velindre Road
Cardiff
CF14 2TL
Tel: 029 2019 6141
Email: Anne.Johnson2@wales.nhs.uk

Prof Derek Jones
Director
Cardiff University Brain Research Imaging Centre (CUBRIC)
School of Psychology
Maindy Road,
Cardiff
CF24 4HQ
Tel: 029 2087 9412
Email: JonesD27@cardiff.ac.uk

Prof Geraint Lewis
Head of Medical Physics
Velindre Cancer Centre
Whitchurch
Cardiff
CF14 2TL
Tel: 029 2031 6913
Email: Geraint.lewis4@wales.nhs.uk

Mr Tony Millin
Head of Radiotherapy Physics Treatment Planning
Velindre Cancer Centre
Whitchurch
Cardiff
CF14 2TL
Tel: 029 2031 6192
Email: tony.millin@wales.nhs.uk

Dr James Powell
Consultant Clinical Oncologist
Velindre Cancer Centre
Whitchurch
Cardiff
CF14 2TL
Tel: 02920 615888

Email: james.powell2@wales.nhs.uk

Dr Najmus Sahar Iqbal
Clinical Research Fellow
Velindre Cancer Centre
Whitchurch
Cardiff
CF14 2TL
Tel: 029 2061 5888
Email: IqbalNS@cardiff.ac.uk

Dr Michelle Smalley
Deputy Head of Neuropsychology Services & Honorary Senior Lecturer
University Hospital of Wales
Heath Park
Cardiff
CF14 4XW
Tel: 029 2074 3224
Email: drmichellesmalley@hotmail.co.uk

Dr Stefan Schwartz
Consultant Neuroradiologist
University Hospital of Wales
Heath Park
Cardiff
CF14 4XW
Tel: 029 2074 3027
Email: Stefan.Schwarz@wales.nhs.uk

Dr Maeve Smyth
Clinical Scientist
Velindre Cancer Centre
Whitchurch
Cardiff
CF14 2TL
Tel: 02920 615888
Email: maeve.smyth2@wales.nhs.uk

Dr John Staffurth
Consultant Clinical Oncologist & Clinical Senior Lecturer in Oncology
Velindre Cancer Centre
Whitchurch
Cardiff
CF14 2TL
Tel: 029 2031 6964
Email: john.staffurth@wales.nhs.uk

Prof Richard Wise
Head of MRI
Cardiff University Brain Research Imaging Centre (CUBRIC)
School of Psychology
Maindy Road,
Cardiff
CF24 4HQ
Tel: 02920 870358
Email: wiserg@cardiff.ac.uk

2. Sponsor

Velindre NHS Trust,
Velindre Cancer Centre,
Whitchurch Road,
Cardiff
CF14 2TL

3. Funding

This study is funded by the Moondance charitable fund and the Headfirst Brain Tumour Appeal at Velindre Cancer Centre.

4. Confidentiality Statement

This document contains confidential information that must not be disclosed to anyone other than the Sponsor, the Investigator Team, Velindre Cancer Centre, Cardiff University, and members of the Research Ethics Committee

5. Investigator Delegation Log

Name	Role
Mr Andrew Bryant	Radiotherapy Physicist, Velindre Cancer Centre Involved in SRS treatment planning Andrew.bryant@wales.nhs.uk
Prof William Gray	Professor of Functional Neurosurgery, Neurosciences and Mental Health, CUBRIC, School of Psychology, Cardiff University Graywp@cardiff.ac.uk
Mr Tony Millin	Head of Radiotherapy Physics Treatment Planning Responsible for SRS treatment planning

	Tony.millin@wales.nhs.uk
Dr Najmus Sahar Iqbal	Clinical Research Fellow, Velindre Cancer Centre, and Cardiff University. Responsible for study design and conduct, consent, providing patient information, MRI data collection and analysis IqbalNS@cardiff.ac.uk
Dr Anne Johnson	Consultant Clinical Psychologist, Velindre Cancer Centre. Responsible for NCF test and data collection Anne.johnson2@wales.nhs.uk
Dr James Powell	Consultant Clinical Oncologist, Velindre Cancer Centre Chief Investigator, Responsible for patient selection and involved in the design of the study James.powell2@wales.nhs.uk
Dr Michelle Smalley	Clinical Psychologist in Neuropsychology. Responsible for NCF test selection and analysis drmichellesmalley@hotmail.co.uk
Dr Maeve Smyth	Clinical Scientist, Velindre Cancer Centre Involved in SRS treatment planning and MRI data analysis Maeve.smyth2@wales.nhs.uk
Dr Owen Tilsley	Consultant Clinical Oncologist, Velindre Cancer Centre. Involved in patient selection Owen.tisley@wales.nhs.uk
Prof. Richard Wise	Principal Investigator, Head of MRI, responsible for set up of the study and for study conduct at CUBRIC. WiseRG@cardiff.ac.uk

6. Glossary of Common Abbreviations

ASL	Arterial Spin Labelling
BOLD	Blood Oxygen Level Dependant
CBF	Cerebral Blood Flow
CT	Computed Tomography
CUBRIC	Cardiff University Brain Research Imaging Centre
DVH	Dose Volume Histogram
fMRI	Functional Magnetic Resonance Imaging
Gy	Gray (Measure of Radiation Dose)
SRS	Stereotactic Radiosurgery
MDT	Multi-Disciplinary Team
MRI	Magnetic Resonance Imaging
NCF	Neurocognitive Function
QoL	Quality of Life
RT	Radiotherapy

WBRT	Whole Brain Radiotherapy
WHO PS	World Health Organisation Performance Status
VCC	Velindre Cancer Centre

7. Purpose of the study and Scientific Rationale

Stereotactic radiosurgery (SRS) and whole brain radiotherapy (WBRT) has demonstrated a survival benefit over WBRT alone, establishing SRS treatment for 1-3 brain metastases. This improved outcome has put greater emphasis on quality of life (QoL) following treatment and particularly on the deleterious effect on neurocognitive function (NCF) of WBRT. Consequently, SRS is increasingly delivered without WBRT, in favour of close surveillance, as a strategy to preserve NCF in patients with brain metastases. Nevertheless, even in patients treated with SRS alone a sizeable proportion of patients (20 – 25% of patients reported in randomised trials) suffer reduced NCF, with memory the most commonly affected neurocognitive domain.

The effect of radiation on neurogenesis in the hippocampus has been implicated in the reduced NCF evident following WBRT and techniques such as hippocampal–sparing radiotherapy have been evaluated to limit hippocampal radiation dose during WBRT. However, limited information exists to define appropriate radiation dose tolerance constraints for the hippocampus either for standard radiotherapy fractionation or for hypofractionated radiotherapy regimens used in SRS. Equally, other structures within the brain important for NCF exist, including the amygdala, striatum, mamillary body and prefrontal cortex, which have not been as extensively evaluated for the effect of radiation on NCF and limited studies have correlated neurocognitive outcomes with radiation dose and neurophysiological change in these structures. Mechanistic understanding of neurocognitive decline following radiotherapy is also limited although different hypotheses exist including vascular injury, white matter injury, loss of brain plasticity and functional network disruption.

We propose conducting a prospective observational study evaluating NCF in 40 patients treated with SRS at Velindre Cancer Centre (VCC) over 2 years, recruiting patients over 18 months. We will correlate clinical changes in NCF with radiation dosimetry to the hippocampus, wider limbic system, and prefrontal cortex. Additionally, in a collaborative, translational study, serial MRI scans will be performed at the Cardiff University Brain Research Imaging Centre (CUBRIC) where functional, physiological, and structural change using functional and spectroscopic MRI techniques will be evaluated in these different structures. Specific neurocognitive and spectroscopic assessments sensitive for detecting changes in hippocampal neurogenesis will also be performed at CUBRIC. NCF will be assessed by performing a formal neurocognitive test battery assessing different cognitive domains including memory, processing, executive function, verbal fluency, and motor dexterity. QoL will be assessed using standardized EORTC assessment of physical, emotional, and social wellbeing. Each patient will undergo neurocognitive testing at VCC pre-treatment and at 1, 3 and 6 months following SRS treatment**.** The translational MRI study will be performed in these patients and for this the patients will have MRI brain scans performed at CUBRIC at baseline and at 1 and 3 months after treatment.

Changes in NCF will be correlated with radiation dose measurements and changes on MRI scans. Our hypothesis is that radiation dose to the cognitive structures will correlate with worsening NCF and with changes in functional MRI markers such as hippocampal blood flow and diffusion. The primary outcome measure of this study will be memory, assessed by formal NCF testing, at 3 months. This study will help define radiation tolerance doses for the cognitive structures described using SRS and may identify radiation induced MRI markers of neurcognitive deterioration offering mechanistic and predictive insights that can evaluated prospectively in a randomized trial.

The purpose of this study is to evaluate the effects of hypofractionated radiation on NCF and function in the cognitive structures including hippocampus, limbic system, and prefrontal cortex in adult patients with brain metastases following treatment with SRS. To do this we will conduct a prospective observational study of NCF in patients receiving this treatment and correlate NCF with radiation dosimetric dose-volume histogram (DVH) data. Our hypothesis is that greater radiation dose to these structures will correlate with post treatment NCF impairment and that dosimetric DVH parameters will be able to be defined that predict for NCF deterioration. NCF impairment will also be correlated with structural and functional changes detected on post treatment MRI scans using latest MRI technology based at CUBRIC.

The main objectives of this study are:

4) To measure changes in NCF in patients receiving SRS at VCC for one to three brain metastases.
5) To correlate radiation dose received by the hippocampus and other cognitive structures with changes in NCF and identify if radiation dose parameters to these structures are predictive for NCF decline.
6) To measure structural and functional changes in the cognitive structures radiation by MRI and correlate these with decline in NCF.

8. Project Summary

Planned Start Date	January 2017
Study Design	Observational
Study Participants	Adult Patients with 1-3 brain metastases eligible for stereotactic radiosurgery treatment
Planned Sample Size	40
Planned Study Period	24 months

Project Aim	The overall aim of the study is to assess changes in neurocognitive function after stereotactic radiosurgery
Primary Objective	To measure neurocognitive function at 3 months after completion of SRS
Secondary Objectives	• Comprehensive measurement of NCF at baseline and at 1, 3 and 6 months following SRS. • Develop standardised protocols for contouring the hippocampus and other cognitive structures at VCC. • Statistical correlation between NCF and radiation dosimetry to hippocampus and associated cognitive structures. • Assess if radiation dosimetric paramaters to cognitive structures predicts NCF impairment after SRS, identify dosimetric parameters most important for predicting NCF decline and produce formal dose constraints based on this work. • Identify structural and physiological changes in the cognitive structures after SRS using structural, spectroscopic, and functional MRI markers.

9. Study Design

a. Participants

We aim to recruit 40 patients to the study. In line with the retrospective analysis we consider this would be feasible to achieve in a 24 month period. All patients will be discussed and assessed at the weekly South Wales Neuro-Oncology multi-disciplinary team meeting (MDT) at University Hospital of Wales. Selection of patients for SRS will be made by the MDT and consideration for neurosurgical treatment will be made in all cases where appropriate. SRS will only be recommended with the collective agreement of the Neuro-Oncology MDT.

Potential participants who fulfil the eligibility criteria will be provided with the study information at their first consultation at Velindre Cancer Centre and will be given as much time as they require (minimum 24 hour) to decide if they wish to participate. Patients will be required to have capacity to consent for the treatment.

b. Summary of Study Design

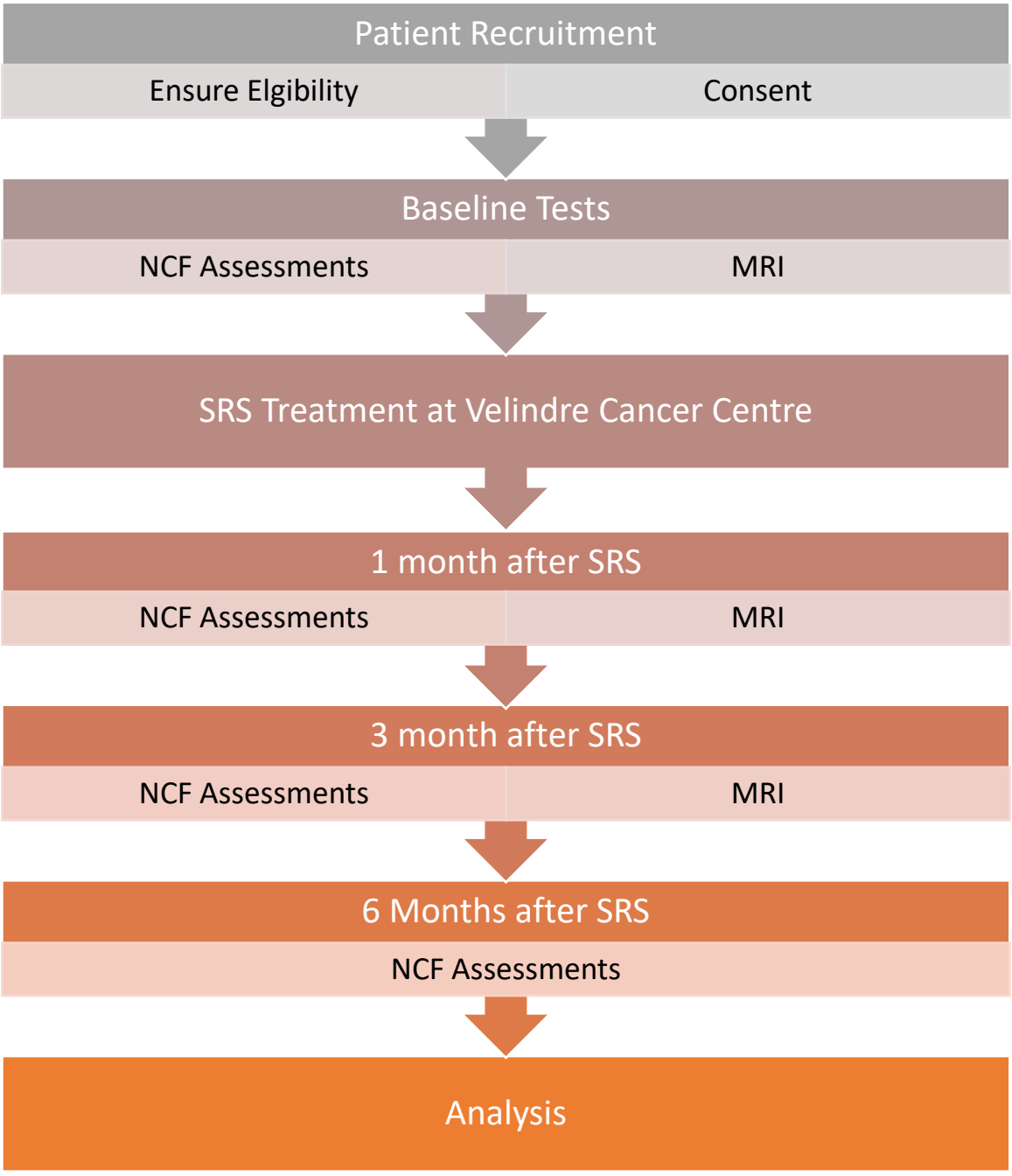

c. Eligibility Criteria

Inclusion criteria:-

- Patients ≥ 18 years of age
- WHO Performance status 0 - 2
- All patients must have undergone prior assessment by the South Wales Neuro-Oncology MDT and SRS must be the recommended treatment with the collective agreement of the MDT.
- Patients will have one to three cranial metastases undergoing stereotactic radiosurgery.
- Patients will have established diagnosis of cancer and absent or controllable primary disease with an estimated prognosis of ≥ 6 months.
- Pre-treatment scans must not show a tumour volume of more than 20cc. This will usually mean that no individual tumour has a diameter in excess of 3cm.
- A brain magnetic resonance imaging (MRI) scan (may be the MRI planning scan) will be required within 1 month of recruitment to the study.

Exclusion criteria:-

- Contra-indication to MRI
- Patients presenting with pressure symptoms best relieved by neurosurgery
- Prior history of neurosurgery, SRS or WBRT
- Histological diagnosis of leukaemia, lymphoma, germ cell tumour or small cell carcinoma.
- Presence of leptomeningeal disease.
- Pregnancy
- Patients with pre-existing diagnosed neurocognitive dysfunction

d. Study Sites

Study site	**Research Activity**
Velindre Cancer Centre	Recruitment of participants Eligibility Screening Reviewing participant medical notes Study Participation Consent Neurocognitive Assessments Stereotactic Radiosurgery
Cardiff University Brain Research Imaging	Study Participation Consent

Centre (CUBRIC)	Neurocognitive Assessments MRI

e. Radiation Dosimetry Protocol

All the patients in the study have detailed radiation dosimetric assessments. The latest version of the Velindre SRS clinical protocol will be followed throughout the study. This protocol is subject to ongoing clinical review at Velindre Cancer Centre and any updates to this clinical protocol will be adopted for this study to ensure that the most up to date standard SRS treatment clinical protocol is followed for the purposes of this study. At present the SRS treatment clinical protocol is as follows:

Technique

Immobilisation will be achieved using the BrainLab Frameless Radiosurgery immobilisation system. All patients will undergo a non-contrast enhanced CT planning scan (0.6 mm slice thickness) and MRI planning scan (1 mm slice thickness). The planning images will be localised and fused using Brainlab CT localiser and target volumes will be defined using the iPlan planning software. All patients will be conformally planned using a dynamic arc treatment technique.

Target Volume Delineation

Target volumes will be delineated using the iPlan RT Image module. Typically, fused contrast-enhanced T1 weighted MRI images are utilised for outlining the gross tumour volume (GTV) and organs at risk. Planning target volume (PTV) are created using advanced manipulation within the software with the following margins applied:
GTV – visible tumour on contrast enhanced T1 weighted image
PTV = GTV + 1 mm

Doses

The dose prescribed for SRS is dependent upon the volume of the PTV. The prescription doses will be as follows:
Single fractions:
21 Gy to 80% isodose, PTV < 7 cc
18 Gy to 80% isodose, PTV 7-13 cc
15 Gy to 80% isodose, PTV > 13 cc
Fractionated course, typically 21 Gy in 3 fractions, delivered over consecutive days, may be considered – prescribed to 90% isodose PTV > 20 cc (diameter > 3.4 cm).

Organs At Risk (OAR) delineation

The following organs at risk are contoured as standard: Brainstem, Optic Nerves, Optic Chiasm, Eyes, Lens, Brain (normal tissue) and Cochlea. These structures will be outlined using the auto segmentation tool on the RT image module on iPlan. In addition to this for this study additional structures, considered critical for cognition, will be contoured including the hippocampus, limbic system, amygdala, striatum, mamillary bodies and prefrontal cortex. These structures will be outlined manually by the clinician. All OARs have a 1 mm symmetrical margin for Planned Risk Volume (PRV).

Considerable age and disease specific variability in hippocampal size and location has been described limiting the applicability of autocontouring techniques for the delineation of the hippocampus using population-generated atlases. Equally, automated atlases do not specifically concentrate on the dentate gyrus, considered to be the critical portion of the hippocampus for memory function. Many neuroanatomical protocols have been published for defining the human hippocampus using cerebral MRI and for this study the hippocampus will be delineated according to the RTOG 0933 Hippocampal Contouring Atlas (Gondi V*et al* 2010). This contouring protocol concentrates particularly on the dentate gyrus and cornu ammonus portions of the hippocampus, where neural progenitor cells important for new memory are considered to be located. For the additional cognitive structures the following cross sectional anatomy and imaging books will be used and contouring reviewed by radiology. Examples of some of these books are:
Diagnostic and Surgical Imaging Anatomy - Brain, Head, Neck & Spine. Harnsburger, Osborn, MacDonbald & Ross
Human Sectional Anatomy. Ellis.

Delineation of the cognitive structures will be performed after completion of SRS treatment to ensure that no inadvertent effort at sparing these structures is undertaken during treatment planning.

Dosimetry paramaters and Re-planning

Reported radiotherapy dose constraints to the hippocampus vary considerably in the literature and these have rarely been correlated with clinical outcome therefore presently there is little to support the routine use of a particular dose constraint. Most groups recommend minimising dose to the bilateral hippocampi but one study of paediatric intracranial tumours spared the contralateral hippocampus only due to the proximity of the PTV to the ipsilateral hippocampus (Marsh JC *et al* 2012). A retrospective study of 18 adults with benign or low grade brain tumours suggested that hippocampal dosimetry predicted for neurocognitive function impairment after *fractionated* stereotactic radiotherapy and reported that radiation dose greater than 7.3 Gy to 40% of the bilateral hippocampi was associated with impaired memory function (Gondi V *et al* 2013). The phase II RTOG 0933 trial demonstrated preservation of quality of life and memory with hippocampal sparing WBRT. In this study 100% of the hippocampus could not exceed 9Gy and maximal hippocampal dose could not exceed 16 Gy in 10 fractions (Gondi V *et al* 2014). The upcoming UK HIPPO trial, is employing similar dose constraints for hippocampal-sparing WBRT with mandatory dose constraints to single hippocampus including mean dose <11 Gy and D2% < 15Gy.

Very few studies have been performed evaluating hippocampal dosimetry specifically in patients undergoing SRS and very few hippocampal dose constraints have been reported for SRS. The SABR UK consortium guidance have not provided hippocampal dose constraints within the CNS dose constraints section in the most recent protocol (version 5, January 2016).

For this study we will look at a series of volumetric dose constraints in the hippocampus and other critical cognitive structures. DVHs will be generated for the left and right hippocampi

individually and for the composite bilateral hippocampi. Doses to deciles (D10% to D100%), and the maximum dose (Dmax), of individual and combined hippocampal volumes, will be determined, and tabulated. Doses to the additional structures will also be reported. Our hypothesis is that hippocampal dosimetry is associated with NCF loss, and we will compare high-dose vs. low-dose groups in terms of NCF impairment with NCF impairment measured in the different neurocognitive domains as a binary outcome variable.

Finally, a radiotherapy modeling study will be performed on the cases identified as having high doses to the neurocognitive structures to evaluate if alternative radiotherapy plans could be generated which will limit dose to these structures. This will involve a formal comparison between different Linac-delivered SRS techniques including static field SRS, dynamic conformal arc SRS and inverse planned SRS, developing class solutions, using Brainlab Elements software. We also aim to perform dose distribution modeling comparisons between these Linac-based methods and gamma knife radiotherapy plans and proton beam radiotherapy plans and this component of the work will require support from Medical Physics.

f. NCF Assessment Protocol

40 patients will be recruited over 24 months and will undergo formal neurocognitive function assessment measuring performance in the following neurocognitive domains:- memory, processing, executive function, verbal fluency, attention span, verbal memory, dexterity, and learning. Testing will involve a battery of different tests taking around 45 minutes per assessment and will be performed by the Clinical Psychology team at Velindre Cancer Centre. To limit additional hospital visits an attempt will be made to perform NCF assessments when patients attend other appointments and travel expenses are available for the psychologist to travel to perform the tests nearer the patients' home where necessary. NCF assessment will be performed at baseline (before start of SRS) and at 1, 3 and 6months following SRS. QoL will be formally assessed using a standardised assessment of physical, emotional, and social wellbeing and fatigue and pain scores will be calculated to control for these confounding factors. Patients will be screened, lasting roughly 5 minutes, for mood, anxiety and IQ at their initial clinic visit to assess their suitability for neurocognitive testing.

The NCF test battery has been chosen as these are widely used, standardised psychometric assessments that have shown sensitivity to the neurotoxic effects of cancer treatment and have been recommended by an International research group for the evaluation of patients with secondary brain tumours. These tests come with data that can be used to minimize the effects of repeat administration and to limit the effect of learning on test outcomes. These NCF tests also align closely with standard assessments used by CUBRIC, for example in the epilepsy surgery service, facilitating possible future comparisons to be made between different patient cohorts. The primary outcome measure of this study will be memory, assessed by formal NCF testing, at 3 months.

NCF results will be compiled by the Clinical Psychology department and presented to the clinical study team with detail of performance of each patient, at each timepoint in each neurocognitive domain. This data will then be correlated with radiation dosimetric information.

g. MRI Protocol

All additional MRI will be performed at CUBRIC, Cardiff University Brain Research Imaging Centre. The CUBRIC facility features state of the art MRI technology and is an internationally recognised brain research imaging centre providing the latest MRI technology and equipment making it a unique facility within Europe. In this study serial MRI scans will be performed on up to 40 patients evaluating functional, physiological, and structural changes in different neurological structures using advanced 3 Tesla, functional metabolic and microstructural MRI techniques.

Patients will undergo formal NCF testing as well as quality of life assessments at VCC prior to SRS and at 1, 3 and 6months following completion of SRS treatment. In addition, patients will have MRI brain scans at baseline, 1 and 3 months at CUBRIC.

MRI Scanning Protocol

Patients will attend CUBRIC in order to have transational MRI which will be in addition to standard MR planning that is carried out in Velindre Cancer Centre. Patients would be expected to arrive 30 minutes before the time given in order to carry out MR safety checks (see appendix 1) and change into a gown. A private room is provided with lockers for this. The scans are expected to last between 90 and 120 minutes and may involve scans in 2 different MRI scanners.

Patients will be provided with ear plugs to reduce the noise being transmitted from the MRI scanner. An emergency button is given to the pariticipants to use, should they require assitance during the scan. There is regular communication between the MR operator and the patient. Thus the patients will be able to come out of the scanner should they need to do so. Patients are constantly observed by the MR operator and instructions are given to the patient via a microphone.

The following MRI scans and measurements will be performed at each visit:-

1) Structural 3 Tesla MRI

   Detailed structural measurements of areas of interest including size, shape and volume using different T1 and T2 sequences in two and three dimensional scanning. Diffusion imaging.

2) Functional 3 Tesla MRI

   Blood flow measurements using the arterial spin labelling (ASL) technique
   Task-related scans to make functional MRI measurements using blood-oxygen-level dependent (BOLD) contrast imaging
   Resting state functional imaging to measure network connectivity

3) 3 Tesla MR Spectroscopy

   Metabolic analysis of left and right hippocampus examining metabolites related to hippocampal neurogenesis. Examples of such metabolites include NAA, Choline, Creatine and Myo-Inositol among others that may be measured during the study.

4) 3 Tesla CONNECTOM microstructural MRI

   Diffusion-weighted MRI techniques to measure fine tissue microstructure and connectivity.

In order to carry out functional analysis, patients may be given tasks to carry out within the scanner that will involve memory tests and instructions for these are relayed through screen visible within the scanner.

MRI Analysis Protocol

Structures within the brain important for neurocognition will be assessed using MRI including the hippocampus, limbic system including amygdala and mammillary bodies, striatum, and prefrontal cortex. Structural and physiological MRI measurements will be made in each of these structures at baseline, 1 and 3 months and comparison made between MRI findings before and after SRS treatment. Structural measurements of organ size, volume and shape, functional measurements of fluctuations in cerebral blood flow using arterial spin labeling, changes in displacement of water molecules and white matter tract integrity using the diffusion tensor imaging, and microstructural measurements of glial structure and white matter tract integrity using diffusion MRI will be made. In addition, in the collaboration with the Gray research group, MR spectroscopic metabolic analysis will be performed examining metabolites related to hippocampal neurogenesis.

This imaging study will provide comprehensive MRI assessment using a combination of different MRI modalities and employing 3 Tesla MRI technology, functional MRI, diffusion MRI and MR spectroscopy at each visit.

10. Ethical Considerations

a. Patient Participation

Patients with brain metastases are often excluded from other clinical trials, hence we envisage that patients will be willing to participate in the study. However, cancer patients can feel compelled to enter clinical trial at times. We will use the following measures to reduce possibility of patients feeling pressurised in any way to enter the study:

1. We will use patient information leaflets written in lay language so participants can read information in their own time and make a decision.
2. We will approach patients in a non-threatening manner to minimise such concerns. Patient and public involvement has been sought throughout the development of this study by the Brainstrust charity, who have formally endorsed the study.
3. All patients will be given a minimum of 24 hours to consider participation in the study.

4. Patients willing to participate will be consented by Dr Iqbal, MD student undertaking this project, who will not be directly involved in patient's care.

b. MRI

Patients undergoing SRS for brain metastases normally have 2 MRI scans of the head before radiotherapy, therefore patients know what to expect during the scans. Although an MRI scan can be claustrophobic, this is less so with the latest, more compact system that is available in the Cardiff University Brain Research Imaging Centre (CUBRIC). Patients will be required to have 3 additional MRI scans at CUBRIC as part of this study, 1 before SRS treatment and 2 afterwards at 1 month and 3 months. Each scan will be approximately 2 hours long. Patient will undergo half the scan and will then have a break with a drink before going into the scanner again. There is no extra radiation involved with MRI scans. If the participants find the experience in the scanner unpleasant they may opt out of the MRI component of the study. CUBRIC has an open and friendly atmosphere with plenty of space available for patients to wait. Patients will be asked to perform some tasks in the scanner that will test their memory in order to gain information such as blood flow changes in areas involved in cognition.

The MRI scans at CUBRIC are for research purposes only and not used for clinical interpretation. The following procedure for incidental MRI findings has been previously approved by NREC for CUBRIC research project entitled, "Predicting the individual's potential for functional recovery in Multiple Sclerosis: a novel clinical and neuroimaging strategy" (REC reference:15/SW/0105, IRAS project ID 165980) CUBRIC is wholly research-orientated and the images of the brain are for specific research purposes only and are not intended for diagnosis of pathology. Participants' scans will undergo review for quality control purposes by a CUBRIC MRI Operator. In the event that an incidental structural abnormalities is suspected (beyond the expected pathology), the CUBRIC procedure for incidental findings will be followed. This includes specialist neuroradiological review and contact with the patient's oncologist or GP, as appropriate, to arrange for follow-up if indicated.

c. Neurocognitive Tests

All patients in the study will be required to undergo neurocognitive testing with a trained psychologist. The tasks are to test memory with simple questioning along with other higher mental functions. Crude neurocognitive assessments of patients is already done in clinical practice, however, these specific tests will distinguish between different neurocognitive domains, such as immediate recall, delayed recall, and motor dexterity. Measure of fatigue, quality of life and pain will also be taken at each visit. Patients will be assessed in a familiar clinical environment in order to minimise confounding factors. To minimise patient visits, base line neurocognitive function is planned to be done combined with radiotherapy planning visit. The battery of neurocognitive tests proposed will typically not take longer than 45 minutes to complete. There is a possibility that participants may become tired during the test. Patients will be assessed in a relaxed environment and may have a break in the middle of the assessments for refreshment and then continue with the remaining assessments.

d. Data Confidentiality - MRI

Data will be stored within a firewall and password−protected computer system (CUBRIC fileserver) within a swipe−card secured building. As is the case with MRI data, CUBRIC researchers associated with the study will have confidential access to files, which allow the matching of recorded data to participants. Any identifying information collected will be kept separately in a locked filing cabinet in the swipe−card secured building. No data will leave CUBRIC without being anonymised, i.e., identifying data will be removed from the dataset. Data will be archived to optical disks or hard-drives.

e. Date Confidentiality - Neurocognitive Tests

Data will be stored within a firewall and password protected encrypted computer system in Velindre NHS Trust. No data will leave Velindre NHS Trust computers without being completely anonymised. Any paper copy will be stored in patient's medical notes that is stored in a swipe card secured area of the hospital.

Anonymised data may be shared with the organisation funding the study. Anonymised data may be shared with researchers at other organisations (non-commercial and commercial) in the UK or overseas and it may be made publicly available. All participant identification and referral procedures as well as procedures for data storage, processing and management will comply with the Data Protection Act 1998. Personal data (for the MRI scanning, the name, sex, age, weight, date of scan, name and address of the person's general practitioner (GP), consultant oncologist, and screening forms and the consent form) will be retained for 10 years and all information will held in a locked filing cabinet within CUBRIC, in line with CUBRIC record keeping rules and regulations. Anonymised non-identifiable data will be stored in locked cabinets and/or on secured computer hard-drives (password protected) in CUBRIC which is an access controlled building within the School of Psychology. This is in compliance with the guidelines set by the Cardiff University Research Governance Framework.

The confidentiality of participants will be preserved in accordance with the Data Protection Act 1998. All participants will be allocated a unique identifier and all data collected will be held in a linked anonymised form.

11. Statistics

a. Sample Size Considerations

This is an exploratory pilot study combining structural and functional MRI data acquisition with measures of neurocognition. We cannot make accurate prior calculations of effect sizes due to an absence of existing comparable data. A sample size of up to 40 patients will be recruited initially, based on feasibility and analysis of patients treated with SRS at Velindre Cancer Centre. As evident from the retrospective study, 30 patients are treated with SRS in 1 year thus by recruiting 40 patients in 2 years we are aiming to recruit 66% of total patient population and that this sample size would allow to estimate this proportion with 95% confidence intervals of 54%-80%.

We would also be able to calculate the standard deviation for your neurocognitive assessments that would allow sample size calculation for a definitive study. Depending on pilot data more participants may be recruited in a future amended study in order to increase power.

b. Data Analysis

Processing and analysis of functional images will be performed using standard methods available within the FMRIB software library and image analysis package FEAT (www.fmrib.ox.ac.uk/fsl) including registration packages and functional image analysis package FEAT as well as in-house Matlab and C shell scripts. Neurocognitive data and QoL questionnaires will be collated and analysed using standard statistical software packages such as SPSS or Matlab before being combined with imaging data. Correlation and regression (where appropriate) analysis between imaging and behavioral outcomes with random permutation testing to correct for multiple comparisons will allow the researchers to reach the study objectives and determine whether the data supports the study hypotheses.

12. Safety reporting

a. Definition of Serious Adverse Events

A serious adverse event is any untoward medical occurrence that:

- Results in death,
- Is life-threatening

NOTE: The term "life-threatening" in the definition of "serious" refers to an event in which the participant was at risk of death at the time of the event; it does not refer to an event which hypothetically might have caused death if it were more severe.

- Requires inpatient hospitalisation or prolongation of existing hospitalisation,
- Results in persistent or significant disability/incapacity, or
- Is a congenital anomaly/birth defect.
- Other important medical events*

*Other events that may not result in death, are not life threatening, or do not require hospitalisation, may be considered a serious adverse event when, based upon appropriate medical judgement, the event may jeopardise the participant and may require medical or surgical intervention to prevent one of the outcomes listed above.

b. Reporting Procedures for Serious Adverse Events

A serious adverse event (SAE) occurring to participants would be reported to the ethics committee that gave a favourable opinion of the study where in the opinion of the Chief Investigator the event was: ‘related’ – that is, it resulted from administration of any of the research procedures; and ‘unexpected’ – that is, the type of event is not listed in the protocol as an expected occurrence. Reports of related and unexpected SAEs would be submitted within 15 days of the Chief Investigator becoming aware of the event. A volunteer may

voluntarily withdraw from the study due to what he or she perceives as an intolerable adverse event (AE). If either of these occurs, the volunteer would be given appropriate care under medical supervision until symptoms cease or the condition becomes stable.

Financing and Insurance

This study is being funded through a grant from Moondance Programme Board which is charitable fund run by Velindre Cancer Centre as well as funding from the Headfirst Velindre Brain Tumour Appeal.

Appendix II – Patient Information Leaflet

An observational study of neurocognitive function in patients undergoing Stereotactic Radiosurgery at Velindre Cancer Centre

Patient Information Sheet and Consent Form

December 2016

REC Number: **16/WA/0374**

Study title

An observational study of neurocognitive function in patients undergoing Stereotactic Radiosurgery at Velindre Cancer Centre

Study Summary

Until recently, the radiotherapy that you would receive if you have cancer that has spread to the brain from somewhere else in the body (secondary cancer) would have been radiotherapy to the whole brain. Due to advances in this treatment we now have more precise radiotherapy treatment, called stereotactic radiosurgery, which allows tumours to be targeted more precisely.This also means that the radiotherapy dose can be increased to small areas of cancer in the brain because the radiotherapy treatment is more focused. Such advances in radiotherapy treatment mean that more people are living longer, so it is important that the side effects of treatment are reduced.

- Despite more targeted treatment some side effects still happen. This includes a reduction in memory which can affect between 25% and 50% of people.
- This reduction in memory following radiotherapy treatment is not fully understood but one important idea is that there are areas within the brain important for forming memories that are very sensitive to radiotherapy.
- When using this targeted radiotherapy it is not currently understood what dose of radiotherapy can be safely given to the areas in the brain which are important for forming memories. Also, it is not clear how radiotherapy has this problematic effect on memory.
- In this study we will perform detailed memory tests before and after radiotherapy treatment. We will also calculate the radiotherapy dose received by important structures within the brain and perform MRI scans of the brain.
- By combining these three pieces of information we predict that we will obtain important new information on which areas of the brain are important when delivering targetted brain radiotherapy treatment and what dose of radiotherapy is safe to deliver to these structures.
- We describe the study in detail in the remainder of this leaflet.

Invitation

Dr James Powell is a consultant oncologist specialising in the treatment of cancer within the brain and Dr Najmus Sahar Iqbal is a researcher with a specialist interest in treating brain tumours. We are particularly interested in researching and reducing the side effects of radiotherapy on memory and would like to invite you to take part in this study.

Before you decide, it is important for you to understand why the research is being done and what it will involve. Please take time to read this information carefully and discuss it with friends, relatives, and your GP if you wish. Please ask us if you would like more information. Take time to decide whether or not you wish to take part.

Why are we doing this study?

As your doctor has discussed with you, you have been diagnosed with cancer that has spread to the brain. You are planning to receive treatment with a targeted radiotherapy technique called stereotactic radiosurgery.

The aim of this study is to assess changes in memory and learning after this targeted radiotherapy treatment for the cancer that has spread to the brain. As part of your standard treatment, you will have already had a MRI brain scan. Following this you will have a MRI scan to help plan your radiotherapy treatment at Velindre Cancer Centre which is part of the standard treatment. If you take part in this study you will also have several assessments of your memory using questions and simple tasks and MRI scans (figure 1) at Cardiff University Brain Research Imaging Centre (CUBRIC). These will be in addition to standard scans that you would otherwise usually have.

The memory assessment will take approximately 45 minutes to complete and the MRI scans will take approximately 2 hours. By doing tests to measure memory and the additional MRI scans at CUBRIC, we can identify changes in memory and link these changes with the doses of radiotherapy given to different areas in the brain important for memory during your treatment. The relationship between these 3 pieces of information will provide important knowledge about the radiotherapy dose limitations of these structures within the brain.

Figure 1. MRI scanner at CUBRIC

Why am I being invited to take part?

This study is planned for patients such as you, who have cancer that has spread to the brain and who are undergoing targeted radiotherapy called stereotactic radiosurgery. Roughly half of patients undergoing this treatment report some reduction in memory when measured with memory assessments. This reduction in memory following radiotherapy is not fully understood, however, certain areas within the brain considered important for memory and learning are thought to be affected by radiotherapy.

What will happen to me if I take part?

In addition to your standard radiotherapy treatment you will have the specialist MRI scans at CUBRIC and memory tests before and after your treatment at specified time points. The MRI scan at CUBRIC is very similar to the MRI scan you will have at Velindre Hospital (see picture 1). Memory tests involve answering some questions relating to memory; you may be given a list of words or pictures and be required to recall these and you may be asked to perform some basic tasks. The MRI at CUBRIC will be done 3 times, once before treatment and twice afterwards at 1 month and 3 months. Memory tests will be done 5 times, once before treatment and 4 times afterwards at 1 month, 3 months, 6 months, and 9 months. It is important to note that the scans in CUBRIC are in addition to the routine follow up NHS MRI scans that are done 3 monthly.

When you come to CUBRIC, you will be asked to fill out MRI screening questionnaires. For your safety, you will be asked to remove all metal objects from your person including keys, coins, jewellery, and watches. We will ask you to change into 'scrubs' (like pyjamas) for the

purpose of the MRI scans and we will need you to remove your underwired bra, should you be wearing one. We have our own private changing room with lockers for you to use.

The MRI scans will involve a series of separate scans acquired one after the other while you rest in the MRI. You will be given a "squeeze ball" which you can use to signal to us if you want to stop the scan. If you squeeze this we will come and get you out immediately. We will also talk to you over the microphone between scans to check that everything is fine. We may ask you to perform one task inside the scanner. This involves pressing buttons in response to pictures or words that may appear on the screen. The task will be explained in more detail on the day. We will ask you to relax and stay very still for the scan session. Around halfway through you can have a break if you want so that you can get out and move around if needed.

What happens if you find something unusual on my scan in CUBRIC?

It is important that you know that the scans in CUBRIC are not intended to provide any information that may help your diagnosis or treatment. The staff conducting your scans will not be able to comment on the results of your MRI scans. Occasionally when a patient has a scan, the staff may be concerned that there is an unexpected abnormality on the scan which hasn't been seen before as this is a more detailed MRI scan than usual MRI scans. In this case, we will ask an appropriate doctor specialising in brain scans, to examine the images. If this doctor feels it to be appropriate, a report will be sent to your GP and/or oncologist, so that they may arrange for you to have further investigations.

Do I have to take part?

No. It is up to you to decide whether or not to take part. If you do choose to take part in the study, you will be asked to sign a consent form. A copy of the consent form and study information sheet will be given to you for your record. Your health care and legal rights are not affected by participation in the study. You will receive the same standard of treatment of care if you decide not to join the study.

What happens if I change my mind or am unable to continue during the study?

You are free to change your mind and withdraw from the study at any time without giving a reason. This will not affect the standard of treatment or care you receive. However, if this was to happen, we would like your permission to continue to collect the information on your progress that is routinely recorded in your medical records after you withdraw from the study. We would also like to retain the data collected up to the point of your withdrawal from the study so that the overall quality of the study is not affected. If, for any medical reason you are unable to continue involvement with the study we would also like your permission to retain the data and information collected up until that point.

What information will you be collecting as part of this study?

We will be collecting data from the memory tests, MRI scans and radiotherapy treatment that we have explained above. As well as this, to help analyse this data it will be important to collect some individual data relating to your personal characteristics such as age and sex as well as information related to your primary cancer treatment, past medical history, and regular medications. A lot of this information will already be recorded from when you meet the doctor for the first visit to assess you for the radiotherapy treatment. We will also be interested in knowing whether this information changes during the months after your treatment and so we will need to ask questions about whether there have been any changes to your general medical condition, treatment, or medications during clinic visits after radiotherapy. It will also be important to collect data relating to the tumour in the brain such as its position in the brain and size and number of tumours.

Will any tissue samples be taken from me?

No tissue samples will be taken from you for the purpose of study.

What are the side effects of any procedure when taking part?

There are no direct side effects of participation in the study, as you will be receiving standard therapy with a few extra scans and tests for memory. You will experience side effects of radiotherapy, which are not related to your participation in the study. Your doctors will discuss side effects of radiotherapy separately in detail with you.

What are the possible disadvantages and risks of taking part?

The MRI scans do not deliver any radiation; however, the extra scans do mean additional trips to the Cardiff University Brain Research Imaging Centre. We will try to minimise this inconvenience by arranging memory tests on the same day as your routine hospital appointment. If your local cancer centre is South West Wales Cancer Centre, we will endeavour to organize memory tests in Swansea. The specialist MRI scans can, however, only be carried out in Cardiff university. The CUBRIC building is a new building that has a friendly environment and plenty of space for you to be seen by the staff there. There is designated patient parking available which is located behind the building.

Will I receive travel expenses for the extra visits required by the study?

Yes, travel expenses will be provided for the additional visits that you are required to make to the CUBRIC building for your MRI scans. Payment will be made either according to mileage travelled if travelling by car or according to the cost of public transport if travelling by public transport. We may require you to keep receipts as a record of your journeys using public transport.

What are the possible benefits of taking part?

There may be no direct benefit for you. Currently, we know from other studies that a significant number of patients have some changes in memory after this treatment. However, there is little known about the effect of radiation on the structures within the brain that are important in memory. The community at large may benefit from the results of the study. This small pilot study might lead to a larger study, aimed at improving side effects for patients treated with radiotherapy, by using the information gathered in this study. It is possible that new information obtained from the research MRI scan may alter your treatment plan though this is considered to be very unlikely as you will already have undergone a detailed MRI scan at Velindre Hospital to provide accurate information about location and size of the secondary brain tumours. If new information is gained from the MRI scan at CUBRIC this will be discussed with you in detail by your consultant.

Will my taking part in this study be kept confidential?

Yes, all information that is collected about you during the course of the study will be kept strictly confidential. Members of the study team, medical team, authorised personnel from Cardiff University and the audit team will have access to your data. All personnel will have a duty of confidentiality to you as a research participant. Your unique trial number will be used to make sure you cannot be identified outside the trial. We will notify your GP to inform them that you are participating in this study. No data will leave Cardiff University or Velindre Cancer Centre without being anonymised, i.e., information identifying you will be removed from it. Custody of the data remains with the Chief and Principal Investigator at Velindre Cancer Centre and CUBRIC. Your data may be used for further research projects within and outside Cardiff University by sharing it with other investigators not involved in the current project. The data may also be used for teaching purposes and may be published in journals, books and electronically and presented at conferences. In any sort of report that we might publish, you might simply be referred to by your gender, age and possibly some characteristic such as location of the cancer. Your data, once anonymised, may be shared with public or commercial bodies in the UK and overseas.

What will happen to the results of the study?

As soon as the data from the study have been analysed, they will be submitted for publication in medical journals and for presentation at meetings. Your identity will not be revealed in any report, publication, or presentation. If you would like to be informed about the results, your consultant will be able to provide you with this information at the end of the study.

How is the trial monitored for safety?

This study has been carefully planned by cancer specialists and has been given a favourable opinion by the Wales Research Ethics Committee 3 and The Velindre Research and Development committee. The members of the study team will be meeting at regular intervals to monitor the progress and safety of the study.

What if something goes wrong?

It is unlikely that anything will go wrong with your treatment or care, but if you wish to complain, you can do so using the normal NHS complaints procedure. If taking part harms you in any way, there are no special compensation arrangements, but the hospital would be liable for any negligence on the part of hospital staff. Your legal rights are not affected by giving consent for the study. Your progress will be watched closely and you will be offered whatever help is available to cope with any side effects.

Who is organising and funding the research?

The study is being funded by charitable funding through the Moondance charitable fund and the Headfirst Brain Tumour Appeal both at Velindre Cancer Centre. The staff involved will not be paid for including you in this study.

What do I do now?

We would be happy to answer any questions you may have about the study. You can telephone us or speak to us again when you come to the clinic. Please discuss this information with your family, friends, or your GP if you wish. If you have any concerns or complaints regarding your participation in this study, please contact us using the contact details given at the top of this page.

Thank you for reading and considering taking part in this study.

An observational study of neurocognitive function in patients undergoing Stereotactic Radiosurgery at Velindre Cancer Centre

CONSENT FORM

REC Study Number: **Patient trial ID:**

Patient hospital number: **Patient's Initials:**

Name of Clinician: **Please initial boxes**

I confirm that I have read and understood the information sheet dated December 2016 (version 2.2) for the above study and that I have had the opportunity to ask questions and these have been answered satisfactorily.	☐
I understand that my participation is voluntary and that I am free to withdraw at any time, without giving a reason, and that my medical care and legal rights will not be affected. Data collected up until my withdrawal may still be used in the study.	☐
If I withdraw from the study, I consent to providing authorised researchers with basic clinical information that would routinely be collected and written in my medical records.	☐
If I withdraw from the study or am unable to continue with the study for any reason, I consent for any data that has been collected on me up until that point to be retained and included in the overall analysis of the study.	☐
I understand and agree that the MRI scan at CUBRIC is not a medical screening procedure and that the researchers are not qualified to provide a clinical diagnosis or identify potential abnormalities.	☐
I understand that, if the researchers are concerned that there may be a potential abnormality on the scan, I consent to them disclosing the scan to a specialist to provide a report on the scan. The results of this can be given to my General Practitioner and / or oncology consultant.	☐

I understand that the information provided by me will be held confidentially. Data from all parts of this study will be stored using a code so that only the researchers can trace this information back to me individually. The information may be retained indefinitely unless I specifically instruct the researchers to delete my data. ☐

I consent to the anonymized data obtained from all parts of this study being shared with other researchers at Velindre Cancer Centre and Cardiff University. ☐

I consent to the anonymised data from all parts of this study being shared with researchers in other organisations outside Cardiff University and Velindre Cancer Centre, including commercial bodies, and being deposited in publicly accessible databases ☐

I agree to participate in the memory tests. ☐

I agree to participate in the MRI assessments at CUBRIC. ☐

_____	_____	_____
Name of Patient	Date	Signature

I confirm that I have explained the nature, purposes, and foreseeable effects of the trial to the subject whose name is printed above.

_____	_____	_____
Name of Person obtaining consent	Date	Signature

(if different from Chief Investigator)

_____	_____	_____
Chief Investigator	Date	Signature

Copies: 1 for Patient, 1 for researcher, 1 to be kept with hospital notes